



Chair of Geology and Economic Geology

Doctoral Thesis



Characterisation and Metallurgical
Treatment of Jarosite Residues from Zinc and
Platinum Production

Gustav Erwin Hanke, BSc MSc

January 2020

Affidavit

I declare on oath that I wrote this thesis independently, did not use other than the specified sources and aids, and did not otherwise use any unauthorized aids.

I declare that I have read, understood, and complied with the guidelines of the senate of the Montanuniversität Leoben for "Good Scientific Practice".

Furthermore, I declare that the electronic and printed version of the submitted thesis are identical, both formally and with regard to content.

Date 14.01.2020

Signature Author
Gustav Erwin Hanke, BSc MSc

Danksagung

Ich danke meinem Doktorvater Frank Melcher für die Möglichkeit, an der Montanuniversität in einer neuen und anfangs eher unbekanntem Thematik zu promovieren und für die gute Betreuung.

Jürgen Antrekowitsch danke ich für die ausführliche Begleitung und die unzähligen Möglichkeiten die mir geboten wurden, bei anderen Projekten mitzuarbeiten und meinen Beitrag zu leisten.

Dem Resources Innovation Center Leoben gilt mein Dank für den finanziellen Rückhalt der letzten Jahre.

Mein Einstieg in das Doktoratsstudium wurde ermöglicht, weil jemand zur richtigen Zeit an mich gedacht hat. Danke, Peter Onuk, für die Vermittlung und das Sprungbrett in meine Karriere an der Montanuniversität und die Unterstützung, vor allem im Bereich der Analytik.

Viele andere nette Kolleginnen und Kollegen am Department für Angewandte Geowissenschaften und Geophysik und dem Lehrstuhl für Nichteisenmetallurgie sind mir oft zur Seite gestanden. Stellvertretend sei Brigitte Mang erwähnt, für die organisatorische, aber vor allem für die moralische Rückendeckung.

Meinen Eltern Suvi und Gustav danke ich dafür, dass sie durch ihre Unterstützung, Förderung und ihren stetigen Glauben an mich den Grundstein für all das Erreichte gelegt haben.

Danke Martina und Ida (+1), für den unersetzlichen seelischen Rückhalt und die vielen Stunden der Ablenkung, die mich immer wieder an das Schönste und Wichtigste im Leben erinnert haben.

Abstract

Metallurgical by-products are often regarded as waste ending up in dumps, even though they may bear considerable amounts of different valuable metals. This does not only cause potential value losses, but also increasing problems of landfilling due to stringent environmental regulations. Adapting or developing processes which allow the treatment of such residues requires detailed knowledge of all properties concerning the material and its components.

This study deals with the characterisation of hydrometallurgical by-products out of zinc and platinum production (jarosite) and the development of a characterisation procedure for similar materials.

By-products of different zinc smelters were investigated. These are usually mixtures of residues from various process steps. The main part of the residue is the precipitation product, consisting of jarosite group minerals $[(K,Na,NH_4)Fe^{3+}_3(SO_4)_2(OH)_6]$. Referring to this main component, the whole material is commonly called “jarosite” as well. Furthermore, a similar residue from platinum production was investigated.

Many different analytical methods were tested on these residues for their applicability. Starting with sample preparation and chemical bulk analysis, electron beam methods and the determination of the mineralogical composition were in focus. Identification of valuable phases was of prime importance. Thereby, the limits and benefits of different methods were demonstrated. In close cooperation with the research fields “nonferrous metallurgy” and “mineral processing,” numerous experimental trials were performed. The (intermediate-) products generated were also characterised in detail for process optimisation.

The jarosite residue from zinc production contains various valuable metals, with zinc (2.2-6.6 %), lead (4.0-7.1 %) and silver (80-219 ppm) being the most important. Copper is commonly around several tenths of a per cent and therefore only of minor importance. Gold concentrations around 1 ppm are due to its heterogeneous distribution (nugget effect).

The small grain size is a challenge for mineralogical characterisation. Grain size analyses showed a distribution of 90 % <30 μm and 57 % <10 μm for the jarosite from zinc production and 100 % <40 μm and 45 % <10 μm for the jarosite from platinum production, respectively.

Jarosite group minerals comprise a main value-bearing phase in the residue from zinc production, as they often contain several per cent of both lead and zinc. Further phases containing considerable amounts of these metals are zinc ferrite (franklinite), sphalerite, galena, anglesite and litharge. Silver appears mainly associated with copper as inclusions in quartz, feldspar and sphalerite particles.

The jarosite residue from zinc production was successfully treated in pyrometallurgical trials in order to produce a slag (low content of heavy metals), a Pb, Ag, Cu, Au- containing metal alloy and an off-gas that contains zinc as zinc oxide. The slag was successfully tested for replacing natural sand in concrete.

The jarosite residue from platinum production is simpler in its mineralogical composition, as it is only a precipitation product and not a mixture of different residues like the jarosite from zinc production. Nickel is the only valuable element (3.7-8.4 %). This material was treated in the same pyrometallurgical process as the jarosite from zinc production. These trials were also successful. The metal alloy in this case consisted of Fe and Ni.

Intermediate and final products of all trials were characterised for process optimisation.

With the insights from the extensive characterisation of these residues, a characterisation procedure for such and similar materials was defined. Such a procedure is of major importance to evaluate the chemical and especially the mineralogical composition of unknown materials in the forefront of a possible (metallurgical) treatment.

Zusammenfassung

Metallurgische Nebenprodukte werden oft trotz ihrer teilweise erheblichen Metallgehalte als Abfälle angesehen und deponiert. Neben dem Verlust an Metallen führt dies häufig auch zu Problemen bei der Entsorgung, da strenger werdende Umweltauflagen immer größere Herausforderungen darstellen. Die Adaptierung und Entwicklung von Verfahren, die eine Verwertung solcher Reststoffe ermöglichen, setzen detailliertes Wissen über die Eigenschaften des Materials und dessen Komponenten voraus.

Es wurden in erster Linie hydrometallurgische Reststoffe verschiedener Zinkhütten untersucht. Dabei handelt es sich um eine Mischung aus unterschiedlichen Nebenprodukten die während des gesamten Prozesses entstehen. Der Hauptteil ist jedoch ein Fällungsprodukt, bestehend aus dem Mineral „Jarosit“ nach welchem oftmals das gesamte Material ebenfalls als „Jarosit“ bezeichnet wird. Außerdem erfolgte auch die Charakterisierung eines ähnlichen Rückstandes der Platinproduktion.

Es wurden mehrere Analysemethoden für die Charakterisierung dieser Reststoffe getestet. Beginnend mit der Probenaufbereitung und chemischen Gesamtanalysen, lag der Schwerpunkt auf Elektronenstrahlmethoden und der Bestimmung der mineralogischen Zusammensetzung. Die Identifizierung der wertmetalltragenden Phasen war von besonderer Bedeutung. Dabei konnten die Grenzen der unterschiedlichen Methoden und deren Nutzen aufgezeigt werden. In enger Zusammenarbeit mit den Forschungsbereichen Nichteisenmetallurgie und Aufbereitung wurde eine Vielzahl an Versuchen mit diesen Materialien durchgeführt.

Der Jarositrückstand aus der Zinkproduktion enthält an Wertmetallen vor allem Zink (2.2-6.6 %), Blei (4.0-7.1 %) und Silber (80-219 ppm). Kupfer kommt im Bereich von einigen Zehntel Prozent vor, ist aber von untergeordneter Bedeutung. Gold wurde bei vielen chemischen Analysen im Bereich um 1 ppm nachgewiesen, was aufgrund der üblicherweise heterogenen Verteilung von Gold (Nuggeteffekt) aber nur als Annäherungswert angesehen werden kann.

Bei der mineralogischen Charakterisierung stellte besonders die durchwegs geringe Korngröße des Materials eine besondere Herausforderung dar. Für das Jarositmaterial aus der Zinkproduktion wurden 90 % <30 µm und 57 % <10 µm sowie für den Jarosit aus der Platinproduktion 100 % <40 µm und 45 % <10 µm ermittelt. Als wertmetalltragende Phasen im Jarosit aus der Zinkproduktion wurde vor allem das Mineral Jarosit identifiziert, welches

einige Prozent Blei und Zink beinhalten kann. Weitere identifizierte Phasen, welche diese Metalle enthalten sind: Zinkferrit (Franklinit), Sphalerit, Galenit, Anglesit und Lithargit. Silber wurde vor allem gemeinsam mit Kupfer als Einschlüsse in Quarz, Feldspat und Sphaleritpartikeln gefunden.

Mit dem Jarositmaterial aus der Zinkproduktion wurden erfolgreich Versuche zur pyrometallurgischen Verwertung durchgeführt. Dabei entstand eine Schlacke, die nahezu frei von Schwermetallen ist, eine Metalllegierung welche Blei, Silber (Kupfer und Gold) sammelte und ein Abgas welches das Zink in Form von Zinkoxid enthielt. Die Schlacke wurde auch positiv auf ihre Eignung als Sandersatz in Beton getestet.

Die Charakterisierung des Jarositrückstandes aus der Platinproduktion erfolgte auf dieselbe Art und Weise. Als einziges Wertmetall ist Ni interessant (3.7-8.4 %). Es wurden pyrometallurgische Versuche durchgeführt, die auf demselben Prinzip beruhen, jedoch mit dem Unterschied, dass das Metallprodukt eine Fe-Ni Legierung ist. Auch diese Versuche verliefen erfolgreich.

Im Zuge der pyrometallurgischen Verarbeitung beider Materialien wurden auch die Zwischen- und Endprodukte im Detail charakterisiert, um die Prozesse optimieren zu können. Anhand der Erkenntnisse aus dieser Arbeit entstand ein Konzept zur Charakterisierung solcher und ähnlicher Materialien. Damit soll die chemische und mineralogische Zusammensetzung von unbekanntem Reststoffen auf deren Nutzen zur Metallgewinnung evaluiert werden können.

Acronyms

AAS	Atomic absorption spectrometry
EDX	Energy dispersive X-ray detector
EMP	Electron microprobe
FEG	Field emission gun
HGMS	High gradient magnetic separator
HPA	High pressure asher
ICP-MS	Inductively coupled plasma - mass spectroscopy
ICP-OES	Inductively coupled plasma atomic emission spectroscopy
LA-ICP-MS	Laser ablation - Inductively coupled plasma - mass spectroscopy
SEM	Scanning electron microscope
S/TEM	Scanning/transmission electron microscope
TBRC	Top blown rotary converter
TEM	Transmission electron microscope
WDX	Wavelength dispersive X-ray detector
XRD	X-ray diffraction analysis
XRF	X-ray fluorescence analysis

List of Mineral Formula

Albite	$\text{NaAlSi}_3\text{O}_8$
Ammoniojarosite	$(\text{NH}_4)\text{Fe}^{3+}_3(\text{SO}_4)_2(\text{OH})_6$
Anglesite	$\text{Pb}(\text{SO}_4)$
Anhydrite	$\text{Ca}(\text{SO}_4)$
Anorthite	$\text{CaAl}_2\text{Si}_2\text{O}_8$
Barite	$\text{Ba}(\text{SO}_4)$
Celestine	$\text{Sr}(\text{SO}_4)$
Covellite	CuS
Feldspar	$(\text{Ba,Ca,Na,K,NH}_4)(\text{Al,B,Si})_4\text{O}_8$
Franklinite	$(\text{Zn,Mn}^{2+},\text{Fe}^{2+})(\text{Fe}^{3+},\text{Mn}^{3+})_2\text{O}_4$
Galena	PbS
Garnet	$(\text{Mg,Ca,Fe}^{2+},\text{Mn}^{2+})_3(\text{Al,Fe}^{3+},\text{Cr}^{3+},\text{V}^{3+})_2(\text{SiO}_4)_3$
Gersdorffite	NiAsS
Gypsum	$\text{CaSO}_4 \cdot 2(\text{H}_2\text{O})$
Heazlewoodite	Ni_3S_2
Hematite	$\text{Fe}^{3+}_2\text{O}_3$
Hexahydrate	$\text{MgSO}_4 \cdot 6(\text{H}_2\text{O})$
Hydroniumjarosite	$(\text{H}_3\text{O})\text{Fe}^{3+}_3(\text{SO}_4)_2(\text{OH})_6$
Jarosite	$\text{KFe}^{3+}_3(\text{SO}_4)_2(\text{OH})_6$
Litharge	PbO
Microcline	KAlSi_3O_8
Natrojarosite	$\text{NaFe}^{3+}_3(\text{SO}_4)_2(\text{OH})_6$
Orthoclase	KAlSi_3O_8
Plumbojarosite	$\text{Pb}_{0.5}\text{Fe}^{3+}_3(\text{SO}_4)_2(\text{OH})_6$
Pyrite	Fe^{2+}S_2
Quartz	SiO_2
Siegenite	$(\text{Ni,Co})_3\text{S}_4$
Sphalerite	$(\text{Zn,Fe})\text{S}$
Talc	$\text{Mg}_3\text{Si}_4\text{O}_{10}(\text{OH})_2$
Trevorite	$\text{NiFe}^{3+}_2\text{O}_4$
Wuestite	Fe^{2+}O

Table of Contents

Danksagung	I
Abstract	II
Zusammenfassung	IV
Acronyms	VI
List of Mineral Formula	VII
Table of Contents	VIII
1. Introduction	1
1.1 The Mineral 'Jarosite'	4
1.2 The Importance of Jarosite Residues	5
1.3 Questions to be Answered	6
1.4 Cooperation	7
2. Jarosite from Zinc Production	8
2.1 Roasting	10
2.2 Leaching	12
2.3 Iron Precipitation	13
2.4 Dumped Material	15
2.5 Jarofix	16
3. Jarosite from Platinum Production	17
3.1 Introduction to Platinum Production	17
3.1.1 Concentrating and Smelting	18
3.1.2 Base Metals Refinery	20
4. Use of Jarosite	21
5. Characterisation	23
5.1 Characterisation of Fine- Grained Material	23
6. Samples	25
7. Methods	27
7.1 Sample Preparation	27
7.2 Grain Size Distribution	28
7.3 Magnetic Separation	28
7.4 X-ray Diffraction Analysis	29
7.5 X-ray Fluorescence Analysis	30
7.6 Inductively Coupled Plasma-Mass Spectroscopy	30
7.7 Electron Beam Methods	31
7.7.1 Automated Analysis	33
7.8 Laser Ablation-Inductively Coupled Plasma-Mass Spectroscopy	33
7.9 RAMAN Spectroscopy	35
7.10 Summary of the Evaluated Methods	35

7.11	Hydro Separation	37
8.	Results.....	39
8.1	Chemical Composition of Various Jarosites from Zinc Production.....	39
8.2	Sample Preparation for Mineralogical Characterisation	42
8.3	Mineralogical Characterisation.....	45
8.4	In-Situ High Resolution Chemical Analysis.....	47
8.4.1	Sample Heterogeneity Measured by LA-ICP-MS.....	47
8.4.2	Phase Identification Using Element Correlation	48
8.5	Grain Size Distribution	51
8.6	Mineralogical Composition.....	52
8.6.1	Jarosite.....	52
8.6.2	Zinc Ferrite and other Zn-Bearing Phases	57
8.6.3	Lead-Bearing Phases.....	58
8.6.4	Silicates	61
8.6.5	Occurrence of Silver	62
8.6.6	Minor Phases	64
8.6.7	Listing of Identified Phases.....	66
8.7	First Insights Using S/TEM	68
8.8	Jarosite from Platinum/Nickel Production	70
8.8.1	Chemical Composition of Jarosite from Platinum Production	70
8.8.2	Grain Size Distribution.....	71
8.8.3	Mineralogical Composition.....	72
9.	Proposal for Utilisation.....	78
9.1	Possible Beneficiation.....	78
9.1.1	Flotation Trials.....	78
9.1.1.1	Results from Flotation Trials.....	80
9.1.2	Grain Size Separation.....	83
9.1.3	Magnetic Separation	85
9.2	Pyrometallurgical Treatment.....	86
9.2.1	Preparation for Pyrometallurgical Treatment.....	87
9.2.2	Calcination	88
9.2.3	Reduction of Jarosite from Zinc Production.....	88
9.2.4	Reduction of Jarosite from Platinum Production	89
9.3	Pyrometallurgical Trials on Jarosite from Zinc Production.....	89
9.3.1	Pre-treatment.....	89
9.3.2	Calcination	90
9.3.3	Reduction.....	91
9.3.4	Use of the Slag.....	94
9.3.5	Summary of Trials on Jarosite from Zinc Production	97

9.4	Pyrometallurgical Trials on Jarosite from Platinum Production.....	99
9.4.1	Pre-Treatment	100
9.4.2	Calcination	101
9.4.3	Reduction.....	101
9.4.4	Summary of Trials on Jarosite from Platinum Production	102
9.5	Benefits of Characterisation on Process Development and Product Optimisation	104
9.5.1	Benefits of Characterisation on Products from Treating Jarosite from Zinc Production	105
9.5.1.1	Characterisation for Pre-Treatment	105
9.5.1.2	Evaluating the Settings for Calcination	106
9.5.1.3	Characterisation of Final Products	107
9.5.2	Benefits of Characterisation on Products from Treating Jarosite from Platinum Production	109
9.5.2.1	Characterisation for Pre-Treatment	109
9.5.2.2	Evaluating the Settings for Calcination	110
9.5.2.3	Characterisation of Final Products	113
9.6	Economic Considerations.....	115
9.6.1	The Important Role of Lead, Silver and Zinc.....	116
9.6.2	The Variable Importance of Gold	118
10.	Concept for a Characterisation Procedure	118
10.1	Proposed Approach for Characterisation of Unknown Material.....	119
11.	Discussion	122
11.1	Questions to be Answered-Jarosite from Zinc Production.....	122
11.2	Questions to be Answered- Jarosite from Platinum Production.....	123
11.3	Evaluated Methods and their Usability for Jarosite-Type Residues.....	124
12.	Summary.....	128
12.1	Outlook	132
13.	Acknowledgements	132
14.	References	133
15.	List of Figures.....	138
16.	List of Tables	143
17.	List of Appendices.....	145
18.	Appendix.....	149

1. Introduction

Every day, huge amounts of by-products of the metal-producing industry are dumped as waste. Due to the lack of suitable processing techniques, these dumps still contain high concentrations of precious and critical metals. In connection with the ever-growing demand for raw materials and the ubiquitous search for deposits, these dumps are becoming increasingly important as secondary deposits (Reuter, 2013).

Besides the continuously formed residues, there is also a high number of old dumps from mining, processing and metallurgical activities. These commonly contain even higher amounts of various metals due to less developed processing methods in the past (Pawlek, 1983). Not only the need for new resources, but also environmental considerations make it necessary to treat these by-products somehow, especially because the amount of by-products will most likely grow in future as the need for raw materials is increasing whilst the quality of ores is getting worse, causing an increase in waste for the same amount of valuables.

Until today, the major part of by-products has been dumped, even though many of them bear considerable amounts of valuable metals (Balladares, et al., 2014, Piatak, et al., 2003, Rizescu, et al., 2010, Vereš, et al., 2015). Some of the reasons for this are:

- The potential of a by-product is not known.
- Smelters focus on their main metals and are not interested in producing others.
- Trials on treating the material might have been unsuccessful due to a lack of specific know-how and therefore the material is treated as valueless, even if it bears valuables.
- The materials cannot be treated by state of the art techniques and the development of new methods is too expensive.
- Dumping of by-products is easier and cheaper than treating it.

In the end, the decision if a material is treated or dumped is an economical one. Therefore, even if a dump or a by-product is not worth further processing at the moment, it might be in the near future.

The development of proper methods requires a full understanding of the complex mineralogical and chemical composition of these heterogeneous waste materials. Due to

their origin, these materials are not comparable to natural ores. Residues are often a mixture of by-products of many different process steps within one process of metal winning. By-products often contain phases which are unnatural, amorphous and/or very small in their grain size.

The present work focuses on the characterisation of residues from primary zinc production. This material is one of the most abundant metallurgical by-products in the world and demonstrates different challenges which can appear during the characterisation of residues in general (Hanke, et al., 2016).

“Jarosite” comprises a family of minerals which are the main components in these residues. Jarosite is, more precisely, a potassium iron sulphate hydroxide but can also accommodate many other elements and form different endmembers, such as natrojarosite (the more important one in the hydrometallurgical zinc winning process), hydronium jarosite, ammoniojarosite and plumbojarosite (Swayze, et al., 2008, Anthony, et al., 1990). However, the final residue from hydrometallurgical zinc winning consists not only of the mineral jarosite, but also of many other residues that occur during the whole process. It bears considerable amounts of zinc, lead, silver, copper and in some cases also gold, indium, germanium and gallium (Sharma, 2016).

The jarosite mineral is formed as a precipitation product after the leaching processes and is sometimes dumped together with a part of the leaching residue; this significantly increases the amount of precious metals as it is an important source for especially lead and silver. This leaching residue is also sometimes sold separately to lead smelters.

Besides the residues from zinc production, a jarosite residue from platinum production was also investigated in the same way. The origin of the jarosite mineral is similar to the jarosite in zinc production. It is used to remove iron from a hydro-sulphuric process solution (Crundwell, et al., 2011, Lamy, 2007). The main difference is that the jarosite from platinum production does carry only nickel as a valuable metal. In case of a pyrometallurgical treatment, iron is also a part of the metal product (iron-nickel alloy), not a slag component.

In this work, detailed trials on mineral processing and pyrometallurgical treatment of the jarosite residues were performed. In this context, characterisation was not only done on

the original residue, but also on the different final- and by-products which occurred during these trials in order to evaluate potential for improvement. Figure 1 shows a sketch of the most important steps of process development from first evaluations up to a feasibility study and where characterisation is needed in this procedure.

For a first impression on the success of a trial, a chemical analysis is usually enough. If a trial was not successful, the reason can often be found in specific phases. Identifying relevant and essential phases is the main task when characterising intermediate or final products.

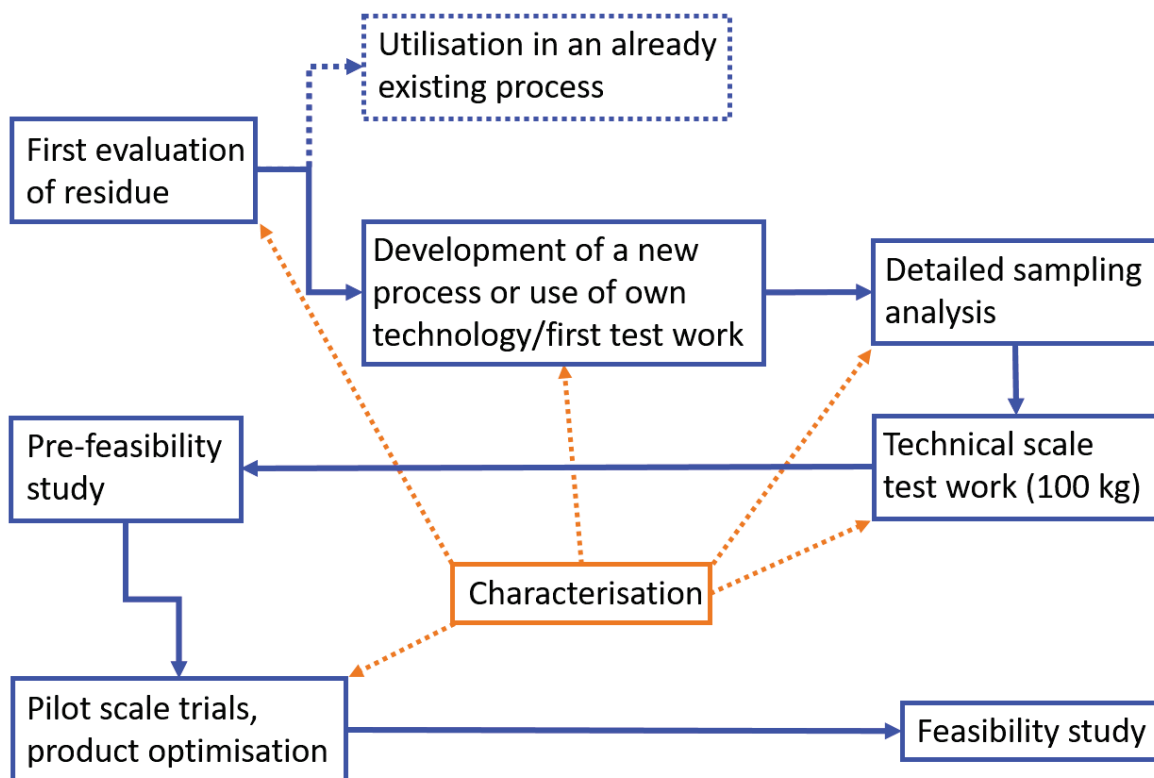


Figure 1: Sketch showing typical steps of the evaluation of a residue, process development and upscaling for process optimisation.

On a larger scale, this work should contribute to the development of an evaluation procedure for secondary resources, where the determination of the chemical and mineralogical characteristics is of major importance. Due to the technical origin of the phases present in a metallurgical residue, characterisation faces other challenges than for primary ores.

For primary ores, there are a number of procedures available, such as JORC or NI 43-101, which allow a serious assessment and certification of primary resources. However, the requirements for the evaluation of a dump and secondary resources are totally different,

as residues pose other challenges that might be more difficult to handle. For natural ores, many state of the art methods in terms of mineral processing are available, whilst residues are often too different to be treated in such an existing process.

1.1 The Mineral 'Jarosite'

Jarosite is the potassium endmember of the jarosite subgroup minerals within the alunite supergroup. The general chemical formula is $DG_3(TO_4)_2(OH,H_2O)_6$. D stands for cations with a coordination number of 9 or greater and is most commonly occupied by K, Na, NH_4 and H_3O but can also be Pb (Table 1) (Dutrizac & Jambor, 2000). All members of the supergroup have a trivalent cation in the G position, commonly Fe^{3+} or Al^{3+} , rarely Ga^{3+} and V^{3+} is also possible. The differentiation of the jarosite- from the alunite family is defined by the dominance of Fe^{3+} (jarosite) or Al^{3+} (alunite) at this position. Within these families, the T position can be occupied by S, P or As, whereby S is dominant for jarosite endmembers. Table 1 lists different jarosite endmembers and their chemical composition (Dutrizac & Jambor, 2000). Complete solid solutions within the alunite supergroup are very common (Scott, 1987). According to Dutrizac (1983) (potassium-) jarosite is the most stable endmember and there is a complete solid solubility among the alkali jarosite types. However, Desborough et al. (2010) showed that the solid solubility of Na and K at low temperatures (<140 °C) is very limited. In their studies on natural jarosite members, they found no indication for significant solid solution of K in Na-jarosite and vice versa at low temperatures. Hydronium substitution (>5 mol %) does not occur, which is most likely due to the very low stability of hydroniumjarosite over geologic timescales.

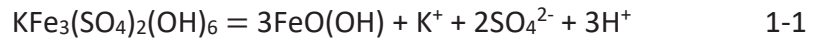
Lead in the D position leads to a slightly different chemical formula, as $2K^+$ is replaced by Pb^{2+} (Table 1). Basciano and Peterson (2010) describe an incomplete solid solution series between jarosite and plumbojarosite and an extremely limited substitution of Pb in jarosite with an occupancy of 2 % in the potassium site.

Table 1: Members of the jarosite subgroup.

Jarosite	$\text{KFe}_3(\text{SO}_4)_2(\text{OH})_6$
Natrojarosite	$\text{NaFe}_3(\text{SO}_4)_2(\text{OH})_6$
Ammoniojarosite	$(\text{NH}_4)\text{Fe}_3(\text{SO}_4)_2(\text{OH})_6$
Hydroniumjarosite	$(\text{H}_3\text{O})\text{Fe}_3(\text{SO}_4)_2(\text{OH})_6$
Plumbojarosite	$\text{PbFe}_6(\text{SO}_4)_4(\text{OH})_{12}$
Argentojarosite	$\text{AgFe}_3(\text{SO}_4)_2(\text{OH})_6$
Beaverite	$\text{Pb}(\text{Fe,Cu})_3(\text{SO}_4)_2(\text{OH})_6$
Dorallcharite	$\text{TlFe}_3(\text{SO}_4)_2(\text{OH})_6$

In nature, jarosite minerals, especially the K and Na endmembers are very widespread and known as an indicator for sulphide mineralisation as they form as a supergene product of Fe-sulphide oxidation (Ripmeester, et al., 1986, Stoffregen, et al., 2000).

Under surficial conditions, jarosite converts to goethite following the reaction (Equation 1-1) (Stoffregen, et al., 2000, Desborough, et al., 2010):



This reaction generates considerable amounts of acid. Many studies have reported natural jarosite to be a significant, natural source of acidity in soils, e.g. of the Australian coast (Welch, et al., 2008).

1.2 The Importance of Jarosite Residues

Zinc is and will also be in future one of the most produced metals in the world. The quality of the ores is continuously decreasing, as is the case for other ores as well. Both factors imply a huge amount of existing and an increase in newly generated residues. There are a couple of reasons why zinc production residues were chosen as the focus for the investigation of metallurgical by-products as secondary resources:

- In contrast to all other metals, Europe is still strong in zinc production.
- The hydrometallurgical process, which jarosite residues originate from, is the main method of zinc winning.
- These residues are very complex in their chemistry and mineralogy.

- They contain valuable metals which could be of interest from an economic point of view.
- Dumping of the material is an increasing problem, as it must be treated as hazardous waste.
- Annually, residues containing metals (Zn, Pb, Cu, Ag) with a value of about €2-3 billion are produced (Hanke & Antrekowitsch, 2018).

Jarosite from platinum production was chosen because it is a similar material concerning its formation, grain size, appearance and problems in dumping, but very different in terms of valuables. The idea of further treatment is also comparable, even though the final products are different.

1.3 Questions to be Answered

The aim of the characterisation procedure is to deliver information to specialists in mineral processing and metallurgy. This is the basis to evaluate the material and develop and optimise processes. The main questions essential for the treatment can be defined as follows:

- Does the material contain any valuables?
 - A first chemical analysis gives evidence, if the material is worth further investigations.
- Does the material contain any hazardous compounds?
 - The presence of hazardous compounds may have a negative effect on treatment, newly formed residues or the final products.
- Which particles contain the valuables?
 - Especially for methods of mineral processing, detailed information concerning properties of host particles is necessary.
- What is the quantity of valuables in specific host particles?
 - Not only finding, but also quantifying phases is of crucial importance for producing a concentrate.

- What is the morphology/size of the (host-)particles?
 - It may be possible to use the grain size or grain morphology for any kind of processing.
- What are the intergrowth relationships and agglomerates?
 - Treatment to break agglomerates, or to reduce the grain size in general (milling) might be necessary.
- What are slag-forming compounds?
 - When it comes to a pyrometallurgical treatment, the composition of the produced slag is critical in order to produce as much metal as possible and produce a slag that fulfils the requirements for further treatment.

1.4 Cooperation

Close cooperation with specialists in metallurgy and mineral processing was needed in order to develop proper treatment procedures for this kind of material.

At Montanuniversität Leoben, a method of pyrometallurgical multi-metal recovery, which is able to treat the jarosite residue as well, has been already developed. The idea behind it is a two-step process that allows the winning of all valuable metals and the production of an inert slag that can be used as construction material or is at least much easier to dump than the original jarosite residue (Pichler, et al., 2013). So far, the cooperation with metallurgists has focused on optimising the existing process for the jarosite material.

As pyrometallurgy is relatively energy consuming and therefore expensive, a prior concentration of valuables is necessary. Screening of typical methods of mineral processing and parallel investigations on intermediate and final products were performed to evaluate techniques which are applicable for this type of material. Due to the properties of the material, special attention was paid to flotation, where an accurate characterisation of all components is necessary to develop reagent regimes enabling productive flotation.

This work was also supported by the FFG project Jaromin – “Mineralogische Charakterisierung von Jarosit als Basis für die metallurgische Verarbeitung.“

At the end, the mineralogical and chemical characterisation delivers the basis for the flotation technology and optimisation of pyrometallurgical metal recovery.

2. Jarosite from Zinc Production

Concentrating sulphide minerals by the development of flotation processes substantially expanded the availability of zinc raw materials. Whilst in former times the zinc production was limited to oxidic ores, this new technology allowed the use of sulphidic ores as well. However, the whole zinc winning process was developed for the use of oxidic ores. According to this, an additional process was needed to convert sulphidic ores to oxidic ones to allow the use of the commonly used zinc process. Firstly, this was done by open heap roasting. This technique was not only quite inefficient, but also very problematic regarding its environmental impact, as the off-gas, which is rich in sulphur, escaped directly into the atmosphere. Subsequently, the capture of the sulphur dioxide formed became a parallel task. This was not only reasonable from an environmental point of view, but also from an economic one, as the sulphur dioxide can be used to produce sulphuric acid, which is later at least partly needed in the leaching processes. However, the sulphuric acid in the zinc winning process is theoretically reused in a closed circle and new acid is only needed to compensate a small loss. Therefore, much more sulphuric acid is produced than is needed for the leaching. The much bigger part of it can be sold in the best case.

About 1.5 million tons of waste are produced annually from hydrometallurgical processes in Europe's zinc smelters (see Chapter 2.4). These wastes are commonly termed "jarosite" even though they contain many other phases than only the mineral jarosite. These residues are usually dumped, although they often contain significant concentrations of valuable metals such as zinc, lead and silver (Ismael & Carvalho, 2003).

Nowadays, about 90 % of the world's total zinc output results from the conventional hydrometallurgical route. Figure 2 shows a simplified sketch of this process. The blue frames and arrows indicate the main steps and streams, while the orange ones point out different types of residues that might be produced.

The input material is a zinc sulphide concentrate. After calcination, the calcine undergoes different steps of leaching in sulphuric acid. The residue from the weak acid leaching, also known as neutral leach residue, is more a historical one. Weak acid leaching is not able to leach the zinc ferrite that is formed during roasting if iron is available in the concentrate. In former times, ore qualities were considerably better (less iron), and therefore the zinc loss due to zinc ferrites low. However, nowadays the iron content and with this the amount of

zinc ferrite is much higher, so this residue is usually further treated with additional leaching steps. After the hot acid leaching, the solution contains not only zinc, but also iron that must be removed in an additional precipitation process to allow the zinc winning via electrolysis. Jarosite and goethite are the common compounds that are formed for iron precipitation nowadays. Both are iron precipitation products of different hydrometallurgical processes and might be dumped as a mixture with leaching residues, intermediate products or other residues from the overall process. As jarosite and goethite are the main “mineral” phases of the dumped material, the residue is also commonly called jarosite or goethite. The residue from the last leaching step is enriched in lead and silver and sometimes sold to lead smelters after additional concentration (Sinclair, 2005, Sahu & Agrawal, 2008).

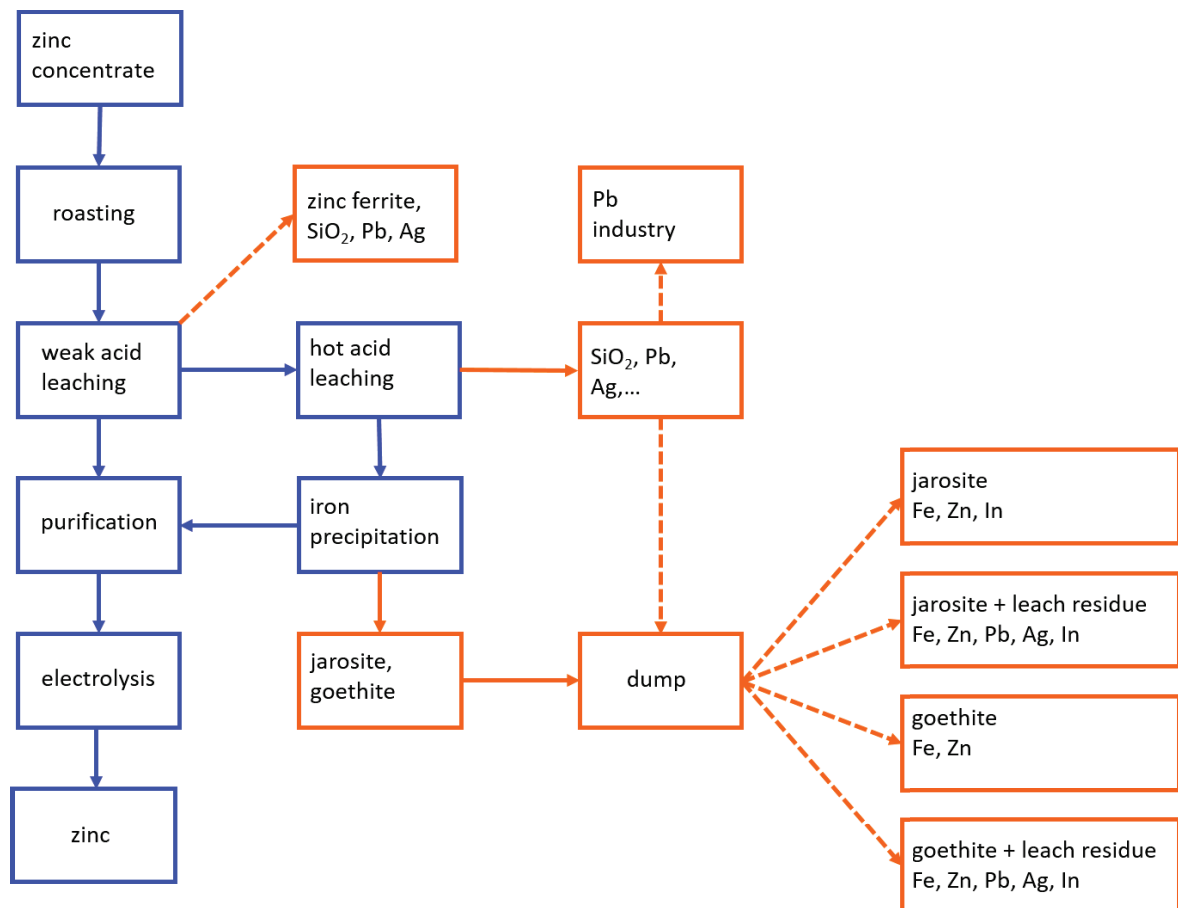


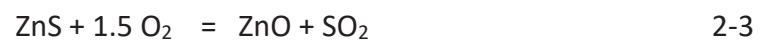
Figure 2: Simplified sketch of hydrometallurgical zinc production showing possible compositions of dumped material. Blue represents different process steps and orange, residues produced.

The following chapters describe the hydrometallurgical route according to Sinclair (2005) in more detail. However, it is still a simplified repetition, as every smelter has a varying

process structure, concerning, for example, the number of leaching steps or the treatment of side streams (Garcia & Valdez, 1996; Rosales, 2016; van Dyk, 2006).

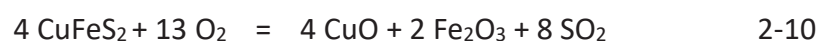
2.1 Roasting

During the roasting process, zinc sulphides turn into zinc oxides. As a by-product, it delivers sulphur which is used to produce sulphuric acid. A part of this sulphuric acid is used for the leaching process. However, the amount of acid produced is much higher than what is needed for the process. The rest must be utilised differently. During the roasting of zinc sulphide, the following reactions occur (Equations 2-1 to 2-4) (Sinclair, 2005):



The reactions are dependent on the temperature, but also strongly controlled by the partial pressures of oxygen and sulphur dioxide in the roaster gas.

Naturally, the concentrates contain other sulphide minerals that also undergo a change in composition. The most important ones are (Equations 2-5 to 2-10):



The amount of sulphate formed depends on the concentration of oxygen and sulphur dioxide as well as on the equilibrium balance for the reversible SO_3 formation (Equation 2-11):



New processes of direct leaching, where a roasting step before leaching is not necessary, might complement the roast-leach process (Svens, et al., 2003). However, the roasting does have advantages in eliminating volatile impurities, such as halides. A main question for choosing the direct leach or roast-leach process is, whether or not there is a market for the sulphuric acid produced or not. The high amount of acid produced in the roast-leach process cannot be used entirely at the plant, so it is necessary to have a client for the rest. In case it is not possible to get rid of the acid, the direct leach method is an alternative.

In addition to the above-mentioned reactions, which are gas-solid reactions (besides SO_2 to SO_3), a number of solid state reactions also occur. The formation of a spinel type structure is of prime importance for the further process, the most important one being the formation of zinc ferrite according to the following reaction (Equation 2-12):



Not only iron containing sphalerite is converted to zinc ferrite; a significant amount is formed from the iron of pyrite and pyrrhotite, which reacts with the zinc oxide. This reaction is favoured by increasing temperature and roasting time. Furthermore, zinc ferrites formed under higher temperatures are more difficult to leach than those formed under lower temperatures. Zinc ferrite contains relatively large amounts of the total zinc. As zinc ferrite is not leachable under the common conditions of neutral leaching, this zinc is either lost or has to be treated in an additional leaching process.

Zinc silicate is another common mineral formed during roasting (Equation 2-13) when there is a close mineral association between sphalerite and quartz. Equal to the formation of zinc ferrite, the formation of zinc silicate is also favoured at higher temperatures and long residence times.



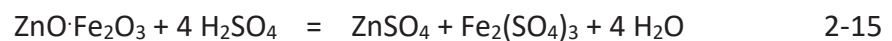
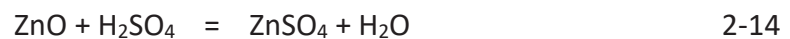
The silicate formation (willemite) can mainly be minimised by limiting the silicate content in the input concentrates.

As mentioned before, the roasting gas can be used to produce sulphuric acid. Of course, the roasting gas contains many different carryover particles which must be removed before the production of sulphuric acid. 9 to 10 % of the gas is usually SO_2 (the rest is N_2 and O_2).

The main part of the dust components (typically around 50 mg/m³) consists of chlorine, fluorine, mercury and selenium.

2.2 Leaching

In the leaching operation, the roasted material is treated with sulphuric acid (Sinclair, 2005). The task is to remove the zinc as selectively as possible in order to reduce impurities and release the following steps of cleaning purification. A high yield is desirable to lose as little as possible in the waste material. Therefore, usually two, sometimes up to five different leaching steps under different conditions are performed. The leaching reactions of the zinc oxide and zinc ferrite are (Equations 2-14 and 2-15):



The sulphuric acid can be used several times. After the electrowinning process it is reused for leaching. Small losses of acid are compensated by input from the sulphuric acid plant which produces the acid from the roast gas.

As already stated, different leaching steps are necessary to leach not only ZnO, but also zinc ferrite. The steps differ in temperature and pH-value. The following are four commonly used regimes:

- neutral leaching: pH 4 – 5.5 at 60°C
- weak acid leaching: 10 g/L H₂SO₄ to pH 4 at 60°C
- hot acid leaching: 30-80 g/L H₂SO₄ at >90°C
- strong acid leaching: >120 g/L H₂SO₄ at >90°C

The first neutral leaching and the weak acid leaching (primary leaching) are intended to leach the zinc oxide, whilst the hot acid leaching and the strong acid leaching (secondary leaching) leach the zinc ferrite. The product of the primary leaching undergoes a solution purification which removes precious metals such as Cu. This is necessary because metals more precious than zinc cannot be removed during electrolysis and will contaminate the product. Iron does not have to be removed, as it is not leached in the primary leaching. The

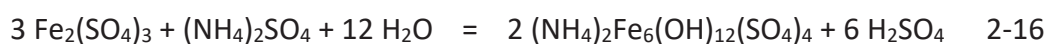
next step is electrowinning which produces zinc with a purity of 99.995 % that is later molten into saleable products.

2.3 Iron Precipitation

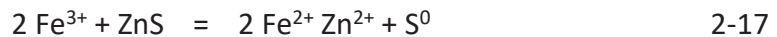
As the solution resulting from secondary leaching does not only contain zinc, but also iron, another step is needed to remove the iron, as it would cause major problems in the electrowinning process.

There are three iron minerals used for iron precipitation: jarosite, goethite and hematite. The jarosite process is currently the most commonly used one. Jarosite is an iron sulphate mineral with the formula $R_2Fe_6(OH)_{12}(SO_4)_4$. R can be K^+ , NH_4^+ , Na^+ , Ag^+ ; Pb^{2+} for R_2 is also possible (Forray, et al., 2010, Swayze, et al., 2008). According to Dutrizac et al., iron can also be partly replaced by gallium (Dutrizac & Chen, 2000) and thallium (Dutrizac, et al., 2005). The formation of jarosite requires high temperatures, close to the boiling point, and low solution acidities. As potassium and sodium are usually present in the concentrate, potassium- and sodium-jarosite are naturally formed in the precipitation product, at least in small amounts. However, the amount is by far not enough to remove all of the iron. Consequently, additional jarosite-building reagents must be added. Today, zinc plants in Europe produce exclusively natrojarosite (sodium endmember). Ammoniojarosite is only present in historical dumps.

As every mol of jarosite formed causes three moles of sulphuric acid (Equation 2-16), neutralisation is necessary to keep the pH-value at a certain level and allow the reaction to proceed. For this, calcine is added to the solution. This causes a loss of zinc, as zinc ferrite does not react under these conditions. Another step of pre-neutralisation and thickening prior to the addition of calcine reduces the amount of calcine needed. It is also possible to leach the precipitation product again, because jarosite has higher stability in acid than zinc ferrite and therefore, the iron in the jarosite remains untouched whilst the zinc ferrites are leached. Typical conditions of jarosite precipitation are 90°C, acidity of around 10 g/L and residence time of about six hours. Equation 2-16 shows the formation of ammoniojarosite:



Besides the jarosite process, the goethite process is a commonly used method for iron precipitation. Whilst hydronium jarosite is stable at an Fe concentration above 12 g/L, goethite is the stable solid phase at Fe concentrations below 2 g/L. For that reason, the usual Fe concentration of 30 g/L must be reduced before goethite precipitation can occur. One method is the Vieille Montagne (VM) goethite process; the other one is the Paragoethite process. The first step of the VM process is reducing the solution following the equation (2-17)



In the next step, the solution is oxidised to ferric iron. Goethite is precipitated simultaneously (Equation 2-18).



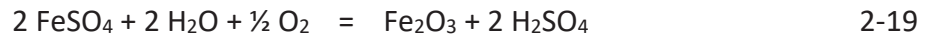
Generally, a pH-value of 4.5-4 and a temperature of 95°C is preferred. Due to the lower stability of goethite compared to jarosite, a recovery of zinc in a re-leach is not possible because the goethite would be leached as well.

The iron content in the goethite is higher than in jarosite with theoretically 69.2 % according to its formula. Due to an uncertain level of hydration and the presence of other phases, it is around 43 %, and thus still higher than 30 % Fe in jarosite. So far, an advantage of the goethite is that the amount of material that goes to the dump is much lower. Furthermore, it is more efficient in removing impurities like As, Sb, In, Tl and F. This is also the reason why zinc producers which recover indium use the goethite process instead of the jarosite process.

However, the loss of zinc is significantly higher in the goethite process. It usually contains up to 10 % of zinc, whilst the jarosite residue contains about three to six per cent. The lower total amount of goethite (about 75 %, compared to jarosite) does not change the relation essentially.

An ancillary alternative is the hematite process. However, it has never been as important as the jarosite or goethite processes and currently this process plays no role. In the hematite process, the feed solution is reduced equally as in the VM goethite process to convert all iron in the ferrous state. At temperatures of 180-200°C, high pressure and under

the addition of oxygen (at former Datteln plant, Ruhr Zinc) the following reaction occurs (Equation 2-19):



The benefit of this method is the high iron content, lowering the total amount of residue to about half compared to the jarosite process, and the very high zinc recovery of about 99%. One essential reason for companies using this process used to be the possibility of selling the hematite for iron production. However, the material proved to be very high in impurity levels, especially in zinc and arsenic. Due to the additional disadvantage of relatively high operational costs, the hematite process is not of prime importance in worldwide zinc production.

The following table (Table 2) compares the characteristics of the four iron removal processes mentioned.

Table 2: Metal contents in by-products of different iron removal processes per 100 t of feed concentrate (Sinclair, 2005).

Process	Jarosite	VM-goethite	Paragoethite	Hematite
Iron residue				
Fe content	29 %	40 %	34 %	57 %
Zn content	3.5 %	8.5 %	13.0 %	1.0 %
Pb content	1.9 %	1.9 %	2.2 %	0 %
Quantity of Fe residue	22.5 t	16.2 t	19.2 t	11.2 t
Zinc loss in Fe residue	1.51 %	2.65 %	4.79 %	0.21 %
Quantity of sec leach residue	6.0 t	6.5 t	6.0 t	8.0 t
Zinc loss in sec leach residue	0.58 %	0.63 %	0.58 %	0.77 %
Overall zinc recovery	97.9 %	96.7 %	94.6 %	99.0 %

2.4 Dumped Material

Having a closer look at the jarosite and goethite material that is available at dumps, there are four combinations possible. As mentioned above, the leaching residue can be sold (after further treatment like flotation) to lead smelters for the recovery of lead and silver. Depending on the amount of leaching residue sold, the dumped material can consist of

either very pure iron precipitate or a mixture of iron precipitate and leach residue. If the leach residue is dumped together with the jarosite, it is considerably higher in valuable metals, especially in lead and silver. Furthermore, different mixtures of iron precipitate and leaching residue are possible, as sometimes not all of the weak acid leaching residue is further treated but directly dumped instead. It also happens that intermediate process steps are overloaded and the surplus then skips some of these. In the end, a large variety of different by-products from many different process steps are dumped together. The case is quite similar in the jarosite and goethite processes. However, the quantity of metals may differ. Depending on the plant technology, the input material, the exact process and other factors, the total amount of residue produced is around 0.5 to 1 ton per ton of produced zinc. Table 3 shows details such as capacity, calculated amount and type of by-products of different zinc plants.

Table 3: Details of zinc plants in Europe. Own investigations, Chair of Nonferrous Metallurgy.

	Annual capacity	Residue (calc.)	Dump	Jarosite/goethite	Valuables (Ag/Pb)	Start of operation
1	155 000	124 000	yes	jarosite	yes	1972
2	485 000	388 000	yes	jarosite	yes/no	1960
3	260 000	208 000	?	goethite	no	1935
4	255 000	204 000	no	jarosite	yes	1974
5	160 000	128 000	?	goethite	no	1975
6	150 000	120 000	yes	goethite	?	1994
7	315 000	252 000	yes	jarosite	yes	1969
8	160 000	128 000	yes	jarosite	yes	1929

2.5 Jarofix

As the dumping of the jarosite residue is problematic, some zinc plants mix it with lime and cement to produce a product called jarofix. This is more stable and easier to dump than the jarosite residue. The benefit of dumping is a disadvantage in processing, if the material is going to be recycled. The overall amount of material also increases. According to Krishnan et al. (2016), jarofix contains about 2 % lime and 10 % cement. Following a European zinc smelter, lime and cement and jarosite residue are mixed in a ratio of 0.3:1.

3. Jarosite from Platinum Production

The use of the jarosite precipitation technique is not only limited to the zinc industry, but is also applied in the nickel route within the production process of platinum group metals. Similar to the jarosite in the zinc winning process, iron removal from a solution is also necessary during nickel production. Opposite to zinc-jarosite, the residue in this case contains only nickel as a valuable metal. In terms of pyrometallurgical treatment of this residue, iron is a component of the metal product, as the nickel is won as an iron alloy. Therefore, the economic value of the material is limited to the concentration of nickel.

The total process of platinum production is, in this case, not limited to the winning of platinum, but is designed to also produce Cu, Ni and Co besides PGMs. Pyrrhotite, pentlandite, chalcopyrite and pyrite are the main sulphide minerals in the ore. PGMs are mainly associated with pentlandite but also with other sulphides and occur as minerals such as braggite, cooperite, laurite and ferroplatinum (Jones, 1999).

In fact, the jarosite precipitation is located in the side stream of Ni and Co production within the overall process. This chapter summarises the origin of this type of jarosite and the basics of the overall process following Crundwell et al. (2011), Lamya (2007) and Cramer (2001).

3.1 Introduction to Platinum Production

The whole process can be subdivided into three stages:

- Concentrating and smelting
 - Production of an oxide slag and a matte
- Base metals refinery
 - Production of Cu, Ni, Co, (Se) and a PGM concentrate
 - Origin of jarosite residue
- Platinum metals refinery
 - Production of Au, Pd, Ru, Pt, Ir and Rh

The following chapters describe the origin of the jarosite residue, which is why the description only gives a superficial overview on the other process steps within the “concentration and smelting” and “base metals refinery” (Figure 3).

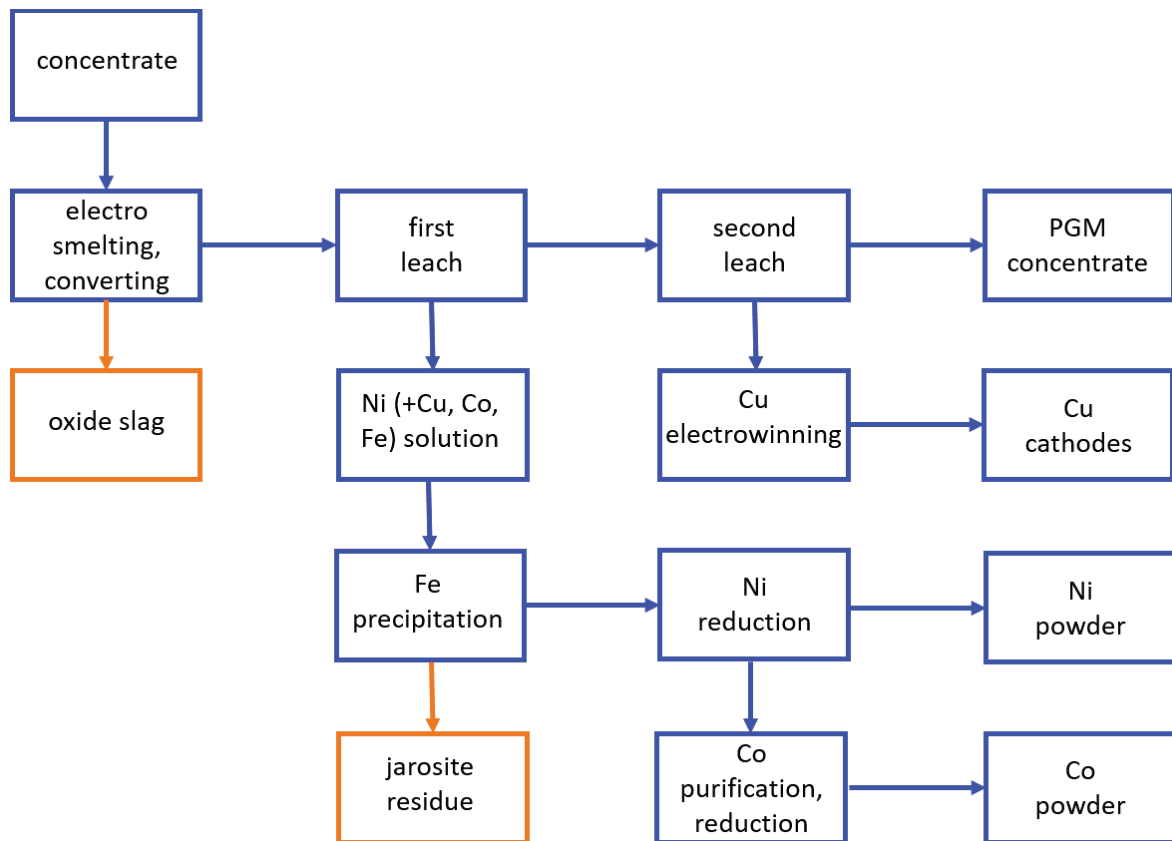
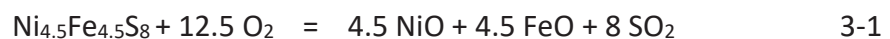


Figure 3: Simplified sketch of the base metals refinery process for winning of Cu, Ni, Co and a PGM concentrate.

3.1.1 Concentrating and Smelting

After beneficiation by means of mineral processing, the produced concentrate is roasted and smelted in order to produce a matte, which is the input material for the following leaching process.

The roasting partly oxidises the concentrate (mainly pentlandite) following the reaction (Equation 3-1)



This reaction is exothermic and can thus be used to heat the incoming concentrate and air. An optimum temperature is between 600 and 760°C and is adjusted by the addition of water to the feed as a cooling reagent. The main objective of the roasting unit is to remove SO₂ from the calcine. It is important that the calcine is not oxidised completely to avoid a higher melting point of the matte for the following smelting process. Typically, 40-70 % of

the sulphur is removed during roasting. The extent of oxidation is controlled by the ratio of input material to input air.

The hot calcine (~300°C) is charged into a furnace. At about 1300°C an iron-silica slag with <0.5 % Ni and a matte with the composition

25–32 % Cu

46–51 % Ni

0.2–0.5 % Co

0.2–1.5 % Fe

19–23 % S

are formed. In order to encourage a clean separation of slag and matte, it is necessary to ensure a reducing environment for minimising the oxidation of Ni. To support this, carbon is added, which reacts with oxygen (Equation 3-2):



During smelting, nickel oxide is sulphidised, which leads to a collection of nickel in the matte instead of the slag (Equation 3-3).



The roasting-smelting process allows a Ni recovery of 98 % to the matte, whilst the major part of iron is collected in the slag.

Before the first leaching step, the matte is milled to 50 % smaller 45 µm particle size (Lamya , 2007).

Typical accompanying elements in a Ni concentrate are Co (dissolved in pentlandite) and copper (mainly in chalcopyrite). The recovery of Cu to the matte is comparable to Ni. Due to the easier oxidisation of Co and therefore a higher loss to the slag, the recovery is

considerably lower at 50–80 % (Grimsey, 1993, Matousek, 1993). Ag, Au and PGMs are not oxidised and recovered nearly totally to the matte.

3.1.2 Base Metals Refinery

After smelting, the milled matte from the pre-treatment is leached in a first leaching step at about 130°C and 9.5 bar in order to leach Ni. The acid originates from the copper electrowinning, so it carries some Cu. Two main reactions occur: The first reaction (Equation 3-4) takes place in the oxidising zone of the autoclave.



Additionally, nickel sulphide reacts with the solution following the formula (Equation 3-5)



The thickener separates the slurry into an overflow, which is then treated in the nickel purification unit and an underflow fraction which is leached again in a second leach step. After the second leaching, copper cathodes are produced from the solution. The leach residue is then, after additional leaching steps, the input concentrate for the PGM refinery. During the first leaching step, about 85 % of the nickel content can be recovered. The solution contains about 100 g/L Ni, 5 g/L Cu and 2 g/L Fe. Cu is removed by cementation with Ni powder. Both Fe and Pb are removed by precipitation of jarosite, similar to the iron removal in zinc production (only iron is removed in the zinc process, as lead is not leached). The jarosite endmembers formed are ammoniojarosite $\text{NH}_4\text{Fe}_3(\text{SO}_4)_2(\text{OH})_6$ and plumbojarosite $\text{Pb}_{0.5}\text{Fe}_3(\text{SO}_4)_2(\text{OH})_6$.

After filtering, the filter cake is dumped (this residue is the material studied in this work) and the filtrate is further treated for the winning of Ni and Co. Both metals are reduced with hydrogen in separate process steps (first Ni) and recovered as powders which are then briquetted and sold.

4. Use of Jarosite

As jarosite is a commonly produced by-product; a number of scientists have worked on possible utilisation concepts, mainly in terms of using it as construction material.

Due to the high concentration of heavy and toxic elements (Pb, Zn, S, Cd, Cr, Cu), jarosite has to be treated as hazardous waste (Rathore, et al., 2014). Besides the winning of valuable metals, difficulties in dumping are also a driving force in developing a useful treatment of the jarosite material. The production of jarofix is one possibility to make the jarosite more stable and easier to dump. Especially when mixed with other materials such as soil, it is suitable to be used as construction material, for example for the construction of embankments and subgrade layers for road pavements (Krishnan, 2016).

The concentration of valuable metals in jarofix is considerably lower compared to that in jarosite. For that reason, jarofix production is rather counterproductive when a further treatment in terms of metal recovery is considered.

According to Katsioti et al. (2005), jarosite can also be used as a substitute for gypsum in Portland cement. Different tests and analyses have proved that a substitution of jarosite for gypsum up to 20 % does not affect the properties of the cement mixture, whilst higher amounts cause a shortening of the setting time and a decrease in water-soluble Cr^{6+} and compressive strength values. Jarosite/alunite material from nickel production was treated for this research.

Pappu et al. (2006) proved a potential use of jarosite as construction material such as bricks, blocks, cements and others. A mixture of jarosite, sand and coal combustion residues gives the material the necessary properties. The production of ceramic materials also offers a possible use for jarosite.

A mixture of jarosite, dumped ferrous slag, aluminium surface cleaning waste and eventually some CaO or Portland cement was tested as a construction material with good characteristics concerning strength and water resistance.

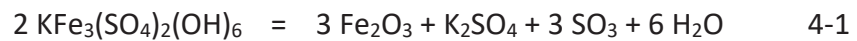
The mixing with other inorganic industrial wastes, such as coal combustion residues, pond coal combustion residues and marble processing residues can also detoxify the jarosite.

Some factories in China produce metals from jarosite residues using rotary kilns and a mass of coal. The method allows a recovery of 75 % Zn, 68 % Pb and 80 % Ge. Weaknesses are high investment costs, high operational costs and air pollution. The top submerged lancing process (TSL) as used at Korea Zinc allows even better recovery of Zn and Pb and

additionally 86 % of Ag and 61 % of Cu (Ju, et al., 2011). However, economic treatment of jarosite material requires an existing recycling complex where it can be added.

The potential for the hydrometallurgical treatment of jarosite was illustrated by Ju et al. (2011). They reached a recovery of about 95 % of Zn, Pb, Ag, Cd and Cu through leaching with aqueous NH_4Cl solution. Additionally, it was also possible to remove 94 % of As and 73 % of Si with another leaching in NaOH at 160°C . The remaining material consisted of 55 % Fe, which could be used for iron production.

Han et al. (2014) published their work on recovering anglesite (lead sulphate) and silver from jarosite through roasting and sulphidisation-flotation. $600\text{-}700^\circ\text{C}$ was evaluated as the optimum roasting temperature for further flotation and allows a recovery of over 65 % of lead and over 80 % of silver. One very important benefit of the roasting procedure is that it breaks agglomerations of different components. Very often, valuable particles are encapsulated by jarosite, prohibiting an enrichment by flotation. The roasting also causes a decomposition of different components such as jarosite and zinc ferrite, as shown in Equations 4-1 and 4-2:



Most of the zinc was transformed into the wash water after roasting, reducing the amount of zinc in the roasted material from 6.37 % to 1.28 %. The wash water after the washing consisted of 11.36 g/L zinc, 0.08 g/L lead and no silver.

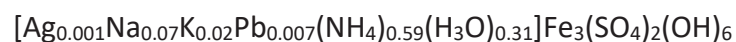
Kangas et al. (2017) developed the so-called Jarogain process, which is a hydrometallurgical process for recovering valuable elements from jarosite-type residues. The method allows a close to zero waste solution. Due to the complexity of the jarosite, the hydrometallurgical route is very complex as well and requires high investment, also causing high operational costs (Kangas, et al., 2017).

The recovery of nickel from jarosite from platinum production was successfully tested in laboratory scale. Malenga et al. (2015) evaluated conditions which allowed a recovery of more than 80 % of nickel out of the jarosite residue using different acids (Nheta & Makhatha, 2013, Ntumba-Malenga, et al., 2014).

5. Characterisation

Numerous publications deal with various by-products and wastes from mining and metallurgical sites. Slag, for example, is often in the focus of interest. Typical analytical techniques like X-ray diffraction analysis, scanning electron microscopy, electron microprobe analysis and Raman spectroscopy have proved to be useful tools for mineralogical characterisation (Antrekowitsch & Steinlechner, 2010). X-ray fluorescence analysis, inductively coupled plasma - mass spectroscopy (ICP-MS) and atomic absorption spectroscopy (AAS) are used for chemical bulk analysis. Compared to slags, the use of these methods for jarosite is limited due to the small grain size and the variable and complex chemical composition of the components.

So far, published articles have dealt with other questions concerning these by-products, not especially with characterisation. Therefore, characterisation has hardly been performed, especially not in a mineralogical way. Salinas et al. (2001) estimated the following as the formula of industrial jarosite mineral produced by a zinc plant in Mexico:



5.1 Characterisation of Fine- Grained Material

For mineralogical and chemical characterisation of other materials than especially jarosite-type residues, there is some literature available. The methods are generally the same as those mentioned in the previous chapter. For chemical analysis, X-ray fluorescence analysis is the commonly used method. However, other methods like ICP-MS have often been used instead or additionally.

X-ray diffraction analysis is mentioned in nearly every paper dealing with any kind of mineralogical characterisation. It is a reliable method if the material meets some demands. Amorphous phases are not detectable and poorly crystallised phases cause problems. This may not be a problem in primary ores or concentrates, but it is in secondary materials. However, qualitative analysis of well-crystallised components in a quantity of more than some per cent is not a challenge. When the amount of a specific component is known (needed as a reference), the Rietveld analysis allows a quantitative analysis.

For the mineralogical characterisation, the light microscope is the typical tool for investigations. It is not well suited, however, for very fine-grained material, as it is limited in its magnification to about 1000x. Moreover, for the identification of particles it is necessary not only to see the particle, but also to evaluate its optical characteristics like colour, shape and cleavage. Sample preparation is generally very difficult, but in the case of light microscopy it is even more difficult. A very common technique for the mineralogical determination of a material (rocks) is working with a thin section. These sections are usually polished to 30 μm thickness, thus making this technique unusable for the jarosite. Microscopy using reflected light is limited to non-transparent minerals, which is why the number of phases, identifiable by reflected light microscopy is very low compared to the overall number of phases in the material.

Scanning electron microscopes equipped with energy dispersive detectors are very common tools and available at many research institutes, making them a main instrument used in characterising different materials. Especially back scattered electron detectors are used to identify different minerals, as the brightness of particles increases with the atomic number, facilitating the differentiation of phases. This helps significantly to find typical ore minerals like sphalerite and galena in a matrix of rock-forming minerals like quartz and feldspar. The great benefit is the potential for displaying particles of sizes down to some micrometres. Using EDX spectra also allows (semi-) quantitative, chemical analysis of single grains, enabling the identification of different components through their chemical composition. As the detection limit of energy dispersive spectroscopy is around 0.5 %, it is not possible to detect trace elements. In contrast to tungsten filament microscopes, field emission microscopes allow images of particles within the submicron range.

Scanning electron microscopes allow a relatively fast characterisation of single grains. This is often enough information for specific questions. Quantification of the components is much more complicated to realise. Besides the Rietveld method for X-ray diffraction analysis, this can also be done by specific software for light microscopes, scanning electron microscopes and electron microprobes.

Johnson et al. (2015) compared two automated electron beam-based mineral mapping techniques: quantitative evaluation of minerals by scanning electron microscopy QEMSCAN[®] and field emission gun electron microprobe analyser FEG-EMPA in detail. As a scanning electron microscope is traditionally used like an optical microscope, it is mainly

designed for the examination of morphological properties, whilst an electron microprobe is primarily designed for accurate chemical measurements. Therefore, the EPMA is superior in terms of detection limits and quantification. Additionally, the field emission gun allows a spatial resolution down to 50-100 nm, significantly lower than $\sim 2 \mu\text{m}$, achievable with a common SEM. Both methods are suitable methods for different questions (Johnson, et al., 2015, Jamieson, et al., 2015).

6. Samples

The materials related to the zinc industry investigated in this work are mainly jarosite residues from five different locations, three of which are zinc smelters that are still in production. Two samples are from historical dumps. One historical site in Africa does not only contain jarosite residue but also other residues from hydrometallurgical zinc winning.

Three locations were analysed in detail:

- jarosite and leaching residue from an active, European zinc smelter
- jarosite and leaching residue from historical zinc production in Africa
- jarosite from platinum production from a plant in Africa

The jarosite from the European plant was mainly used for characterisation, grain size measurements (sieving) and trials for magnetic separation. This jarosite was chosen due to the good cooperation with this company and therefore availability of sample material. The same plant provided a leaching residue which was also investigated.

The zinc production residues from Africa were available and investigated because of a serious interest in treating this material in the near future. Flotation trials were mainly performed on what is called the leaching residue from this plant.

Jarosite from platinum production is very different from the zinc jarosite, as the main metal of economic interest is nickel. Furthermore, in this case, iron is also seen as a valuable and not as a slag component. However, this type of jarosite has many similarities to the jarosite from zinc production as it is produced for the same reason, namely iron precipitation. Therefore, the main mineralogical phase is the same (jarosite) and the overall appearance according to grain size, for example, is similar.

A series of pyrometallurgical 50 kg scale trials were performed with this material.

Macroscopically, the jarosites from zinc production from different locations are very similar to each other. The colour is generally ochre and ranges from yellowish to brown (Figure 4 A, B, C). The grain size is fine-silt to clay. The leaching residue is grey and relatively dry, as it comes directly from a filter press (Figure 4 D). It has a light grey colour and on the surface of agglomerates, the pattern of the filter is sometimes still visible.

Jarosite from platinum production is also in the fine-silt to clay grain size range, but is brownish-red in colour (Figure 5).

The jarosite residue is usually wet. When delivered in rigid boxes, it commonly comes to a separation of fluid and mud.

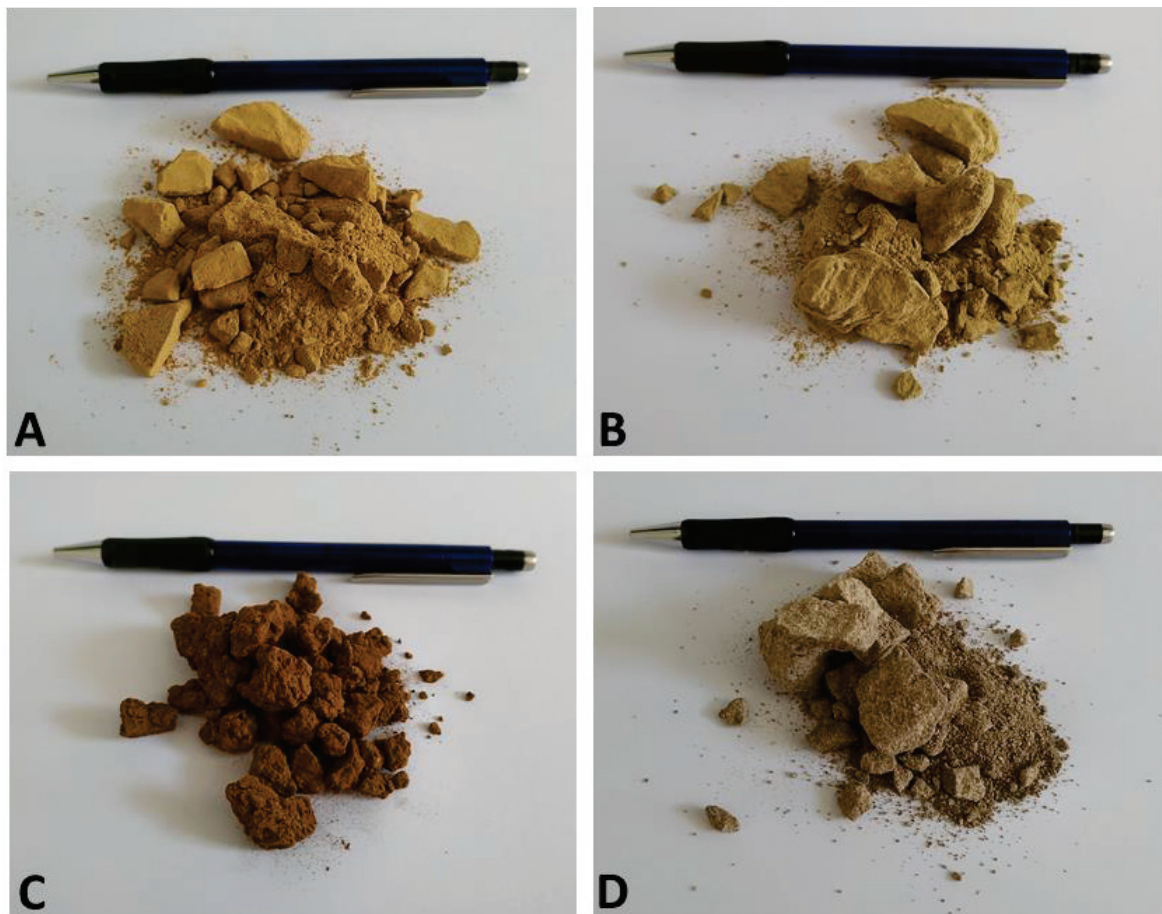


Figure 4: Photographs of four different dried residues from zinc production. A, B and C show jarosite materials from different plants and D a pure leaching residue.



Figure 5: Dried jarosite residue from platinum production.

7. Methods

Different methods are available for the characterisation of chemical, mineralogical and morphological properties. Metallurgical residues are often inhomogeneous and contain unnatural and amorphous phases. As a result, the use of specific analytical methods can be challenging.

Currently, there is no procedure for the evaluation of complex residues. In order to evaluate proper methods, many different types of analysis were tested.

7.1 Sample Preparation

Due to the special condition of the material (small grain size and wet) compared to natural rock samples, the preparation of sections is challenging. A major difficulty for sample preparation is the presence of agglomerates of small particles that mainly form during drying. The resin used in sample preparation only fixes the outer core of each agglomerate and cannot reach the inner part. During grinding and polishing, the weak inner part will most likely break out. Beside the fact that the specific particles are not well polishable, the chipped components also destroy other, well-polished particles.

Low viscosity resins are more suitable in order to infiltrate these agglomerates. Furthermore, resins with long curing times allow air inclusions to be removed from the section. Due to the porosity of the agglomerates, air is embedded into the material, causing porous sections which make grinding and especially polishing problematic. Different trials

of treating the resin-sample mixture with vacuum and/or overpressure did not show any notable benefits.

Pre-treatment in order to break the agglomerates or avoid the agglomeration appears meaningful. As the jarosite is wet when it arrives from the plant, the drying procedure could bear a potential for treatment, concerning temperature and time, as the agglomerates also form during drying. There are some common additives to loosen agglomerates, e.g. sodium citrate. It was tested but it did not make any difference.

When destroying agglomerates with a mill or a mortar, it must be ensured that each single grain stays as unchanged as possible.

7.2 Grain Size Distribution

The grain size of the samples studied was generally very small; a large part of the material was found in grain sizes below 10 μm . Classic sieving analysis of such small grain sizes is difficult, but with specific sieves, a grain size distribution with a particle size down to 10 μm can be determined. Sieves of such small mesh size are not producible as classic wire sieves, but need to be etched. Additionally, ultrasonic handling is needed in order to get the material through the sieves. The wet sieving was not performed on a sieve stack, but with each sieve separately to increase precision.

7.3 Magnetic Separation

Separation of different phases using magnetic properties is widely used in mineral processing. It is not only possible to separate magnetic phases from non-magnetic ones, but also to reach a separation within the (para-)magnetic phases. However, it faces similar problems to other techniques. First of all, agglomerates cannot be separated properly. The small grain size is not a big problem, as the whole separation is performed with water as the transport medium.

The HGMS device used for the separation was a matrix separator of the type Metso laboratory HGMS; the settings used are listed in Table 4. The matrix type was XM0. "XM" indicates the mesh size (Figure 6) and "0" the distance between each grid. In this case, no spacers were used. The washers used had a diameter of 6 and 6.8 mm.

Table 4: Settings used for magnetic separation by HGMS.

Tap	Voltage, V	Current, A	Transformer setting, %	Magnetic induction, T
1	3.00	200	100	0.150
2	9.00	510	100	0.342
3	14.00	810	100	0.580
4	19.00	1040	100	0.750
5	24.00	1280	100	1.020

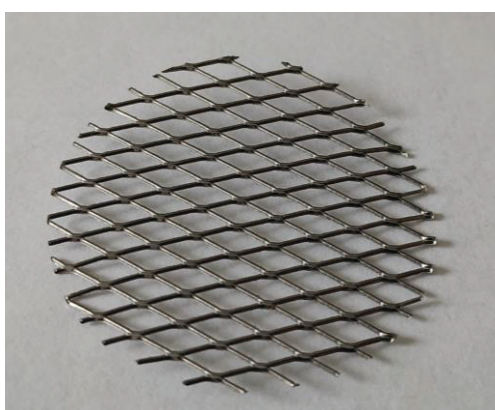


Figure 6: Matrix grid of the type XM. The diameter of the disc is 3.5 cm.

7.4 X-ray Diffraction Analysis

X-ray diffraction analysis (XRD) is a state of the art method for the determination of the main mineral phases in a sample. Crystalline phases with a quantity of more than several per cent can be detected. A semi-quantitative analysis is also possible if the material allows a precise measurement. One big advantage is that it works practically independently of grain size. As the jarosite residue very often causes problems due to the small grain size, XRD is a promising method. Different mineral phases are determined by means of their crystallographic properties (d-values). Therefore, reliable results require well crystallised material. It is also possible to identify different polymorphs, as well as different minerals from one mineral group, for example the various jarosite types. Measurements were done on a powder pellet. The precision of a measurement can be improved, for example, by a longer measuring time or by rotating the sample holder while measuring. Rotation reduces the error caused by cleavage effects of the crystals.

A Siemens D-5000 with a Cu anode, operated at 40kV and 40 mA and hosted by the Institute for Earth Sciences at University of Graz, as well as a Panalytical X'Pert³ (CuK α -radiation; 35 kV, 35 mA) with sideward-filled powder mounts from the Chair of Petroleum Geology at Montanuniversität Leoben were used. Interpretation of the results was made according to Schultz (1964).

7.5 X-ray Fluorescence Analysis

X-ray fluorescence analysis allows relatively fast, quantitative element analysis of main components and trace elements. The sample can be prepared as a fused disc or as pressed powder pellets. As volatile elements (e.g. S and Na) will get lost during the procedure of loss on ignition (LOI at 1050°C) and when producing a fused disc (1050°C), measurements were only performed on pressed powder pellets. However, the grain size- and matrixeffects of powder samples must be taken into account. Therefore, it is necessary to produce an analytically fine powder.

The device used is a PANalytical Axios mAX advanced. Measurements were performed on powder pellets consisting of 4 g of sample material and 1 g of Höchst Wax C, pressed with 10 t to pellets of 35 mm in diameter and analysed using the software Omnian by Panalytical.

7.6 Inductively Coupled Plasma-Mass Spectroscopy

Inductively coupled plasma mass spectroscopy is a method for the chemical analysis of liquid and solid phases and allows a detection limit below ng/g, depending on the element. The device used for chemical bulk analysis is an Agilent[®] 8800 triple quadrupole ICP-MS located at the Chair of General and Analytical Chemistry, Montanuniversität Leoben. Merck 6 ICP-MS multi-element standard and Merck single-element standards for Zn, In and Pb were used for calibration. As internal standards, 1 $\mu\text{g/l}$ of scandium and rhenium were added to the sample. The acids for sample leaching were HNO₃, HCl and a mixture of 3HNO₃ + 1HCl; the dilution factor was 1:25 000. The ICP-MS is tuned on maximum intensities, reaching a Th/ThO factor of <0.3.

7.7 Electron Beam Methods

Scanning electron microscopy and electron microprobe analysis are common methods for investigating different samples in nearly every field of science. Depending on equipment, these methods allow chemical analysis in the form of single point measurements and element mappings as well as imaging with a high resolution down to very small grain sizes. Two different methods of imaging are common. Using a backscattered electron detector (BSE) allows light and heavy elements, or particles consisting of light or heavy elements, to be distinguished by their brightness in the image. A secondary electron detector (SE) gives a more three-dimensional image but does not distinguish the composition of different grains (Goldstein, et al., 2017). Furthermore, there are different limits in magnification caused by the detector used and electron beam source. The most common version is an energy dispersive X-ray detector and a tungsten cathode. This setup allows imaging of particles with grain sizes down to a few microns. A Zeiss EVO MA-10 equipped with a Bruker Quantax EDX Detector 60 mm², installed at the Montanuniversität Leoben, Chair of Geology and Economic Geology was used, employing 15-20 keV acceleration voltage, a beam current of 80 µA and a working distance of 8-11 mm in most cases.

Chemical analysis is also possible with common electron microscopes, but the applicability is limited and very dependent on the surface of the sample. A flat and even surface is important for a reliable analysis. The diameter of the electron beam limits the size of the point measurement and the resolution of the element mapping to several µm. Whilst a scanning electron microscope has its advantages in high resolution imaging, electron microprobe analysis is superior in chemical analysis, in qualitative as well as in quantitative measurements. The detection limit of an energy dispersive X-ray detector of a scanning electron microscope is usually about 0.5 %, depending on the measured material, the surface and the general settings. An electron microprobe equipped with wavelength dispersive X-ray detectors allows reliable measurements with a detection limit of some hundreds of ppm. Furthermore, the software used for quantitative analysis allows automated evaluation of the measurements, facilitating the handling of a large number of measurements. The electron microprobe utilised is a Jeol JXA-8200 equipped with 5 WDX spectrometers with different analyser crystals at Montanuniversität Leoben, Chair of

Resource Mineralogy. Conditions for WDX measurement were 15 kV acceleration voltage and a beam current of 10 nA. More details are shown in Table 5.

Table 5: Calibration parameters and standards used for measurements with electron microprobe analysis.

Element	Line	Crystal	Standard
Al	Ka	TAP	corundumLB1
Pb	Ma	PETJ	galena15kv
Zn	Ka	LIF	SPIsphal20new
Si	Ka	PETH	wollast15kv
Ag	La	PETH	AgBiSe2_cap499
Ba	La	PETJ	Baritespi15Kv
Cu	Ka	LIF	CupriteSPI15KV
In	La	PETH	In-metal
S	Ka	PETJ	MolySPI15KvLB
Fe	Ka	PETJ	KaerSPI15KV

Both scanning electron microscopy and microprobe analysis are important tools in characterising fine-grained material. Even though tungsten cathode SEMs do not allow high quality imaging of the smallest grain fractions, they enable basic investigations on morphology and intergrowth relationships. The possibility of qualitative and semi-quantitative chemical measurements makes the identification of mineralogical phases according to their chemical composition possible. Identification based on morphology/crystal forms is not possible. Chemical measurements must be treated with care, as the polishing is often bad and the grain size is simply too small, namely smaller than the size of the electron beam. The surface condition is even more critical if a strewn slide is prepared instead of a polished section.

Transmission electron microscopy allows investigations up to atomic scale. Contrary to SEM and EMP, the electron beam of a transmission electron microscope is not reflected from the specimen, but penetrates it (Pennycock & Nellist, 2011) (Von Heimdahl, 1970) (Williams & Carter, 2009). For this, the sample must be accordingly thin, between 10-100 nm, to allow penetration of part of the electrons. In some cases, depending mainly on the material and the acceleration voltage used, it may be necessary to use much thicker samples, up to some

μm . Sample preparation differs totally from the other methods. The jarosite material, even though it is already very small in its grain size, must be milled, to produce particles within the mentioned grain size. After mixing the powder with ethanol, the suspension is spread on a carbon grid.

The device employed is a FEI Talos™ F200X G2 scanning/transmission electron microscope (S/TEM) equipped with the detectors STEM BF/DF2/segmented, DF4/HAADF incl. ADF (16 MPx) and Super-X EDX. It also uses a CETA 16M camera with speed update and a FEI Velox™ S/TEM control software. It is located at Montanuniversität Leoben, Chair of Nonferrous Metallurgy.

7.7.1 Automated Analysis

An initial idea at the project start was to calibrate and use software for automated analysis called SMART-PI. Combined with a Zeiss EVO MA-10 SEM, it allows automated characterisation of samples in terms of quantification of phases and/or grain sizes. The process is briefly explained in the following. First of all, specific phases have to be defined by chemical composition. For the differentiation of separate particles, optical parameters also have to be calibrated and defined. The system recognises different phases due to grey levels in BSE mode, caused mainly by their density. After measuring the particle size and composition (semi-) quantitatively, the particle is designated as programmed by the operator. Another very important factor is the orientation of the surface compared to the electron beam and detector. Therefore, a perfectly polished surface without topography and any scratches is critical. This is actually not feasible with jarosite material. Additionally, the problem of the very small grain size would make it necessary to use a different microscope, as the magnification of a tungsten cathode SEM is not enough and the electron beam is too large to measure the small particles, especially automatically.

7.8 Laser Ablation-Inductively Coupled Plasma-Mass Spectroscopy

The ICP-MS can be coupled with a laser in order to expand the applicability of the technique. The photon-matter interaction of the laser ablates particles of low nm size from the sample, which are then measured with ICP-MS. The size of these craters can be adjusted to different diameters and depths ($>5 \mu\text{m}$). Thus, LA-ICP-MS measurement is

always a bulk analysis, but of a very small volume. Measurement of single grains in order to detect and quantify trace elements is a typical scope of application. The detection limit is about 0.01 µg/g, depending on the size of the laser beam and the element measured.

For every measurement, the concentration of a reference element is needed to quantify the results. Furthermore, very heterogeneous material requires a combination of different standards, as every standard is only suitable for specific elements within a specific concentration range. Matrix-matched reference materials are not available.

The system is a New Wave Research (NWR 213) Nd: YAG 213 nm Nano second laser ablation system updated with a TV2 ablation cell, coupled to an Agilent® 8800 triple quadrupole ICP-MS (QQQ-ICP-MS).

As mentioned before, different standards are needed. In these trials the following two were used:

- For quantification of the elements hosted in sulphides and sulphates, namely Mn, Fe, Cu, Zn, Ga, Ge, Ag, Cd, In, Au and Pb, the matrix matched sintered powder pressed pellet MUL-ZnS 1 reference material was used (Onuk, et al., 2017). For the quality control of these elements, the USGS powder pressed polysulphide reference material MASS-1 was measured as an unknown sample.
- The elements hosted in silicates like Na, Mg, Al, Si, K, and Ca were quantified by using the USGS-BCR-2G silica glass. NIST SRM 612 reference material conducted as internal reference material to monitor these elements (Wilson, et al., 2002).

The laser beam size was 10, 30 and 60 µm to get information about heterogeneity and determine the best fitting spot size for the task. The analysis time for each sample was 120 seconds, 30 seconds for measuring the background and laser warm-up with closed aperture, 60 seconds analysis with laser on and 30 seconds wash out time.

Iron was quantified using WDX-XRF analysis on each pressed powder pellet and later on calculated as the internal standard element to quantify the major and trace element content of each single analysis (Hanke, et al., 2018).

The measurements were performed on pressed powder pellets, with 35 mm in diameter, made of 4 g of sample material and Elvacite as the binder.

The idea for use, in the case of characterising metallurgical by-products, is a different one from what LA-ICP-MS is usually used for. It may occur that chemical analysis of a material indicates a considerable concentration of a specific element, but no host particle can be found. In this case, the following procedure might help:

- Numerous spots spread on the whole sample to produce a lot of small bulk analyses.
- Correlation of different elements can then help to identify host particles.

An example:

A material is rich in lead and the lead phases are known. The material is also rich in silver, but no silver particles can be found. If the LA-ICP-MS indicates a positive correlation between lead and silver, the lead phases will very likely be host particles for silver and are worth further investigation. If measurements with low lead are also low in silver, it indicates as well that silver might not be present in any other phases. This will also be indicated by a negative correlation of silver with other elements.

7.9 RAMAN Spectroscopy

For the identification of single mineral phases, RAMAN spectroscopy is a fast and easy method. It uses a laser beam and measures the scattered light pattern characteristic for each mineral (Graves & Gardiner, 1989; Nasdala, et al., 2004). It requires a polished surface and is limited to grain size due to the size of the laser beam and the use of a light microscope. The device used is a Horiba LabRAM HR Evolution with a SIN-EM FIVIS detector, MPlan N 100x objective, 532nm laser wavelength and a confocal hole of 100 μm .

7.10 Summary of the Evaluated Methods

In the following table (Table 6), the methods of analysis are summarised with a short comment on their usability on the characterisation of morphology, chemistry and mineralogy of a material.

Table 6: Summary of evaluated analytical methods.

	Morphology	Chemistry	Mineralogy
Light microscopy	Suitable for thin- or thick sections and strewn slides with grain sizes down to 10 μm	Not possible.	Defined by various optical properties.
Scanning electron microscope	Characterisation of optical properties to grain size of some μm , or nm when equipped with appropriate tools. High resolution images.	(Semi-)quantitative point measurements (detection limit: >5 mg/g) and qualitative element mapping.	Defined by chemistry.
Electron microprobe	Characterisation of optical properties to grain size of some μm , or nm when equipped with appropriate tools.	Quantitative single point measurements (detection limit: >100 $\mu\text{g/g}$, depending on element) and qualitative element mapping.	Defined by chemistry.
X-ray fluorescence analysis	Not possible.	(Semi-)quantitative analysis of solid samples like powder pellets or fused discs. Applicable for many different elements, especially slag components. Detection limit >10 $\mu\text{g/g}$ for fused discs.	Not possible.

	Morphology	Chemistry	Mineralogy
Inductively coupled plasma – mass spectroscopy	Not possible.	Quantitative analysis of liquids, or leached sample material, gas and solid phases. Detection limit >ng/g for liquids.	Not possible.
Laser ablation - Inductively coupled plasma – mass spectroscopy	Possible with the coupled light microscope that is used to position the points for laser measurements.	Single point measurements with detection limits (>1 µg/g spot size-dependent) and small bulk analysis on solid samples. Best suitable for trace element analysis.	Possible with the coupled light microscope that is used to position the points for laser measurements.
X-ray diffraction analysis	Not possible.	Not possible.	Qualitative and semi-quantitative analysis of crystalline mineral phases (detection limit some %). Rietveld method allows quantification.
RAMAN spectroscopy	Possible with the coupled light microscope.	Not possible.	Qualitative and quantitative mineralogical analysis of grains >1 µm in size.

7.11 Hydro Separation

A special method of separation was performed by Thomas Aiglsperger from the University of Barcelona. A jarosite sample was sieved with a 30 µm mesh size. The smaller 30 µm fraction was treated by hydro separation. This technique uses a flow of water to separate heavy minerals (Figure 7). It does not separate minerals only due to their density, but also due to their grain size and morphology. With this method, a concentrate of heavy grains

with a grain size of about 30 μm was produced. It allowed the production of a well-polished, monolayer sample (Figure 8). Such a sample is much more suitable for measurements with electron beam methods. However, the concentrate is not representative for the starting material, attributed to the following reasons:

- The 30 μm fraction is less than 2 % of the whole material, according to the grain size distribution.
- It is not only a separation due to grain size, but also of density and grain morphology.
- Even if the concentrate were representative for this grain size, it would not mean that it is comparable to other grain size fractions.

However, such a sample can be of help when investigating specific phases that are enriched in this concentrate. For example, the three different lead phases (oxide, sulphate and sulphide) can be investigated much better than in a section containing the whole jarosite material, because of the better polishing of the section.

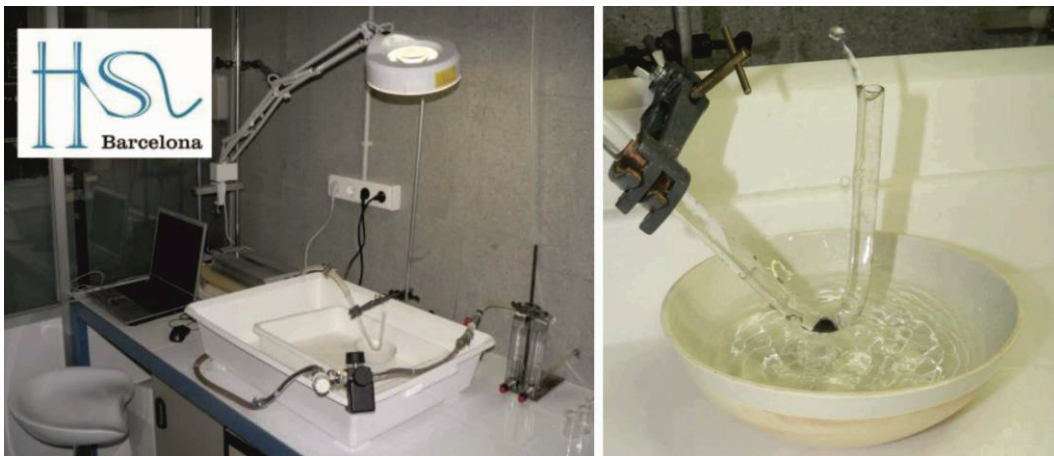


Figure 7: Overview (left) and detail (right) of the hydro separation used for producing a 30 μm concentrate out of jarosite.

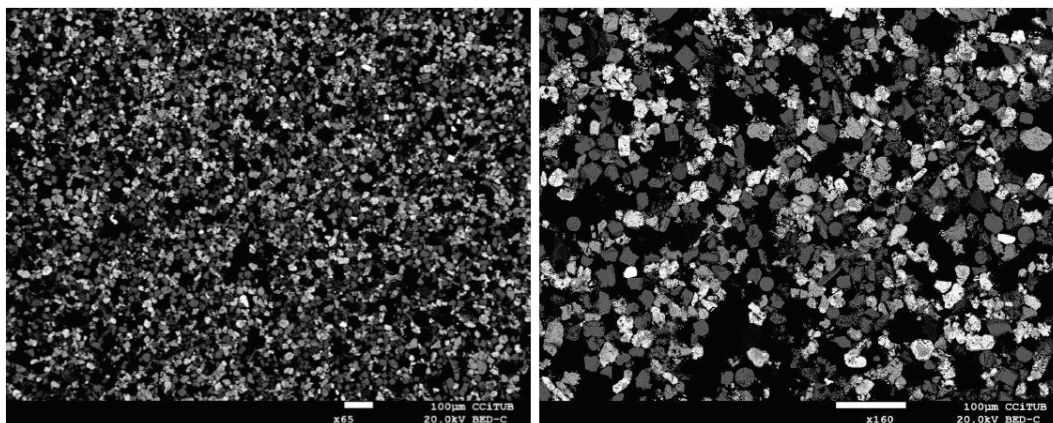


Figure 8: Two BSE images of the monolayer section from hydro separation using a field emission gun- scanning electron microscope. Note the well-separated grain size fraction.

8. Results

Bulk chemistry of the jarosite material can be determined by standard methods of chemical analysis. For methods that require leaching of the sample, special attention must be paid to a proper acid composition to leach all components. X-ray fluorescence analysis is a good method within its known limitations. Determination of mineralogical composition and especially quantification of identified phases is more challenging.

A number of different methods commonly used for the characterisation of various materials were tested in order to evaluate their usability for jarosite residues. Especially the small grain size causes problems; firstly, in the preparation of proper sections, and secondly, in the limits of magnification of common analytical methods. Moreover, the synthetic origin of some phases, especially the jarosite, limits the use of methods that rely on crystallographic properties, as these phases are often not well crystallised.

8.1 Chemical Composition of Various Jarosites from Zinc Production

Even though the process of hydrometallurgical zinc winning is a standard procedure, the residues differ to a certain extent from one plant to another. This is attributed to both the input material from different mines and small but significant variations in the process. Variations in the input material are obvious, as no concentrate is absolutely similar to another. Differences within the hydrometallurgical process mainly concern the treatment of the numerous residues and by-products that occur during every process step. While in the principle process there is one neutral leaching step and the residue is treated by one

hot acid leaching, in fact, more steps are often applied. It is also common that not all of the leaching residue is leached in the next step; part of it is frequently dumped together with other residues.

As mentioned in a previous chapter, the formation of the jarosite mineral is used to remove the iron from the solution. Different types of jarosite can be applied for this.

Natro- and ammoniojarosite are the two commonly used endmembers. This also explains the differences in sodium in the residue, as it must be added to the process if natrojarosite should be formed. This also applies to the ammonium for ammoniojarosite, but neither hydrogen nor nitrogen is measurable by the methods of chemical analysis used in this study.

Another important factor affecting the amount of valuables in the dumped material is the treatment of the final leaching residue. Some plants concentrate and sell their leaching residue as lead-silver concentrate, lowering the amount of specific elements (mainly silver and lead) at the dump. Other plants dump it either together or separately from the iron precipitation product.

Summarising, there are many different reasons for the differences in the chemistry of jarosite material:

- Input material (Zn concentrate)
- Number of leaching steps
- Further treatment of (leaching) residues
- Type of jarosite endmember formed
- Mixed or separate dumping of residues

The following table displays the chemical composition of five different jarosite residues, analysed by A.M.C.O. united samplers and assayers GmbH, an accredited analysis laboratory, using ICP-OES on aqua regia digestion (Table 7).

Table 7: Chemical composition of five different jarosite residues from zinc production.

	Residue 1	Residue 2	Residue 3	Residue 4	Residue 5
Pb %	4.0	4.7	6.5	7.1	4.55
Zn %	2.2	4.0	6.6	3.7	4.65
Cu %	0.4	0.42	0.5	0.4	0.75
Ag ppm	213	219	162	159	80
In ppm	<20	25.7	193	116	210
Fe %	25.3	25.2	28.0	18.8	32.5
Si %	2.8	2.6	2.9	1.2	3.6
Na %	4.7	2.3	0.12	1.0	0.04
Al %	1.1	1.0	0.74	0.32	1.28
Ca %	2.5	0.87	0.54	5.6	1.3
K %	0.42	0.44	0.22	0.1	0.09
Mg %	0.12	0.09	0.04	0.06	0.15
Mn %	0.1	0.22	0.41	0.08	0.68

Additionally, the jarosite residue number 4 in Table 7 was also analysed by different methods at Montanuniversität Leoben in order to evaluate their applicability. Table 8 shows the results from various analyses by different institutions and methods on the same sample material. For comparison, the AMCO result from Table 7 is shown in the first column.

Comparison of results from different chemical analyses show considerable differences in many elements. A main reason valid for every element is the heterogeneity of the sample material. For acid digestion, it is essential that the sample is fully leached and stays in solution. The high concentration iron can be problematic concerning the saturation of the acid and for analysis using ICP-OES. Analyses 4 and 5 are considerably lower in Ag and In. This might be due to the precipitation of AgCl and InCl. Silicates are difficult to leach with the acids used, resulting in unreliable values for elements common in quartz and feldspar as well as for Ag and Cu, as both are often found as inclusions in these silicates. Differences in Ca are probably caused by the formation of gypsum during drying of the jarosite material. Whether the sample for chemical analysis was taken from an area with visible gypsum or not might cause the difference in gypsum and subsequently in all other elements.

Table 8: Results of different analytical methods and institutions. GEG-Chair of Geology and Economic Geology, Chem-Chair of Analytical Chemistry MUL.

Analysis	1	2	3	4	5	6	7
Laboratory	AMCO	GEG	GEG	GEG	GEG	GEG	Chem
Method	ICP-OES	ICP-MS	ICP-MS	ICP-MS	ICP-MS	ICP-MS	XRF, analytical
Preparation	Aqua Regia	5 ml HNO ₃ 2 ml HCL 1 ml H ₂ O ₂ HPA	3HNO ₃ +HCl 400 ml	3HNO ₃ +HCl 100 ml	HCl 100 ml	HNO ₃ 100 ml	powder pellet 1 g wax
Sample		0.2 g	10 g	0.5 g	0.5 g	0.5 g	4 g
Pb %	7.1	7.64	5.14	11.40	11.34	11.74	6.38
Zn %	3.7	6.49	15.46	10.44	9.60	10.00	4.62
Cu %	0.4	0.47	0.19	0.15	0.15	0.15	0.26
Fe %	18.8	26.33	17.55	11.84	12.35	11.17	24.69
Si %	1.2						1.99
Na %	1.0	1.33	0.84	2.09	2.13	2.19	0.72
Al %	0.32	0.41	0.21	0.07	0.07	0.08	0.39
Ca %	5.6	10.87	23.12	18.04	18.19	18.45	3.51
K %	0.1	0.21	0.13	0.06	0.07	0.12	0.14
Mg %	0.06	0.07	0.05	0.02	0.02	0.02	0.04
Mn %	0.08	0.12	0.14	0.03	0.03	0.03	0.13
Ag ppm	159	329	335	96	5	87	239
In ppm	116	123	122	39	41	39	173
As %		0.34	0.38	0.15	0.14	0.05	0.80
Cd %		0.09	0.06	0.16	0.14	0.14	0.07

Heterogeneity of the sample material is an important factor for chemical analysis and limits the comparability of the presented results.

The analyses from AMCO might be the most reliable ones, as it is an accredited laboratory. From the methods performed at MUL, ICP-MS on HPA digestion is the most suitable from the wet chemical methods for also measuring elements bound to silicates. However, due to the beneficial sample preparation and acceptable results, XRF measurement on powder pellets is the overall preferable method.

8.2 Sample Preparation for Mineralogical Characterisation

Strewn slides are relatively fast and easy to prepare. For investigations with a scanning electron microscope, the dried sample is dispersed on a double-sided adhesive carbon tape. For determining morphological properties, this is an appropriate type of preparation.

For precise chemical analysis with electron beam methods, an even surface is necessary. The only way to get a polished surface is embedding the sample material in epoxy resin. This is state of the art and works well for many different materials. However, the preparation of polished sections of jarosite proved to be difficult, starting with the first step of treating the sample, namely the drying. The muddy sample turns into a solid mass, especially when using higher temperatures of around 100°C. During the embedding of the sample, the epoxy resin is not able to infiltrate all of the material. When the sample is then ground and polished, parts that are not fixed by epoxy resin break out, causing holes in the sample and scratches in the already polished parts. To minimise this problem, the sample material must be milled, scaling down the already very small grain size and distorting the material in terms of intergrowth relationships as well as grain size.

Drying at low temperatures, with help of silica gel, for example, seems to reduce the cementation of the material. What is more, the use of a slow hardening, low viscosity epoxy resin proved to be beneficial. Figure 9 shows two sections of jarosite material for which a fast hardening (about 3 minutes) and high viscous resin were used (ebalta SG 2000). Numerous air bubbles are imbedded and the (large) agglomerates are only fixed at their rims, while the cores of many particles broke out.



Figure 9: Example of two jarosite sections using a fast hardening and high viscosity epoxy resin. The sections are 4 cm in diameter.

Table 9 shows a selection of different resins used and grinding and polishing devices which were tested on the jarosite material for their applicability and showed good results.

Table 9: List of resins and grinding and polishing devices used for preparation of polished sections of jarosite material.

	Resin	Grinding wheel	Pre-polish			Final polish	
			cloth	polishing agent		cloth	polishing agent
1	Araldit DBF BD, Huntsman	Plato diamond grinding wheel 74 μm and 10 μm	Alpha, ATM	Silicon carbide 9 μm and Aluminium oxide 3 μm	in water	Gamma, ATM	Dia-Complete poly 1 μm
2	Araldit 2020, Huntsman						
3	Epoxy resin "wasserklar", r&g						
4	Araldit DBF BD, Huntsman				in Ethanol-based lubricant	DP-PAN, Struers	Aluminium-oxide 1 μm in Ethanol-based lubricant
5	Araldit 2020, Huntsman						
6	Epoxy resin "wasserklar", r&g						

The best results were performed with the Epoxy resin "wasserklar," whereby the water free-treatment did not show a significant increase in the quality of the section. Representative SEM images using the secondary electron detector are shown in Figure 10. The numbering of the images is linked to the first column in Table 9. Trials using overpressure and vacuum did not show a significant difference in the final result.

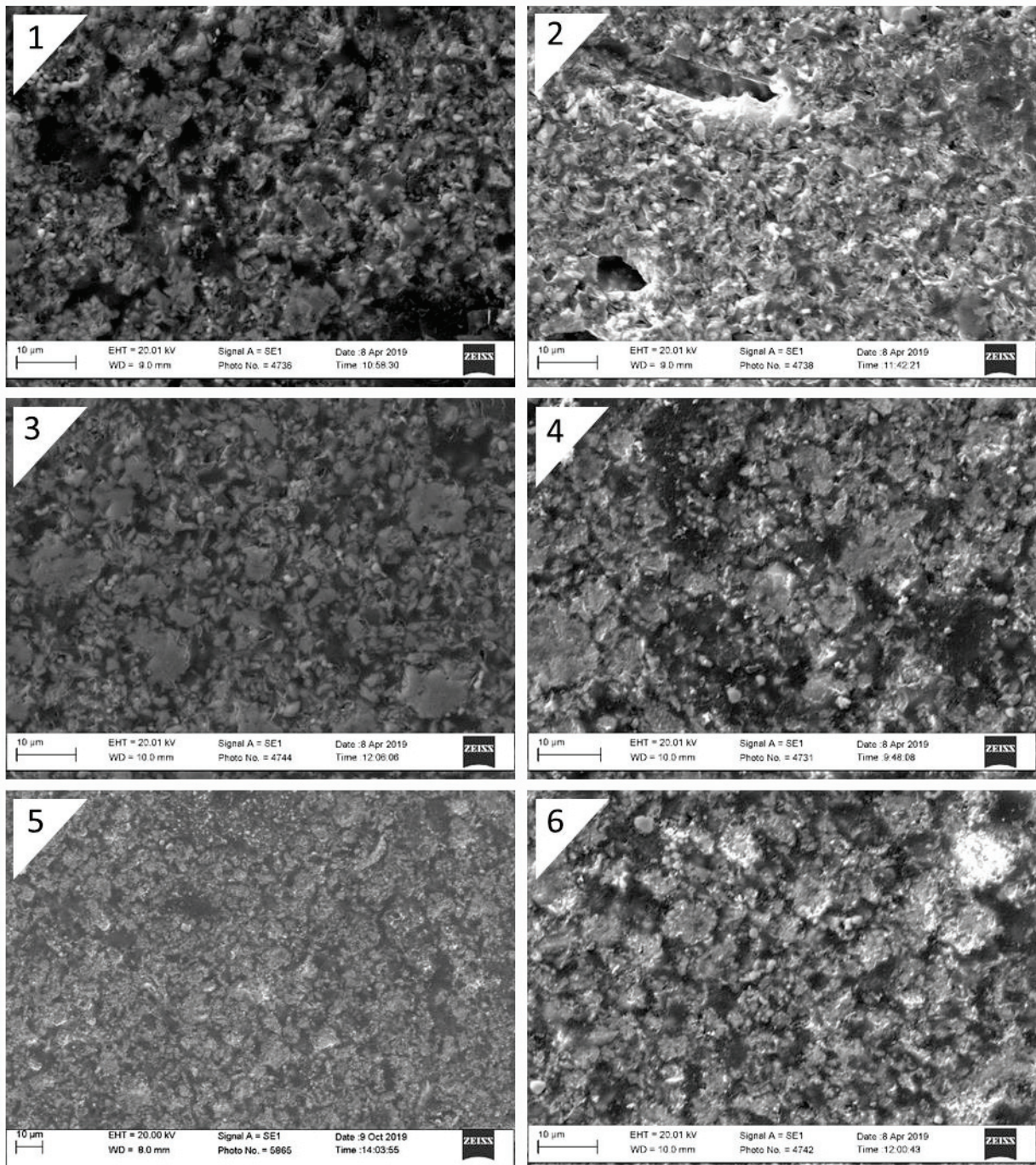


Figure 10: Examples of polished jarosite sections. The numbering corresponds to Table 9.

8.3 Mineralogical Characterisation

X-ray diffraction analysis is a standard method for identifying the main mineralogical phases, even though the jarosite material must be treated with care. Grain size of the material does not influence the analysis. Due to its synthetic origin, the jarosite mineral is fast grown and poorly crystallised. This is reflected in the magnitude and shift of d-values in the XRD spectra and causes major problems in distinguishing the jarosite minerals,

rendering a serious quantification impossible. Sample rotation and longer measuring time effectively decreases the background of a spectrum. The main advantage is the easy sample preparation and its usability independent of grain size.

An XRD spectrum of a typical jarosite from zinc production is shown in Figure 11. Whilst jarosite is clearly identified, the differentiation of the different endmembers is very difficult. In this case, natrojarosite and jarosite are identified. Additionally, plumbojarosite, ammoniojarosite and hydroniumjarosite are most likely also present. Gypsum is detected as well. Quartz and hexahydrate are also illustrated, but are too low in quantity to be seriously identified.

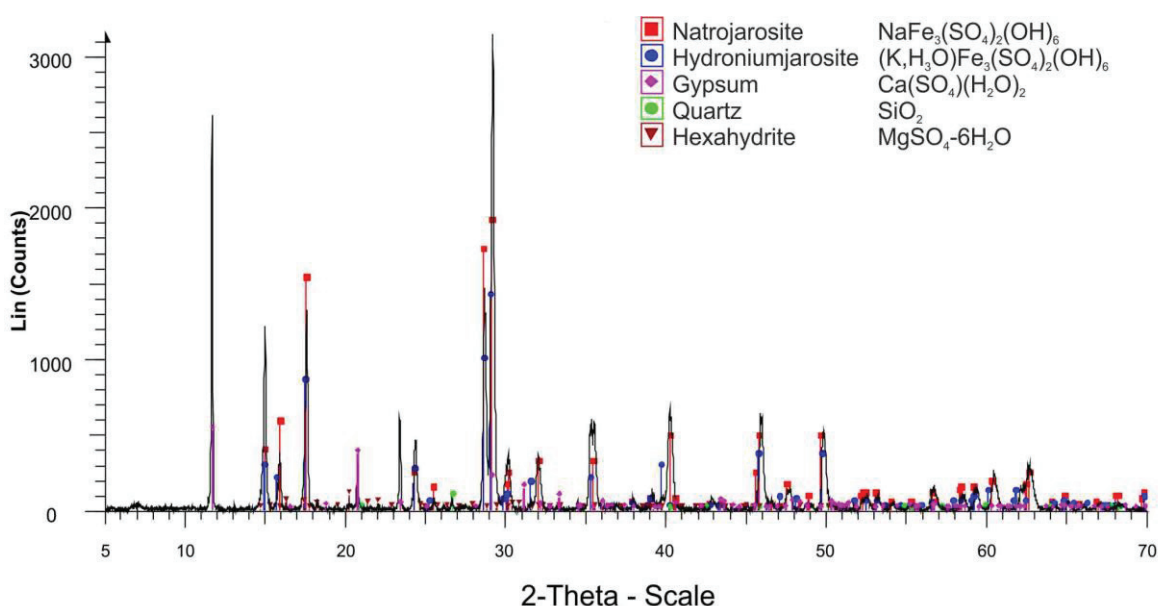


Figure 11: XRD spectrum of a jarosite from zinc production. Different jarosite endmembers and gypsum are clearly detected. Step size: 0.010° , step time: 11 s.

Another XRD spectrum is shown in Figure 12. The analysed material is a sieve fraction smaller than $10 \mu\text{m}$ from the same jarosite residue measured in Figure 11. The only appreciable difference is the absence of gypsum. Instead of quartz and hexahydrate, franklinite is tagged but the concentration is also too low for clear identification.

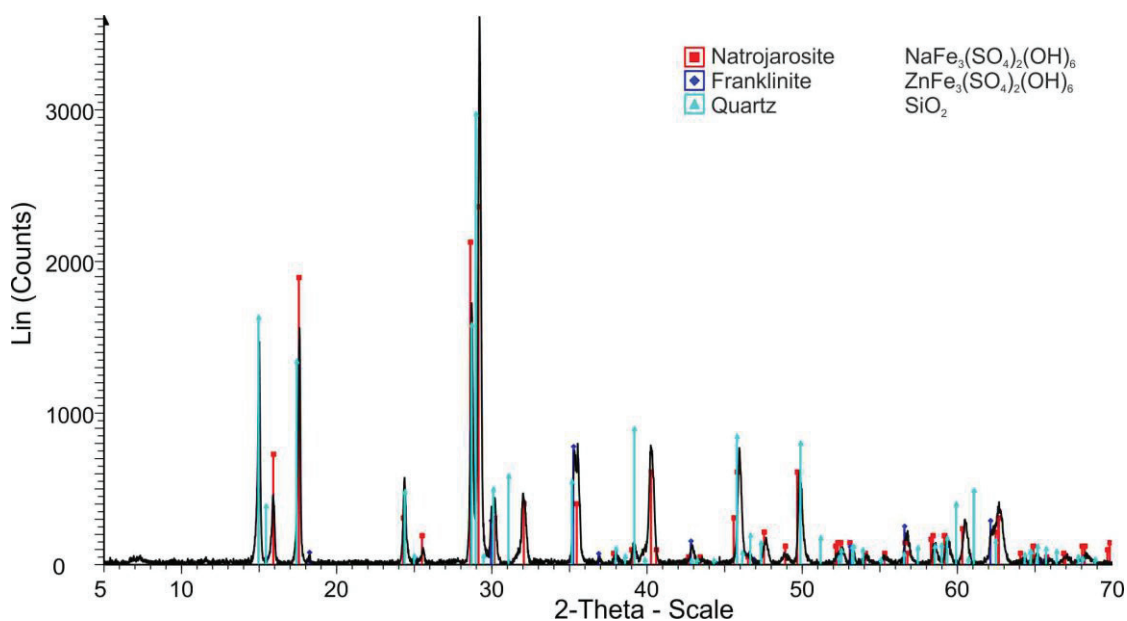


Figure 12: XRD spectrum of a jarosite sieve fraction smaller than 10 μm . The absence of gypsum makes this fraction different from the whole jarosite sample as shown in Figure 11. Step size: 0.020°, step time: 14 s.

8.4 In-Situ High Resolution Chemical Analysis

LA-ICP-MS and EMP were used for small-scale chemical analyses to determine the distribution of elements within the material and identify host phases for valuable elements.

8.4.1 Sample Heterogeneity Measured by LA-ICP-MS

The sample was prepared as a pressed powder pellet (3.1 cm in diameter) with 4 g of sample material and Elvacite as the binder. Along a line, 30 points were defined for chemical analyses using LA-ICP-MS. The diameter of the laser beam was 30 μm for all points and the measurement time for analysis 60 seconds. Iron was used as the reference element and measured using XRF on the same pressed powder pellet that was used for LA-ICP-MS. Figure 13 and Figure 14 display two line plots for main and trace elements. At this scale the material is more homogeneous for trace elements than for main elements. Measurement 25 differs significantly. The elevated concentrations of Na, K, Si, Al point to the presence of a large silicate (feldspar) grain. Silver and gallium are also considerably enriched. The high concentration of silver might be due to a silver inclusion like it is often found in silicates using SEM. Indium and gallium show a similar distribution, except for measurement 25, where gallium increases with silica and silver, whereas indium decreases.

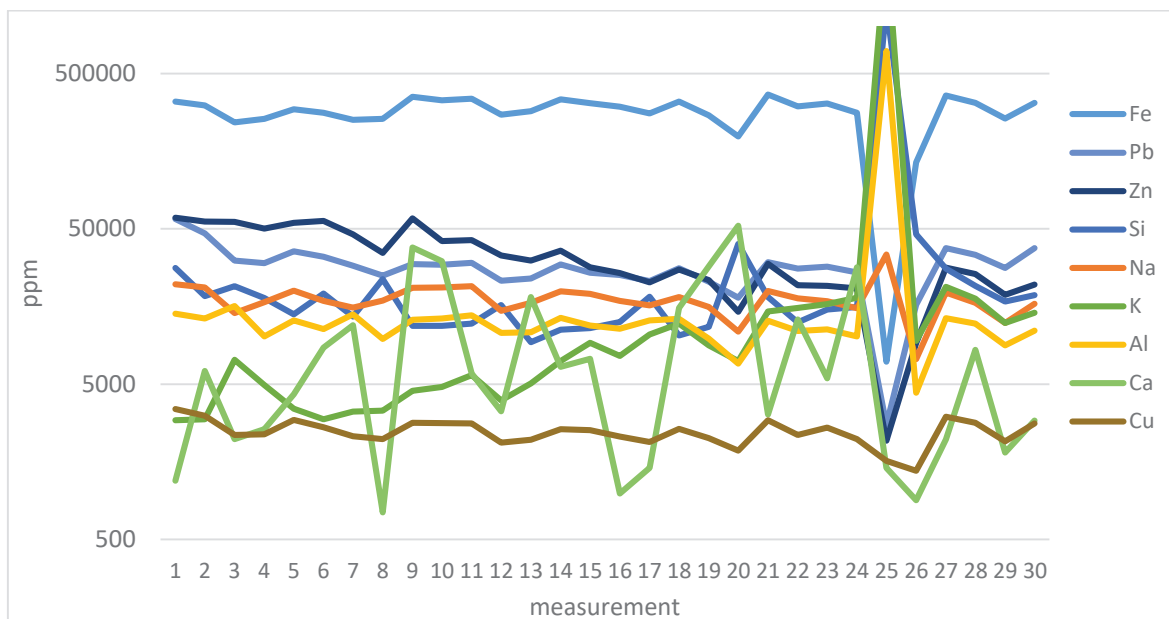


Figure 13: Distribution of main elements measured using LA-ICP-MS on a pressed powder pellet.

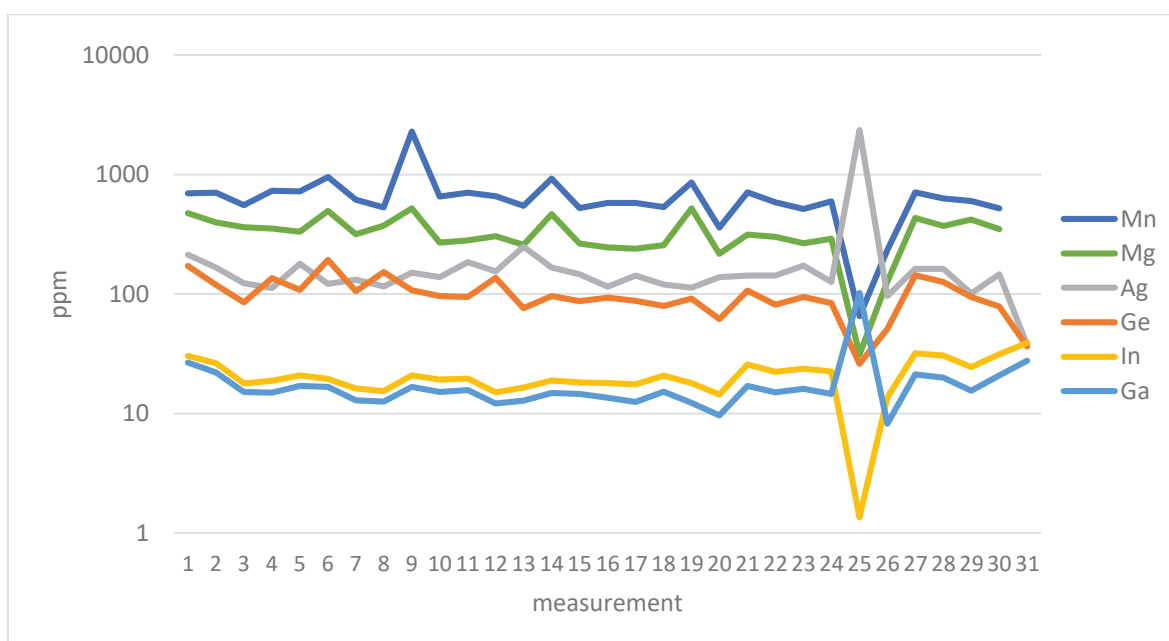


Figure 14; Distribution of trace elements measured using LA-ICP-MS on a pressed powder pellet.

8.4.2 Phase Identification Using Element Correlation

Correlating element distribution “in-situ” with LA-ICP-MS proved to be more complicated than expected. Every single measurement needs a known concentration of a reference element; this cannot be ensured in a powder pellet where every selected point definitely consists of other phases. Therefore, an evaluation of the results is complex. Implementing the same idea with an electron microprobe seems to be more promising. The results are

not that precise compared to (calibrated) LA-ICP-MS and the detection limits are higher, but the results can be used in order to find element correlations. Table 10 shows an example of a correlation matrix of electron microprobe measurements on a representative jarosite section. The basis of this correlation matrix is 414 point measurements. In a representative area of the jarosite section, a pattern of point measurements with a distance of ten microns was chosen for automated chemical analysis.

When comparing the table with investigations with SEM, the following conclusions can be drawn:

- Lead correlates very well with sulphur ($r=0.72$). This corresponds to the appearance of lead as sulphate and sulphide (Figure 15).
- Iron correlates with sulphur ($r=0.39$) due to the jarosite mineral as the main phase (Figure 16).
- Positive correlation of iron and lead ($r=0.45$) indicates that lead is bound to jarosite.
- The main zinc-bearing phase is zinc ferrite, indicated by the correlation of zinc and iron ($r=0.42$)(Figure 16).
- The correlation of zinc and iron indicates zinc ferrite and jarosite as important zinc-bearing phases but in addition, the negative correlation ($r=-0.40$) of zinc and sulphur shows the jarosite mineral to be not especially important as a zinc carrier.
- Silicon has a clear negative correlation with sulphur ($r=-0.42$) and iron ($r=-0.48$)(Figure 17).
- Silver correlates with copper ($r=0.65$)(Figure 18).
- Barium always appears as barite and is often intergrown with lead phases, illustrated by the correlation of barium with lead ($r=0.53$)(Figure 18) and sulphur ($r=0.72$)(Figure 15).

Table 10: Correlation matrix of selected elements. Measurements made by electron microprobe on a jarosite section.

	Al	Pb	Zn	Si	Ag	Ba	Cu	Cl	In	S	Fe
Al	1.00										
Pb	0.03	1.00									
Zn	0.21	-0.17	1.00								
Si	-0.01	-0.28	-0.08	1.00							
Ag	0.39	-0.12	-0.07	0.06	1.00						
Ba	-0.02	0.53	-0.25	-0.16	-0.11	1.00					
Cu	0.35	0.43	0.08	-0.20	0.65	0.18	1.00				
Cl	-0.12	-0.56	-0.18	0.22	0.08	-0.27	-0.27	1.00			
In	0.17	-0.08	-0.06	0.15	0.21	-0.03	0.03	0.10	1.00		
S	0.01	0.72	-0.40	-0.42	-0.07	0.51	0.25	-0.54	-0.05	1.00	
Fe	-0.13	0.45	0.42	-0.48	-0.19	0.25	0.22	-0.64	-0.16	0.39	1.00

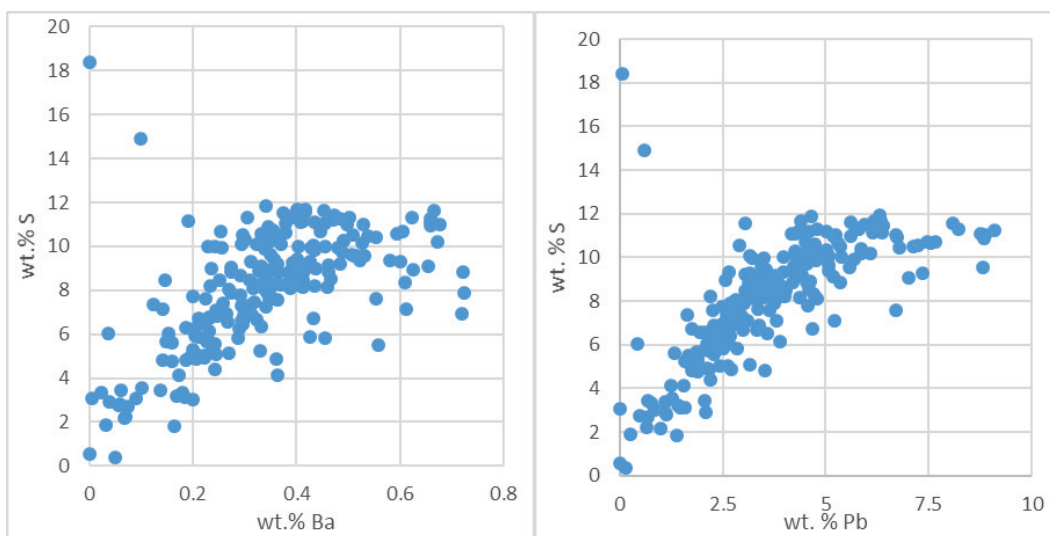


Figure 15: Positive correlation of sulphur with barium (left) and lead (right).

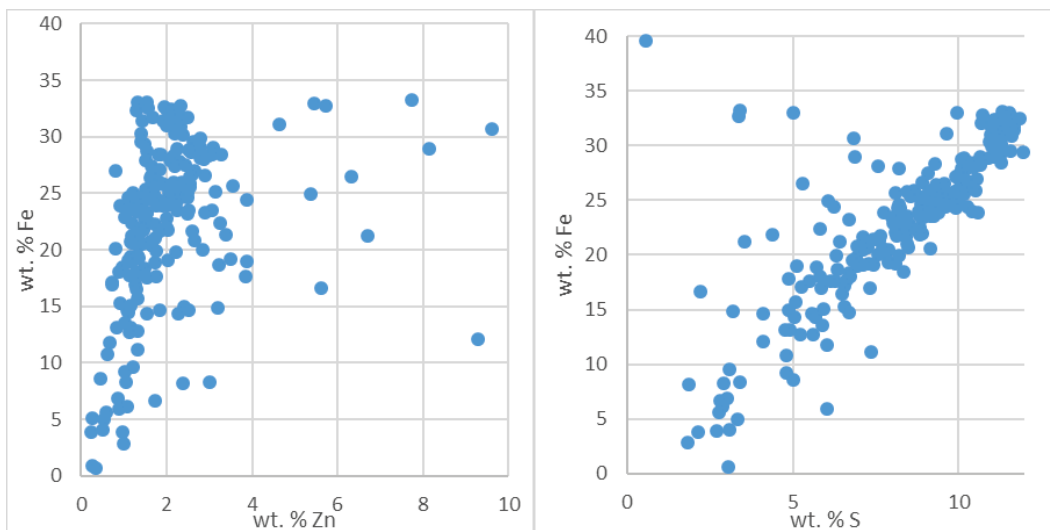


Figure 16: Correlation of Fe-Zn (left) and Fe-S (right).

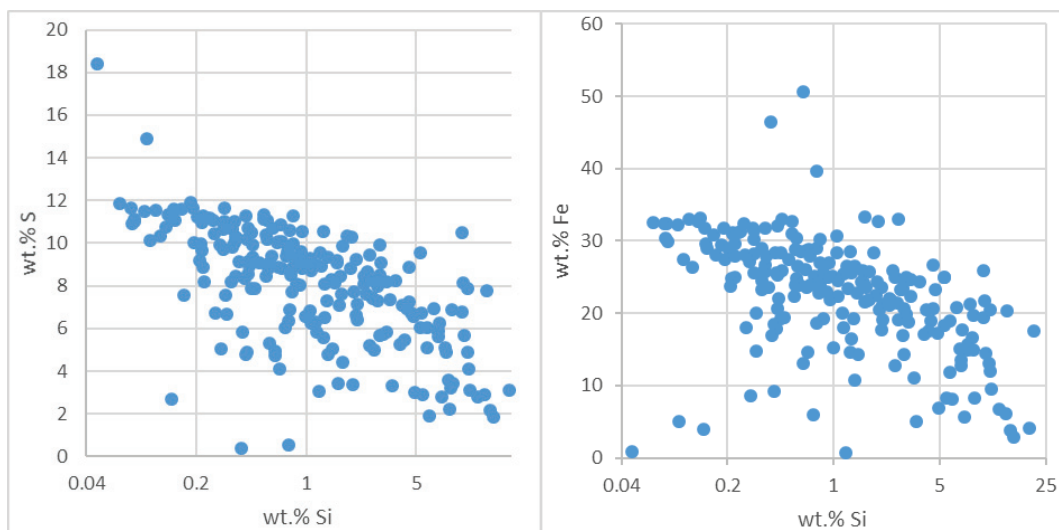


Figure 17: Negative correlation of Si-S (left) and Fe-Si (right).

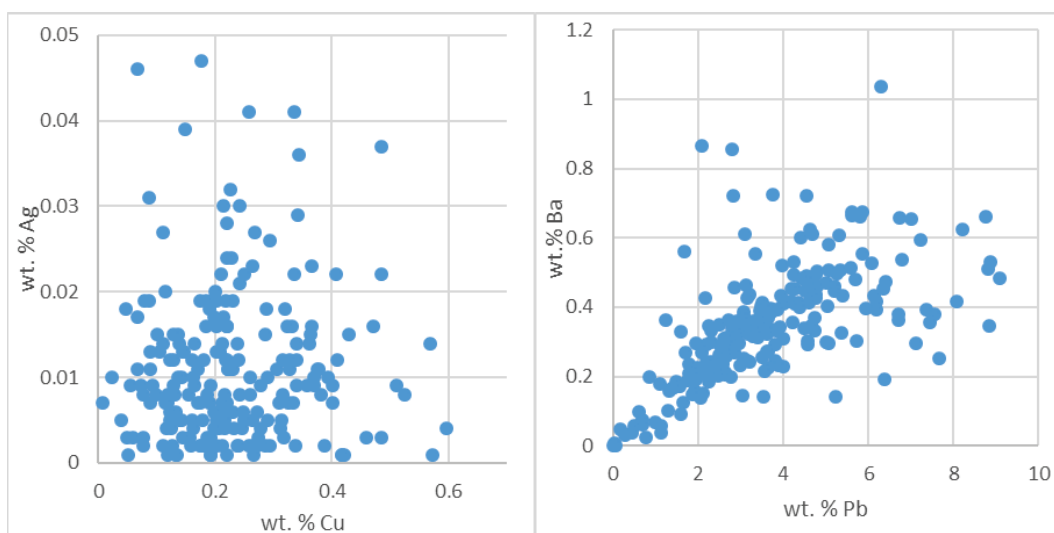


Figure 18: Correlation of Ag-Cu (left) and Ba-Pb (right).

8.5 Grain Size Distribution

The jarosite material from zinc production is generally very fine grained. The grain size was determined by sieve analysis (Figure 19). Twelve different mesh sizes were used and showed a distribution of about 50-60 % of the grains being smaller than 10 μm . SEM analysis of the sieving fractions showed a significant amount of agglomerates. According to information from the staff of a zinc plant, laser granulometry shows a very similar distribution.

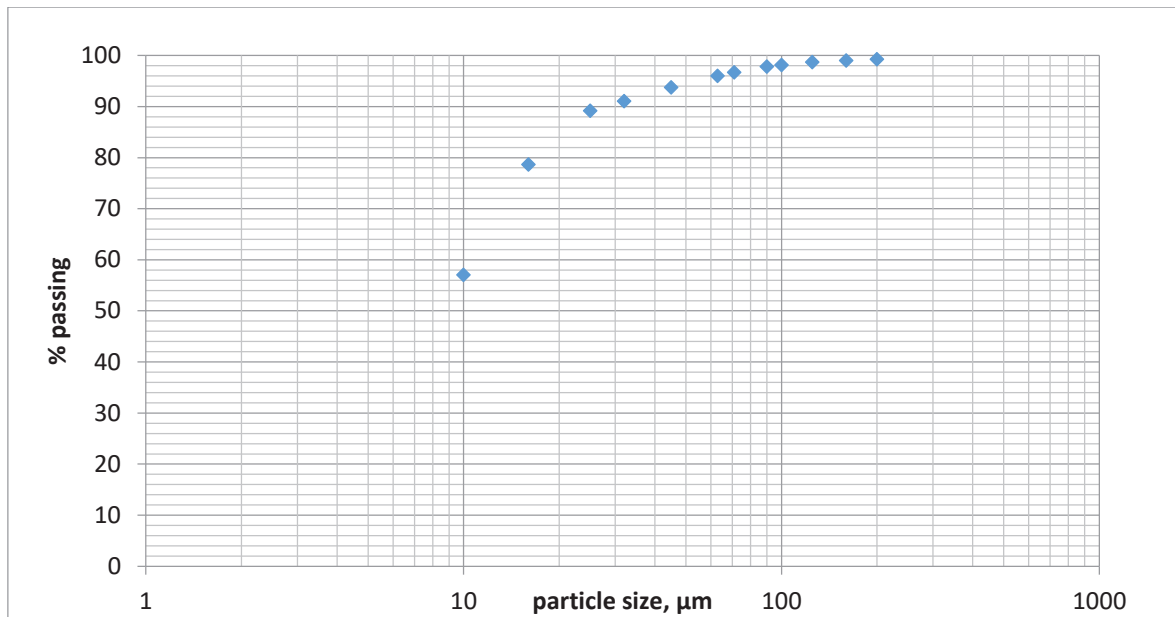


Figure 19: Screening curve of a jarosite from zinc production.

8.6 Mineralogical Composition

The phases appearing in the residues can be assigned to three origins:

- chemical precipitates such as jarosite
- roasted but unleached phases like zinc ferrite
- geogenic, unchanged minerals from the ore, for example quartz

8.6.1 Jarosite

The mineralogical type of jarosite depends on the specific plant and production process; usually it is natro- or ammoniojarosite. Additionally, hydroniumjarosite is also formed. (K-) Jarosite was identified using RAMAN spectroscopy (Appendix 10). Figure 20 shows a typical natrojarosite from a residue from a European zinc smelter.

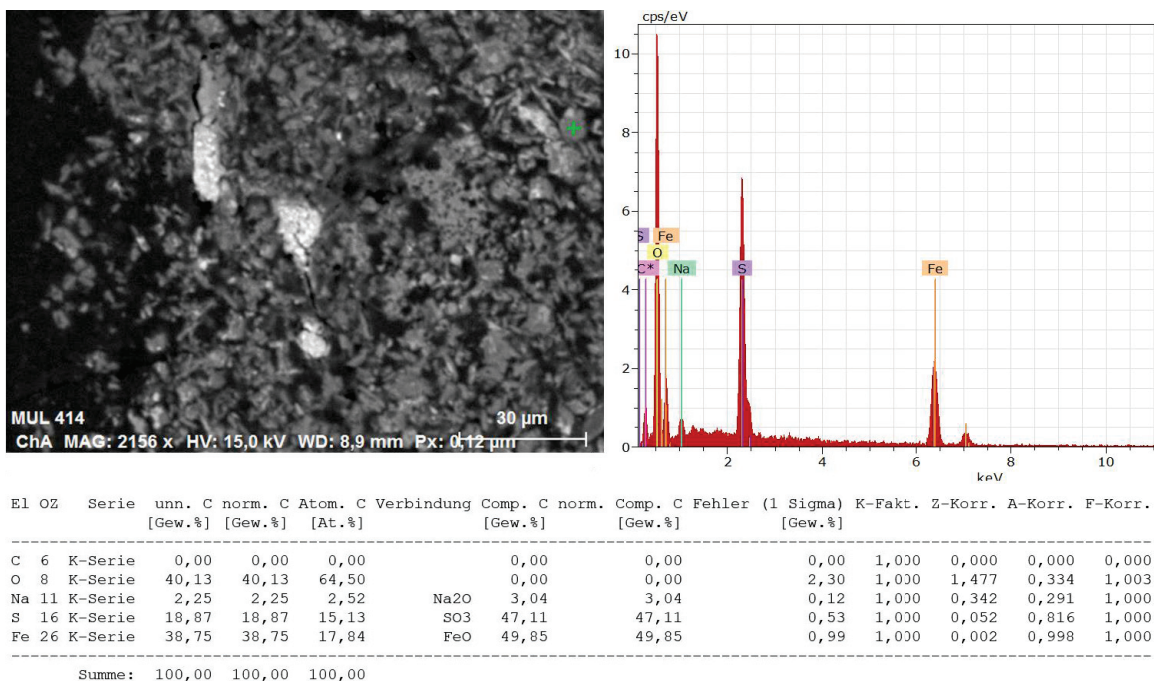


Figure 20: BSE image of a natrojarosite from a residue from a European zinc smelter measured by SEM-EDX.

The jarosite phase can also incorporate Pb, Ag, Cu, Ca, Al, Ba, K, As and Tl (Dutrizac & Jambor, 2000). From these elements, especially lead and silver are interesting in terms of the jarosite process in zinc winning. Theoretically, none of them should be present in the stage of jarosite formation. However, plumbojarosite is confirmed in the residue. Having a closer look at the process of one specific zinc plant, the source of plumbojarosite becomes obvious. After the first, neutral leaching step, a thickener separates the fluid solution from the solids. As this separation is not a very precise one and the hot acid leaching plant is too small for all of the incoming material, a part of the undissolved material (lead and silver bearing) takes the direct way to the jarosite precipitation site. Furthermore, all of the final leach residue is sold as a lead and silver concentrate, so all of the lead and silver in the jarosite residue is due to this direct way from thickener after neutral leach to the jarosite precipitation step.

As the jarosite process is introduced for removing iron from the solution, jarosite is the main, but not only carrier of iron. Jarosite may also carry considerable amounts of lead. Whilst the presence of lead in the jarosite phase was proven by EMP in this material (Figure 21), the presence of silver and copper has not been verified yet.

The grain size of the jarosite particles is generally small, below several micrometres. This is due to the fact that the minerals are precipitates from a solution within the process.

	1	2
Element	wt.%	wt.%
Na ₂ O	2.1	3.3
MgO	0.0	0.0
BaO	0.4	0.3
SiO ₂	1.3	3.0
Al ₂ O ₃	2.4	2.2
Fe ₂ O ₃	28.9	32.8
MnO	0.0	0.0
ZnO	5.4	4.1
PbO	10.9	9.4
Ag ₂ O	0.0	0.0
SO ₃	26.5	28.3
K ₂ O	0.7	0.8
CaO	0.1	

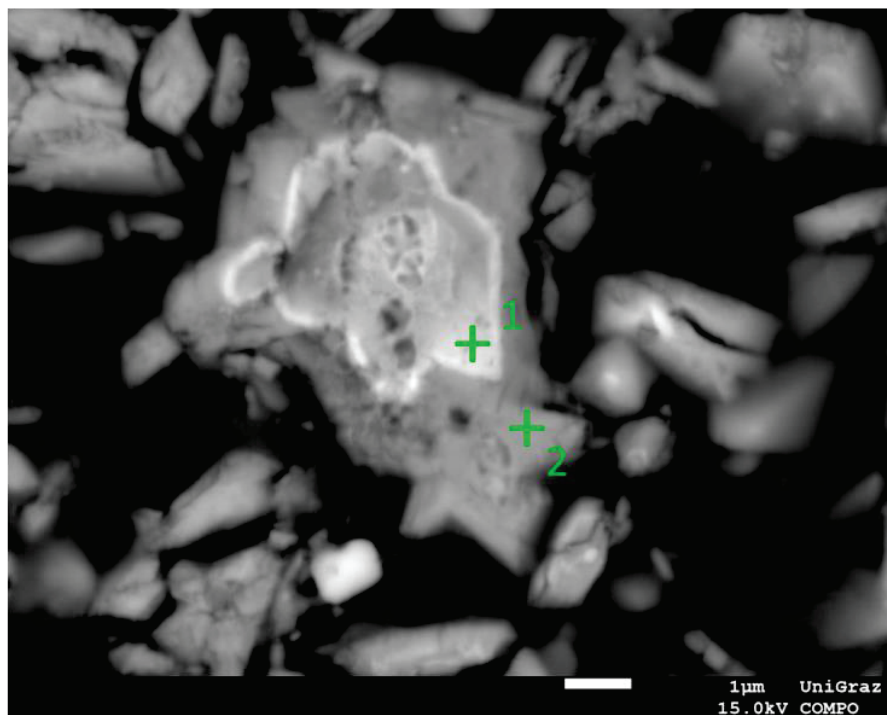


Figure 21: BSE image (FEG) and two WDX measurements of a jarosite particle. Due to the small scale, a precise measurement is not possible but the bright areas are richer in lead than the darker ones. Analysis was performed using a FEG EMP at University of Graz.

Table 11 lists chemical analyses using SEM-EDX and EMP-WDX and calculated atoms per formula unit for several selected jarosite particles. The right columns show an ideal natrojarosite composition for comparison, two EMP-WDX measurements and the mean values of 25 measurements. Elements are organised in groups of possible components in the A (Na, K, Pb) and B positions (Fe, Zn, Al, Ca, Cu). Arsenic in the sulphate group is possible, but occurs only to a minor extent. The bottom lines of the table give the atoms per position and the sum of both. Bad totals are mainly due to bad polishing of the surface, missing calibration and inclusions or surrounding material that was also analysed accidentally. Mean and EMP-EDX measurements are very close to the ideal values. The A position is dominated by Na, as all samples were from plants where natrojarosite is formed. Pb is often present and also reports to the A position. Ti and Si are not common elements in jarosite and may refer to small impurities of other phases. Small impurities and intergrowths are possible in all measurements and cannot be omitted due to the small grainsize.

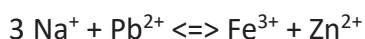
Table 11: Element composition and calculated atoms per formula unit normalised to 11 oxygen for selected jarosite particles. The right columns show the composition of an ideal natrojarosite, the mean values of all measurements (n=25) and two EMP-WDX measurements. All other columns refer to SEM-EDX measurements.

wt.% oxide	strewn slides																		EMP WDX		ideal
	3.9	5.8	4.9	4.7	5.9	5.2	7.2	2.4	4.6	5.1	3.7	3.7	6	4.7	6.6	6.1	6.8	1.3	2.1	3.3	
Na ₂ O	3.9	5.8	4.9	4.7	5.9	5.2	7.2	2.4	4.6	5.1	3.7	3.7	6	4.7	6.6	6.1	6.8	1.3	2.1	3.3	6.4
K ₂ O	0.5	0.8	1.1	1	1.2	1.1	1.3	0	0.7	0.9	0.6	0.7	1	1	0.6	1	0.7	0	0.7	0.8	0
PbO	19	0	0	0	0	0	0	20	9.6	9.9	18	16	0	6.6	5.4	0	0	10	11	9.4	0
Fe ₂ O ₃	36	45	46	51	47	47	47	34	38	38	35	36	42	38	32	38	47	56	29	33	49
ZnO	9.3	3.6	4	3	4.5	3.6	0	6.1	5.2	3.9	5.7	4.9	3.4	3.1	2.9	1.7	0	2.6	5.4	4.1	0
Al ₂ O ₃	4.2	1.9	1.2	1.2	1.8	1.7	2.3	2.3	3.9	2.8	1.6	2.8	2.9	2.3	2.2	1.6	1.3	0	2.4	2.2	0
CaO	0	0	0	0	0	0	0	0	0	0	0	0	1.8	1.8	0	0.7	0	0	0.1		0
Cu ₂ O	0	0	0	0	0	0	0	2.2	1.7	1	2.1	2.1	1	0.8	0.9	0.7	0	0			0
TiO ₂	0	0	0	0	0	0	0	0	0.9	0	0	0	0	0	0.3	0	0	0			0
SiO ₂	0.6	0.9	4.6	0	0	0	0	0	1.5	0	0.5	0.4	4.7	3.8	0.6	0.3	0	0.6	1.3	3	0
SO ₃	31	38	34	37	36	39	39	28	31	33	28	29	37	29	28	33	40	35	27	28	33
As ₂ O ₃	0	0	0	0	0	0	0	0	1.7	0	0	0	3.9	0	0.6	2.6	0	0			0
BaO	0	0	0	0	0	0	0	0	0	0	0	0.7	0.4	0.4	0	0	1.1	0	0.4	0.3	0
MgO	0	0	0	0	0	0	0	0	0	0	0	0	0	0.3	0	0	0	0	0	0	0
sum	105	96	96	97	96	97	97	95	99	95	95	96	104	91	80	86	97	106	79	84	82

atoms per formular unit		strewn slides																		EMP WDX		mean	ideal
A position		0.6	0.8	0.7	0.7	0.9	0.7	1	0.4	0.7	0.8	0.7	0.6	0.8	0.8	1.2	1	1	0.2	0.4	0.6	0.7	1
Na ⁺		0.6	0.8	0.7	0.7	0.9	0.7	1	0.4	0.7	0.8	0.7	0.6	0.8	0.8	1.2	1	1	0.2	0.4	0.6	0.7	1
K ⁺		0.1	0.1	0.1	0.1	0.1	0.1	0	0.1	0.1	0.1	0.1	0.1	0.1	0.1	0.1	0.1	0.1	0	0.1	0.1	0.1	0
Pb ²⁺		0.4	0	0	0	0	0	0.5	0.2	0.2	0.4	0.4	0	0.1	0.1	0	0	0.2	0.3	0.2	0.2	0	
B position		2.2	2.5	2.6	2.8	2.7	2.6	2.6	2.3	2.3	2.4	2.4	2.2	2.4	2.3	2.4	2.6	3.1	2.2	2.3	2.6	3	
Fe ³⁺		2.2	2.5	2.6	2.8	2.7	2.6	2.6	2.3	2.3	2.4	2.4	2.2	2.4	2.3	2.4	2.6	3.1	2.2	2.3	2.6	3	
Zn ²⁺		0.6	0.2	0.2	0.2	0.3	0.2	0	0.4	0.3	0.2	0.4	0.3	0.2	0.2	0.1	0	0.1	0.4	0.3	0.2	0	
Al ³⁺		0.4	0.2	0.1	0.1	0.2	0.1	0.2	0.3	0.4	0.3	0.2	0.3	0.2	0.2	0.2	0.1	0	0.3	0.2	0.2	0	
Ca ²⁺		0	0	0	0	0	0	0	0	0	0	0	0.1	0.2	0	0.1	0	0	0	0	0	0	
Cu ⁺		0	0	0	0	0	0	0.2	0.1	0.1	0.2	0.2	0.1	0.1	0.1	0.1	0	0	0	0	0	0	
Ti ⁴⁺		0	0	0	0	0	0	0	0.1	0	0	0	0	0	0	0	0	0	0	0	0	0	
Si ⁴⁺		0	0.1	0.3	0	0	0	0	0.1	0	0	0	0.3	0.3	0.1	0	0	0	0.1	0.3	0.1	0	
S ⁴⁻		1.9	2.1	1.9	2	2	2.1	2.1	2	1.9	2	1.9	1.9	1.9	1.8	2	2.1	2.1	1.9	2.0	1.9	2	2
As ⁴⁻		0	0	0	0	0	0	0	0.1	0	0	0	0.2	0	0	0.1	0	0	0	0	0	0	0
sum A+B		4.25	3.70	3.71	3.85	4.04	3.75	3.87	4.10	4.07	4.09	4.32	4.24	3.67	4.11	4.24	3.85	3.73	3.67	3.71	3.70	3.95	4.00
A pos		1.08	0.88	0.81	0.76	0.97	0.83	1.12	0.92	1.00	1.13	1.15	1.11	0.90	1.04	1.42	1.09	1.05	0.39	0.81	0.92	0.93	1.00
B pos		3.16	2.82	2.90	3.09	3.07	2.92	2.75	3.18	3.07	2.96	3.16	3.13	2.77	3.07	2.82	2.76	2.68	3.28	2.90	2.78	3.02	3.00

Figure 22 and Figure 23 show different correlation diagrams of 25 SEM-EDX and 2 EMP-WDX measurements on jarosite particles, some of which are presented in Table 11. Zn and

Iron does not show significant correlation with other metals. Lead and Zn correlate slightly positively, indicating an occupation of different positions in the structure (A and B) (Figure 22). In accordance with literature, Na and Pb are both part of the A site (Dutrizac & Jambor, 2000), also visualised by a slightly negative correlation. A similar trend is presented for Zn and Na (Figure 22 and Figure 23). Na-Fe and Pb-Fe do not correlate (Figure 24). Due to the observed, although weak, correlations of Na, Pb, Fe and Zn, a coupled substitution such as (Equation 8-1)



8-1

is proposed for jarosite forming in residues from zinc production.

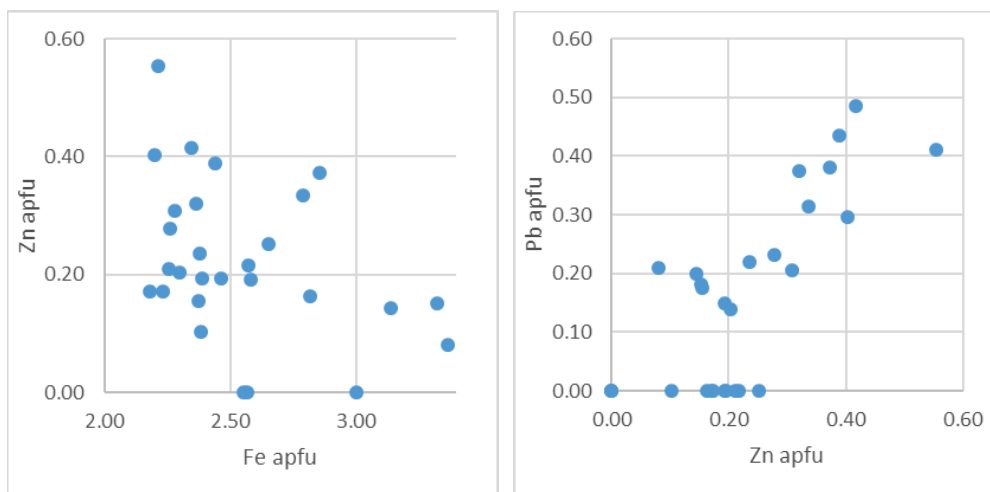


Figure 22: Correlation of atoms per formula unit for Zn-Fe (left) and Pb-Zn (right).

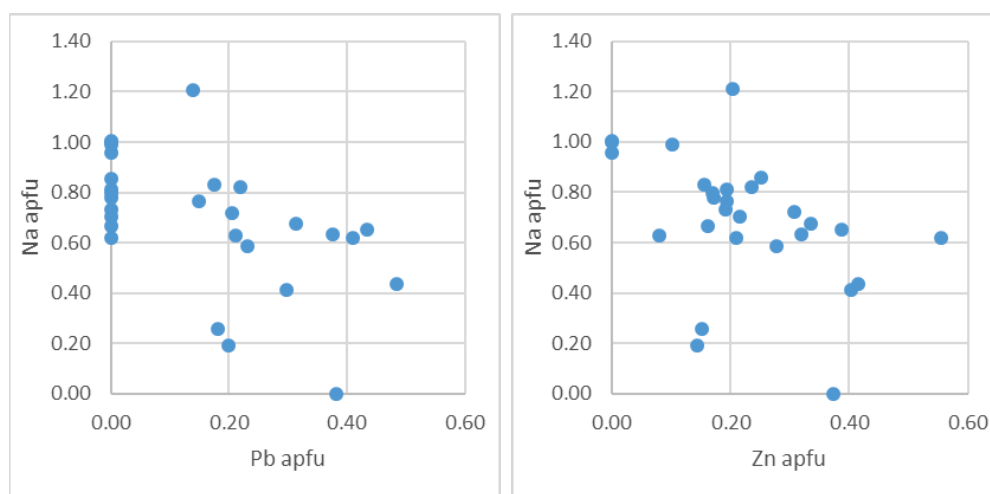


Figure 23: Correlation of atoms per formula unit for Na-Pb (left) and Na-Zn (right).

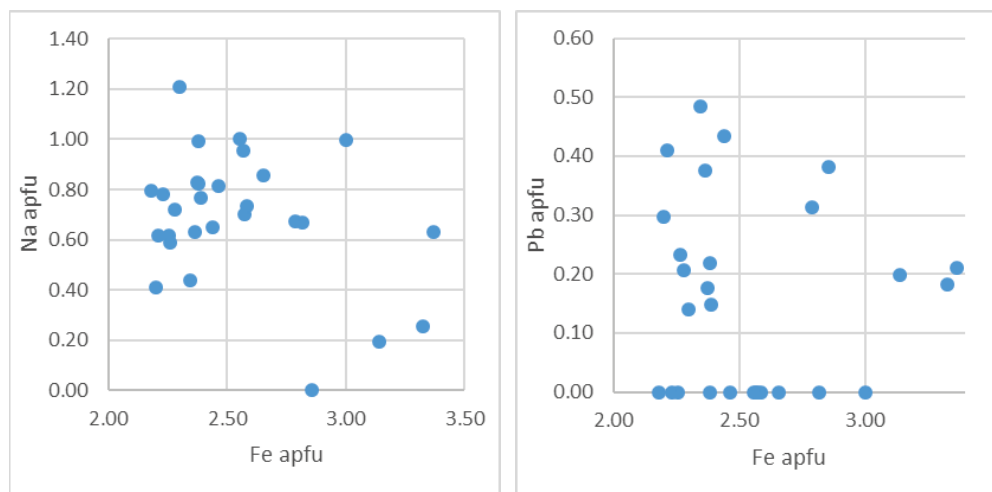


Figure 24: Correlation of atoms per formula unit for Na-Fe (left) and Pb-Fe (right).

8.6.2 Zinc Ferrite and other Zn-Bearing Phases

Zinc ores usually contain considerable amounts of iron. Besides the iron content of the sphalerite, iron also originates from minerals like pyrite, marcasite and chalcocopyrite, which are commonly associated with sphalerite. The problem for the zinc winning process in the presence of iron in the zinc concentrate is the formation of zinc ferrite during roasting (Figure 25). This newly built phase is more difficult to leach in sulphuric acid than zinc oxide, the desired product after roasting. Another (hot-acid) leaching step is necessary to leach zinc ferrite and therefore prohibit zinc loss. After this, some roasted material is added to the solution for neutralisation which then cannot be totally leached. Furthermore, the residue after the first leaching step that goes directly to the jarosite precipitation also contains some zinc ferrite.

Zinc ferrite is an important zinc carrier in the residue. Sphalerite should not be present in the residue according to the process. However, due to incomplete roasting, a small amount of sphalerite was found in several samples (Figure 26). It was also identified using RAMAN spectroscopy (Appendix 11). Even though sphalerite grains sometimes contain small silver inclusions (Figure 26), the phase itself is too rare to be of any economic importance. Single grains of gahnite (Zn-Al spinel) were identified as well.

The size of the particles ranges from several microns to a few tens of microns. This is due to grinding and milling during mineral processing as well as milling after roasting. Investigations by electron microprobe analysis also indicate a small amount of zinc bound to the jarosite mineral.

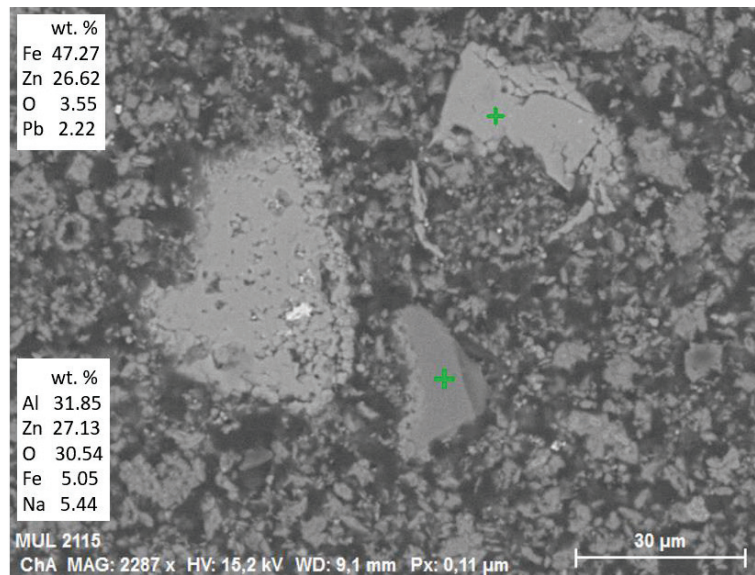


Figure 25: SEM image of zinc ferrite (upper cross and table) and gahnite (Zn-Al spinel, lower cross and table).

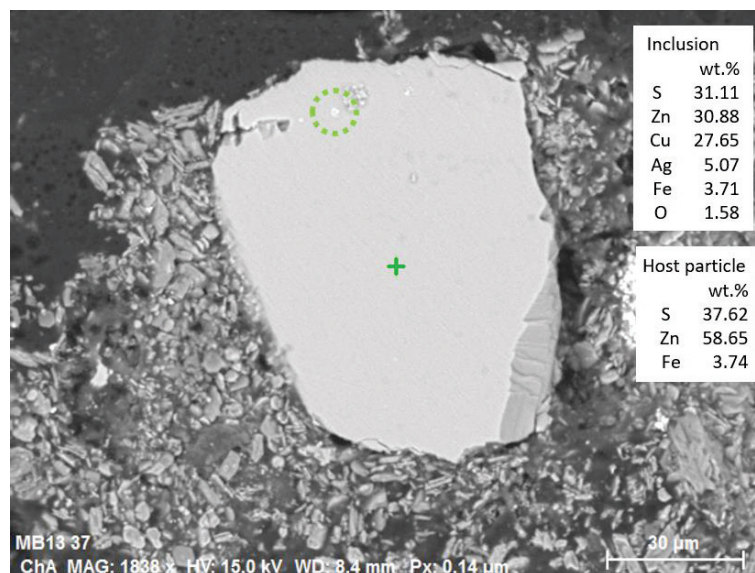


Figure 26: SEM-image of a sphalerite grain (containing 3.74 % Fe) with a silver-bearing covellite inclusion (green circle).

8.6.3 Lead-Bearing Phases

Lead is one of the main metals of interest in the jarosite residue. It is always present in zinc ores in considerable amounts. Often a lead-silver concentrate, the leaching residue, is separated during the zinc winning process and sold to lead smelters. The reasons, why lead bearing phases appear in the residues are:

- A part of the residue after the first leaching step is sometimes dumped when the following process steps are overloaded.
- Roasted material is added to the solution after the final leaching for neutralisation

- Leaching residues might be dumped together with precipitation residues.

In the residue, lead occurs as oxide, sulphate and sulphide within the same material (Figure 27 and Figure 28). Sulphides (galena) are geogene remnants from the original ore, oxides are formed during roasting and sulphates are formed during the leaching process with sulphuric acid. Close intergrowth with barite is very common (Figure 29 and Figure 30). Additionally, the jarosite mineral also contains a small amount of lead sometimes. Silver usually appears together with lead, or in lead phases. Interestingly, there is no evidence for lead phases containing silver in the investigated jarosites.

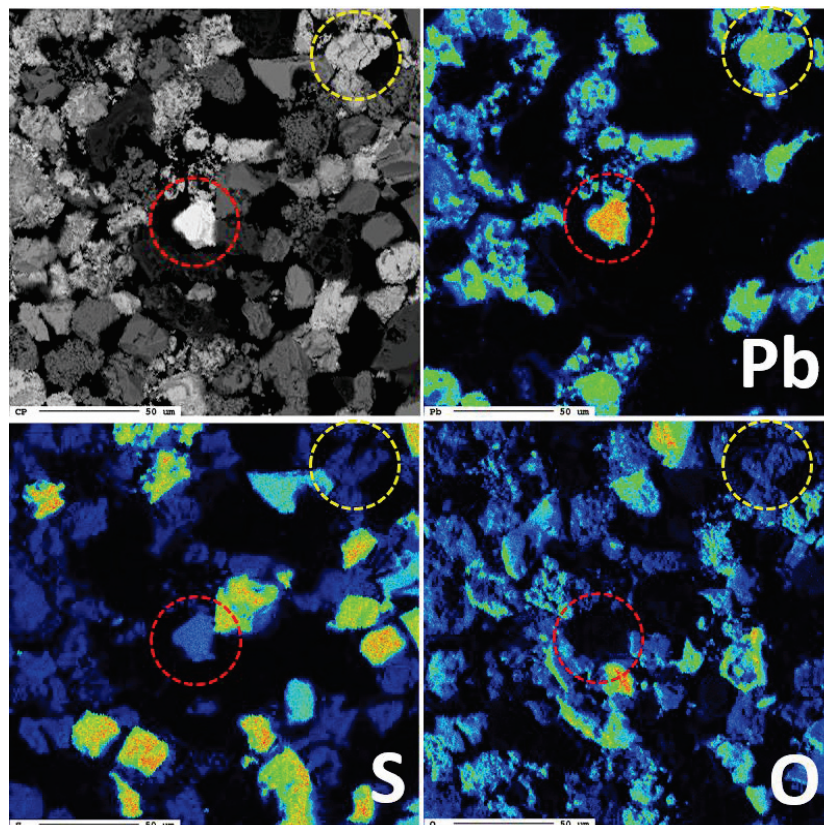


Figure 27: EMP-WDX mapping of Pb, S and O on a section of hydro separated jarosite material. Note the different lead phases anglesite (yellow circle) and galena (red circle).

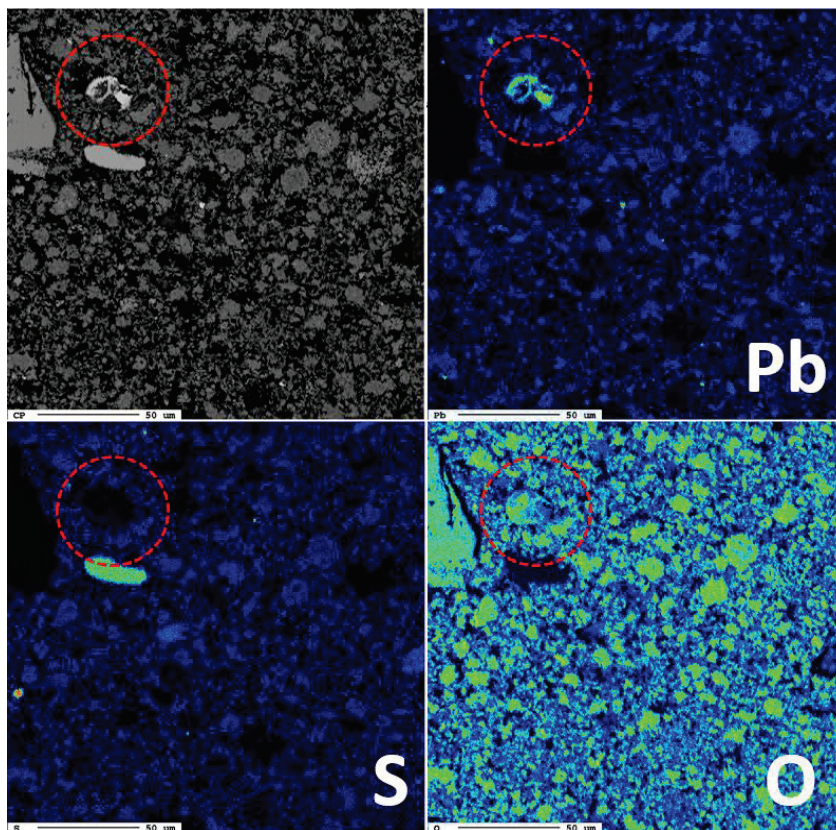


Figure 28: EMP-WDX mapping of Pb, S and O on a characteristic section of jarosite residue from zinc production.

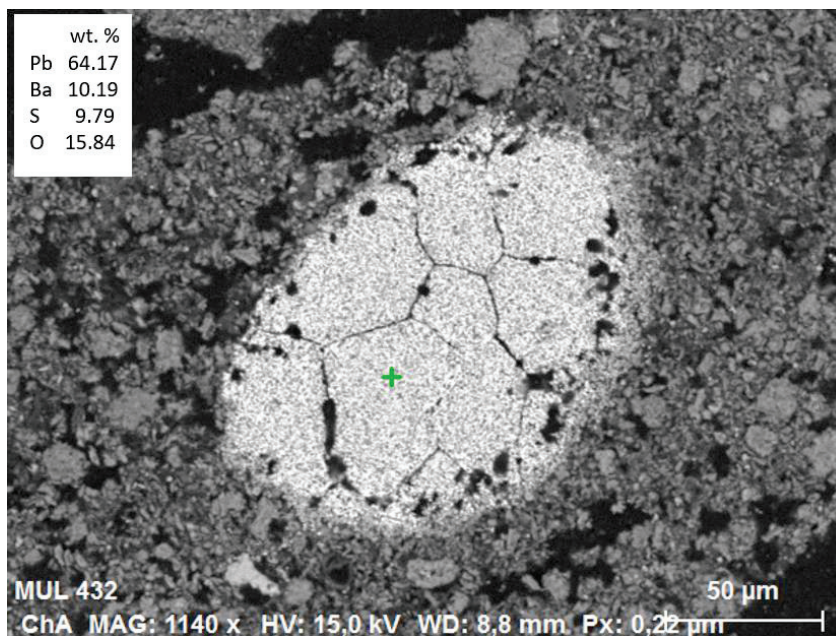


Figure 29: Large particle of a lead-barium sulphate particle.

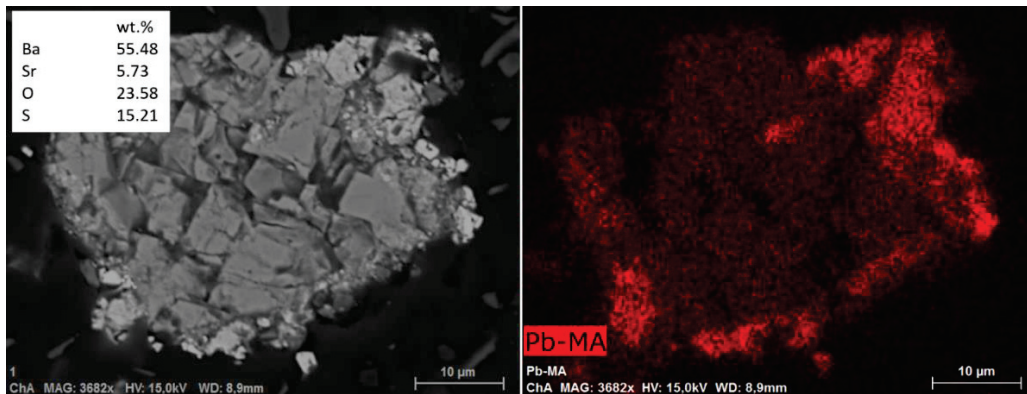


Figure 30: BSE and X-ray distribution image of a strontium-bearing barite surrounded by galena (brighter grains).

8.6.4 Silicates

The main silica-bearing phases are quartz and feldspar (e.g. anorthite and albite). Due to their chemical resistance, both phases are not influenced by any of the metallurgical steps in the zinc winning process. The grain size is caused by crushing and milling, as roasting has no influence on these minerals and no shrinking of the particles takes place. Therefore, the grains are generally large compared to other phases. For the characterisation of the material and a further treatment in terms of metal winning, quartz and feldspar are of interest from two points of view:

- Both phases are the main carriers of silica, influencing slag basicity for a pyrometallurgical treatment process
- Both phases often bear metal inclusions. Copper inclusions that are sometimes also high in silver are of greatest interest (Figure 31).

Other silicates, for example garnet (Figure 32), appear as accessories.

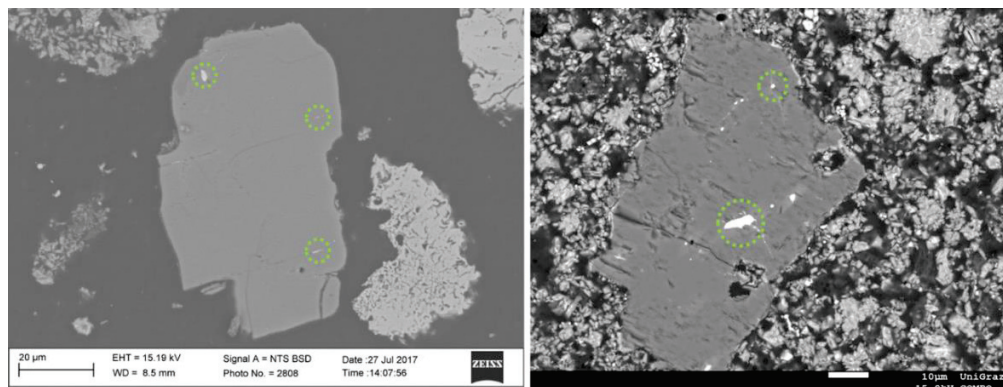


Figure 31: Left: Large orthoclase with silver and copper-bearing inclusions. Right: Potassium feldspar. The circled inclusion in the middle is galena with copper-bearing zones. The upper circle marks a copper-silver-bearing inclusion

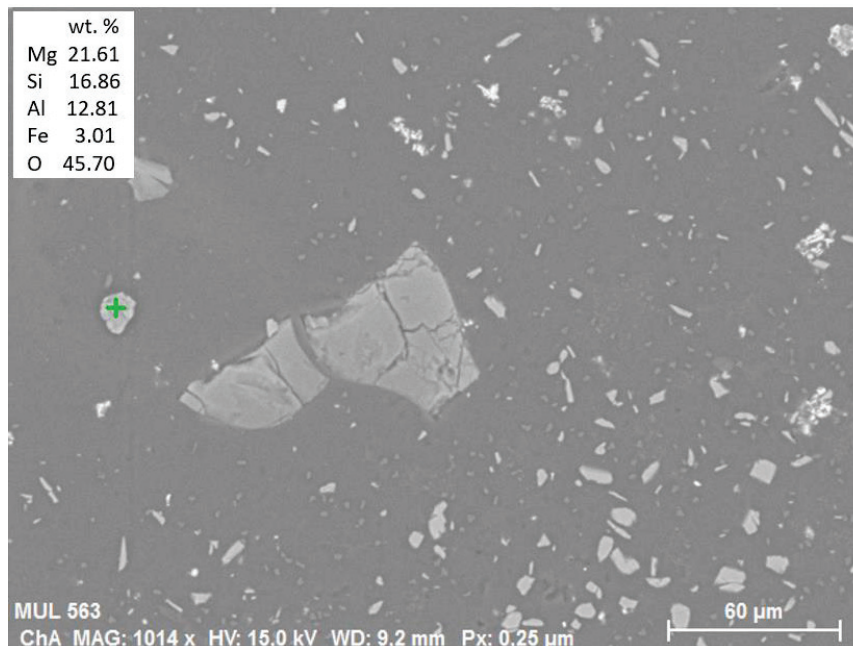


Figure 32: BSE image of a garnet grain.

8.6.5 Occurrence of Silver

Silver is one of the most important valuable elements in the jarosite residue from zinc production. The concentration varies from 80 to 220 ppm according to the AMCO analyses, but can reach up to 600 ppm in specific cases. Table 12 shows a selection of different silver- and silver-bearing phases. The chemical compositions refer to SEM-EDX measurements. Due to the very small grain size of these particles (<3 μm), the analyses also partly affect the surrounding material. If the silver phase is embedded in another particle, the host particle is named in the first column. "Agglomerate" means that an agglomerate of very small grains was measured and no mineralogical identification is possible. Grains that are not embedded or agglomerated with other phases are termed as "free grain."

Silver often appears as inclusion in silicates (Figure 31). Sphalerite and anglesite were also identified as host particles, but only in subordinate amounts.

Jarosite was not clearly identified as a carrier of silver. Table 12 shows one particle named "jarosite" that also contains silver. However, due to its small grain size, it was not possible to determine if the measurement contains not only a jarosite grain, but also a separate silver phase.

Figure 33 displays an SEM-EDX mapping of an Mn oxide grain. It is huge compared to the rest of the material (~400 μm in length) and is clearly layered. The embedded silver layer consists of mainly 74 % silver and 9.1 % chlorine (see last line in Table 12).

Table 12: Identified silver (-bearing) particles in residues from zinc production. Values are given in wt.%.

Host particle	Ag	Cu	Si	O	Al	Fe	S	Zn	Mg	Cl	Na
quartz	4.0		44.9	51.1							
orthoclase	8.1	54.4	2.8	6.9	1.4	1.3	25.1				
orthoclase	6.0	1.1	28.7	40.0	10.3						
orthoclase	13.6	3.8	22.3	36.2	8.9		3.9				
sphalerite	2.7	8.1		1.8	0.1	3.8	26.4	44.0			
anglesite	82.6		2.3	7.2	3.3			0.8		3.9	
jarosite ?	1.3	0.9	1.1	50.9	1.2	25.2	13.6	2.3			3.6
agglomerate	4.8		1.1	26.8	0.7	9.4	37.3	16.6			3.3
free grain	45.9	2.1	0.6	25.9	0.9	4.4	10.0	4.2		4.8	1.2
free grain	40.1	1.5	0.8	33.3	1.1	7.1	5.9	4.1		4.4	1.7
free grain	35.0		1.8	18.1	2.1	1.7	15.2	21.6	1.2	2.8	
sphalerite	6.8		1.0	7.2	1.1	1.5	30.1	50.5	0.7		
agglomerate	6.2		20.4	27.8	1.8	1.8	12.2	24.3	1.6		3.4
agglomerate	5.6		19.8	31.0	1.7	8.0	13.2	14.7	1.4		3.7
agglomerate	27.8		0.9	37.2	1.6	5.4	8.8	8.3	2.2	4.6	2.8
agglomerate	3.2	0.6	2.7	52.2	1.4	15.1	12.1	6.2	1.6		5.0
covellite	1.8	62.5		2.0			33.7				
covellite	2.4	60.6		2.5		0.6	33.9				
quartz	2.0	49.6	18.7	17.2			12.5				
quartz	0.9	22.9	29.8	33.9	0.2		6.5	5.9			
quartz	4.0	23.3	21.4	23.5	0.7		14.6	12.6			
quartz	3.0	7.1	32.5	43.5	0.1	2.2	4.6	1.6			
quartz	3.5	15.1	34.2	43.6			3.6				
microcline	6.6	70.9	0.7	1.9	0.3		19.7				
MnO	74.2			6.5	2.4		0.6			9.1	

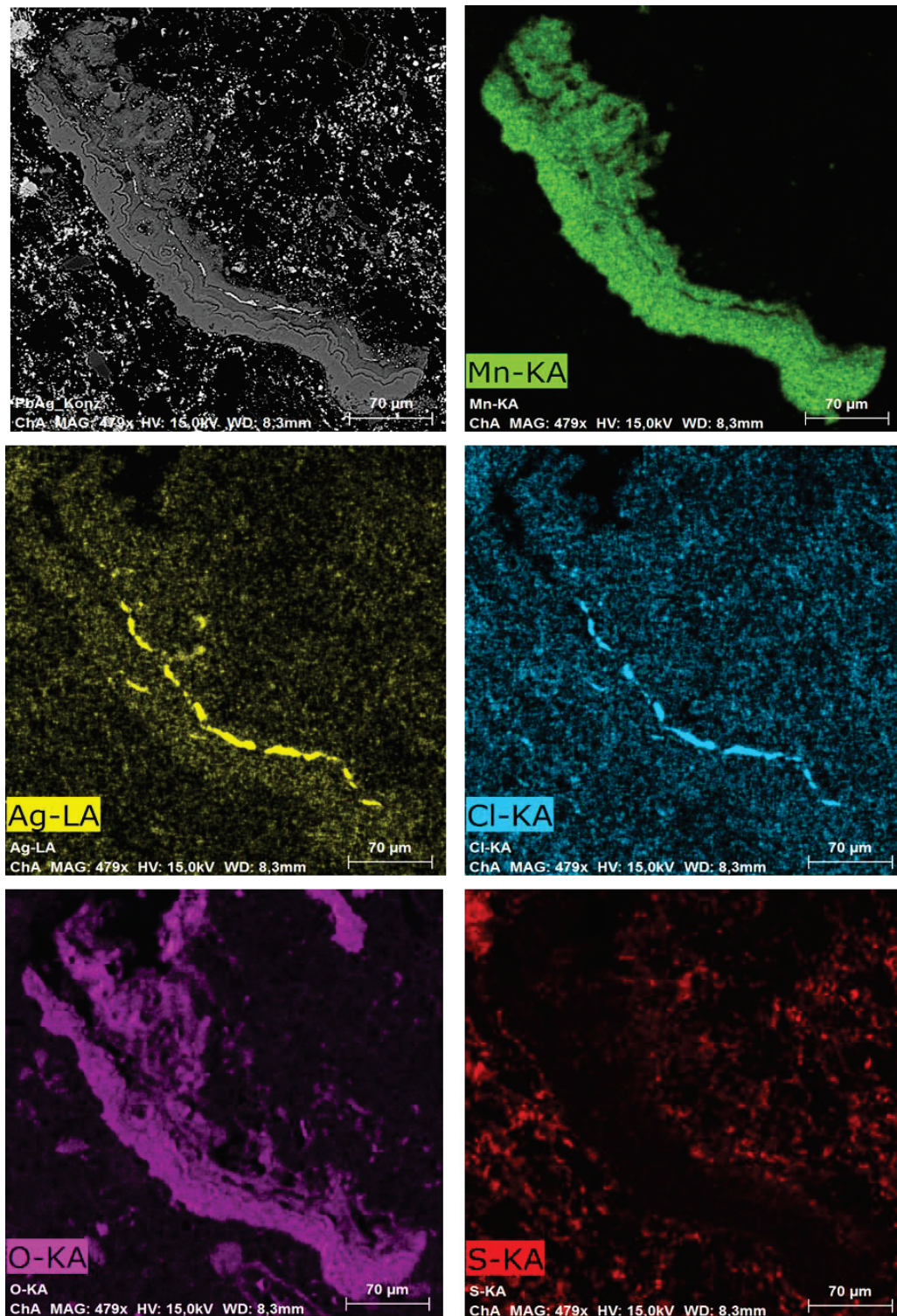


Figure 33: SEM-EDX mapping of a large MnO particle with a layer of silver chloride.

8.6.6 Minor Phases

Although a quantification of phases is currently not possible, minor phases are - in this case - those that are too rare to be of process-technical interest. Examples are: chalcocite and

barite (Figure 34), talc, cassiterite, wuestite, magnetite, amphibole, olivine, chlorite and apatite.

Gold is important despite the low concentration and heterogeneous analyses. According to chemical analysis, gold concentrations may reach up to 10 ppm in different jarosite residues. One single gold grain was identified (Figure 35) using the SEM; it is about 17 μm in diameter, which is quite large for jarosite material. Nevertheless, the gold grade is as high as several ppm in some cases, close to the values in primary ores. According to the calcination-reduction process, there is no need to adapt the process to recover gold. When using a lead bath, it will be collected in the alloy.

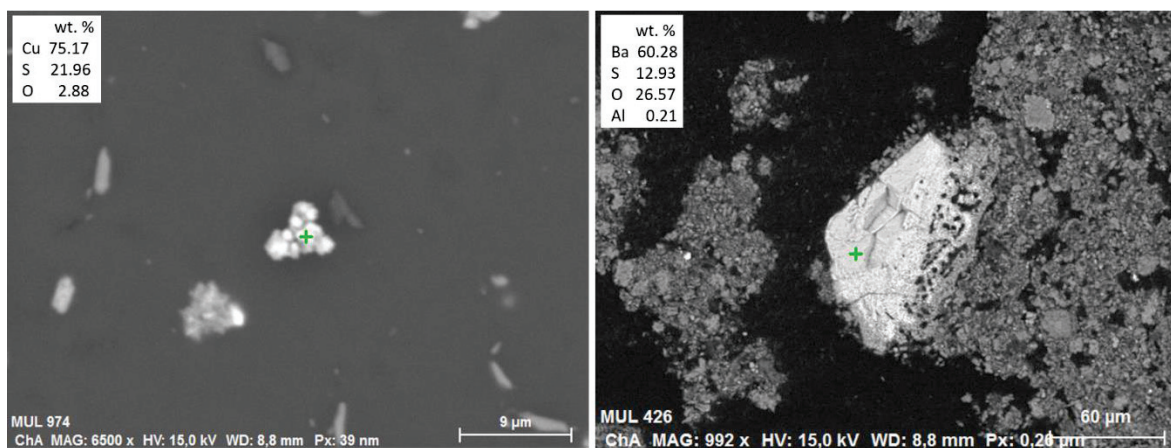


Figure 34: SEM image of a chalcocite particle (left) and barite grain (right).



Figure 35: SEM image of a gold particle.

8.6.7 Listing of Identified Phases

An area of the monolayer sample from the hydro separated concentrate was chosen for a manual, quantitative phase determination using SEM-EDX. As this kind of separation refers not only to a specific physical property, but also to grain size, shape and density, the results are representative neither for the whole material nor the corresponding grain size. Figure 36 shows the area that was selected for quantitative mineralogical analysis and Table 13 and Figure 37 the identified phases.

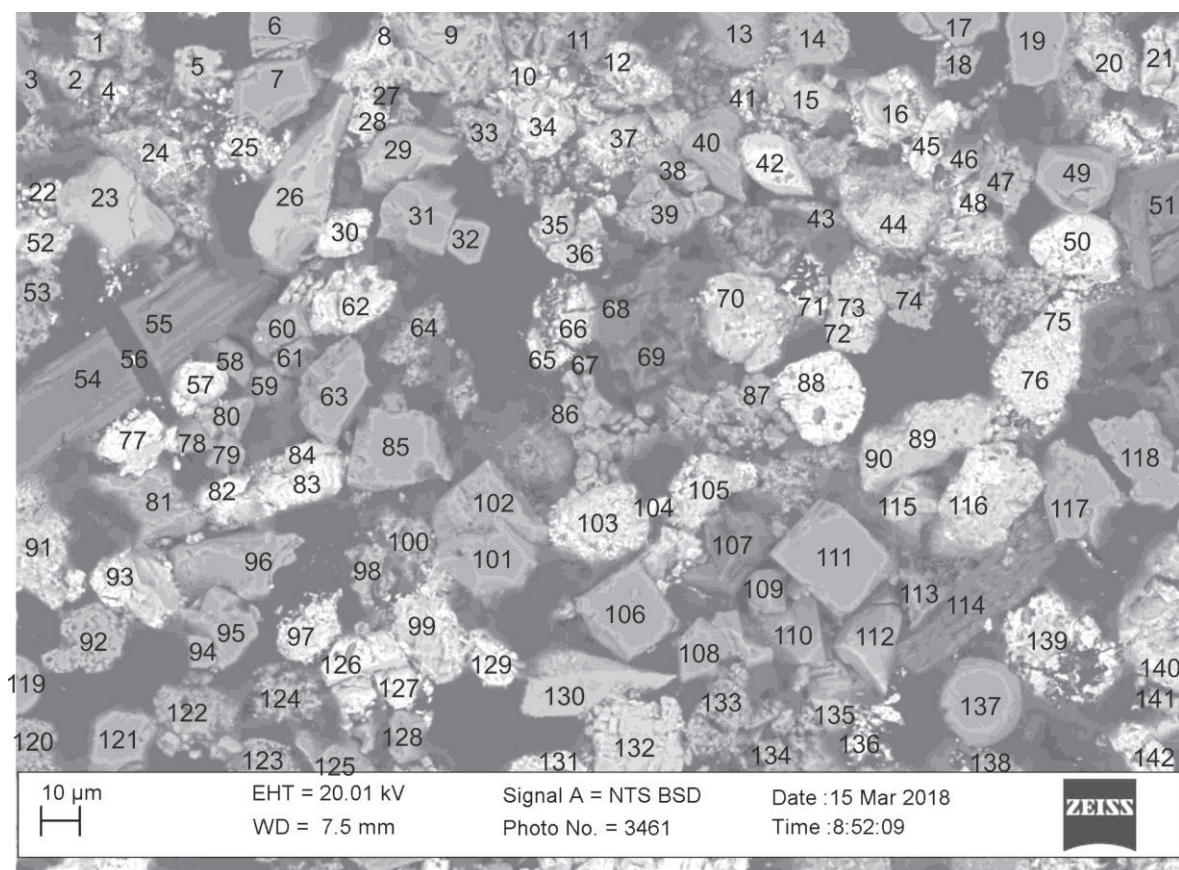


Figure 36: Selected area of a section of the hydro separated concentrate for quantitative mineralogical analysis (SEM-EDX).

Table 13: Identified phases in the hydro separated jarosite sample. The numbering corresponds to Figure 36.

1	Sph	31	Py	61	Py	91	Ba	121	Py
2	Sph	32	Py	62	Ang	92	Fra	122	ni
3	Py	33	Fra	63	Py	93	A-B	123	Wue
4	Ang	34	Ang	64	Wue	94	Py	124	Fra
5	Sph	35	Ba	65	Ang	95	Py	125	Py
6	Py	36	Ba	66	Ang	96	Py	126	Ang
7	Py	37	Ang	67	Fra	97	A-B-C	127	Ang
8	Ang	38	Sph	68	ni	98	Fra	128	Py
9	Sph	39	Py	69	Qz	99	A-B-C	129	Ang
10	Ang	40	Py	70	Ba	100	Fe-Zn	130	Sph
11	Fe	41	Ang	71	Ang	101	Py	131	A-B-C
12	Ang	42	Ang	72	Ba	102	Py	132	Ba
13	Sph	43	Fsp	73	Ang	103	A-B-C	133	Fra
14	Py	44	A-B-C	74	Fra	104	Ang	134	Fra
15	Ba	45	Ang	75	Ang	105	A-B-C	135	Sph
16	Ba	46	Ang	76	A-B	106	Py	136	Ang
17	Py	47	Py	77	Ang	107	Qz	137	Wue
18	Wue	48	Ang	78	Py	108	Py	138	Fra
19	Py	49	Py	79	Py	109	Py	139	Ba
20	A-B-C	50	Ga	80	Py	110	Py	140	A-B-C
21	Ba	51	An	81	Py	111	Py	141	Co
22	Ang	52	Ang	82	Ang	112	Sph	142	Ang
23	Sph	53	Wue	83	Ang	113	ni		
24	Ang	54	An	84	Ang	114	Fsp		
25	Ang	55	An	85	Py	115	Ba		
26	Sph	56	Ang	86	Fra	116	Ang		
27	Ang	57	Ang	87	Fra	117	Py		
28	Ang	58	Py	88	Ang	118	Py		
29	Si	59	ni	89	Ang	119	Wue		
30	Ang	60	Py	90	Ba	120	Wue		
Shortcut	Mineral name			Count		Shortcut	Mineral name		Count
Ang	Anglesite			39		Fra	Franklinite		11
A-B	Anglesite-Barite			2		Ga	Galena		1
A-B-C	Anglesite-Celestine-Barite			8		not	not identified		4
Ba	Barite			12		Py	Pyrite		36
Cov	Covellite			1		Qz	Quartz		2
Fsp	Feldspar			5		Si	Siegenite		1
Fe	Fe			1		Sph	Sphalerite		11
Fe-Zn	Fe-Zn Sulphate			1		Wue	Wuestite		7

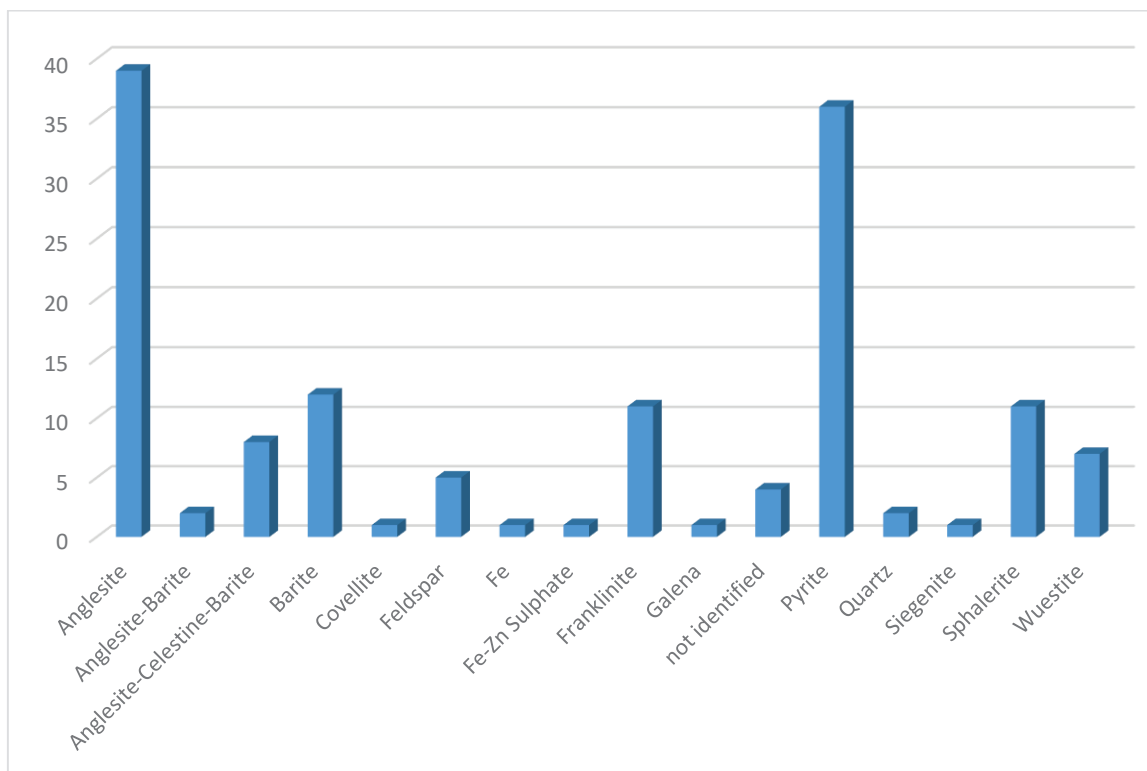


Figure 37: Number of identified phases in a hydro separated sample corresponding to Figure 36 and Table 13.

8.7 First Insights Using S/TEM

Analytical trials to characterise the properties of jarosite in the submicron range using a transmission electron microscope verified already existing indications and also provided new insights into the appearance of elements, especially silver, in the jarosite. Because of the extensive milling that is necessary during sample preparation, investigations on grain morphology are not possible, but the huge magnification allows observation of intergrowth relationships at a very small scale. Figure 38 shows a natro-/plumbojarosite particle and its chemical composition and Figure 39 a mapping of Fe, Zn, Na, Pb, Cu, Ag, Ca, Si, S, Al, K and In in the same grain.

The main components of this jarosite particle (Fe, Na, S) show a similar distribution. The grain is clearly zoned; a ring-shaped area is enriched in Zn, Pb, Cu, Al and K. Si and Ca are present in two separate phases and probably not part of the jarosite. The maps for silver and indium might be a result of background effects.

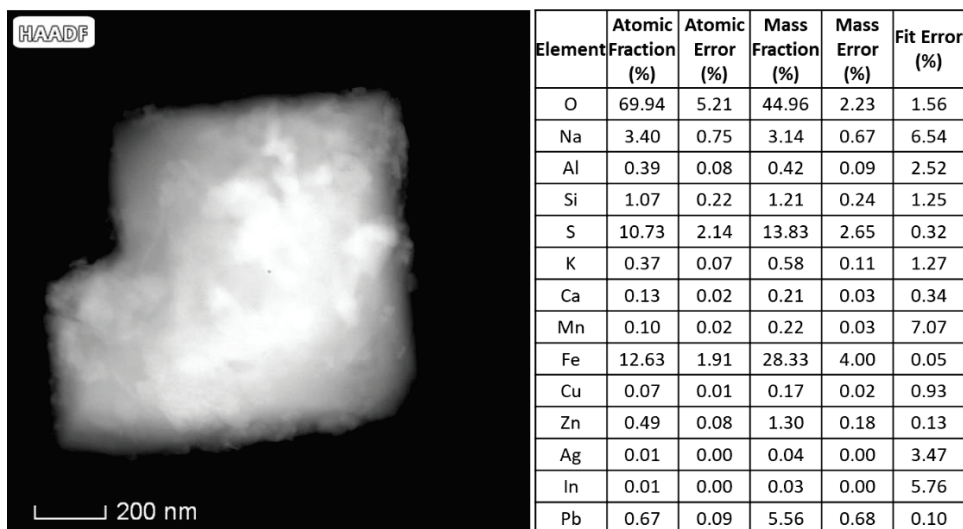


Figure 38: S/TEM image of a natro-/plumbojarosite and chemical analysis of the whole grain (EDX).

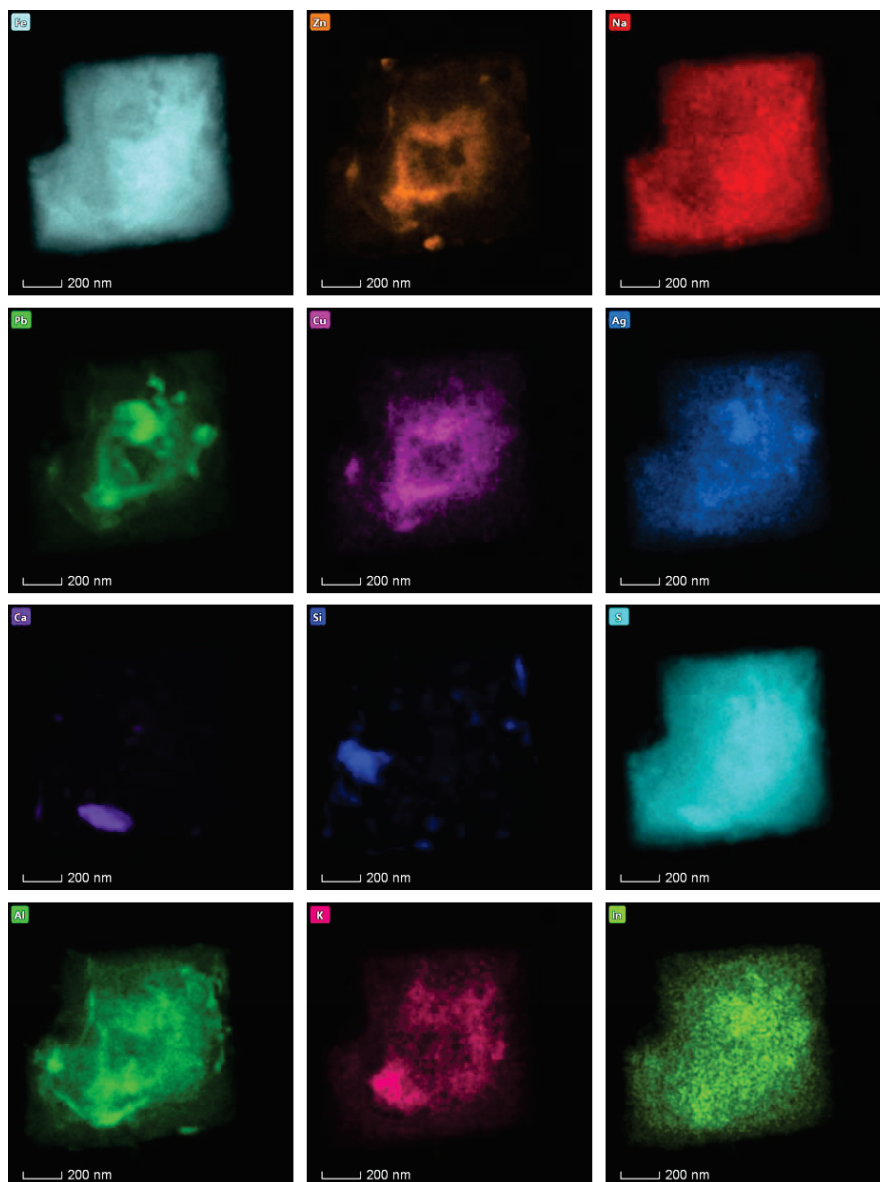


Figure 39: EDX mapping of Fe, Zn, Na, Pb, Cu, Ag, Ca, Si, S, Al, K and In using an S/TEM. The particle is the same as in Figure 38.

8.8 Jarosite from Platinum/Nickel Production

Whilst the jarosites from different zinc plants show comparable characteristics, e.g. in chemistry, grain size and mineralogy, the jarosite from platinum production is different. The iron content is higher (around 42 wt.% Fe). The only metal that is of economic interest is nickel (3-6 wt.%), so the possible final product can only be an alloy of nickel and iron, the latter of which is a main slag component in the treatment of zinc-jarosite.

Due to an extensive experimental series, a lot of information concerning the pyrometallurgical treatment and the characterisation of the final and intermediate products was collected for the jarosite from platinum production.

Compared to jarosite from zinc production, the preparation of polished sections is facilitated because the material is looser, favouring infiltration of resin into agglomerates and preventing particles from breaking out. Figure 40 shows polished sections of slag, calcine and original jarosite from platinum production as well as a strewn slide of the same, original jarosite material.



Figure 40: Different samples prepared for investigations using a scanning electron microscope. The three samples to the left are embedded in epoxy and polished. The diameter is 4 cm each. From left to right: final slag, roasted pellets (calcine) and original residue. The sample on the right is a strewn slide on double-faced adhesive tape.

8.8.1 Chemical Composition of Jarosite from Platinum Production

The main element in this residue is iron, making up about 42 wt.% of the material. It is mainly bound to ammoniojarosite, also explaining the high amount of sulphur (>15 wt.% SO₃). The significant element in this residue is nickel. Depending on the yield of the process in the platinum plant, the jarosite contains between 3 and 6 wt.% nickel according to assertions from staff of the plant. Valuable metals of major importance in the zinc jarosites

(Zn, Pb, Cu, Ag), hardly occur in the nickel jarosite and are therefore of no economic interest. Silicon and aluminium are the only slag-forming elements worth mentioning. The residue contains around half a percent arsenic, making a special off-gas treatment necessary. Table 14 gives the chemical composition of a nickel jarosite, measured by AMCO (ICP-OES) and MinProSol (XRF, powder pellets). Differences in the results are caused by sample heterogeneity, indicated especially by the considerably high amount of nickel in the ICP-OES measurement and the differences between the two XRF analyses. Furthermore, the high amount of iron may also cause some inaccuracy for ICP-OES.

Table 14: Chemical composition of jarosite from nickel production measured by AMCO (ICP-OES, aqua regia digestion) and MinProSol (RFA, powder pellets). The left and middle columns are original jarosite residues; the right column is the same material but with calcium hydroxide added as a binder prior to calcination trials.

wt.%	ICP-OES	XRF	XRF mix
As	0.54	0.34	0.48
Cu	<0.01		
Fe	42	48.56	49.06
Hg	<0.001		
K	<0.01	0.22	0.15
Na	<0.01	0.11	0.09
Ni	8.40	3.72	4.48
Pb	0.25	0.88	0.23
Al	0.16	0.63	0.41
Ca	0.01	0.11	3.05
Mg	<0.01		
Si	0.43	1.94	1.41
Pt	<0.001		
S		6.59	5.12
P		0.21	0.19
Co		0.05	0.06
Zn		0.01	0.01
Ti		0.01	
Cr		0.10	0.06
Ta		0.4	

8.8.2 Grain Size Distribution

The grain size of the nickel jarosite was measured by an external institution (ARP) using laser granulometry. The analysis shows 100 % below 40 μm and about half of the particles being smaller than 10 μm . Very small grain sizes, below 2 μm , are relatively rare (Figure 41). This is a main difference to jarosite from zinc production.

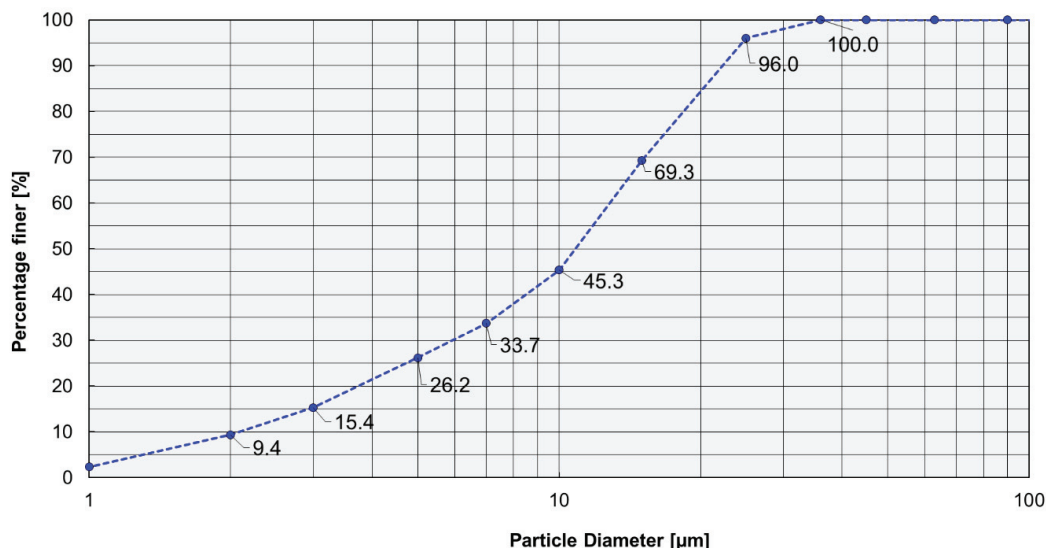


Figure 41: Grain size distribution of a jarosite from platinum production measured by laser granulometry (ARP).

8.8.3 Mineralogical Composition

Due to the less variable origin and chemical composition of this material, the variety of phases is also limited. The reason for this is that this type of residue only contains the iron precipitation product opposite to the jarosite from zinc production, which is a mixture of many different residues from a complex process. According to an XRD analysis, the main phases are ammoniojarosite, (K-)jarosite and hematite. Minor peaks indicate the presence of nickel sulphide, nickel magnesium silicate, gersdorffite and lead oxide (Figure 42). Investigations with a digital microscope and a scanning electron microscope showed that most components are rounded and spherical to elongated. The rim and core of the particles often consist of different phases. An example is a core of iron oxide with a rim of a similar but also nickel and sulphur-containing phase (Figure 43, Figure 44 and Figure 45). The jarosite mineral is mainly ammoniojarosite and often forms rims around iron oxides. It mainly appears as elongated, relatively idiomorphic crystals. In some cases, they also carry up to 1.5 wt.% of nickel and arsenic (Figure 46 and Figure 47). Table 15 shows the chemical composition and calculated atoms per formula unit for 14 jarosite particles, measured using SEM-EDX. According to the process, ammoniojarosite forms. K is totally absent, and Na is only present in small amounts. The limited content of lead in the material also makes plumbojarosite rare; only one of the 15 measurements indicates a jarosite with 4.12 wt.% of Pb. A pure plumbojarosite should contain about 18 wt.% of lead. Ni (<3.76 wt.%) and As (<1.60 wt.%) are very common in the jarosite phase.

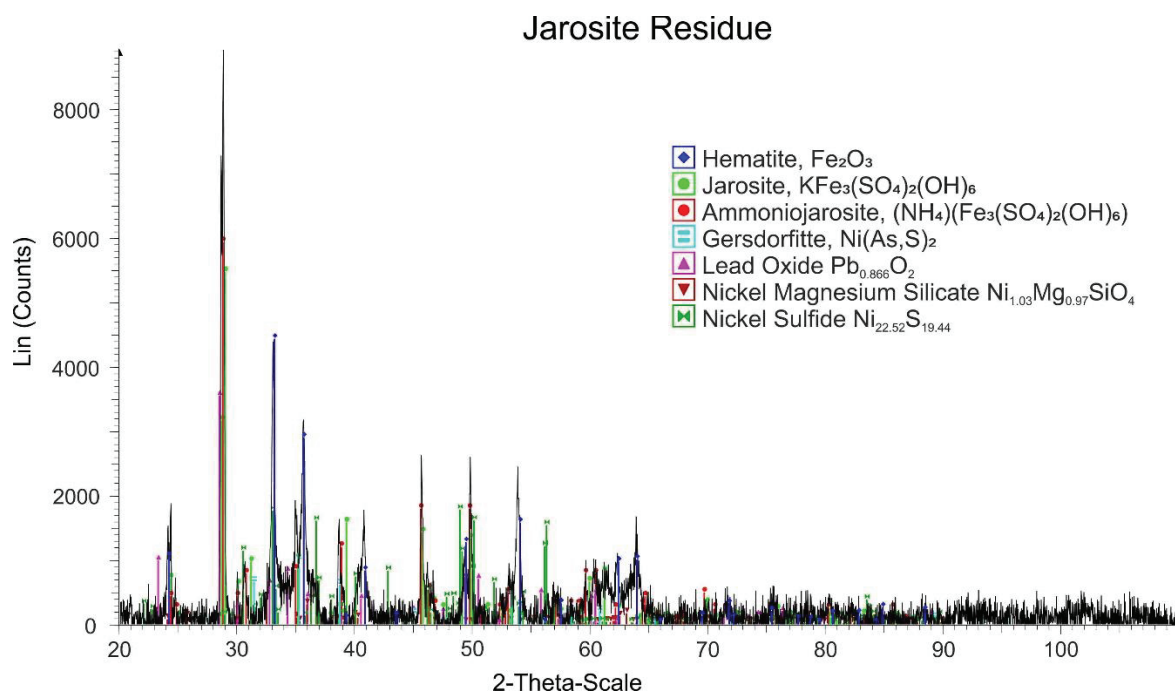


Figure 42: XRD spectra of a jarosite from platinum production. measured by Materials Center Leoben.

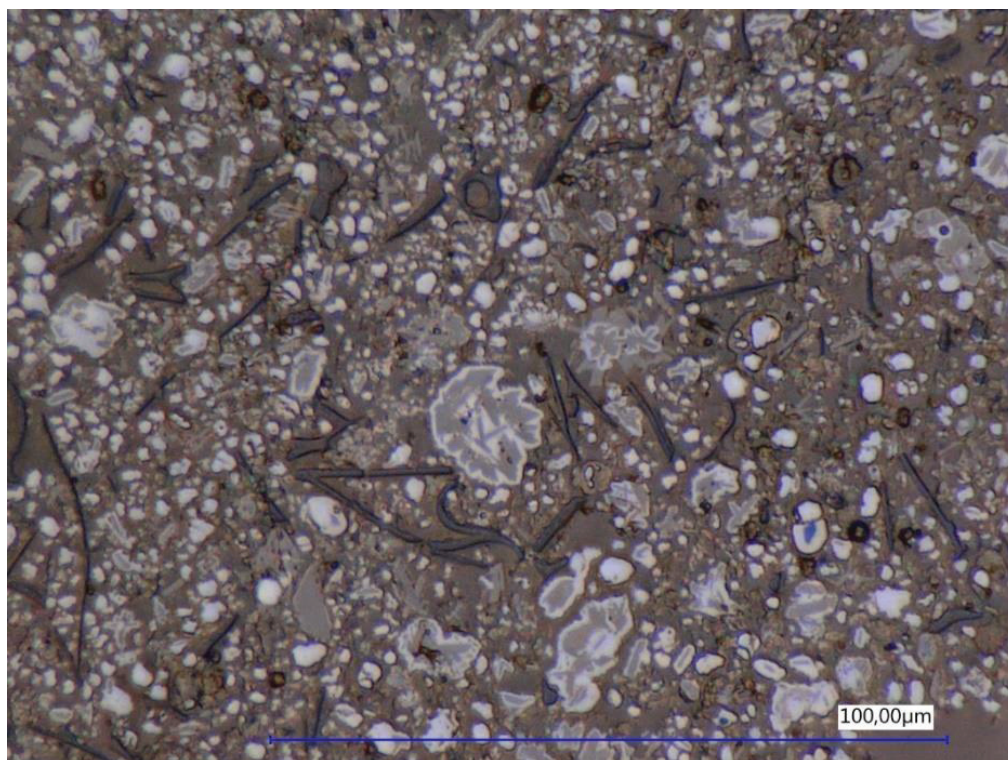


Figure 43: Reflected light photomicrograph of a polished jarosite sample.

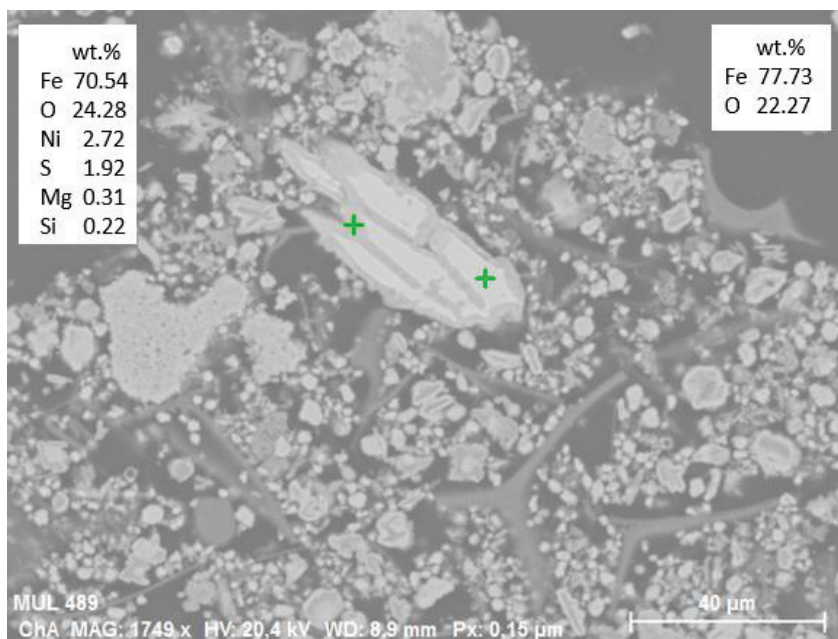


Figure 44: SEM-BSE image of a wuestite grain (right cross and analysis). The surrounding, darker phase (left cross) is also iron oxide, but contains sulphur and nickel in addition (left analysis).

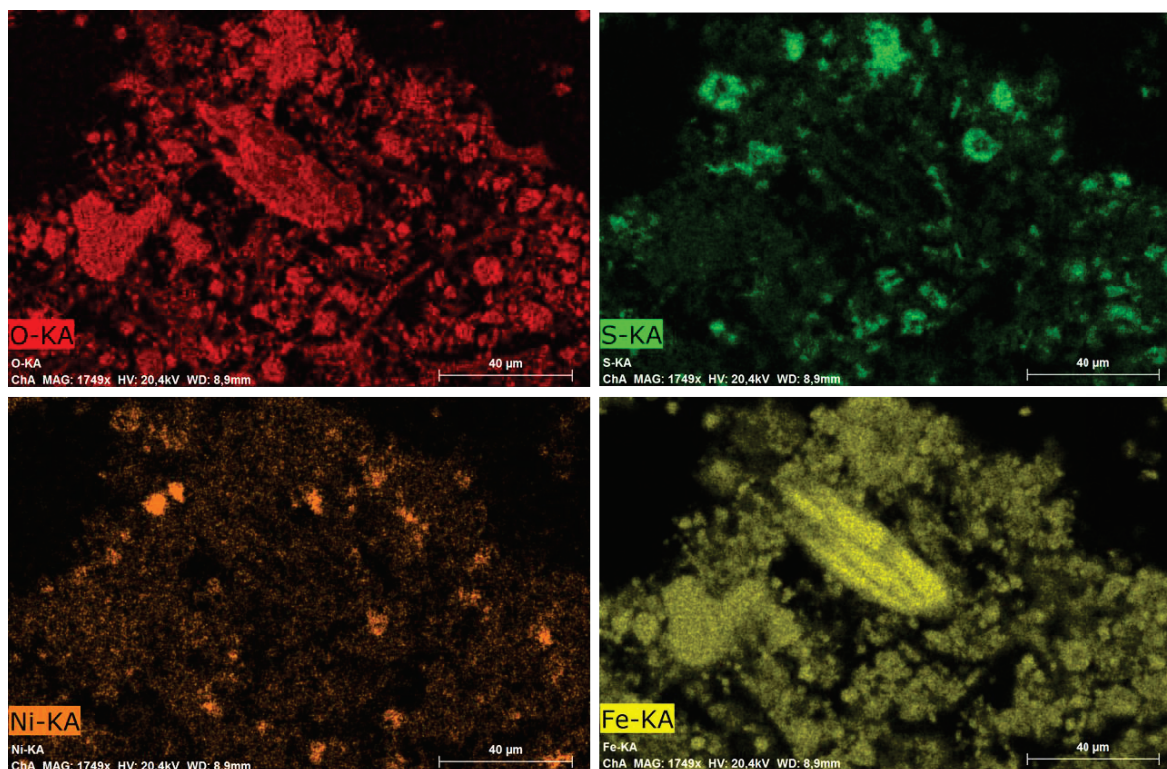
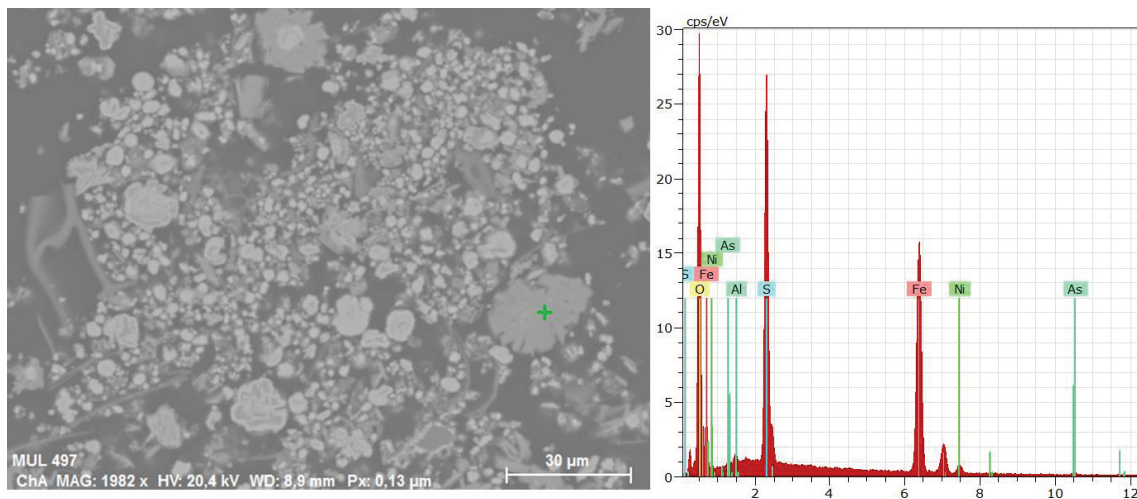


Figure 45: SEM element mapping of the same area as in Figure 44. Opposed distribution of iron and nickel is visible.



Spektrum: Ni Jsit2- 16

El	OZ	Serie	unn. C [Gew. %]	norm. C [Gew. %]	Atom. C [At. %]	Verbindung	Comp. C [Gew. %]	norm. Comp. C [Gew. %]	Fehler (1 Sigma) [Gew. %]
O	8	K-Serie	31,92	38,18	64,25		0,00	0,00	3,93
Al	13	K-Serie	0,36	0,43	0,43	Al2O3	0,81	0,68	0,05
S	16	K-Serie	13,94	16,68	14,00	SO3	41,64	34,81	0,53
Fe	26	K-Serie	34,58	41,36	19,94	FeO	53,21	44,48	0,96
Ni	28	K-Serie	1,52	1,82	0,84	NiO	2,32	1,94	0,09
As	33	K-Serie	1,28	1,53	0,55	As2O3	2,02	1,69	0,11
Summe:			83,60	100,00	100,00				

Figure 46: Example of a large particle of ammoniojarosite in the jarosite residue from platinum production, containing more than 1 wt.% of Ni and As.

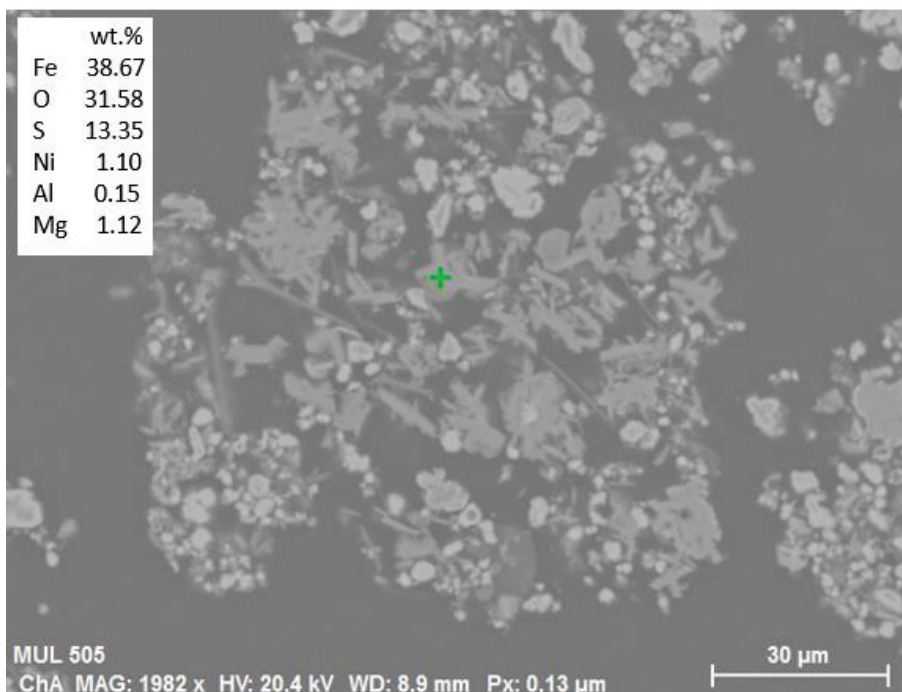


Figure 47: Typical appearance of a jarosite material from platinum production using a scanning electron microscope and a BSE detector. The chemical composition (SEM-EDX) refers to the green crosses and indicates ammoniojarosite.

Table 15: Element composition (SEM-EDX) and calculated atoms per formula unit normalized to 11 oxygen for selected jarosite particles (jarosite from platinum production). Right columns show the composition of an ideal ammoniojarosite and the mean values of all measurements (n=14). Hydrogen and nitrogen are not measurable by the method used.

wt.% oxides															mean	ideal	
H ₂ O	n.a.	n.a.	n.a.	n.a.	n.a.	n.a.	n.a.	n.a.	n.a.	n.a.	n.a.	n.a.	n.a.	n.a.	n.a.	n.a.	11.3
(NH ₄) ₂ O	n.a.	n.a.	n.a.	n.a.	n.a.	n.a.	n.a.	n.a.	n.a.	n.a.	n.a.	n.a.	n.a.	n.a.	n.a.	n.a.	5.4
PbO	0	0	0	0	0	0	0	0	4.4	0	0	0	0	0	0	0	0
Na ₂ O	0	0	0.4	0.9	0	0	0.6	0	0.4	0.8	0	0	0.6	0	0	0	0
NiO	2.3	4.8	2.1	2.3	1.9	1.9	1.8	1.4	2.2	2.1	1.8	1.8	1.7	0	0	2.0	2
Fe ₂ O ₃	46.2	48.7	49.6	53.0	50.1	49.4	47.2	55.3	51.2	49.7	49.0	47.1	45.0	51.3	49.5	49.9	
Al ₂ O ₃	0.4	0.4	0.6	3.0	0.8	0.4	0.3	0.2	0.5	2.4	0.6	0.3	0.3	0	0.7	0	
SO ₃	30.4	27.3	30.0	26.5	32.6	34.8	34.4	33.3	27.5	25.0	31.9	33.4	33.0	31.1	30.8	33.4	
As ₂ O ₃	0.4	1.2	2.1	1.8	1.7	1.7	1.9	0	0	1.7	1.7	1.6	1.8	0	1.2	0	
SiO ₂	1.0	0.8	0.5	0	0	0.0	0.0	0.7	0.5	0	0	0	0	0	0.2	0	
MgO	0	0	0	0	0	0	0	0	0	0	0	0	0	0.2	0	0	
sum	80.7	83.2	85.3	87.5	87.0	88.2	86.1	90.9	86.7	81.8	85.1	84.2	82.3	82.7	85	100.0	
atoms per formula unit															mean	ideal	
A position																	
NH ₄	n.a.	n.a.	n.a.	n.a.	n.a.	n.a.	n.a.	n.a.	n.a.	n.a.	n.a.	n.a.	n.a.	n.a.	n.a.	n.a.	1.0
Pb	0	0	0	0	0	0	0	0	0.1	0	0	0	0	0	0	0	0
K	0	0	0	0	0	0	0	0	0	0	0	0	0	0	0	0	0
Na	0	0	0.1	0.1	0.0	0.0	0.1	0.0	0.1	0.1	0.0	0.0	0.1	0	0	0	0
Ni	0.2	0.3	0.1	0.2	0.1	0.1	0.1	0.1	0.2	0.2	0.1	0.1	0.1	0	0.1	0	0
B position																	
Fe	3.0	3.3	3.2	3.4	3.1	3.0	2.9	3.3	3.4	3.4	3.1	3.0	2.9	3.3	3.2	3.0	
Al	0	0	0.1	0.3	0.1	0	0	0	0.1	0.3	0.1	0	0	0	0.1	0.0	
S	2.0	1.8	1.9	1.7	2.0	2.1	2.1	2.0	1.8	1.7	2.0	2.1	2.1	2.0	2.0	2.0	
As	0	0.1	0.1	0.1	0.1	0.1	0.1	0	0	0.1	0.1	0.1	0.1	0	0.1	0.0	
Si	0.1	0.1	0	0	0	0	0	0.1	0	0	0	0	0	0	0	0.0	
Mg	0	0	0	0	0	0	0	0	0	0	0	0	0	0	0	0.0	
sum A + B	3.4	3.8	3.6	4.1	3.4	3.2	3.2	3.4	3.8	4.1	3.4	3.2	3.2	3.3	3.5	4.0	
A pos	0.2	0.3	0.2	0.3	0.1	0.1	0.2	0.1	0.3	0.3	0.1	0.1	0.2	0.0	0.2	1.0	
B pos	3.1	3.3	3.2	3.7	3.2	3.0	2.9	3.3	3.4	3.7	3.2	3.0	2.9	3.3	3.2	3.0	
Rest A site	0.8	0.7	0.8	0.7	0.9	0.9	0.8	0.9	0.7	0.7	0.9	0.9	0.8	1.0	0.8	0.0	

Iron oxide, and iron-nickel oxides are very common (Figure 48). Table 16 shows SEM-EDX measurements of iron and nickel-bearing phases. “NiJsit2 11” is a jarosite mineral and “NiJsit2 25” is a trevorite, the latter of which appears as an accessory. All other phases are iron oxides containing up to 6.85 wt.% Ni and up to 3.32 wt.% As. Si and Al are, with a few exceptions, below 1 wt.%.

Gangue minerals are also present, but only in small quantities. Quartz can be mentioned as the most frequent one.

Table 16: SEM-EDX measurements on selected grains (iron-nickel phases) on a polished section of jarosite from platinum production.

wt.%	Fe ₂ O ₃	NiO	As ₂ O ₃	SO ₃	SiO ₂	Al ₂ O ₃	sum
NiJsit2 1	56.71	4.15	1.11	22.27	0.64	0.74	85.62
NiJsit2 2	79.48	4.66	3.47	4.04	1.05	0.00	92.70
NiJsit2 3	77.29	5.12	1.72	3.80	2.52	0.79	91.23
NiJsit2 4	87.15	4.30	2.38	3.87	0.86	0.00	98.55
NiJsit2 11	46.24	2.32	0.38	30.36	0.00	0.00	79.30
NiJsit2 12	64.09	4.31	1.78	14.33	0.77	0.00	85.29
NiJsit2 13	83.47	4.84	1.69	3.99	1.20	0.42	95.60
NiJsit2 14	73.22	5.68	1.57	6.47	2.10	0.45	89.49
NiJsit2 21	60.26	4.33	1.65	13.71	0.86	0.55	81.35
NiJsit2 22	79.31	5.12	2.77	5.04	2.16	0.87	95.27
NiJsit2 23	61.10	15.46	0.77	5.59	5.80	1.66	90.38
NiJsit2 24	75.54	7.14	0.66	3.37	4.23	0.00	90.95
NiJsit2 25	23.47	26.25	0.13	6.64	8.30	2.85	67.65

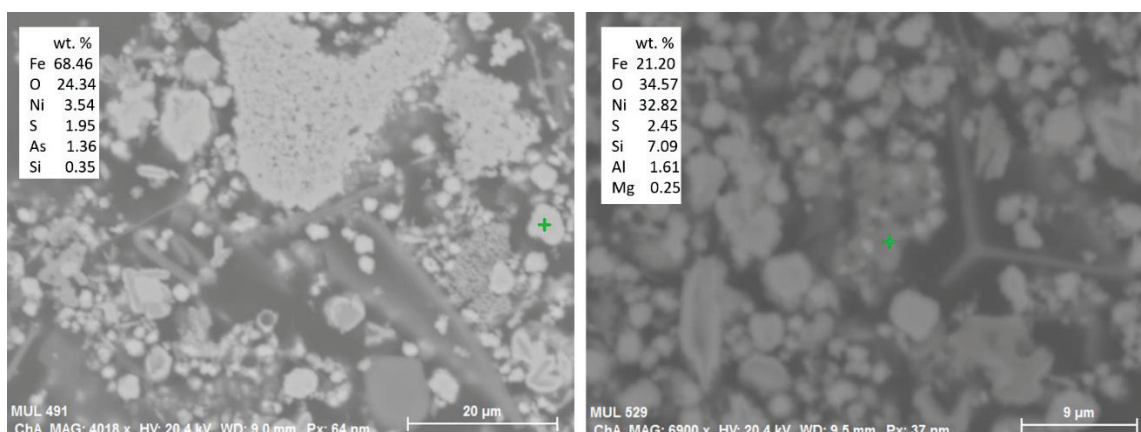


Figure 48: SEM-BSE image and EDX measurements of iron-nickel oxide grains.

9. Proposal for Utilisation

Generally, extraction of only one valuable metal from jarosite residues would be uneconomical. The only way to make the material worth treating is a method that produces several metals in one process. A new process of pyrometallurgical treatment was developed at Montanuniversität Leoben that allows the winning of various metals within a two-step process (calcination-reduction).

As the major part of the material would not be valuable metals, but slag components (in the proposed treatment), a large amount of material must be melted in comparison to the valuable output. This is very energy-intensive and therefore a serious problem in the economic consideration of this kind of treatment. A pre-treatment in terms of mineral processing would be a benefit for the overall process.

9.1 Possible Beneficiation

An important reason for the mineralogical characterisation of residues is to gain information that can be used to develop or adapt proper methods of mineral processing. In the case of a usual jarosite residue, this is not possible, since the jarosite mineral, the main component in the residue, contains considerable amounts of lead and zinc. As both are main metals of interest, it does not make sense to separate the jarosite mineral. Furthermore, other phases that are valueless are too small in quantity to be worth any treatment for removing one.

The situation is similar for the jarosite from platinum production. Due to the importance of iron and thus the jarosite mineral, a beneficiation of this material is not reasonable. Phases that are free of nickel or iron are too low in quantity to be worth any beneficiation steps.

9.1.1 Flotation Trials

Flotation uses the different wettability of minerals and is predominantly performed in an aqueous environment. As most minerals show hydrophilic behaviour, the addition of various reagents which convert the surface properties of specific components to hydrophobic is necessary to achieve a separation of phases. These “collectors” usually consist of a hydro-carbon chain and a positively or negatively charged polar head. Minerals often show a similar affinity for the same group of collectors. A combination of collectors

and the use of other reagents that work as activators, depressants, modifiers and pH regulators allows a more selective separation of specific phases (Metso Corporation, 2015). The flotation tests were performed using a standard Denver D12 laboratory flotation machine at the company MinProSol in Leoben. The steel flotation cell has a volume of 1.2 dm³. The rotor and stator material are polyurethane. A standard Rushton turbine, such as the one provided with the Denver flotation machine, was used as an impeller. Drying of the material before flotation is not necessary, and would actually cause serious problems due to the formation of hard agglomerates. Therefore, the jarosite material was added to the flotation exactly the way it was received from the production site, without any treatment. The gas velocity in the cell was adjusted by the rotational speed of the rotor in order to achieve conditions comparable to industrial-scale flotation machines. The reagents used are also of industrial quality.

The aforementioned residue from an African zinc plant proved to be treatable in terms of flotation. It is a special kind of leaching residue and is comparable to common jarosite residues concerning valuables but has a much lower amount of iron and much higher amount of calcium (Figure 49). It was shown, that up to 50 % of the material is gypsum. A flotation of gypsum in this special case could substantially increase the economic potential of this material, as it would considerably relieve the following pyrometallurgical process in terms of energy consumption.

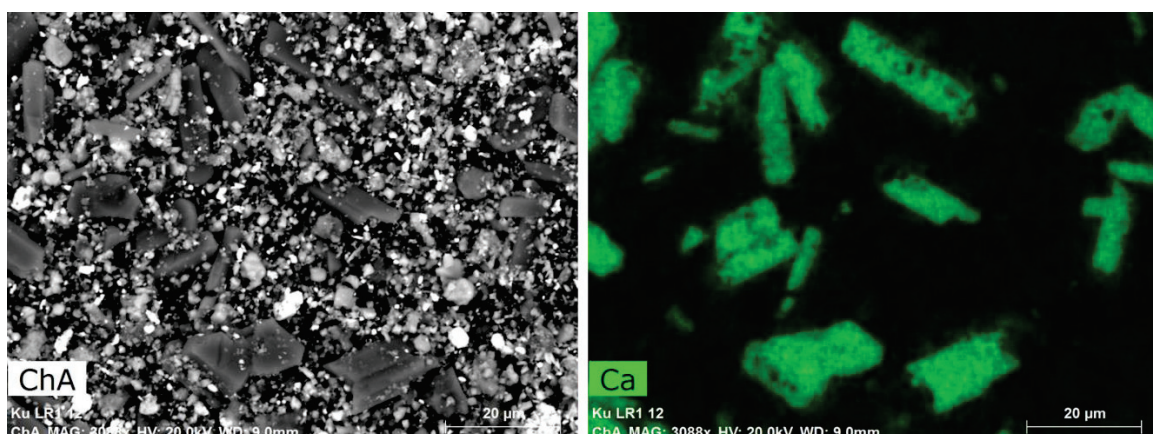


Figure 49: SEM element mapping of an African leaching residue. The calcium distribution matches the appearance of gypsum, as it is the only calcium bearing phase.

9.1.1.1 Results from Flotation Trials

The trials were performed for two different jarosites. Sample 1 is the above-mentioned special type of jarosite with a high amount of gypsum. Sample 2 is a very typical jarosite and representative of most zinc plants. Contrary to many other common methods of mineral processing, the material can be concentrated by means of flotation despite the frequently mentioned small grain size. However, there are several challenges to be managed:

- The small grain size requires a long residence time to achieve satisfying separation.
- Due to the complex chemistry of the material, a change in the properties of particles due to the formation of layers of various phases around the particles may occur.
- The formation of microflocs decreases the concentration grade considerably, as non-floating particles are locked in flocks of floating particles.
- The development of a reagent regime which allows a high selectivity between valuable phases and those with no value and which is applicable for such a complex material in terms of appearing mineralogical phases.

For both samples, different reagent regimes were used, since the targeted minerals were different ones. Whilst the task for sample 1 was to remove gypsum, the trials for sample 2 focused on removing the jarosite mineral. Even though sample 2 also contains some gypsum, it is by far not enough to be of importance.

However, the results of the gypsum removal were surprising, as lead bearing phases were recovered to the froth phase. After some adjustments in the reagent regime, it was possible to remove a major part of the gypsum and concentrate the valuables (mainly lead). The highest lead recovery was achieved in one trial with 85 % of lead in 62 % of the material (Figure 50). The concentration of zinc was not as successful as the one for lead. However, the best reagent regime for zinc is the same as for lead.

Copper enrichment was also best with the same composition of additives, with about 75 % of copper in 62 % of the material (Figure 51). The following figures show two diagrams of lead and copper concentration out of two test series. The amount of material transferred to the concentrate is illustrated on the horizontal axes; the vertical axes show the recovery of the element in the concentrate in wt.%.

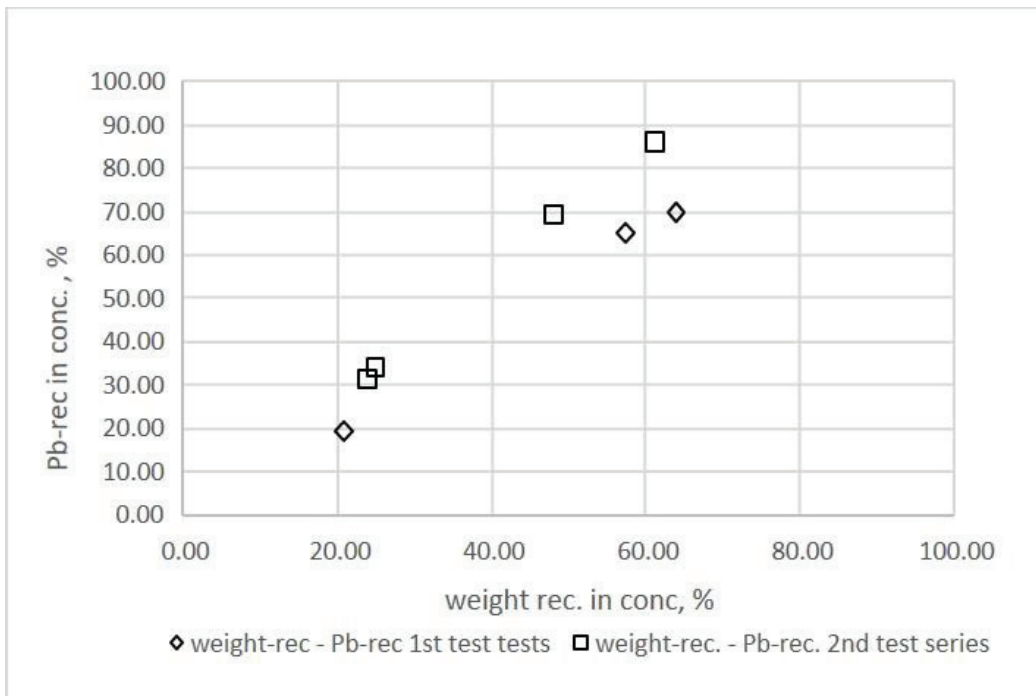


Figure 50: Lead recovery achieved in concentrate out of flotation trials with two different reagent regimes and parameter settings with the aim of removing gypsum from a jarosite residue.

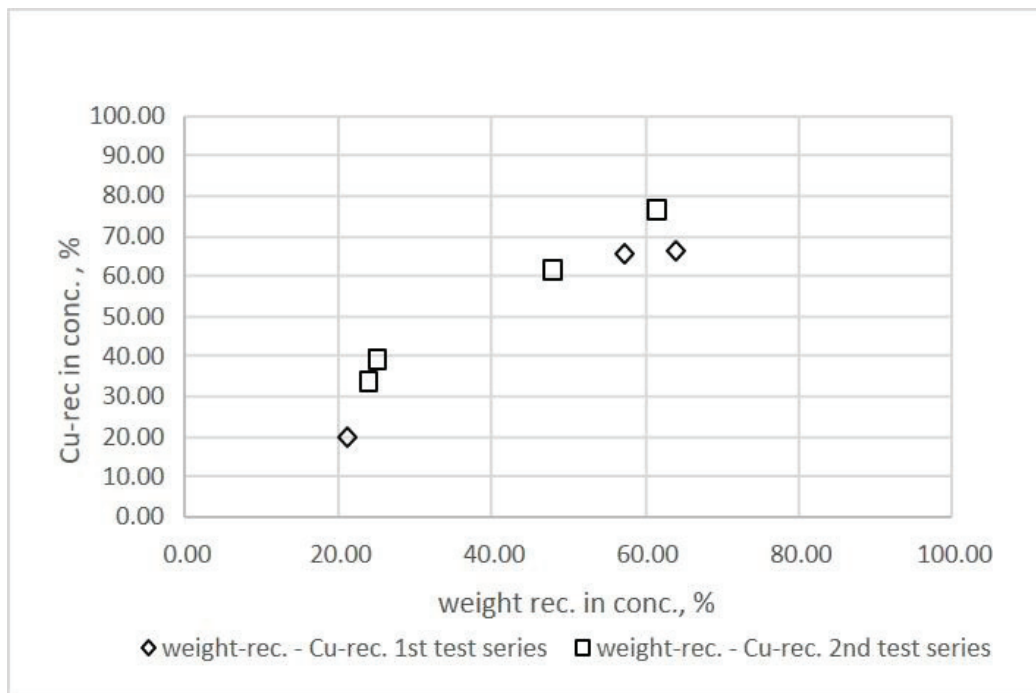


Figure 51: Copper recovery in concentrate after removing gypsum from a jarosite residue from trials with two different reagent regimes and parameter settings.

Not only the concentration of valuables and a reduction of the material that must be treated is beneficial for the following process; gypsum, or its water free equivalent anhydrite, which is formed by the loss of water at temperatures above 190°C, is stable in the roasting step, keeping sulphur in the calcine. In the following reduction, this sulphur would cause problems when forming sulphide phases with valuable metals which are then lost. A removal of gypsum is therefore not only beneficial in reducing the amount of material and concentrating the valuables, but also in increasing the output of metals in the final product.

The trials on sample 2, which is a more typical jarosite, were not as successful. Removal of the jarosite mineral did not show any positive effects on the amount of valuables. This is obviously due to the fact that the jarosite mineral hosts a considerable amount of the total valuables. This mainly affects lead, as the main value carrier in the jarosite material. Removal of any other phase is not relevant due to their small quantity.

It must be concluded that a beneficiation by flotation is only promising in special cases. Figure 52 and Figure 53 show the recovery of lead and zinc in the flotation concentrates.

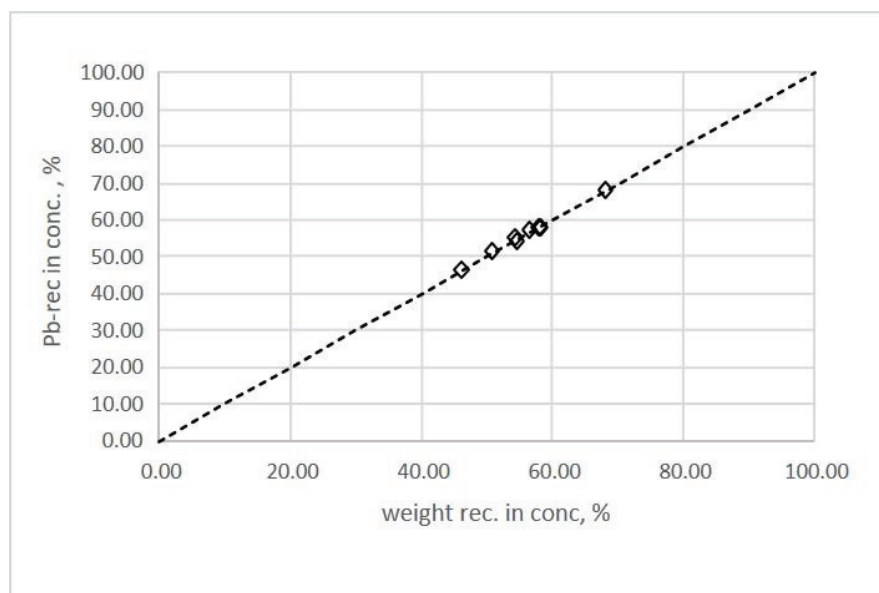


Figure 52: Results from flotation trials on a typical jarosite sample. The diagram shows the recovery of lead achieved with different reagent regimes and parameter settings.

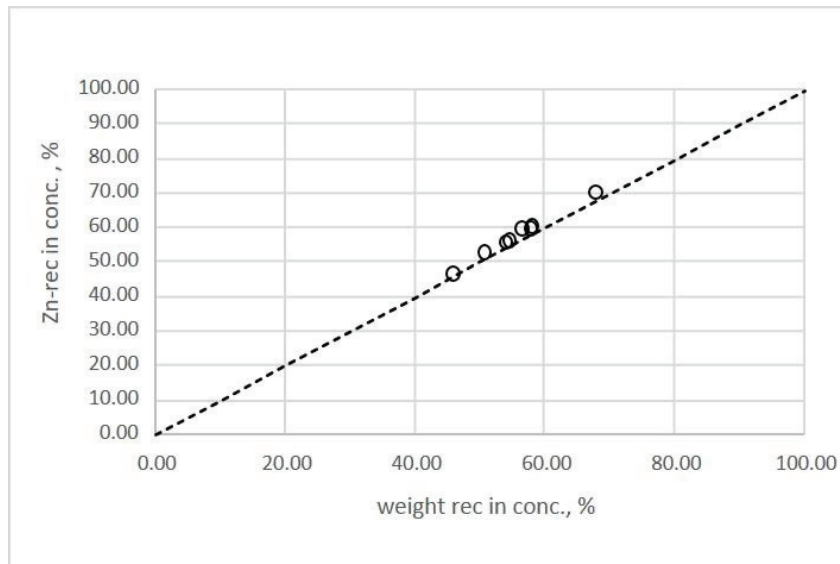


Figure 53: Results from flotation trials on a typical jarosite sample. The diagram shows the recovery of zinc achieved with different reagent regimes and parameter settings.

9.1.2 Grain Size Separation

The grain size distribution was determined by a sieving analysis. Unlike other methods like CILAS, this method has the advantage that each grain size fraction is available as a sample. Chemical and mineralogical investigations on selected fractions did not show any difference in the valuables. Microscopic investigations also indicated poorly separated fractions due to abundant agglomerates (Figure 54 and Figure 55). This problem adulterates the distribution only towards larger grain sizes, as particles which pass a specific mesh size cannot be larger than the targeted diameter. Table 17 shows a comparison of silver, lead and zinc of the original, untreated jarosite material and the fraction smaller than 10 μm . Regardless of any troubles during sieving, the finest fraction definitely only contains particles below this grain size. However, the chemical analyses of the fractions are too similar to leave any room for interpretation concerning the usability of grain size separation.

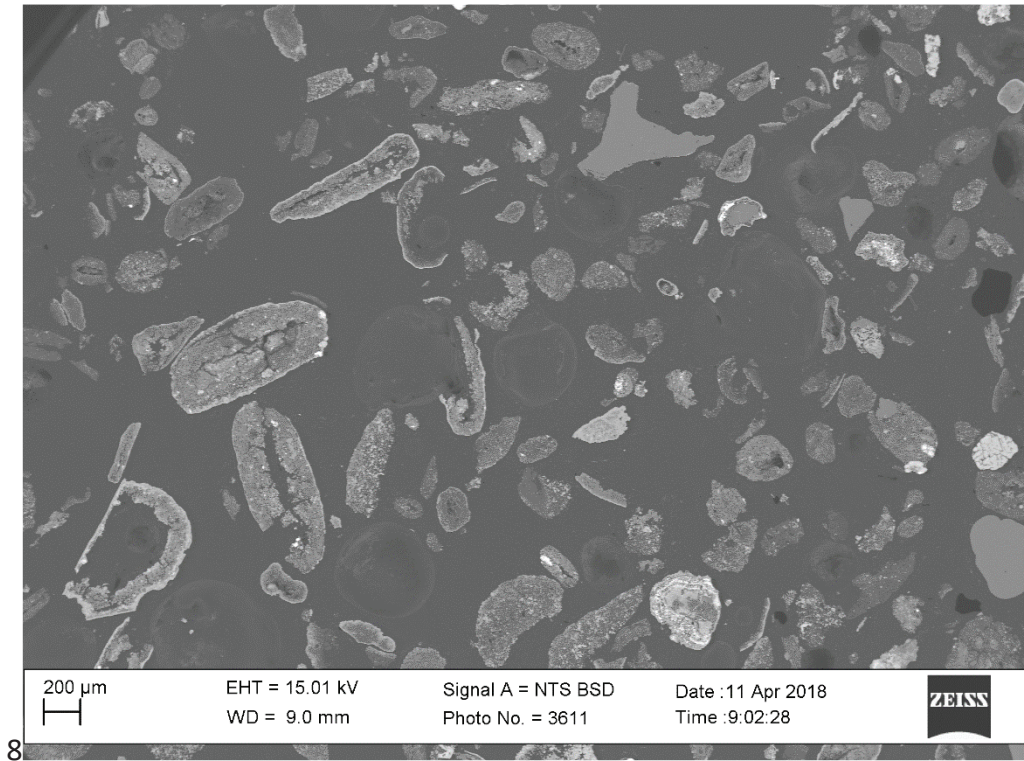


Figure 54: SEM image of the sieve fraction larger than 200 μm prepared as a polished section. Most of the particles are not single grains, but agglomerates.

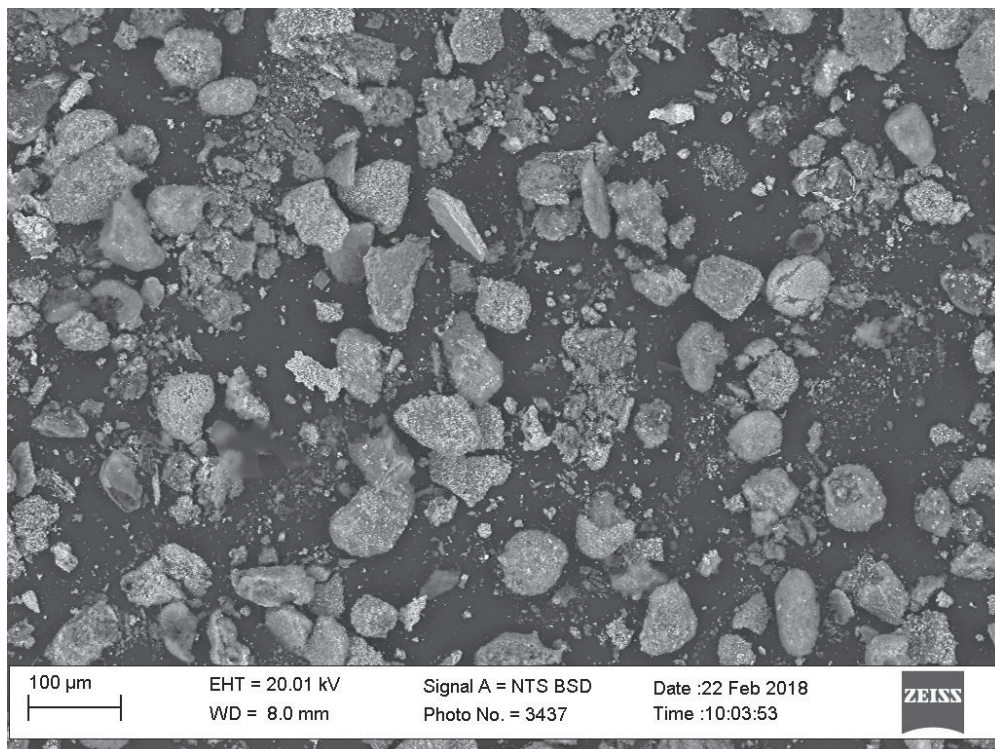


Figure 55: SEM image of the fraction 45-63 μm prepared as a strewn slide, showing numerous agglomerates.

Table 17: Comparison of valuable elements in a jarosite residue and the fraction smaller than 10 µm measured by AMCO with ICP-OES.

	Total jarosite	Fraction <10 µm
Ag	235 ppm	235 ppm
Pb	5.0 %	5.2 %
Zn	4.2 %	3.8 %

9.1.3 Magnetic Separation

High gradient magnetic separation was tested on the jarosite material at MinProSol. The challenges and results are very similar to those for the grain size separation.

Trials V1 to V5 were individual tests with increasing magnetic field strength, whereas in V6 the non-magnetic fraction of one trial was treated again in another trial with increasing magnetic field strength, and so forth (V6 Tap 1- V6 Tap 5). “V6 Tailings” is the non-magnetic fraction of the last run. The fractions contain numerous agglomerates which exclude a serious separation of phases (Figure 56). Chemical analysis showed only minor, negligible differences.

The fractions from trials V6 Tap 1 and V6 Tap 2 show a decrease in lead and an increase in zinc (Table 18). However, there is in fact no benefit to this, because lead and zinc were enriched in both separated products after magnetic separation and no valueless fraction was created.

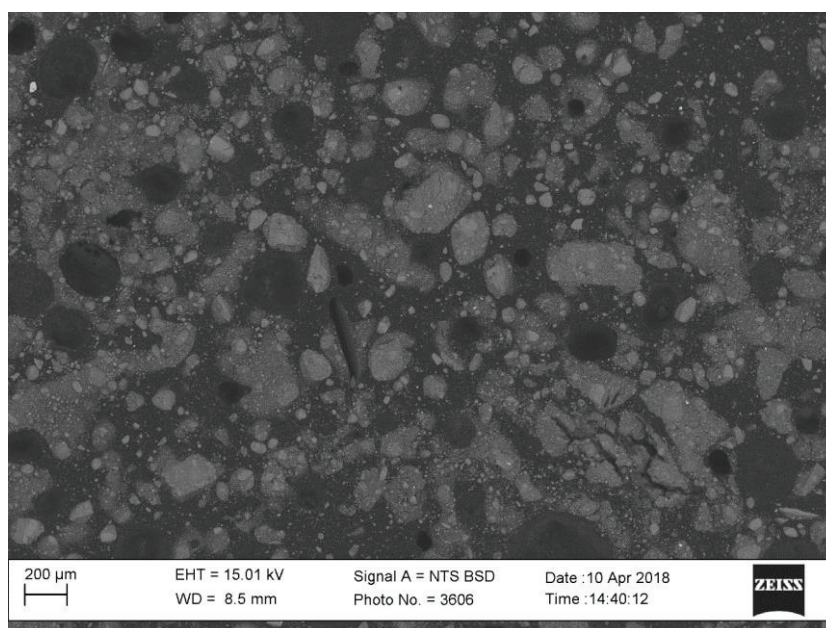


Figure 56: SEM BSE image of a sample from the non-magnetic fraction of V6 Tap 5 showing numerous agglomerates.

Table 18: Chemical analyses of fractions from HGMS trials performed by MinProSol.

wt.%	PbO	Ag ₂ O	ZnO	CuO	Fe ₂ O ₃	SiO ₂	CaO	Al ₂ O ₃	Na ₂ O	SO ₃
V1 mag	No analyses; insufficient sample material.									
V1 nmag	7.04	0.04	4.56	0.75	45.80	7.07	0.39	2.37	4.16	24.98
V2 mag	No analyses; insufficient sample material.									
V2 nmag	7.61	0.05	4.61	0.82	47.86	5.97	0.53	2.06	3.50	24.05
V3 mag	6.82	0.03	7.16	0.77	50.25	4.38	0.32	2.16	3.91	21.34
V3 nmag	7.56	0.05	4.55	0.77	47.60	6.50	0.46	2.00	3.54	24.04
V4 mag	7.11	0.03	6.71	0.85	50.77	3.56	0.32	2.06	3.66	21.99
V4 nmag	7.31	0.05	4.51	0.52	47.06	7.29	0.50	2.06	3.70	24.09
V5 mag	7.29	0.03	6.95	0.82	61.08	3.28	0.31	1.96	3.47	21.99
V5 nmag	7.60	0.05	4.61	0.52	47.61	7.26	0.48	2.04	3.47	23.32
V6 Tap 1	3.11	0.02	14.59	0.72	57.22	10.84	0.39	2.12		10.84
V6 Tap 2	5.04	0.03	9.31	0.66	48.13	7.77	0.34	2.63	5.04	18.07
V6 Tap 3	6.20	0.03	6.99	0.49	46.85	6.04	0.29	2.64	4.74	22.75
V6 Tap 4	7.06	0.03	5.75	0.54	48.05	4.74	0.30	2.41	4.32	24.02
V6 Tap 5	7.60	0.04	5.46	0.79	49.48	3.84	0.34	2.23	3.66	23.61
V6 Tailing	7.16	0.04	3.95	0.75	45.56	6.35	0.28	2.19	4.18	26.87

9.2 Pyrometallurgical Treatment

The idea behind the process is a combination of calcination and reduction. The first step (calcination) removes all volatile compounds, especially the sulphur, through the off-gas. In the second step (reduction) the remaining material is melted. A metal bath is used to collect most of the valuables (Figure 57). Additionally, volatile metals and compounds are collected in the off-gas. Finally, three products are produced:

- At the bottom of the furnace, the metal bath contains most of the valuable metals. Lead and silver are of the highest interest, as they constitute most of the value, but other metals such as copper and gold also are collected in the alloy.
- The off-gas from the reduction process contains the zinc. As it is very easily re-oxidised in contact with air, it appears as relatively pure ZnO. Furthermore, indium is also usually associated with the zinc and is found in the off-gas. Due to the low boiling point of lead oxide (1 470°C), which is very close to the aimed process temperature, some lead oxide will also be volatilised and escape through the off-gas.

- The final slag, which is a fayalitic slag when treating the jarosite from zinc production, will only contain very little remnants of metals. It may be used as construction material or as an additive or replacement for natural components. If it is not usable as such, it is at least much easier to dump than the jarosite.

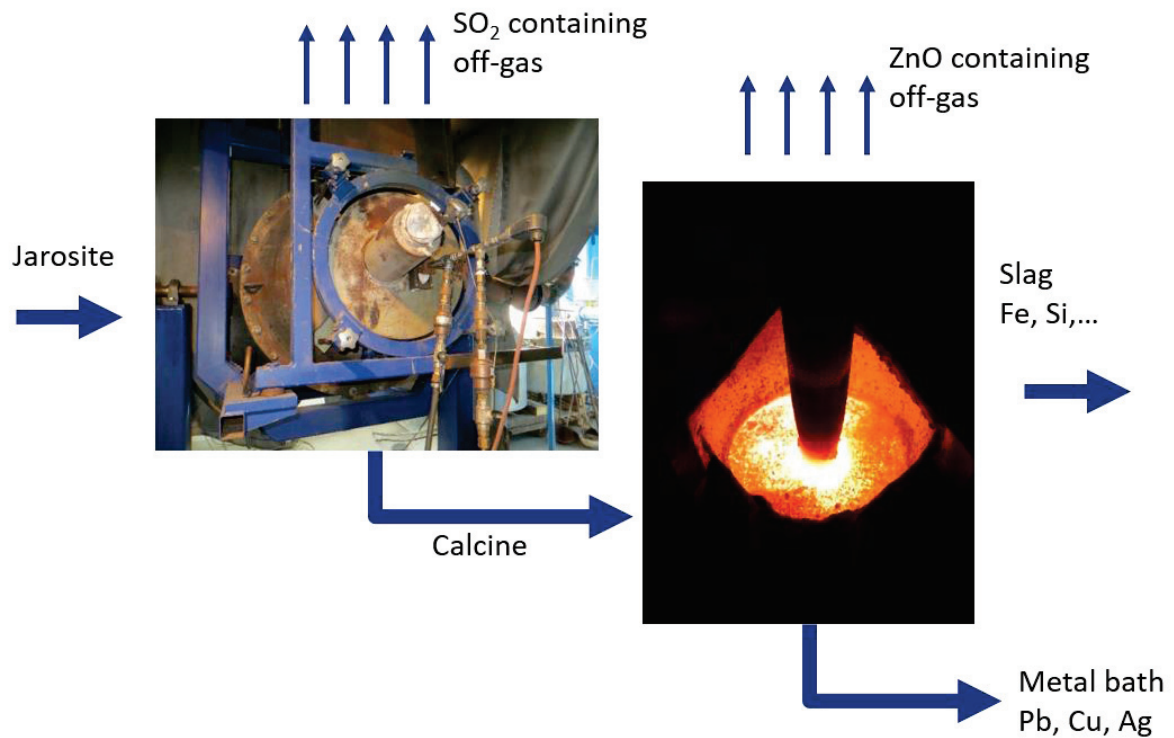


Figure 57: Sketch of the roasting-reduction process for jarosite.

9.2.1 Preparation for Pyrometallurgical Treatment

The very small grain size would cause different problems during further treatment. As soon as the material is dry, it would generate a lot of dust that is difficult to handle and contaminates devices and facilities. Furthermore, a significant part of the material would be lost in the off-gas stream. Therefore, it is necessary to increase the grain size. This can be done by agglomeration with state of the art devices. If the material itself does not agglomerate well, it is necessary to use an additive as a binder. Calcium hydroxide and bentonite are commonly used additives.

9.2.2 Calcination

The first pyrometallurgical step is the calcination of the material between 800-900°C. Volatile phases, especially sulphur, are removed in this process step through the off-gas. The temperature is the essential factor, since it should be high enough to remove specific components but must not remove any of the valuable elements. Removal of sulphur is important, as it would produce sulphidic phases instead of metal during reduction.

9.2.3 Reduction of Jarosite from Zinc Production

After roasting, the calcine is melted in an electric furnace under reducing conditions. Zinc is reduced, volatilised and immediately re-oxidised when coming in contact with oxygen in the off-gas unit. Other valuable metals are collected in a metal bath. Lead, iron and copper are the metals that are at least theoretically usable for this bath. The following table (Table 19) summarises the three possible collector metals and their advantages and disadvantages:

Table 19: Pros and cons of different metals used as collectors.

	Pros	Cons
Lead	Relatively high amount in jarosite. Superior collector for various metals like silver, copper and gold. Low temperature needed and easy to reduce from its oxide.	Difficult to handle due to low evaporation point and low viscosity. Iron stays in the slag, so a high amount of slag is produced.
Copper	Easier to handle than lead and also a good collector for other metals.	Copper scrap must be added, as the jarosite contains only little amounts of Cu. Copper scrap is very pure and expensive. During the process the added copper loses value because it becomes less pure compared to the scrap. Furthermore, it is not as good as a collector compared to lead and more energy-intensive due to its higher melting point. Iron also stays in the slag.

	Pros	Cons
Iron	Low amount of slag, as iron is recovered in the metal bath.	Very energy-intensive. Not really usable as a collector for other metals.

Due to the reasons stated, lead remains the only alternative as the collector in the metal bath, even though it is difficult to handle because of its very low viscosity when liquid and its toxicity when vaporised. In this case, iron forms the main part of the fayalitic slag (Fe_2SiO_4). In all of the investigated jarosites, SiO_2 is too low to bind all of the iron in fayalite. Hence, quartz sand has to be added to achieve the correct chemical composition.

9.2.4 Reduction of Jarosite from Platinum Production

Whereas the calcination is analogous in both types of jarosite, the process of reduction is different even though the process design is similar. The main difference is that iron and nickel are reduced and the final product is an iron-nickel alloy that can be sold as such. As a result, for the jarosite from platinum production, an iron bath is the only option. The iron is not a slag forming element in this case, but rather a main component of the alloy.

9.3 Pyrometallurgical Trials on Jarosite from Zinc Production

The idea of pyrometallurgical multi-metal recovery was verified on jarosite material with a number of trials in different scales. The slag produced from two batches (9.3 kg) was evaluated at W2V in Guimarães (Portugal) for usability as a replacement for sand in concrete. One representative trial is described in this chapter.

9.3.1 Pre-treatment

The jarosite was dried and afterwards pelletized with a disc pelletizer. In this case, the addition of water was enough to produce stable pellets (Figure 58). No other additives were necessary. The final grain size of the pellets produced was about 3-10 mm in diameter.



Figure 58: A disc pelletizer (left) was used to agglomerate the jarosite. The right picture shows the jarosite pellets.

9.3.2 Calcination

In the first step of the pyrometallurgical treatment, 33.36 kg of pellets were treated in a top-blown rotary converter for two hours at a temperature of about 850°C. After calcination, 19.10 kg of material was left, representing a weight loss of about 43 %. Theoretically, mainly SO₂ and OH groups were removed. In fact, other elements were also at least partly volatilised. The reason is the technical layout of the TBRC, where the flame itself is naturally hotter and heats parts of the charged material higher than the targeted temperature, causing evaporation of other elements as well. This problem will not occur in a larger TBRC, as the distance between the flame and charge (Figure 59) is larger. Jarosite is the main carrier of sulphur, hydrogen and oxygen. The following reaction equations (9-1 to 9-4) describe the decomposition of the different jarosites:

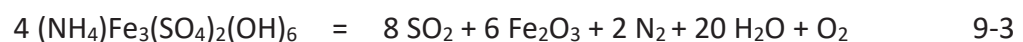
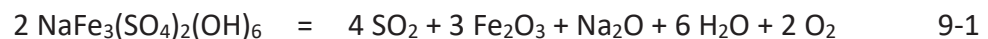




Figure 59: Left: Tapping of calcine from the TBRC. Upper right: opened cap of the TBRC. Note the flame of the gas burner. Lower right: freshly calcined, still-glowing jarosite pellets.

9.3.3 Reduction

For proper separation of slag and metal, it is helpful to add the jarosite material to an already molten slag and an existing metal bath. Therefore, 1.87 kg of synthetic fayalite slag was produced prior to the jarosite trials to act as a starting slag in the actual trial (Figure 60). The following components were added to the fully liquid pre-slag in order to increase the amount of slag and receive a slag as similar as possible to a slag expected to form from jarosite reduction:

5.87 kg	Fe_3O_4
0.33 kg	Al_2O_3
0.20 kg	CaO
2.28 kg	SiO_2

After all of the slag components were molten, a metal-bath was prepared. This consisted of 26.64 kg of metallic lead. Within 35 minutes, all of the jarosite was charged in small batches into the fully liquid load (Figure 61). 5.99 kg quartz sand and 2.14 kg magnetite

were also added to adjust the slag resulting from the jarosite to a correct fayalite composition. According to the amount of metals to be reduced, 0.5 kg of carbon should have sufficed, but as a precaution, 1.2 kg of petroleum coke were added. As expected, the liquid lead percolated through the furnace due to its very low viscosity. To avoid this, an airstream was installed to cool the bottom of the furnace. However, a reliable analysis of the metal bath is not possible. The success of the trial was controlled by the amount of the valuables in the slag. Even though the share of metals did not get as low as expected (2.3 % ZnO and 2.8 % PbO), the trial was ended after 3 hours. Most of the slag was tapped into water to produce slag grains the size of around one centimetre (Figure 62). Investigations showed that the slag contained drops of metallic lead, most likely resulting from the turbulent conditions within the furnace. Another (larger) facility might reduce or even avoid this problem. Other trials proved that a much lower amount of under 1 % for lead and zinc in the slag is definitely feasible.

The most important reactions during the reduction are (equations 9-5 to 9-8):



Figure 60: Synthetic pre-slag of fayalite composition. The mould is about 15 cm wide.



Figure 61: Left: Electric furnace used for reducing the jarosite calcine. Upper right: Calcine is fed but not yet completely molten. White smoke indicates evaporating zinc. Lower right: The whole load is molten. White smoke is nearly gone.

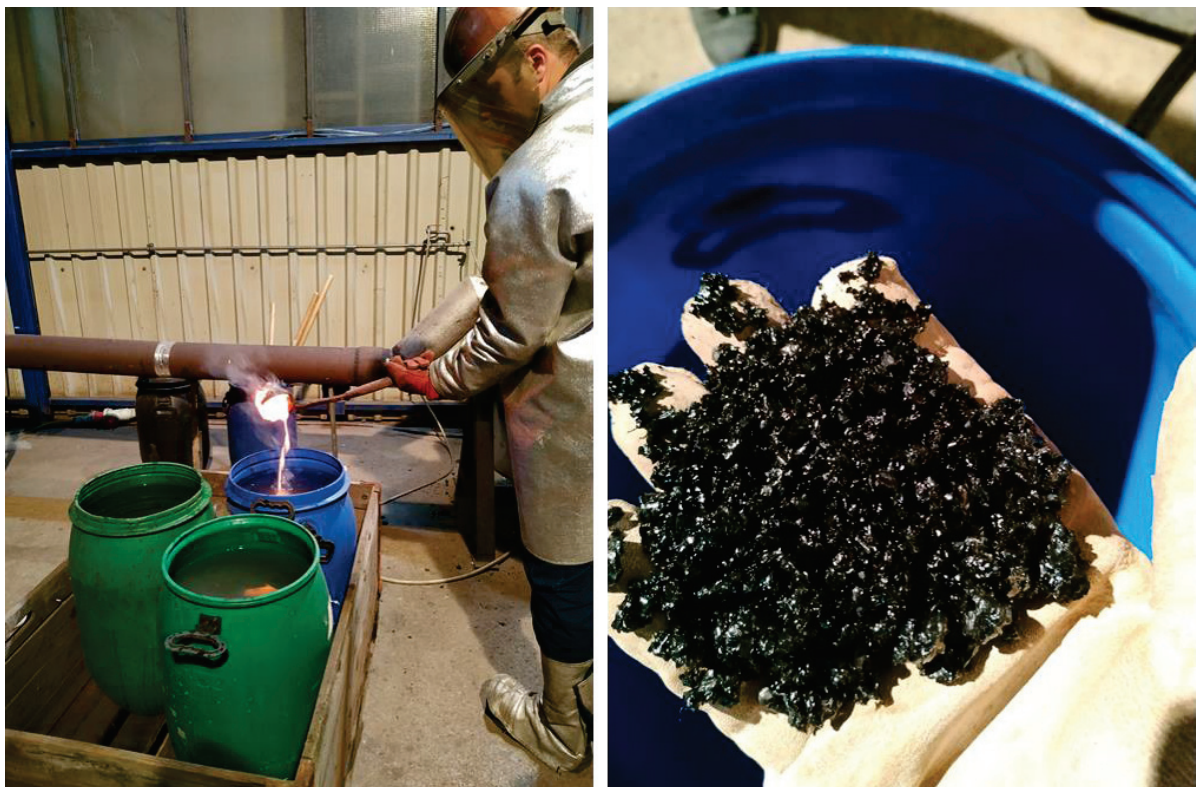


Figure 62: Left: tapping of slag into a water drum. Right: Quenched slag.

9.3.4 Use of the Slag

After the pyrometallurgical trials, about 10 kg of slag were sent to an external institution (W2V, Guimarães, Portugal) in order to evaluate the usability of the slag as construction material. The mechanical behaviour and environmental compliance were evaluated. The objective was, to replace natural aggregates, such as sand, with slag in a Portland cement based concrete.

The slag used was from two reduction trials of jarosite from a European zinc smelter. After 3 hours of treatment, the slag was quenched in water (Figure 62). The grain size distribution was as follows (Figure 63):

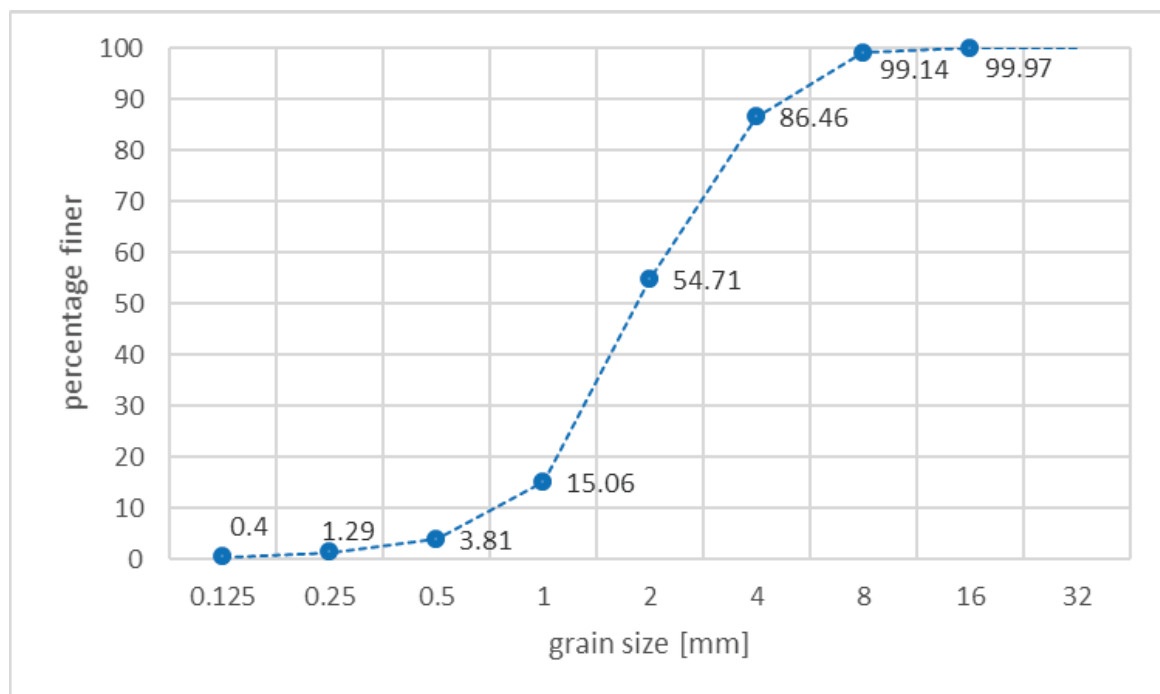


Figure 63: Grain size distribution of the slag determined by sieve analysis at W2V.

After crushing, the sample material was divided into three different grain fractions:

- <1 mm
- 1-2 mm
- 2-4 mm

For the following compressive and flexural strength tests, different concrete samples were mixed. Each consisted of 25 % Portland cement (strength class 32.5) and normalised sand (EN 196), which was replaced by different ratios of slag (Table 20).

Table 20: Composition of the different cement-sand-slag mixtures.

Reference	% Cement	% Sand	% Slag <1mm	% Slag 1-2mm	% Slag 2-4 mm
1	25	75	0	0	0
2	25	72	5	0	0
3	25	65	10	0	0
4	25	55	20	0	0
5	25	72	0	5	0
6	25	65	0	10	0
7	25	55	0	20	0
8	25	72	0	0	5
9	25	65	0	0	10
10	25	55	0	0	20

The amount of added water was between 13 and 16 %. This was done with all three grain size fractions. One sample was tested without slag in order to get values for comparison. In total, ten mixtures were evaluated. For each mixture, 12 samples were tested for compressive strength and 6 for flexural strength evaluation. One half of each was tested after 7 days of curing time; the other half after 28 days. The following figures show the results of the tests (Figure 64 and Figure 65).

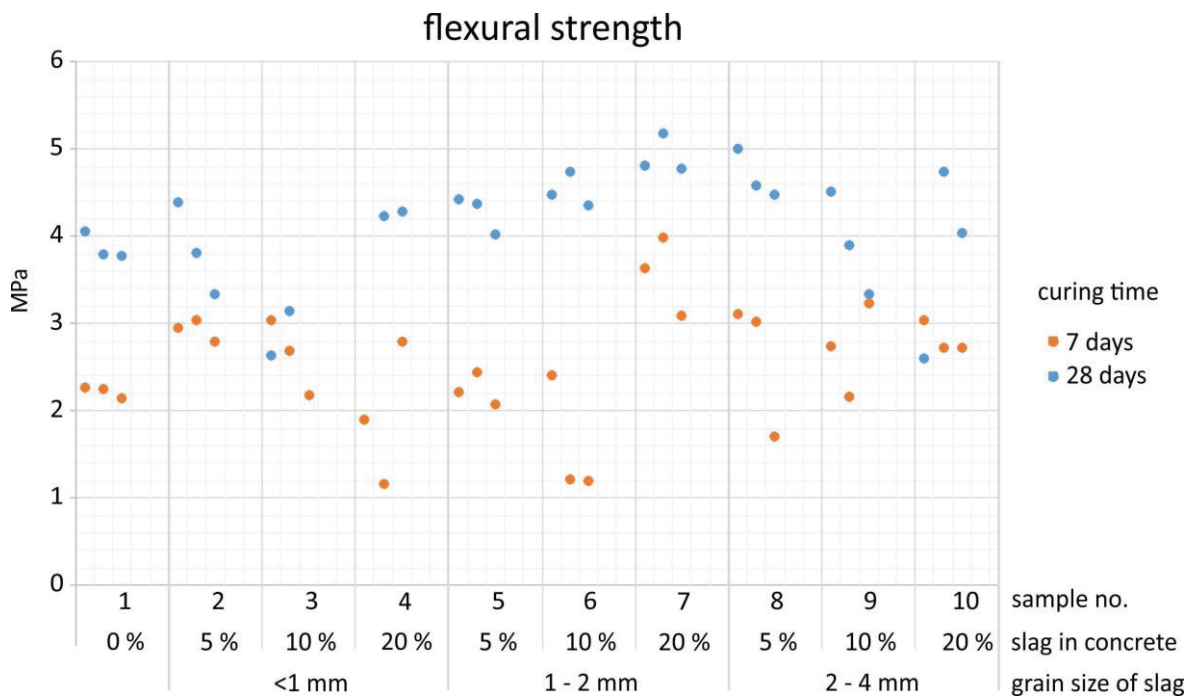


Figure 64: Trials for evaluation of flexural strength on 10 different mixtures of cement, sand and slag.

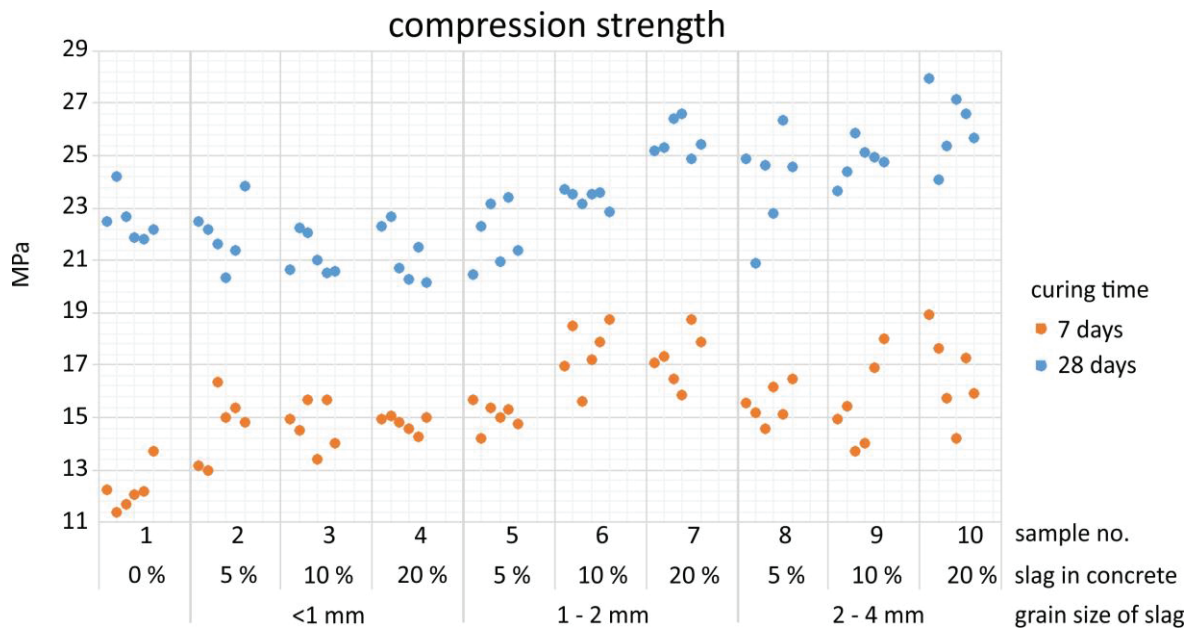


Figure 65: Trials for evaluation of compressive strength on 10 different mixtures of cement, sand and slag.

Both, compressive strength and flexural strength increased, if more slag was incorporated, at least for some mixtures. This applies for the tests after 7 days of curing time, but even more after 28 days. For flexural strength, the results are more variable and not that obvious. However, especially the slag with grain sizes of 1–2 mm increased the values (samples 5-7) particularly after 28 days of curing. For the other mixtures, the spread is quite large, but somewhat in the same range as the reference material.

For compressive strength, the impact of the slag is much more clearly visible. After 7 days of curing, all of the samples containing slag showed a higher strength than the reference sample. Samples 6-10 had the highest strength, but also a high spread, whereas the results of samples 2-5 were lower (still higher than the reference sample) but had a much smaller spread. The trend changed after 28 days of curing. Samples 2-5 showed very similar or slightly lower values compared to the reference material. Samples 6-10 were still considerably higher, even though the spread was still quite large.

Generally, it can be said that the slag bears high potential in replacing sand in concrete. The results from mechanical testing were quite promising, as the mechanical properties are similar, or even better than the ones for the reference sample.

Eluate testing was performed on a crushed (< 10 mm) mixture of samples 4, 7 and 10, all bearing 20 % slag. The leaching was done with a ratio of 10 l water/1 kg of sample material.

Table 21 lists the results from the leaching trials. Lead values exceeded the allowed limits almost twice; 0.93 mg/kg at a limit of 0.5 mg/kg. One reason may be the inclusions of metallic lead in the slag. As discussed in Chapter 9.3.3, there is room for improvement in this task. Moreover, the material used for this test series was relatively high in lead compared to slags from other pyrometallurgical trials. Leaching of concrete with lower amounts of slag will most likely also have a positive effect on the leached lead.

All other measured elements stayed clearly below the limits and elevated high lead values seem to be remediable by adaptations in the pyrometallurgical process and by using less slag in the concrete.

Table 21: Results from leaching trials on crushed concrete samples (<10 mm) containing 20 % slag, measured by AAS at W2V.

Parameters	Analytical methods	Specification mg/kg	Result mg/kg
As	US EPA 200.8, CSN EN ISO 17294-2	0.5	<0.01
Ba		20	4.4
Cd		0.04	0.003
Cr total		0.5	<0.01
Cu		2	<0.05
Hg		0.01	<0.002
Mo		0.5	0.38
Ni		0.4	<0.01
Pb		0.5	0.93
Sb		0.06	0.01
Se		0.1	<0.01
Zn		4	<0.1
Chloride		CSN EN ISO 10304-1	800
Fluoride	10		3
Sulphate	1000		48
Phenol index	CSN ISO 6439	1	<0.10
Dissolved organic carbon	CSN EN 1484	500	36

9.3.5 Summary of Trials on Jarosite from Zinc Production

Several trials with different jarosite residues in laboratory to technical scale proved the material to be treatable in the pyrometallurgical two-step process. Concentration of valuables in terms of mineral processing is not possible, except for very specific materials, like the gypsum-rich residue from the African plant. Pelletizing the jarosite material is necessary in order to avoid a high loss as carry-over in the off-gas. The handling of the

material is also facilitated and cleaner when pelletized (avoiding dust). For the jarosite residues used in the trials, no binder was necessary. The pellets were stable enough without any additives, except water.

A calcination step is needed prior to the reduction. Special attention must be paid to the temperature, as a loss of valuables, especially lead, due to evaporation will occur when reaching too high temperatures.

In the reduction step, three products were generated:

- A fayalitic slag, which bears the potential of being used as a construction material.
- Zinc as zinc oxide can be recovered from the off-gas. According to literature, indium can also be found with zinc, at least when treated together with electric arc furnace dust (Wegscheider, et al., 2017).
- The metal alloy consists of lead, copper and silver. In some cases, gold might also be accumulated.

In summary, the most important conclusions from the trials are:

- Pre-treatment
 - Beneficiation is only possible by flotation and only in exceptional cases.
 - Pelletizing is necessary to avoid carry-over and facilitate material handling in general.
 - No binder is necessary (only water).
- Calcination
 - Calcination is necessary for volatilising SO_2 as well as water and hydroxides.
 - The temperature should be around 850°C to vaporise SO_3 and OH groups.
 - Avoidance of evaporation and therefore loss of PbO limits the maximum temperature.
- Reduction
 - Production of a fayalitic slag.
 - A lead bath is the most promising collector.
 - Use of a copper or iron bath may be possible, but has serious disadvantages, as described in Table 19.
 - Off-gas contains zinc oxide and, theoretically, indium oxide.

- The alloy consists of mainly lead and contains silver, copper and gold, if available.
- Turbulent conditions in the metal bath cause a loss of metal to the slag, in the form of inclusions
- <1 % of lead and zinc in the slag is possible.
- External heating is necessary.
- Zero waste
 - The slag bears high potential of being used as construction material due to good mechanical properties.
 - Leachability of lead is problematic, but there is room for improvement in terms of reducing the amount of lead in the slag.
 - Leachability of other elements is below the common limits.

So far, the trials can be seen as successful and the jarosite material as potential input material for such pyrometallurgical treatment. The limiting factor for industrial implementation is the energy consumption of the calcination and especially in the reduction step.

9.4 Pyrometallurgical Trials on Jarosite from Platinum Production

The usability of the pyrometallurgical two-step process for jarosite from nickel production was tested in an extensive series of trials. The final products are very different to those from jarosite from zinc production:

- The off-gas from the calcination is rich in arsenic. Removing all of the arsenic, separating it and binding it to a stable phase was a key task in these trials. It was successful, but this topic will not be pursued further in this thesis.
- The off-gas from the reduction does not contain any valuables.
- The final slag is only regarded as waste at this point, although tests on its use as construction material might be of interest.
- The only valuable product is the iron-nickel alloy.

9.4.1 Pre-Treatment

Beneficiation is not possible, as iron is a dominating metal of interest and is present in the jarosite phase.

The jarosite was treated as both non-agglomerated and pellets. The non-pelletized jarosite is difficult to handle due to the dust that causes carry-over. For pelletizing, water and two different additives were used as a binder (Figure 66). In the first trial, calcium hydroxide was chosen. The jarosite contains more SiO_2 than CaO , so in the final reduction step calcium must be added to reach a proper slag composition. Therefore, it is obvious to use a Ca-containing phase as a binder from the start. It worked well as a binder, but had the big disadvantage that, due to its high affinity to sulphur, it formed anhydrite and kept the sulphur in the calcine (anhydrite is stable until 1200°C). In the following process, this hinders the removal of all of the sulphur. Hence, another binder, namely bentonite, was used for the following trials. This resulted in a much better sulphur removal during calcination.



Figure 66: Upper left: jarosite from platinum production mixed with calcium hydroxide ready for pelletizing (first trial). Right: Agglomeration process. The pelletizing disc is the same as in Figure 58. Lower left: finished pellets of about 0.5-1.7 cm in diameter.

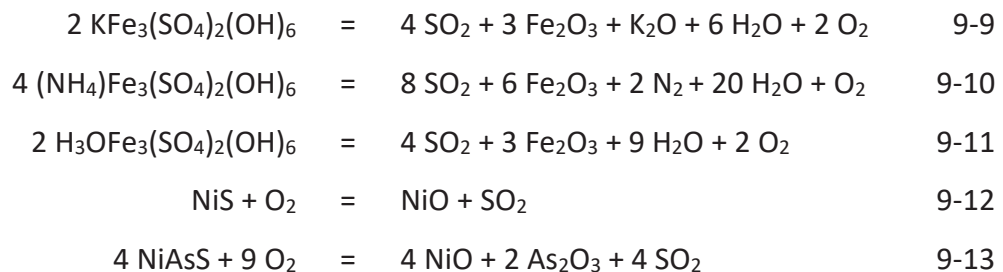
9.4.2 Calcination

A top-blown rotary converter was used for calcining the jarosite pellets and thus splitting the sulphate phases to remove the sulphur as SO₂ and water. The temperature was between 900 and 1000° C, because arsenic-containing phases must also be decomposed and the arsenic must be vaporised as an oxide.

The off-gas treatment is crucial, seeing that the arsenic must be bound in a safe way. A newly developed off-gas unit was tested in these trials to deal with this problem.

As the jarosite contains no sulphides which would allow exothermic reactions, the whole process needs to be heated by a gas burner. The treatment time was about 2 hours.

Important reactions were (Equations 9-9 to 9-13):



9.4.3 Reduction

The calcine pellets were molten to produce an inert slag and an iron alloy. The main value carrier is nickel. The higher the nickel value in the alloy, the higher the price is, but the more iron there is in the alloy, the less slag remains. Nickel is easier to reduce than iron and therefore always completely in the metal alloy. The percentage of iron in the alloy is relatively easy to adjust, by longer treatment time and the addition of carbon. The targeted slag basicity (B2) was 1-1.2 (CaO/SiO₂). If any sulphur or arsenic is still left in the material, this slightly basic slag helps to keep the alloy clean and keep the sulphur and arsenic in the slag.

As the addition of Ca during pelletizing had the above-mentioned drawback, Ca was added during the reduction process as CaCO₃. Besides SiO₂ and CaO, MgO and Al₂O₃ are also present as slag components, but in much smaller amounts. After the amount of iron and nickel in the slag dropped below a certain level, the melt was tapped into a mould (Figure 67).

The most important chemical reactions are (Equations 9-14 to 9-16):



Figure 67: Tapping of the jarosite from platinum production after reduction. The sparks on the floor are caused by oxidation of metallic iron and the rising burning carbon powder.

9.4.4 Summary of Trials on Jarosite from Platinum Production

The characterisation of jarosite from platinum production showed that the material is less complex in its composition. Know-how from the work on jarosite from zinc production also simplified and shortened the process of characterisation for this residue. It became clear at the beginning of the project already that there would not be any efforts on mineral processing for concentrating the valuables (Ni). For that reason, the emphasis changed to the characterisation of intermediate and final products from the pyrometallurgical treatment. Main insights and consequences are described in one of the following chapters in detail.

In contrast to the residues from zinc production, the reasons why beneficiation of valuables is not reasonable are:

- Jarosite as the main phase, is also the main carrier of iron required for the formation of the ferro-alloy.
- A main task is to avoid dumps. A removal of valueless phases would again cause a residue that is as difficult to dump as the original jarosite material.

Instead, the off-gas treatment was a primary task, as the high amount of arsenic causes serious problems.

The main points of treating the jarosite from platinum production are:

- Pre-treatment
 - Beneficiation is not reasonable.
 - Pelletizing is necessary to avoid carry-over and facilitate material handling in general.
 - The binder for pelletizing must be free of calcium.
- Calcination
 - It is necessary to volatilise SO₂, water and hydroxides.
 - High temperature (900-1000°C) is necessary to split arsenic-bearing phases and vaporise arsenic.
 - Maximum temperature is defined by the avoidance of sintering and/or melting of compounds, not by losing valuables.
 - The off-gas contains no valuables, but hazardous components (arsenic).
 - An off-gas unit able to separate arsenic in the form of stable compounds is of prime importance.
 - External heating is necessary, as no exothermic reactions occur.
- Reduction
 - Use of an iron bath.
 - Slag basicity of 1-1.2 (CaO/SiO₂) to keep sulphur and arsenic in the slag (if still present in the calcine).
 - Adjustment of nickel content in the metal alloy is possible by partial reduction of iron. Longer treatment time and the addition of carbon increase the percentage of iron.
 - Turbulent conditions in the metal bath cause a loss of metal to the slag.

Numerous trials showed that a pyrometallurgical treatment of jarosite from platinum production to generate a nickel alloy is possible. Even though the process is similar to the one for treating the jarosite from zinc production, many details vary considerably. This is mainly due to the different chemistry of the slag and the use of iron instead of lead as the metal bath.

The off-gas unit which needs to bind the arsenic in stable phases is essential in the trials and in a following upscaling. Its performance was successful in these trials and is promising for further development.

The main product, namely the nickel-iron alloy, proved to be of a good quality concerning impurities (S, Cu, As). A big advantage is the possibility to adjust the nickel grade in the alloy in order to react to requests from the market. This can be done by reducing only part of the iron. Nickel, as the more noble metal, is always reduced before iron.

9.5 Benefits of Characterisation on Process Development and Product Optimisation

Not only the input material was characterised, but also all intermediate products as well as the final products in order to optimise the proposed and investigated processes. The main questions to be answered are:

- Did the process work well?
 - Is the calcine free of sulphur and arsenic (jarosite from platinum production)?
 - Is the slag free of metals?
- If the process did not work well:
 - Which phases carry the valuable elements?
 - What are the characteristics of these phases?

The question of the success of a process step can often be answered with a chemical bulk analysis of the products, showing if quantitative transfer occurred.

However, if specific elements occur in a product where they were not supposed to be, finding a reason for this is often complicated. It demands detailed investigations, especially concerning the appearance of phases. The identification of phases which bear critical elements is essential for finding solutions, as to how to shift these elements from one product to another. The following two chapters show examples where the characterisation of products from pyrometallurgical trials on jarosite from zinc production and jarosite from platinum production provided essential input for the process optimisation.

9.5.1 Benefits of Characterisation on Products from Treating Jarosite from Zinc Production

Many trials of different jarosites from zinc production underlined the need for detailed characterisation of various (intermediate) products. This might be obvious in terms of chemical composition, but also, or even more so, for identifying specific phases. The following section gives a summary of important findings gained by the mineralogical characterisation of various products that occur during the treatment procedure and their impact on the process.

9.5.1.1 Characterisation for Pre-Treatment

Detailed investigations showed that the initial idea of separating the jarosite mineral from the value-bearing residue is not possible, as the jarosite mineral itself contains considerable amounts of lead. Therefore, even if the jarosite-free fraction were enriched in other valuables, the loss of lead would be too high to allow an economic process concept.

Silver is usually bound to lead phases and even the jarosite mineral is able to host small amounts of Ag (see Chapter 5). However, in the investigated jarosite material, there is no evidence for such phases carrying silver, so a concentration of lead phases (other than jarosite) by mineral processing does not necessarily increase the silver value.

Treatment of gangue minerals such as quartz and feldspar is not effective, due to the fact that their amount is too small to allow a significant concentration of valuables when removed. Furthermore, they often bear copper and silver inclusions which would be lost.

Consequently, a beneficiation of the jarosite material, without losing a large amount of valuables, is not possible.

In spite of this, there is one special residue that is different to the others in one point. In the case of the Zn-bearing residue from Africa, a very high amount of gypsum was detected. Figure 49 shows a qualitative element mapping of calcium on a representative sample using SEM; calcium in this case is an equivalent for gypsum. It can be removed in order to concentrate the valuables. Removal of gypsum by flotation is a state of the art technique. It is beneficial in that it reduces the overall amount of material for the calcination and reduction; the prime task of beneficiation because it also reduces the energy consumption. Furthermore, decomposition of sulphur from anhydrite in the calcination would need a very high temperature of about 1200°C. This high temperature for calcination is not realisable, not only owing to economic and technical reasons, but also due to other phases that were identified in the material, that would evaporate and escape in the off-gas.

Evaluation of grain size distribution proved that the jarosite is too fine-grained to be treated without agglomeration. The clay to silt-sized material would be difficult to handle, and during the pyrometallurgical treatment a lot of material would be lost through the off-gas, making pelletizing before further treatment necessary.

9.5.1.2 Evaluating the Settings for Calcination

Removal of sulphur is the main reason for the calcination step in the proposed process, which is why it is essential to identify the main sulphur-bearing phases to determine the conditions for sulphur removal. Mineralogical characterisation identified jarosite as the most important sulphur carrier. Based on this finding, together with thermodynamic equilibrium calculations, 800°C is defined as the minimum temperature for calcination, as this is sufficiently high to split off sulphur from the jarosite, lead, iron and other sulphates. Besides a minimum temperature, the mineralogical composition also dictates a maximum temperature for calcination. Too high temperatures would cause the evaporation of phases that should stay in the calcine. Lead oxide was identified as an important lead phase in the calcine. Calcination with more than 900°C would cause at least partial evaporation and thus a high loss of lead in the form of lead oxide. As pointed out in the chapter before, a temperature that would be high enough to decompose anhydrite is therefore not feasible.

As a consequence of the mineralogical composition, the calcination temperature must be between 800-900°C.

Characterisation of the calcine proved the chosen temperature to be a good choice. Nearly all of the sulphur was removed. However, small remnants are still present. Silver and copper-rich inclusions in quartz, feldspar and wollastonite, to mention the most common ones, still contain sulphur.

In some cases, characterisation of the calcine showed that the retention time in the TBRC or the required surface was not sufficient to remove all of the sulphur.

9.5.1.3 Characterisation of Final Products

Characterisation of the final slag showed that, as expected, some sulphur was still present in the calcine, causing the formation of lead and zinc sulphides. Whilst chemical bulk analysis proved the presence of sulphur, investigations using a scanning electron microscope allowed the sulphur-carrying phases to be determined. Figure 68 shows an element mapping of a polished section of a slag sample from a jarosite reduction trial. The bright particles in the BSE image are clearly identified as zinc sulphide phases.

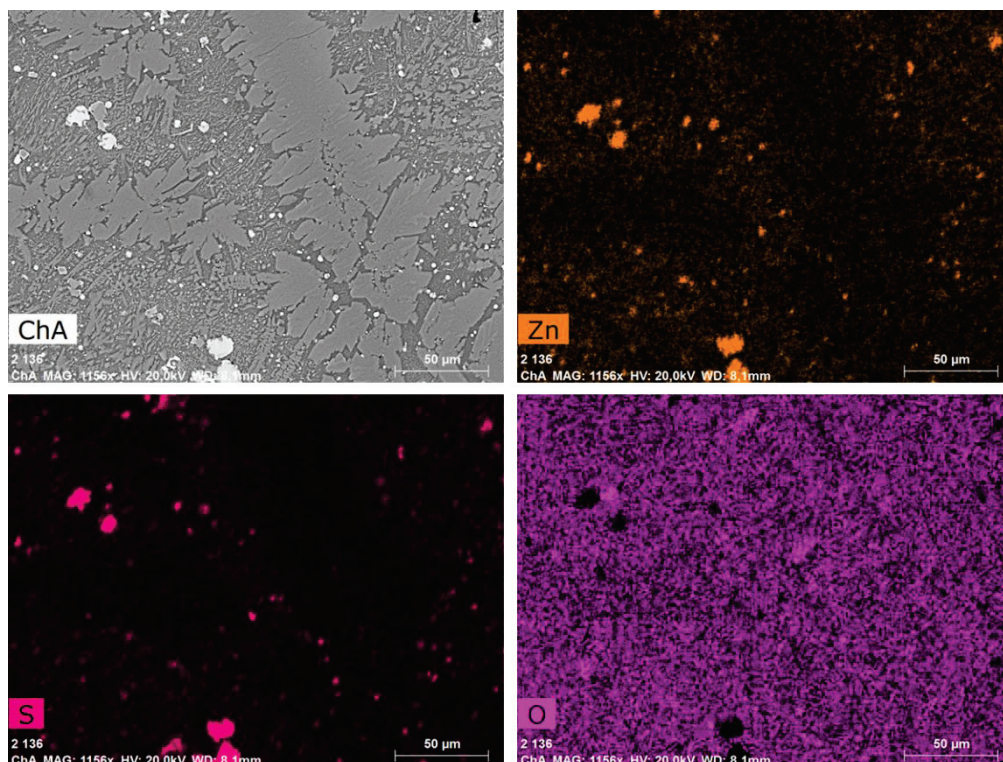


Figure 68: SEM Image (BSE detector) of a polished section of a slag sample from treating jarosite from zinc production. Note the presence of zinc sulphide.

Besides zinc, the slag also often contained much higher lead values than expected. The investigation of slag samples showed the presence of drops of metallic lead (Figure 69). Therefore, missing lead yield is not only a matter of poor reduction, but also of poor settling behaviour. This is an important finding, as the process works better than indicated by chemical analysis.

The composition of the slag is not only significant in terms of a further use, but also for its behaviour during reduction. Characterisation of the slag allowed an optimisation of the process temperature, evaluation of necessary additives and the proportion of the main slag compounds (fayalite, calciumsilicate).

Stable slag composition and missing refractory particles in the slag revealed that there was only very little interaction with the lining.

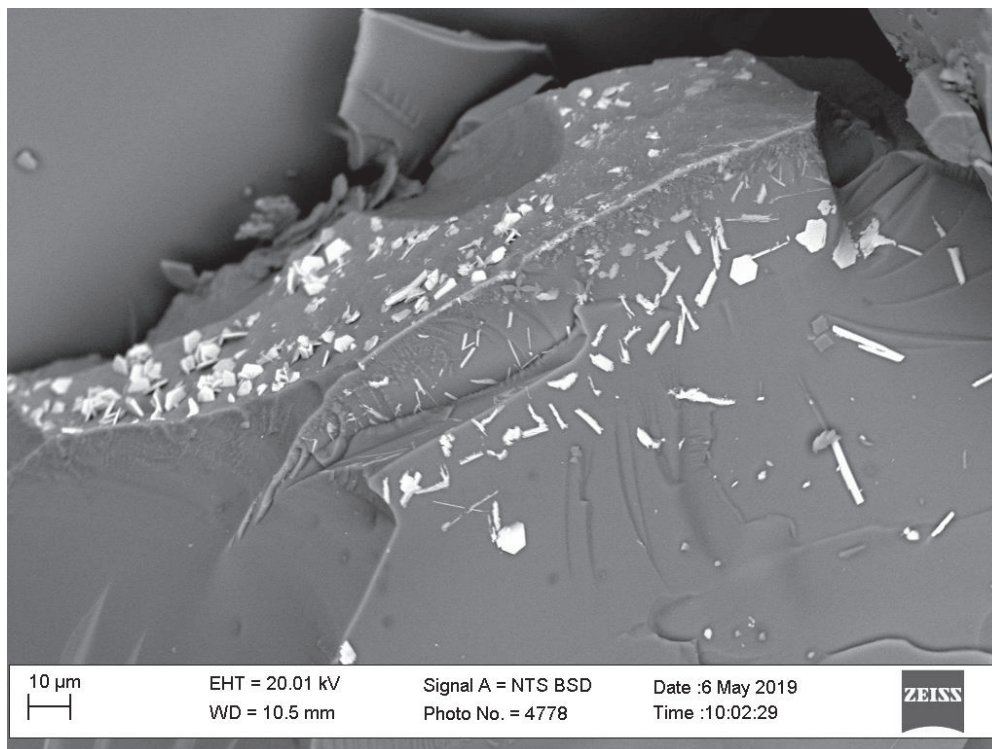


Figure 69: Slag sample from a reduction trial on jarosite-calcine. The bright phases are lead-iron particles; the matrix is the fayalitic slag

Residues deposited in the off-gas unit were evaluated for the determination of evaporated phases, also providing information for optimising the charging procedure to avoid mechanical carry-over. As expected, the off-gas is very rich in zinc oxide. However, it also

contains considerable amounts of lead oxide, most likely due to low reduction intensity or too much influence of the hot spot caused by the electrode (Figure 70).

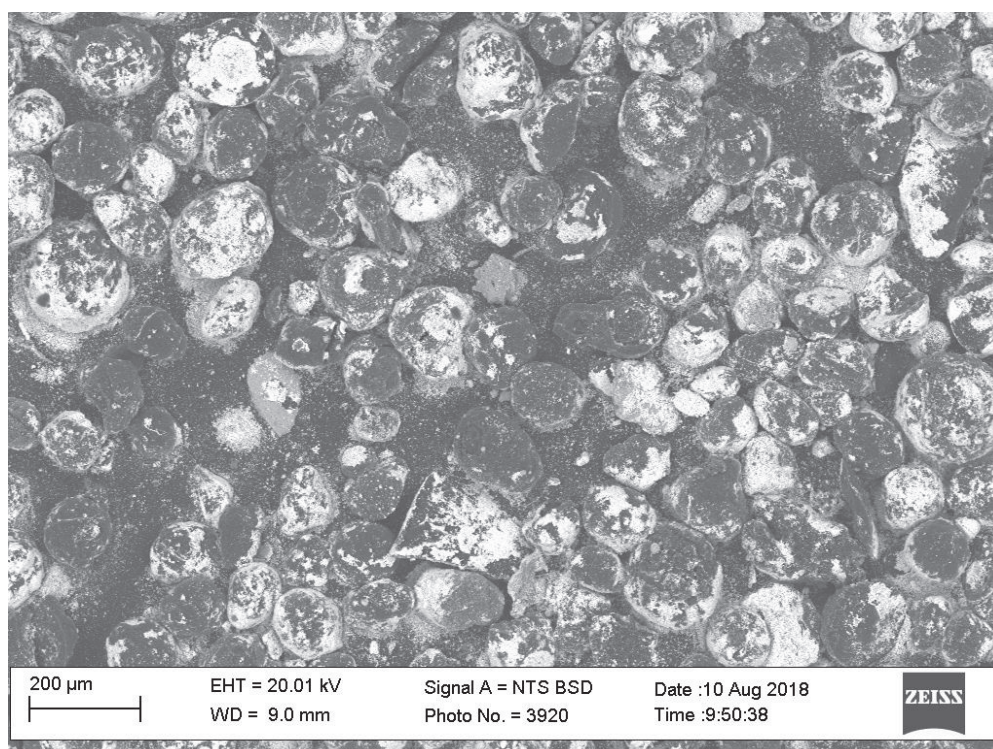


Figure 70: The off-gas of a reduction trial showed considerable amounts of lead (white in the picture).

9.5.2 Benefits of Characterisation on Products from Treating Jarosite from Platinum Production

Many trials on jarosite from platinum production were performed with the same material and within a short period of time, which allowed the immediate use of the information delivered by detailed characterisation of the products for the planning and implementation of the following trials.

This chapter focuses on the characteristics of intermediate and final products of trials on the jarosite from platinum production and the influence on further trials. Detailed characteristics of the original jarosite material can be found in Chapter 8.8 .

9.5.2.1 Characterisation for Pre-Treatment

As a first step, grain size analysis showed that the grain size distribution was very similar to the jarosite from zinc production - clay to silt-size. Therefore, the problem of material

handling and carry-over would be the same, necessitating an increase in the grain size by agglomeration.

In this case, a binder was added to increase the stability of the pellets. For the first run, calcium hydroxide was used and for all of the following runs, bentonite. The reason for the change of binder was a recognition from characterising the calcine and is described in the next chapter.

Any kind of beneficiation is obsolete for this material, as there are no phases present which do not contain valuables and are of high quantity. The main mineralogical phase is jarosite. Other important phases are hematite and various nickel phases. As the final product will be an iron-nickel alloy, none of these phases can be removed without losing valuables. Another important point is avoiding waste or producing inert waste (slag).

9.5.2.2 Evaluating the Settings for Calcination

It was necessary to increase the grain size of the material by pelletizing. In the first trials, calcium hydroxide was added as a binder for the following reason: according to the chemical analysis of the original material, it was clear that calcium must be added during reduction to achieve the correct slag basicity. Some calcium hydroxide was added at the beginning of the treatment, since it can also act as a binder.

However, due to the high affinity of calcium hydroxide to sulphur, anhydrite formed and the results in sulphur removal during calcination were not satisfying. This was verified by means of SEM, as shown in Figure 71.

Even though evaporation of valuables is not a problem for this material (as opposed to jarosite from zinc production), temperatures high enough to decompose anhydrite are not possible. Sintering of the calcine would occur, causing a negative effect on de-sulphurisation. In addition, the energy consumption would increase significantly.

As a consequence, for the following trials, bentonite was used as a binder instead of calcium hydroxide to avoid this problem and calcium was added separately during the reduction process.

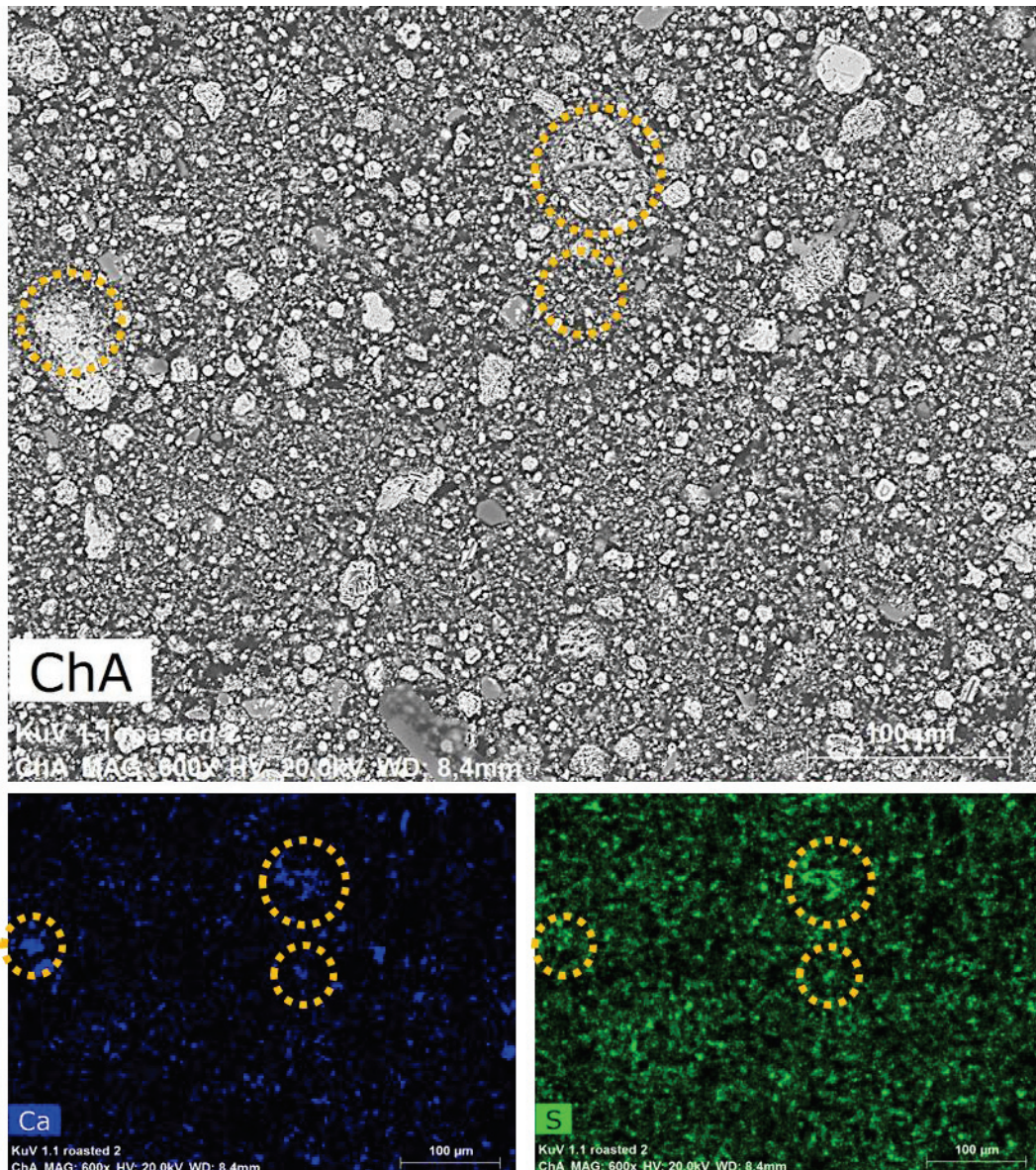


Figure 71: BSE image and qualitative calcium and sulphur mapping of a representative area of calcinated jarosite from platinum production. Note the correlation of calcium and sulphur caused by the formation of anhydrite.

The identification of sulphates and arsenic-bearing compounds (jarosite) allowed the determination of the optimum temperature for calcination. 900-1000°C was chosen as an appropriate temperature range to split sulphates and remove sulphur and arsenic through the off-gas. The XRD spectrum in Figure 72 exclusively shows oxidic phases. Semi-quantitative analysis by scanning electron microscopy did not detect sulphur either, but mainly iron, nickel and small amounts of silicon and aluminium (Figure 73), making the calcination a success.

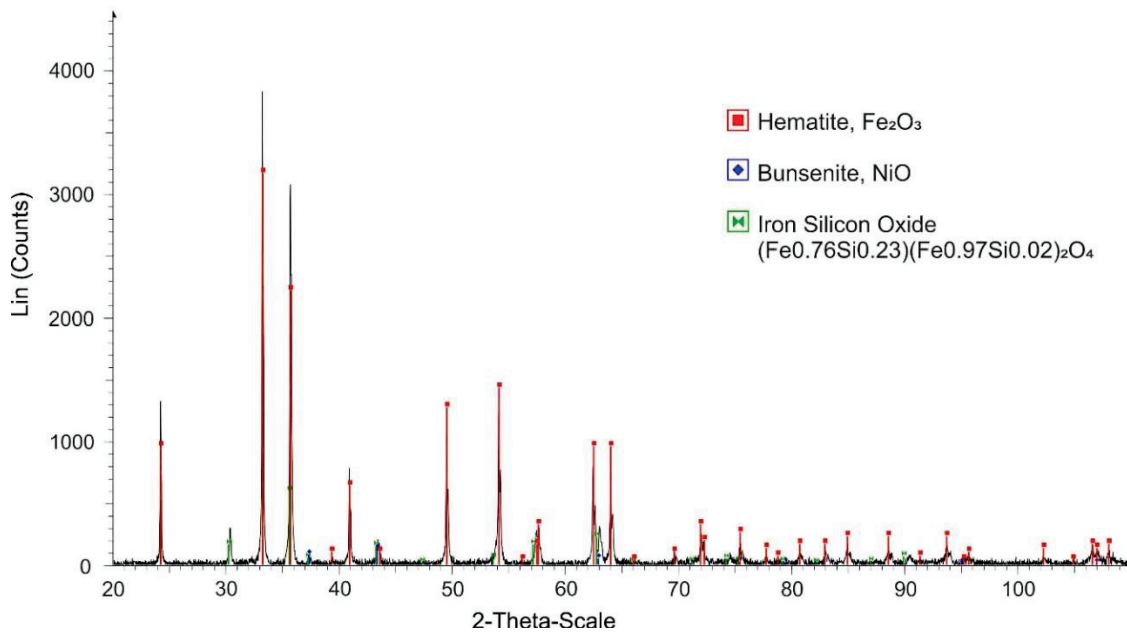


Figure 72: XRD analysis of jarosite from platinum production after calcination.

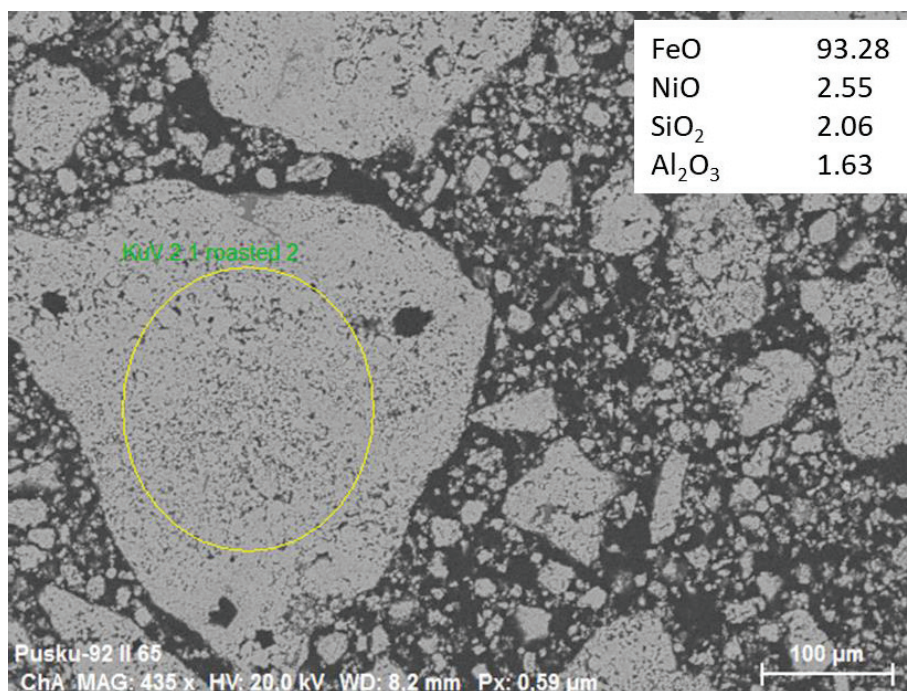


Figure 73: Image of a calcinated jarosite from platinum production. The chemical composition concerns the area in the yellow circle.

In contrast to the calcination of jarosite from zinc production where it is crucial to avoid any loss of lead during calcination, the evaporation of lead in this case is intended. However, lead influences neither the overall process nor the products. The partial removal of lead was verified on the one hand by chemical analysis of the calcine and on the other hand by investigating dust from the off-gas. Samples taken from the off-gas unit close to

the TBRC clearly showed lead oxide. In samples taken after scrubbing with diluted sulphuric acid in the off-gas unit, lead sulphate was found (Figure 74). Small amounts of lead still present in the calcine occurred as lead oxide.

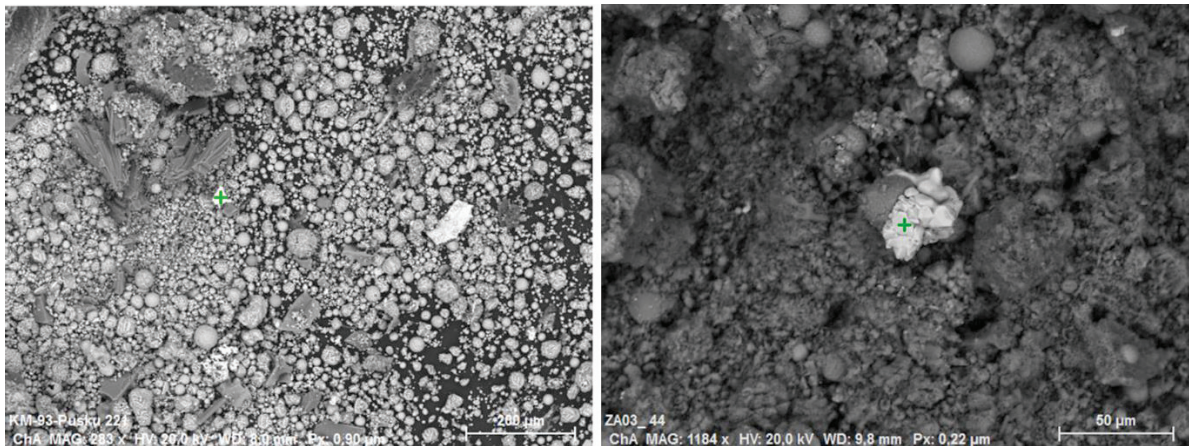


Figure 74: Lead oxide (left) and lead sulphate (right) from different parts of the off-gas unit.

9.5.2.3 Characterisation of Final Products

The final slag was also investigated with the aim of optimising the reduction step and the overall process. The formation of nickel sulphide was expected to be a problem, that would lead to a decrease in the nickel output. However, chemical analysis of the slag showed a very low nickel concentration, even though some nickel-sulphur particles were found using a scanning electron microscope (Figure 75).

According to the chemical analysis, after elevated production time, the iron content in the slag stopped decreasing and stayed at a certain level. Detailed investigations of the iron compounds in the slag showed that metallic iron particles are embedded in the slag (Figure 76). Therefore, the occurrence of iron in the slag is not a function of temperature or reduction potential (reduction of iron is very energy-consuming and requires high reduction potential), but of the settling behaviour, very similar to the trials on jarosite from zinc production. Some iron was also bound to slag components and remnants of arsenic and sulphur were found in the metal product, caused by a low slag basicity. As a consequence, the slag composition was corrected by the addition of lime.

An opportunity from this process is the possibility to adjust the value of the product by regulating the amount of iron in the alloy. A higher nickel content increases the value of the alloy, whereas a higher iron content in the slag increases the amount of slag. Iron also

influences the melting temperature of the slag. Finally, the degree of iron reduction has a major influence on energy consumption.

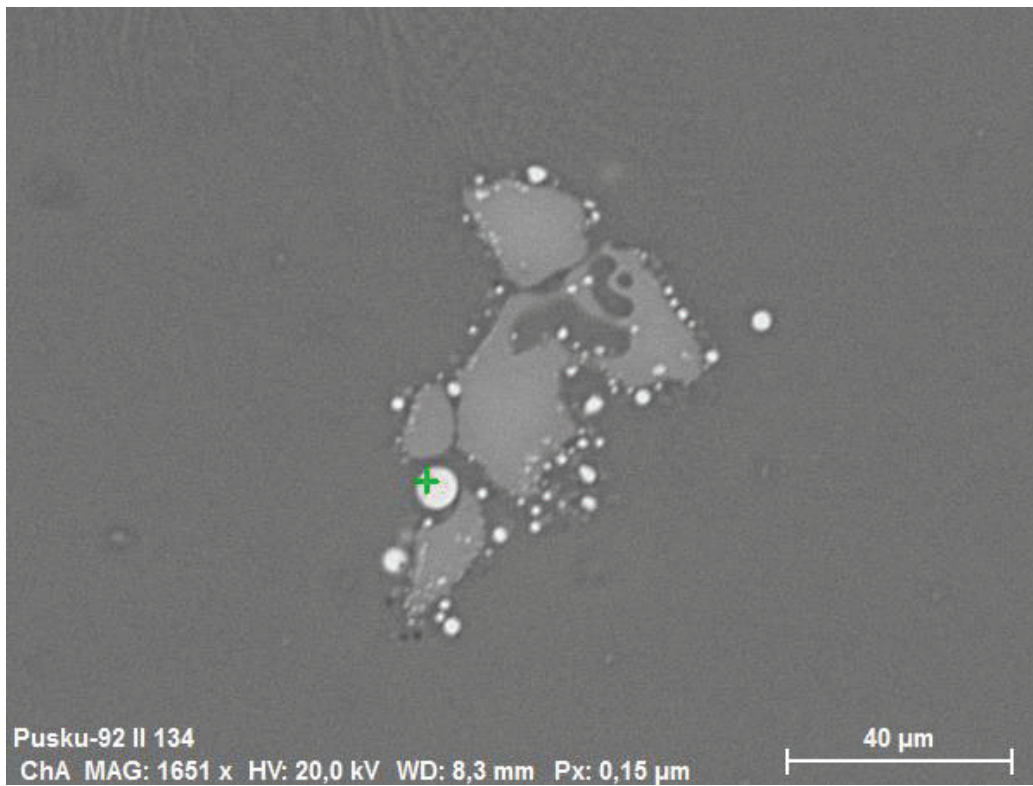


Figure 75: Nickel-iron-sulphur particle. The right half of the spherical grain is an iron nickel alloy (90 %-10 %) whilst the left half has the chemical composition of a heazlewoodite (Ni_3S_2).

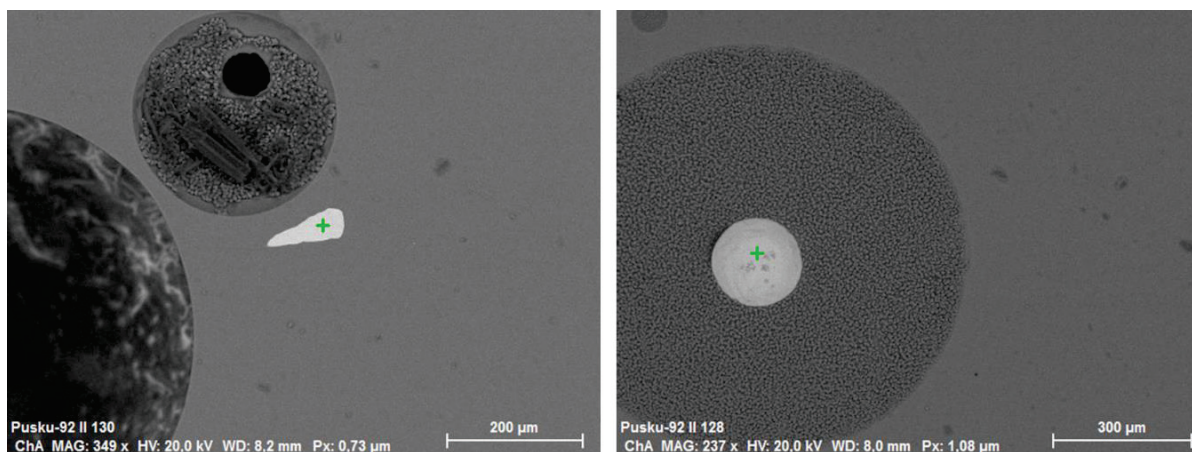


Figure 76: Two different inclusions in a final slag from a reduction trial on jarosite from platinum production. Both consist of about 90 % iron and 10 % nickel.

9.6 Economic Considerations

The residues from hydrometallurgical zinc production contain considerable amounts of different valuable metals. Many of them would be economically recoverable in primary ores at even lower concentrations (Table 22). The main problem is that beneficiation in terms of mineral processing is not possible, as most of the valuables are evenly distributed in the jarosite residue. However, even the combined winning of different metals, as proposed and tested in this work, can hardly assure an economical process. Europe is a big player in zinc production; therefore, a lot of material is available which is one big requirement for the installation of a treatment facility. Unfortunately, Europe is also expensive in terms of electrical energy and this is a limiting factor for the whole process, as the reduction process is very energy-intensive. This applies to the treatment of both types of jarosite, but even more so for the jarosite from platinum production, because of the need to reduce iron instead of reducing lead (and producing a fayalitic slag), as in the case of jarosite from zinc production. Other limiting factors are the metal content and metal prices. The metal content of a currently produced jarosite residue might be relatively constant within a plant, while the content within dumps needs to be evaluated separately. A change in the metal price can also change the economics of the whole process considerably.

Table 22: Comparison of common minimum metal contents in primary ores and average chemistry from jarosite from zinc production (Pawlek, 1983).

	Economically recoverable in ores	Average amount in Zn-jarosite
Zn %	>4.0	1.5-7.1
Pb %	>2.0	0.5-7.1
Cu %	>0.3	0.4-0.7
Ag ppm	>100	<600

As environmental considerations will gain more importance in the future, the jarosite residue must not only be regarded as a resource for metals, but also as a hazardous waste that must be treated. Zinc plants devote enormous efforts to define new dumpsites. The Boliden smelter in Odda, for example, builds huge caverns into solid rock, only to dump the

residues from the plant (Boliden, 2019). In another case, the leaching residue, which is produced separately and bears high potential for being sold as lead-silver concentrate, is mixed with the iron precipitation product, only to be able to realise a minimum value and justify internal treatment. The environmental aspect is sometimes difficult to calculate, but somehow represented in the increasing landfilling costs and efforts on treating residues; not only those from zinc production, but metallurgical by-products in general. As ores are getting worse in their quality (lower grade, more impurities), the amount of residues will also increase. A treatment of residues will most likely be mandatory in the future.

The amount of nickel in jarosite from platinum production is about 10 times the profitability of primary ores (Pawlek, 1983) but also faces the problem of high energy costs if treated, even worse than for the jarosite from zinc production. The main reason why natural ores are recoverable with much lower content is the relatively simple beneficiation, most importantly by means of flotation. For the jarosite from platinum production, beneficiation is neither possible nor desired as it would produce large amounts of residues to be dumped. However, for this jarosite process, avoiding residues is already vital.

Fundamentally, the pyrometallurgical treatment of jarosite residues, as described above, proved to be a promising method in terms of recovering the valuables and further use or dumping of the slag. In the best case, it could become a perfect example of the modern and popular zero-waste philosophy.

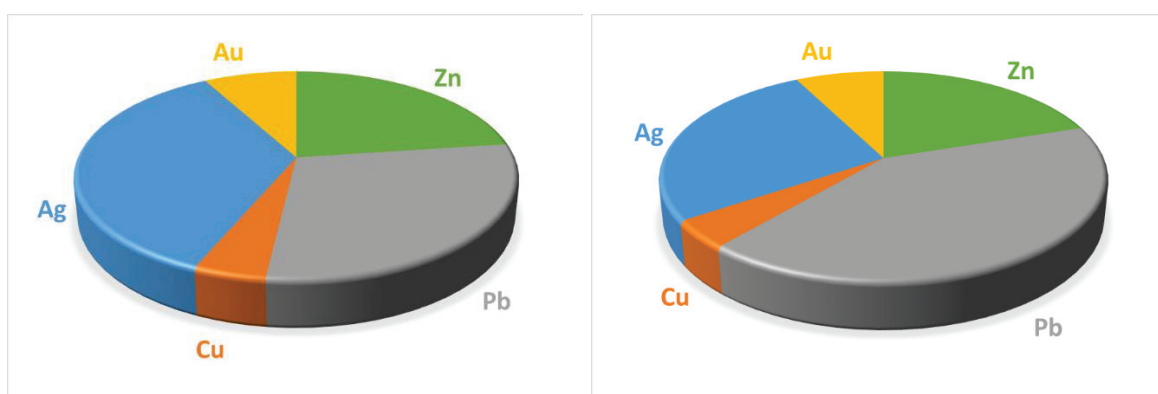
However, for both jarosite residues (from zinc and platinum production), energy consumption is, besides metal content and actual metal prices, a limiting factor, as the reduction is very energy-intensive and therefore expensive. Keeping this in mind, it is obvious that cheap energy could make the whole process economical.

9.6.1 The Important Role of Lead, Silver and Zinc

Due to the very different metal prices, the share of financial outcome for each metal is not obvious. Figure 77 shows two pie charts describing the share of values of two different, but still very typical jarosite residues from zinc production. For these calculations, the metal prices were corrected with a specific factor which considers the treatment charges of the smelter. This is necessary for the following reason:

As the metal alloy produced in the pyrometallurgical process is not a final product, but an intermediate one containing different metals, it can only be sold to a smelter which has to put it into its standard process. Depending on where the alloy has to be implemented, the price paid for it will be adapted. Lead, for example, is the main element in the final alloy. It is already present as a metal and is of good quality concerning accompanying elements. In a lead smelter it would only be necessary to refine it, putting the correction factor closer to 1. The recovery of silver and gold is also state of the art during the final steps of lead refining, causing a correction factor even higher than that for lead. For gold the factor of 1 is somehow optimistic, but as the amount of gold in general is highly variable, the error caused by the correction factor can be ignored.

The dominant roles of lead and silver are clearly visible. Generally, it can be said that these two metals account for more than two thirds of the value of a typical jarosite residue. Zinc is also important, but not as much as the other two. Copper has its share in each of the jarosite residues evaluated, but is only of subordinate importance.



	Metal price (17.10.2019)	Correction factor	Left example		Right example	
			Chemical composition	€/t jarosite	Chemical composition	€/t jarosite
Zn	2 038.40 €/t	0.7	4.0 %	62	3.7 %	57
Pb	1 856.40 €/t	0.85	4.7 %	78	7.1 %	118
Cu	5 182.45 €/t	0.6	0.4 %	12	0.4 %	12
Ag	16.75 €/oz	0.95	219 ppm	96	160 ppm	77
Au	1 383.54 €/oz	1	0.5 ppm	22	0.5 ppm	22
Total				270		286

Figure 77: Calculated share of value from two different jarosite residues.

9.6.2 The Variable Importance of Gold

The importance of gold is very difficult to evaluate, as the determination of the real gold content in the residue is challenging. This is due to sampling, especially because of the “nugget effect,” very typical for gold analysis. The “nugget effect” describes the behaviour of an element to form nuggets instead of being evenly distributed in the material. The difference from one analysis to another within the same sample material can vary considerably. For both examples in Figure 77, 0.5 ppm of gold was assumed. However, in different chemical analyses, gold contents up to 11 ppm were found. Due to the high price of gold compared to the price of the other metals, even a small increase (or decrease) in the amount of gold can influence the total value of the residue significantly. A serious estimation of the importance of gold is not possible without a much more extensive and detailed sampling.

10. Concept for a Characterisation Procedure

Due to the high versatility of by-products in general and especially for jarosite, the characterisation procedure needs to be versatile as well. The first step in any kind of characterisation will be a chemical bulk analysis of the whole material in order to see if the material is worth further considerations for metal recovery. Special attention must be paid to the selection of a suitable method, as each one has its strengths and weaknesses. Very heterogeneous material is more challenging, as some elements might only be measurable with specific analytical techniques. Acid hydrolysis, for example, leaches most of the jarosite material, but not barite. Fused discs, often used in geology, are not applicable for such material because volatile components will be lost during the sample preparation. In many residues, these volatile components are extremely important and cannot be ignored.

Light microscopy is often the first method used when investigating a material from a mineralogical point of view. In the case of the jarosite material, its applicability is very limited due to its limits in magnification.

Electron beam methods are the method of choice for investigating the mineralogy, morphology, grain size, etc. Material that fulfils some requirements such as grain size in

some tens of microns and a well polishable surface can be quantified using automated methods. Major elements in the phases can be identified by semi-quantitative and quantitative element measurement using SEM-EDX and WDX. Many questions concerning intergrowth relationships and qualitative determination of the mineralogy can be answered using a scanning electron microscope on polished sections and strewn slides.

For the detection of elements with low concentration (<0.5 %), such as silver, indium and germanium, it is necessary to use other methods if these elements are not enriched in specific host particles above the stated detection limit. Electron microprobe and LA-ICP-MS are both methods which allow the detection of elements with a concentration of some 100 ppm and below, under suitable conditions. However, a limiting factor is the grain size. The diameter of the laser beam for LA-ICP-MS, for example, can be adjusted and is usually 30-60 μm and a minimum of 3 μm . The electron beam of an electron microprobe is comparable to that of a scanning electron microscope and spot sizes of 0.5-1 μm are achievable. Considering that about 60 % of the jarosite material is smaller than 10 μm , this illustrates the problem of in-situ analysis.

Identifying particles which contain valuables, but not as main components, is very difficult. Element correlation may help to identify host particles within any material (see Chapter 8.4).

For characterisation of host particles, electron beam methods help to determine the particle morphology and may provide precise point analyses. Depending on the characteristics of the host particles, automated methods of quantifying phases can also be an option (e.g. MLA, QEMSCAN[®], ZEISS MinSCAN, RAMAN-HMA (Lünsdorf, et al., 2019)).

10.1 Proposed Approach for Characterisation of Unknown Material

Figure 78 summarises a proposed characterisation procedure for potentially valuable secondary resources in general, but especially metallurgical by-products. The main steps and requirements are:

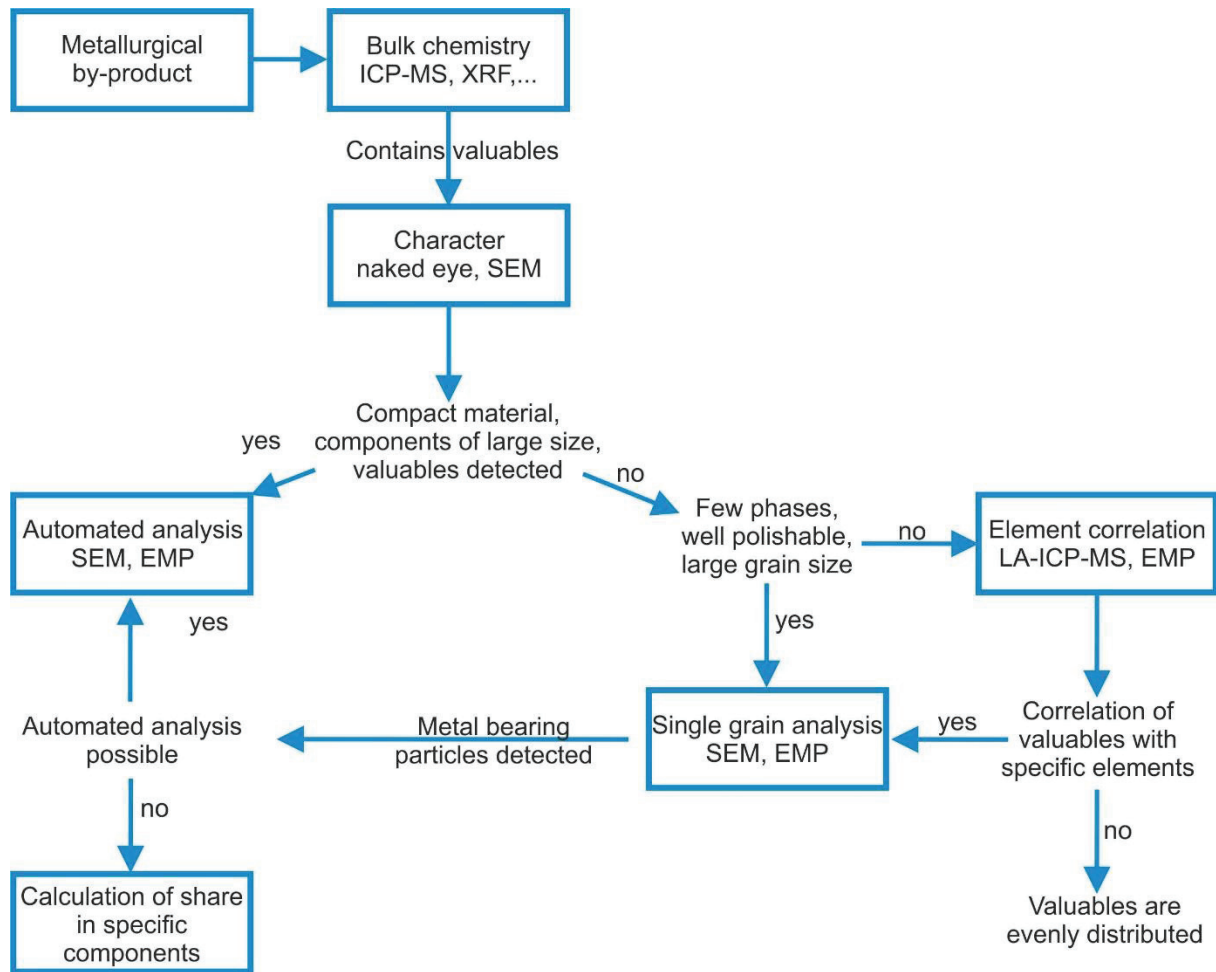


Figure 78: Proposal for a characterisation procedure for fine grained material.

- Chemical analysis
 - The material must contain enough valuables to be of interest from an economic point of view.
 - This can be provided by standard procedures of chemical analysis on solid samples.
- A characterisation of principle properties
 - Investigations by unaided eye, light microscope or scanning electron microscope on strewn slides allow a first impression of the material properties.
 - When the particles in the material are compact, well polishable, consist of particles larger than about 20 μm and all phases of interest are detected, it could be analysed directly by automated electron beam methods.

- Automated phase analysis
 - A number of different software packages are available for automated analysis using a scanning electron microscope, an electron microprobe or a light microscope. When the above-mentioned requirements are fulfilled, these programs can produce a detailed listing of the measured particles concerning grain size, chemistry, morphology and intergrowth relationships.
- Detailed search for host particles
 - If the valuables cannot be detected, but the other requirements are fulfilled, methods which allow lower detection limits, such as electron microprobe, can help to identify the host particles.
 - If host particles are identified, again automated methods could be used.
- Correlation of elements
 - In case no host particles are found, element correlation, as described above, can be useful. It allows the interpretation of whether the valuable metal is concentrated at all or if it is evenly distributed in the sample material.
 - A large number of measurements with electron microprobe analysis or LA-ICP-MS on one sample will provide correlations of valuable metals with other elements. A correlation indicates the possible host particles. No correlation means an even distribution of the metal.
 - If the metal-bearing phase has been identified, again automated methods might be applied to quantify them.
- No clear enrichment detectable
 - A possible situation, like it is for the jarosite material, is that a proportion of a metal is enriched in a host mineral, but it also exists in other phases. In this case it might be necessary to estimate the share with the help of different trials in terms of mineral processing.

The characterisation procedure for jarosite materials is clearly dominated by the search for phases bearing valuable elements and the generally very small grain size. For other materials, a distinct shift in the focus to different methods, like light microscopy, will be meaningful and necessary. Other methods that proved promising for the jarosite residue, like element correlation, might be much less important.

11. Discussion

Based on the investigations, most of the questions defined in the introduction can be answered for both jarosite materials. Even though the major part of the material consists of similar phases (diverse jarosite group minerals), the two types of residues investigated proved to be very different concerning their mineralogical and chemical composition.

11.1 Questions to be Answered-Jarosite from Zinc Production

As the jarosite material from zinc production is a mixture of many different residues, it not only consists of the iron precipitation product (jarosite mineral) but also of leaching residues, other precipitation products, calcine and other materials. It carries different valuables which are partitioned into various phases.

- Which particles contain the valuable elements?

The zinc and lead phases identified are well known. Zinc ferrite, sphalerite and the three lead phases lead oxide, lead sulphide and lead sulphate are common zinc and lead carriers. Additionally, the jarosite mineral also contains considerable amounts of both metals. According to literature (e.g. Dutrizac & Jambor, 2000), there is the possibility of silver being bound to jarosite even though it is very unlikely due to the procedure of the zinc winning process. So far, this has not been verified, even though first attempts at using a transmission electron microscope indicate that this could be the case as well. Even a very small amount of silver bound to the jarosite mineral would have a large impact on the silver distribution.

Silicates (quartz and feldspar) which occur as undigested input from the ore very commonly bear inclusions that contain high amounts of copper and silver. Some sphalerite grains with the same kind of inclusions were also found.

- What is the quantity of valuables in specific host particles?

This is actually the most difficult question to answer. Automated software for quantification - SMART PI, for example - cannot be applied, as it was not

possible to produce microscopic sections in a quality needed for automated analysis. Additionally, the small grain size limits the use of such software. Most of the material is too fine-grained for reliable analysis.

If it appears that the jarosite mineral is free of silver, the material could be highly concentrated in silver by removing the jarosite mineral.

- What is the morphology/size of the (host-)particles?

The morphology of the particles is highly versatile, but in general angular to subrounded. The grain size is very small with at least 80 % smaller than 20 μm and at least 60 % smaller than 10 μm . It must be taken into account that the agglomerates render the measurement of grain size distribution difficult.

- Which intergrowth relationships and agglomerates occur?

Lead phases are sometimes closely intergrown with barite. Silver-copper particles were mainly found as inclusions in quartz, feldspar and other phases. To liberate these inclusions, the material would need to be ground down to one micron and below. This is not realistic due to economic reasons. Agglomerates of any kind are common.

11.2 Questions to be Answered- Jarosite from Platinum Production

Jarosite material from platinum production is a pure residue from one process step (iron precipitation) and therefore less variable compared to the jarosite from nickel production. As the economic value is limited to Ni, the value-bearing phases are also very limited.

- Which particles contain the valuables?

Nickel is the only valuable element in this material, even though iron is also a part of the product. Magnetite, trevorite, nickel magnesium silicate, nickel sulphide and gersdorffite are identified as Ni carriers. The precipitated jarosite phase also contains small amounts of nickel (~1.5 wt.%).

- What is the quantity of valuables in specific host particles?
Single particles with high amounts of nickel are mainly trevorite and magnetite. A major importance of these phases is unlikely, as nickel is distributed in the whole material, even in the jarosite mineral.
- What is the morphology/size of the (host-)particles?
Grains are mainly spherical, sometimes elongated and angular to rounded. The grain size is mainly clay to silt-sized with 96 % smaller than 25 μm and 45 % smaller than 10 μm .
- Which intergrowth relationships and agglomerates appear?
Core-rim relations are very common. Jarosite often coats other particles, for example wuestite. Rims also frequently consist of the same phase as the core, but additionally contain several per cent of nickel and sulphur.

11.3 Evaluated Methods and their Usability for Jarosite-Type Residues

For chemical analysis, X-ray fluorescence analysis on pressed powder pellets delivers fast and precise results. ICP-MS is a better tool for trace elements, but is difficult due to the need for dissolving sample material that is mineralogically very heterogeneous and partly inert.

For mineralogical bulk analysis XRD is applicable for identification of major components, despite the technical origin of many components in the jarosite material. Differentiation of jarosite endmembers and quantification of phases is hardly possible. RAMAN spectroscopy was not successful because the grain size of the particles was too small. Furthermore, the database used is for identifying mineralogical phases and many of the present (unnatural) phases are not included in this database.

Electron beam methods are appropriate methods, within their limits of grain size caused mainly by the size of the electron beam. The limits of magnification and imaging can be pushed further, using, for example, an electron microscope equipped with a field emission gun. Besides the technical limits, sample preparation is a major problem that needs further attention. The reason for the problems with the preparation is the small grain size and agglomerates. Strewn slides are a useful addition for investigations using a scanning

electron microscope, but cannot replace a polished section, since only the surface of particles is visible. Grains are often coated by other phases, particularly for jarosite from platinum production.

Quantification of LA-ICP-MS analysis requires a known concentration of a reference element in the analysed spot. In very fine-grained samples, it is barely possible to provide a reference element for every measurement. In order to identify metal-carrying phases, it can be of help if elemental correlations are calculated. These correlations may be performed with quantified results (keeping the error of the reference element in mind) or even with untreated raw data.

Another possibility for treating the reference element is to define points to be measured with electron beam methods before using LA-ICP-MS on the same spot. It is challenging to stay oriented in the very homogeneous sample material, and locate the same spot again on another instrument. The use of coordinates may solve this problem. Special arrangements in the sample preparation may also help. The problem is that the penetration depth of electron beam methods is different to that of LA-ICP-MS.

In summary, the correlation of elements is possible by LA-ICP-MS but EMP allows the same procedure while minimising the problems of calibration. However, EMP is limited to a concentration of >200 ppm depending on, for instance, the element measured and sample preparation.

The correlation method helps to identify valuable-bearing phases. If the element of interest is bound to many different phases, quantification is a major difficulty.

The basics of the methods used were already summarised in Chapter 7.10 . The following table (Table 23) is supplemented by conclusions gathered from their implementation on the different jarosite residues.

Table 23: Usability of evaluated methods for characterising jarosite-type material.

	Morphology	Chemistry	Mineralogy
Light microscopy	Limited usability for a first, general impression of the material. Not applicable for detailed analysis.	Not possible.	Isolated, large particles can be identified. No significance for detailed analysis.
Scanning electron microscope	Of prime importance for characterisation of grain morphology, intergrowth relationships, grain size. Limited to particles larger than some microns.	Only tool (besides electron microprobe) to identify single particles. Element mapping is of inferior importance due to the small grain size. Automated analysis is not possible. Serious analysis of the smallest particles (<1 µm) is not possible.	Defined by chemistry. Differentiation of jarosite endmembers is hardly possible due to the small grain size and the limitations of EDX. Automated analysis is not possible.
Electron microprobe	Characterisation of morphological properties is possible, but inferior to the scanning electron microscope.	Superior method for determination of chemical composition of specific phases. Serious chemical analyses are applicable for the largest particles. For the method of “element correlation” it is the best analytical apparatus.	Allows determination of solid solutions but spatial separation of intergrown endmembers is not possible due to the small scale.

	Morphology	Chemistry	Mineralogy
X-ray fluorescence analysis	Not possible.	Only applicable for powder pellets. Fast method for determination of main elements. Evaluation of measurement results is difficult for original jarosite material, due to non-measurable elements and mixture of oxides, sulphides and sulphates. Superior for online analysis of slag samples during trials.	Not possible.
Inductively coupled plasma – mass spectroscopy	Not possible.	Reliable but complex method for chemical analysis due to difficult leaching of different materials. Well suited for measuring minor elements.	Not possible.
Laser Ablation - Inductively coupled Plasma – Mass Spectroscopy	Not possible.	Limited use for chemical analysis of small spots (>5 μm) for determination of sample heterogeneity and element correlation.	Not possible.

	Morphology	Chemistry	Mineralogy
		Intricate calibration, but lower detection limits than electron microprobe.	
X-ray diffraction analysis	Not possible.	Not possible.	The main phases are detectable, but different types of jarosite cannot be differentiated. Quantification is not possible.
RAMAN spectroscopy	Limited usability due to small magnification.	Not possible.	Identification of large particles is possible. As many phases are anthropogenic, typical geological databases may not be able to identify them.

12. Summary

Different metallurgical by-products are produced all over the world in increasing amounts. Many of these residues are interesting in terms of a further treatment for mainly two reasons: They are

- rich in valuables and therefore potential secondary resources,
- hazardous and a danger to the environment.

For the jarosite residues, chosen for this case study, both reasons apply.

“Jarosite” is a commonly used mineral formed to remove iron from solutions during the hydrometallurgical processes of zinc and nickel production. In these processes, sodium or ammonium are usually added in order to precipitate natrojarosite or ammoniojarosite.

Besides iron forming the main component, it also hosts more valuable metals. The jarosite material from zinc production carries considerable amounts of zinc, lead, silver, copper and

in some cases also gold and indium. Dumping this material causes major problems (=costs), as it must be treated as hazardous waste. The reason why these residues are dumped despite their value is that there is no proper technique for concentration available. This makes an economical recovery of the valuables difficult, even though the amount of some metals is much higher than in primary ores.

Several methods of characterisation were tested in order to evaluate the properties of the jarosite residues and to find proper methods for characterising such material in general. The main difficulty is the small grain size, which limits the use of common imaging techniques and chemical point measurements, or small-scale bulk measurements. For chemical analysis, the heterogeneity of the material is a challenge when using methods that require leaching of the sample. Mineralogical bulk analysis by means of XRD is applicable for the determination of main components but is problematic for amorphous phases and solid solutions. It was not possible to distinguish different types of jarosite reliably. Furthermore, a serious quantification was not possible.

For detailed mineralogical and morphological investigations, the preparation of proper sections is of prime importance. Strewn slides allow an evaluation of grain size and morphology. For detailed analysis concerning valuable phases, intergrowth relationships and inclusions, polished sections are necessary. Due to the small grain size and the tendency to form agglomerates, low viscosity and slow hardening epoxy resins are favourable.

Electron beam methods are the most useful tool to identify major and minor and observe morphological properties. SEMs using tungsten cathodes are very close to their limits of magnification when investigating jarosite residues but are crucial for qualitative analyses and phase characterisation. Electron microscopes equipped with field emission guns allow higher magnification but hardly any improvement in analytical resolution. For the chemical analysis of single grains, electron microprobe analysis is the only applicable technique, but is also limited to the measurement of the larger particles within a jarosite residue.

In order to identify valuable phases, correlation of elements is a promising method. For this, a large number of very small-scale bulk analyses (>5 μm , depending on the method) distributed in a representative section were measured to find correlations between different elements. This was tested using LA-ICP-MS and EMP; the latter emerged as the

more promising method, mainly because of the advantages in calibration, measurement and smaller spot size.

The following main characteristics were determined for the jarosite material from zinc production:

- It contains considerable amounts of lead (4-7.1 %), zinc (2.2-6.6 %), copper (0.4-0.75 %) and silver (80-219 ppm), and sometimes also gold (<11 ppm) and indium (<210 ppm). Deleterious elements like arsenic and cadmium appear in small amounts (0.81 % As and 0.16 % Cd).
- The distribution of elements in the 30 μm scale is generally homogeneous.
- The grain size is very small; 50-60 % finer than 10 μm .
- The main phases are different types of jarosite; mainly natrojarosite but also ammoniojarosite, plumbojarosite and hydroniumjarosite.
- Jarosite minerals may carry several per cent of lead and zinc.
- Other phases are: franklinite (Zn), sphalerite (Zn), anglesite (Pb), galena (Pb), litharge (Pb), feldspar and quartz (bearing Cu and Ag inclusions).
- Gypsum is removable by means of mineral processing. However, only in one specific jarosite residue was the amount high enough to allow a beneficiation under economical conditions.

For the jarosite from platinum production, the main characteristics are:

- Nickel is the main element of value (~4.4 %).
- Particle size is smaller than 40 μm and about 50 % smaller than 10 μm .
- The main phase is ammoniojarosite.
- Nickel is distributed in many different phases and often associated with iron minerals.

This work also presents an approach for a characterisation procedure for metallurgical residues. Even though it was not possible to quantify specific phases, this procedure can help to evaluate unknown materials.

A significant part of this research was done in close cooperation with industrial partners in order to develop a proper process for treating the different jarosite materials. The

importance of characterisation in general was demonstrated according to the accompanying trials of mineral processing and pyrometallurgy, not only for the input material, but also for intermediate and final products.

In most cases, the extensive beneficiation trials using magnetic and granulometric methods were not able to produce a reasonable concentrate from the jarosite material. This is mainly because the jarosite mineral obviously hosts considerable amounts of the valuable metals (lead, zinc and nickel). This is in contrast to theory, where lead is removed before the iron precipitation step where the jarosite mineral is built and zinc stays in the solution. Beneficiation was successful in one specific case, namely where the residue was rich in gypsum. By means of flotation, the removal of gypsum allowed an enrichment of the valuables.

The pyrometallurgical two-step process was successfully tested on both jarosite types.

Tests on jarosite from zinc production produced three products:

- zinc oxide in the off-gas,
- a fayalitic slag
- and an alloy which collects mainly lead, copper and silver.

The slag was very low in valuables, respectively in heavy metals that would cause problems in further use or dumping. It was evaluated to replace sand in concrete. In these tests, eluate testing was not satisfying, as the amount of leached lead was too high, most likely due to inclusions of metallic lead in the slag. Solutions for treating this problem include the use of another furnace for the reduction step, which allows better settling conditions for the liquid metal, and a reduced amount of slag in the concrete. Mechanical testing showed very positive results with hardly any cement-slag-sand mixtures having worse properties compared to the reference concrete sample. Most slag mixtures showed even considerably higher compressive and flexural strength.

The roasting-reduction trials on jarosite from nickel production were also successful. Arsenic was effectively removed during calcination and the possibility of producing an iron-nickel alloy with adjustable Ni content was demonstrated. Further treatment of the formed slag was not evaluated, but might also be worth further considerations.

12.1 Outlook

Extensive work on characterisation produced extensive know-how concerning the properties and composition of the jarosite residues evaluated. This work was planned to form the basis for the characterisation of other, potential secondary resources. Even though a final characterisation procedure that can answer all questions concerning a residue has not been defined yet, the evaluation of unknown material will be facilitated if the approach presented is followed. A major challenge is the quantification of identified phases and ongoing work will focus on this task. Furthermore, the applicability of this procedure needs to be tested and possibly adapted for other materials.

Successful trials on beneficiation, pyrometallurgy and the use of slag demonstrated what this material and its products can be used for. It remains to be seen if the industry is interested in continuing research on this promising treatment, or if dumping will stay the preferred way. In the latter case, treatment of these residues is certainly not being abandoned, but rather just postponed.

13. Acknowledgements

Thank you to MinProSol, ARP and Fernando Castro (W2V and University of Minho) for being reliable partners for trials of mineral processing and pyrometallurgy as well as for the discussions and analytics.

Many thanks as well to all other partners who contributed over the years with know-how, sample material, for good discussions and deep insights into their metallurgical processes.

14. References

- Anthony, J. W., Bideaux, R. A., Bladh, K. W. & Nichols, M. C., 1990. *Handbook of mineralogy, volume I. Elements, sulfides, sulfosalts, Miner..* s.l.:s.n.
- Antrekowitsch, J. & Steinlechner, S., 2010. Characterization of Zinc Containing Residues from Nonferrous Industry. In: *PbZn 2010*. New Jersey: John Wiley & Sons, Inc. Hoboken, pp. 153-164.
- Balladares, E. et al., 2014. Chemical-mineralogical characterization of copper smelting flue dust.. *Dyna*, 81(186), pp. 11-18.
- Basciano, L. C. & Peterson, R. C., 2010. A crystallographic study of the incomplete solid-solution between plumbojarosite and jarosite.. *The Canadian Mineralogist*, 48(3), pp. 651-659.
- Boliden, 2019. *Boliden Odda*. [Online] Available at: <https://www.boliden.com/operations/smelters/boliden-odda/> [Accessed 31 10 2019].
- Cramer, L. A., 2001. The extractive metallurgy of South Africa's platinum ores. *Jom*, 53(10), pp. 14-18.
- Crundwell, F. et al., 2011. *Extractive metallurgy of nickel, cobalt and platinum group metals..* s.l.:Elsevier.
- Desborough, G. A. et al., 2010. Mineralogical and chemical characteristics of some natural jarosites.. *Geochimica et Cosmochimica Acta*, 74(3), pp. 1041-1056.
- Dutrizac, J. E. & Chen, T. T., 2000. The behaviour of gallium during jarosite precipitation.. *Canadian metallurgical quarterly*, 39(1), pp. 1-14.
- Dutrizac, J. E., Chen, T. T. & Beauchemin, S., 2005. The behaviour of thallium(III) during jarosite precipitation.. *Hydrometallurgy*, 79(3-4), pp. 138-153.
- Dutrizac, J. E. & Jambor, J. L., 2000. Jarosites and Their Application in Hydrometallurgy. *Geochemistry*, 40(1), pp. 405-452.
- Dutrizac, J. E., n.d. Factors affecting alkali jarosite precipitation.. *Metallurgical Transactions B*, 14(4), pp. 531-539.
- Forray, F. L. et al., 2010. Synthesis, characterization and thermochemistry of a Pb-jarosite.. *Geochimica et Cosmochimica Acta*, 74(1), pp. 215-224.
- Garcia, A. & Valdez, C., 1996. Jarosite disposal practices at the Penoles zinc plant. *Iron Control and Disposal*, pp. 643-650.

- Goldstein, J. I. et al., 2017. *Scanning electron microscopy and X-ray microanalysis*. s.l.:Springer.
- Graupner, T. et al., 2007. Formation of sequences of cemented layers and hardpans within sulfide-bearing mine tailings (mine district Freiberg, Germany).. *Applied Geochemistry*, 22(11), pp. 2486-2508.
- Graves, P. & Gardiner, D., 1989. *Practical raman spectroscopy*. s.l.:Springer.
- Grimsey, E. J., 1993. Metal recovery in nickel smelting and converting operations. *Extractive Metallurgy of Copper, Nickel and Cobalt.*, 1, pp. 1239-1251.
- Han, H. et al., 2014. Anglesite and silver recovery from jarosite residues through roasting and sulfidization-flotation in zinc hydrometallurgy. *Journal of Hazardous Materials* 278, pp. 49-54.
- Hanke, G. & Antrekowitsch, J., 2018. Characterisation and Pyrometallurgical Recycling of Jarosite Type Residues out of Zinc Primary Metallurgy. *World of Metallurgy – ERZMETALL* 71/1, pp. 25-30.
- Hanke, G., Melcher, F. & Antrekowitsch, J., 2016. Characterisation of By-products of the Zinc Industry. *OPMR 2016 Opportunities in Processing of Metal Resources in South East Europe*, pp. 184-190.
- Hanke, G., Onuk, P. & Antrekowitsch, J., 2018. *Characterization Strategies for Metallurgical By-Products: Case Study Jarosite*. s.l., FLOGEN.
- Ismael, M. R. C. & Carvalho, J. M. R., 2003. Iron recovery from sulphate leach liquors in zinc hydrometallurgy. *Minerals Engineering*, 16(1), pp. 31-39.
- Jamieson, H. E., Walker, S. R. & Parsons, M. B., 2015. Mineralogical characterization of mine waste.. *Applied Geochemistry*, 57, pp. 85-105.
- Johnson, C., Pownceby, M. I. & Wilson, N. C., 2015. The application of automated electron beam mapping techniques to the characterisation of low grade, fine-grained mineralisation; potential problems and recommendations.. *Minerals Engineering*, 79, pp. 68-83.
- Jones, R. T., 1999. Platinum smelting in South Africa. *South African Journal of Science* 95, pp. 525-534.
- Ju, S. et al., 2011. Clean hydrometallurgical route to recover zinc, silver, lead, copper, cadmium and iron from hazardous jarosite residues produced during zinc hydrometallurgy.. *Journal of hazardous materials*, 192(2), pp. 554-558.

- Kangas, P. et al., 2017. *The Jarogain Process for Metals Recovery from Jarosite and Electric Arc Furnace Dust: Process Design and Economics.*, s.l.: s.n.
- Katsioti, M. et al., 2005. Use of jarosite/alunite precipitate as a substitute for gypsum in Portland cement.. *Cement and concrete composites*, 27(1), pp. 3-9.
- Krishnan, V., 2016. *Evaluation of Jarofix Soil Embankment using Numerical Modelling.* Kurukshehra: Department of Civil Engineering, National Institute of Technology.
- Lamya , R. M., 2007. *A fundamental evaluation of the atmospheric pre-leaching section of the nickel-copper matte treatment process.* University of Stellenbosch: s.n.
- Lünsdorf, N. K. et al., 2019. Semi-Automated Heavy-Mineral Analysis by Raman Spectroscopy. *Minerals*, 9(7), p. 385.
- Malenga, E. N., Mulaba-Bafubiandi, A. F. & Nheta, W., 2015. Alkaline leaching of nickel bearing ammonium jarosite precipitate using KOH, NaOH and NH₄OH in the presence of EDTA and Na₂S.. *Hydrometallurgy*, 155, pp. 69-78.
- Matousek, J. W., 1993. The Behavior of Cobalt in Pyrometallurgical Process. *Extractive Metallurgy of Copper, Nickel and Cobalt.*, 1, pp. 129-142.
- Matthes, S., 1996. *Mineralogie: Eine Einführung in die spezielle Mineralogie, Petrologie und Lagerstättenkunde.* 5 ed. s.l.:Springer-Verlag.
- Metso Corporation, 2015. *Basics in Minerals Processing.* s.l.:s.n.
- Nasdala, L., Smith, D. C., Kaindl, R. & Ziemann, M. A., 2004. Raman spectroscopy: analytical perspectives in mineralogical research. *Spectroscopic methods in mineralogy*, pp. 281-343..
- Nheta, W. & Makhatha, M. E., 2013. *Leaching of nickel from a jarosite precipitate with hydrochloric acid.* s.l., s.n.
- Ntumba-Malenga, E., Mulaba-Bafubiandi, A. F. & Nheta, W., 2014. *Ni recovery using KOH, NaOH, and NH₄OH in the presence of EDTA and Na₂S from jarosite precipitated from a PGM plant.* s.l., The Southern African Institute of Mining and Metallurgy.
- Onuk, P. et al., 2017. Development of a Matrix-Matched Sphalerite Reference Material (MUL-ZnS-1) for Calibration of In Situ Trace Element Measurements by Laser Ablation-Inductively Coupled Plasma-Mass Spectrometry.. *Geostandarts and Geoanalytical Research.* 41(2), pp. 263-272.
- Pappu, A., Saxena, M. & Asolekar, S. R., 2006. Jarosite characteristics and its utilisation potentials. *Science of the total environment* 359 (1-3), pp. 232-243.

- Pawlek, F., 1983. *Metallhüttenkunde*. Berlin, New York: Walter de Gruyter & Co.
- Pennycock, S. J. & Nellist, P. D., 2011. *Scanning transmission electron microscopy: imaging and analysis*. s.l.:Springer Science & Business Media.
- Piatak, N. M. et al., 2003. *Geochemical Characterization of Slags, Other Mine Waste, and Their Leachate from the Elizabeth and Ely Mines (Vermont), the Ducktown Mining District (Tennessee), and the Clayton Smelter Site (Idaho)*. , s.l.: US Geological Survey.
- Pichler, C., Unger, A. & Antrekowitsch, J., 2013. Rückgewinnung von Wertmetallen aus Stahlwerkstäuben durch ein reduzierendes Metallbad. In: *Aschen-Schlacken-Stäube*. Neuruppin: TK Verlag Karl Thomé-Kozmiensky, pp. 587-598.
- Rathore, E. N., Patil, M. P. & Dohare, E. D., 2014. Utilization of jarosite generated from lead-zinc smelter for various applications: A review.. *IJCIET*, 5(11), pp. 192-200.
- Reuter, M. A., 2013. *UNEP Metal Recycling: Opportunities, Limits, Infrastructure.*, s.l.: International Resource Panel.
- Ripmeester, J. A., Ratcliffe, C. I., Dutrizac, J. E. & Jambor, J. L., 1986. Hydronium ion in the alunite-jarosite group.. *The Canadian Mineralogist*, 24(3), pp. 435-447.
- Rizescu, C., Bacinschi, Z., Stoian, E. & Polinescu, A., 2010. *Characterisation of steel mill electric-arc furnace dust.* s.l., s.n.
- Rosales, C. R., 2016. Treatment of High Iron Calcines in the Electrolytic Zinc Plant of Metallurgica Met-Mex Penoles, S.A. De C.V.. *Iron Control: Practice and Research*, pp. 239-246.
- Ruşen, A., Sunkar, A. S. & Topkaya, Y. A., 2008. Zinc and lead extraction from Çinkur leach residues by using hydrometallurgical method.. *Hydrometallurgy* 93,(1-2), pp. 45-50.
- Sahu, K. K. & Agrawal, A., 2008. Lead Zinc Extraction Processes..
- Salinas, E. et al., 2001. Characterization and alkaline decomposition–cyanidation kinetics of industrial ammonium jarosite in NaOH media.. *Hydrometallurgy*, 60(3), pp. 237-246.
- Schultz, L. G., 1964. Quantitative interpretation of mineralogical composition from X-ray and chemical data for the Pierre Shale. *US Geol. Surv. Prof. Pap.*, 391-C.
- Scott, K. M., 1987. Solid solution in, and classification of, gossan-derived members of the alunite-jarosite family, northwest Queensland, Australia.. *American Mineralogist*, 72(1-2), pp. 178-187.

- Sharma, P., 2016. Feasibility Study of Industrial Jarosite Waste as Vital Material for Construction: Positive and Negative Aspects. *Malaysian Journal of Civil Engineering* 28(1), pp. 139-154.
- Sinclair, R. J., 2005. *The Extractive Metallurgy of Zinc*. Victoria: The Australasian Institute of Mining and Metallurgy.
- Stoffregen, R. E., Alpers, C. N. & Jambor, J. L., 2000. Alunite-jarosite crystallography, thermodynamics, and geochronology.. *Reviews in mineralogy and geochemistry*, 40(1), pp. 453-479.
- Svens, K., Kerstiens, B. & Runkel, M., 2003. Recent experiences with modern zinc processing technology.. *Erzmetall*, 56(2), pp. 94-103.
- Swayze, G. A. et al., 2008. Understanding Jarosite—From Mine Waste to Mars.. *US Geological Survey Circular*, 1328, pp. 8-13.
- van Dyk, J. P., 2006. An Overview of the Zincor Process. *Southern African Pyrometallurgy*, pp. 273-282.
- Vereš, J., Šepelák, V. & Hredzák, S., 2015. Chemical, mineralogical and morphological characterisation of basic oxygen furnace dust.. *Mineral Processing and Extractive Metallurgy*, 124(1), pp. 1-8.
- Von Heimdahl, M., 1970. *Einführung in die Elektronenmikroskopie: Verfahren zur Untersuchung von Werkstoffen und anderen Festkörpern*. s.l.:Vielweg.
- Wegscheider, S., Hanke, G., Steinlechner, S. & Antrekowitsch, J., 2017. *Process development for a combined treatment of EAFD and jarosite*. Porto, s.n., pp. 37-44.
- Welch, S. A. et al., 2008. Jarosite dissolution II—Reaction kinetics, stoichiometry and acid flux.. *Chemical Geology*, 254(1-2), pp. 73-86.
- Williams, D. & Carter, C. B., 2009. *Transmission Electron Microscopy A Textbook for Material Science*. s.l.:Springer US.
- Wilson, S. A., Ridley, W. I. & Koenig, A. E., 2002. Development of sulfide calibration standards for the laser ablation inductively-coupled plasma mass spectrometry technique.. *Journal of Analytical Atomic Spectrometry*, 17(4), pp. 406-409.

15. List of Figures

Figure 1: Sketch showing typical steps of the evaluation of a residue, process development and upscaling for process optimisation.	3
Figure 2: Simplified sketch of hydrometallurgical zinc production showing possible compositions of dumped material. Blue represents different process steps and orange, residues produced.	9
Figure 3: Simplified sketch of the base metals refinery process for winning of Cu, Ni, Co and a PGM concentrate.	18
Figure 4: Photographs of four different dried residues from zinc production. A, B and C show jarosite materials from different plants and D a pure leaching residue.....	26
Figure 5: Dried jarosite residue from platinum production.	27
Figure 6: Matrix grid of the type XM. The diameter of the disc is 3.5 cm.	29
Figure 7: Overview (left) and detail (right) of the hydro separation used for producing a 30 μm concentrate out of jarosite.	38
Figure 8: Two BSE images of the monolayer section from hydro separation using a field emission gun- scanning electron microscope. Note the well-separated grain size fraction.	39
Figure 9: Example of two jarosite sections using a fast hardening and high viscosity epoxy resin.....	43
Figure 10: Examples of polished jarosite sections. The numbering corresponds to Table 9.	45
Figure 11: XRD spectrum of a jarosite from zinc production. Different jarosite endmembers and gypsum are clearly detected. Step size: 0.010° , step time: 11 s.	46
Figure 12: XRD spectrum of a jarosite sieve fraction smaller than 10 μm . The absence of gypsum makes this fraction different from the whole jarosite sample as shown in Figure 11. Step size: 0.020° , step time: 14 s.	47
Figure 13: Distribution of main elements measured using LA-ICP-MS on a pressed powder pellet.	48
Figure 14; Distribution of trace elements measured using LA-ICP-MS on a pressed powder pellet.	48
Figure 15: Positive correlation of sulphur with barium (left) and lead (right).	50
Figure 16: Correlation of Fe-Zn (left) and Fe-S (right).	50

Figure 17: Negative correlation of Si-S (left) and Fe-Si (right).	51
Figure 18: Correlation of Ag-Cu (left) and Ba-Pb (right).	51
Figure 19: Screening curve of a jarosite from zinc production.	52
Figure 20: BSE image of a natrojarosite from a residue from a European zinc smelter measured by SEM-EDX.	53
Figure 21: BSE image (FEG) and two WDX measurements of a jarosite particle. Due to the small scale, a precise measurement is not possible but the bright areas are richer in lead than the darker ones. Analysis was performed using a FEG EMP at University of Graz.	54
Figure 22: Correlation of atoms per formula unit for Zn-Fe (left) and Pb-Zn (right).	56
Figure 23: Correlation of atoms per formula unit for Na-Pb (left) and Na-Zn (right).	56
Figure 24: Correlation of atoms per formula unit for Na-Fe (left) and Pb-Fe (right).	57
Figure 25: SEM image of zinc ferrite (upper cross and table) and gahnite (Zn-Al spinel, lower cross and table).	58
Figure 26: SEM-image of a sphalerite grain (containing 3.74 % Fe) with a silver-bearing covellite inclusion (green circle).	58
Figure 27: EMP-WDX mapping of Pb, S and O on a section of hydro separated jarosite material. Note the different lead phases anglesite (yellow circle) and galena (red circle).	59
Figure 28: EMP-WDX mapping of Pb, S and O on a characteristic section of jarosite residue from zinc production.	60
Figure 29: Large particle of a lead-barium sulphate particle.	60
Figure 30: BSE and X-ray distribution image of a strontium-bearing barite surrounded by galena (brighter grains).	61
Figure 31: Left: Large orthoclase with silver and copper-bearing inclusions. Right: Potassium feldspar. The circled inclusion in the middle is galena with copper-bearing zones. The upper circle marks a copper-silver-bearing inclusion	61
Figure 32: BSE image of a garnet grain.	62
Figure 33: SEM-EDX mapping of a large MnO particle with a layer of silver chloride.	64
Figure 34: SEM image of a chalcocite particle (left) and barite grain (right).	65
Figure 35: SEM image of a gold particle.	65

Figure 36: Selected area of a section of the hydro separated concentrate for quantitative mineralogical analysis (SEM-EDX).....	66
Figure 37: Number of identified phases in a hydro separated sample corresponding to Figure 36 and Table 13.....	68
Figure 38: S/TEM image of a natro-/plumbojarosite and chemical analysis of the whole grain (EDX).....	69
Figure 39: EDX mapping of Fe, Zn, Na, Pb, Cu, Ag, Ca, Si, S, Al, K and In using an S/TEM. The particle is the same as in Figure 38.....	69
Figure 40: Different samples prepared for investigations using a scanning electron microscope. The three samples to the left are embedded in epoxy and polished. The diameter is 4 cm each. From left to right: final slag, roasted pellets (calcine) and original residue. The sample on the right is a strewn slide on double-faced adhesive tape.	70
Figure 41: Grain size distribution of a jarosite from platinum production measured by laser granulometry (ARP).....	72
Figure 42: XRD spectra of a jarosite from platinum production. measured by Materials Center Leoben.....	73
Figure 43: Reflected light photomicrograph of a polished jarosite sample.....	73
Figure 44: SEM-BSE image of a wuestite grain (right cross and analysis). The surrounding, darker phase (left cross) is also iron oxide, but contains sulphur and nickel in addition (left analysis).	74
Figure 45: SEM element mapping of the same area as in Figure 44. Opposed distribution of iron and nickel is visible.	74
Figure 46: Example of a large particle of ammoniojarosite in the jarosite residue from platinum production, containing more than 1 wt.% of Ni and As.	75
Figure 47: Typical appearance of a jarosite material from platinum production using a scanning electron microscope and a BSE detector. The chemical composition (SEM-EDX) refers to the green crosses and indicates ammoniojarosite.....	75
Figure 48: SEM-BSE image and EDX measurements of iron-nickel oxide grains.	77
Figure 49: SEM element mapping of an African leaching residue. The calcium distribution matches the appearance of gypsum, as it is the only calcium bearing phase.....	79

Figure 50: Lead recovery achieved in concentrate out of flotation trials with two different reagent regimes and parameter settings with the aim of removing gypsum from a jarosite residue.....	81
Figure 51: Copper recovery in concentrate after removing gypsum from a jarosite residue from trials with two different reagent regimes and parameter settings.	81
Figure 52: Results from flotation trials on a typical jarosite sample. The diagram shows the recovery of lead achieved with different reagent regimes and parameter settings.	82
Figure 53: Results from flotation trials on a typical jarosite sample. The diagram shows the recovery of zinc achieved with different reagent regimes and parameter settings.	83
Figure 54: SEM image of the sieve fraction larger than 200 μm prepared as a polished section. Most of the particles are not single grains, but agglomerates.	84
Figure 55: SEM image of the fraction 45-63 μm prepared as a strewn slide, showing numerous agglomerates.	84
Figure 56: SEM BSE image of a sample from the non-magnetic fraction of V6 Tap 5 showing numerous agglomerates.	85
Figure 57: Sketch of the roasting-reduction process for jarosite.....	87
Figure 58: A disc pelletizer (left) was used to agglomerate the jarosite. The right picture shows the jarosite pellets.	90
Figure 59: Left: Tapping of calcine from the TBRC. Upper right: opened cap of the TBRC. Note the flame of the gas burner. Lower right: freshly calcined, still-glowing jarosite pellets.....	91
Figure 60: Synthetic pre-slag of fayalite composition. The mould is about 15 cm wide. ...	92
Figure 61: Left: Electric furnace used for reducing the jarosite calcine. Upper right: Calcine is fed but not yet completely molten. White smoke indicates evaporating zinc. Lower right: The whole load is molten. White smoke is nearly gone.	93
Figure 62: Left: tapping of slag into a water drum. Right: Quenched slag.....	93
Figure 63: Grain size distribution of the slag determined by sieve analysis at W2V.	94
Figure 64: Trials for evaluation of flexural strength on 10 different mixtures of cement, sand and slag.	95
Figure 65: Trials for evaluation of compressive strength on 10 different mixtures of cement, sand and slag.....	96

Figure 66: Upper left: jarosite from platinum production mixed with calcium hydroxide ready for pelletizing (first trial). Right: Agglomeration process. The pelletizing disc is the same as in Figure 58. Lower left: finished pellets of about 0.5-1.7 cm in diameter.	100
Figure 67: Tapping of the jarosite from platinum production after reduction. The sparks on the floor are caused by oxidation of metallic iron and the rising burning carbon powder.	102
Figure 68: SEM Image (BSE detector) of a polished section of a slag sample from treating jarosite from zinc production. Note the presence of zinc sulphide.....	107
Figure 69: Slag sample from a reduction trial on jarosite-calcine. The bright phases are lead-iron particles; the matrix is the fayalitic slag	108
Figure 70: The off-gas of a reduction trial showed considerable amounts of lead (white in the picture).....	109
Figure 71: BSE image and qualitative calcium and sulphur mapping of a representative area of calcinated jarosite from platinum production. Note the correlation of calcium and sulphur caused by the formation of anhydrite.	111
Figure 72: XRD analysis of jarosite from platinum production after calcination.	112
Figure 73: Image of a calcinated jarosite from platinum production. The chemical composition concerns the area in the yellow circle.	112
Figure 74: Lead oxide (left) and lead sulphate (right) from different parts of the off-gas unit.	113
Figure 75: Nickel-iron-sulphur particle. The right half of the spherical grain is an iron nickel alloy (90 %-10 %) whilst the left half has the chemical composition of a heazlewoodite (Ni_3S_2).	114
Figure 76: Two different inclusions in a final slag from a reduction trial on jarosite from platinum production. Both consist of about 90 % iron and 10 % nickel.	114
Figure 77: Calculated share of value from two different jarosite residues.	117
Figure 78: Proposal for a characterisation procedure for fine grained material.	120

16. List of Tables

Table 1: Members of the jarosite subgroup.....	5
Table 2: Metal contents in by-products of different iron removal processes per 100 t of feed concentrate (Sinclair, 2005).....	15
Table 3: Details of zinc plants in Europe. Own investigations, Chair of Nonferrous Metallurgy.....	16
Table 4: Settings used for magnetic separation by HGMS.....	29
Table 5: Calibration parameters and standards used for measurements with electron microprobe analysis.....	32
Table 6: Summary of evaluated analytical methods.....	36
Table 7: Chemical composition of five different jarosite residues from zinc production..	41
Table 8: Results of different analytical methods and institutions. GEG-Chair of Geology and Economic Geology, Chem-Chair of Analytical Chemistry MUL.....	42
Table 9: List of resins and grinding and polishing devices used for preparation of polished sections of jarosite material.....	44
Table 10: Correlation matrix of selected elements. Measurements made by electron microprobe on a jarosite section.....	50
Table 11: Element composition and calculated atoms per formula unit normalised to 11 oxygen for selected jarosite particles. The right columns show the composition of an ideal natrojarosite, the mean values of all measurements (n=25) and two EMP-WDX measurements. All other columns refer to SEM-EDX measurements.....	55
Table 12: Identified silver (-bearing) particles in residues from zinc production. Values are given in wt.%.....	63
Table 13: Identified phases in the hydro separated jarosite sample. The numbering corresponds to Figure 36.....	67
Table 14: Chemical composition of jarosite from nickel production measured by AMCO (ICP-OES, aqua regia digestion) and MinProSol (RFA, powder pellets). The left and middle columns are original jarosite residues; the right column is the same material but with calcium hydroxide added as a binder prior to calcination trials.....	71
Table 15: Element composition (SEM-EDX) and calculated atoms per formula unit normalized to 11 oxygen for selected jarosite particles (jarosite from platinum production). Right columns show the composition of an ideal ammoniojarosite and	

the mean values of all measurements (n=14). Hydrogen and nitrogen are not measurable by the method used.	76
Table 16: SEM-EDX measurements on selected grains (iron-nickel phases) on a polished section of jarosite from platinum production.	77
Table 17: Comparison of valuable elements in a jarosite residue and the fraction	85
Table 18: Chemical analyses of fractions from HGMS trials performed by MinProSol.	86
Table 19: Pros and cons of different metals used as collectors.	88
Table 20: Composition of the different cement-sand-slag mixtures.	95
Table 21: Results from leaching trials on crushed concrete samples (<10 mm) containing 20 % slag,	97
Table 22: Comparison of common minimum metal contents in primary ores and average chemistry from jarosite from zinc production (Pawlek, 1983).	115
Table 23: Usability of evaluated methods for characterising jarosite-type material.	126

17. List of Appendices

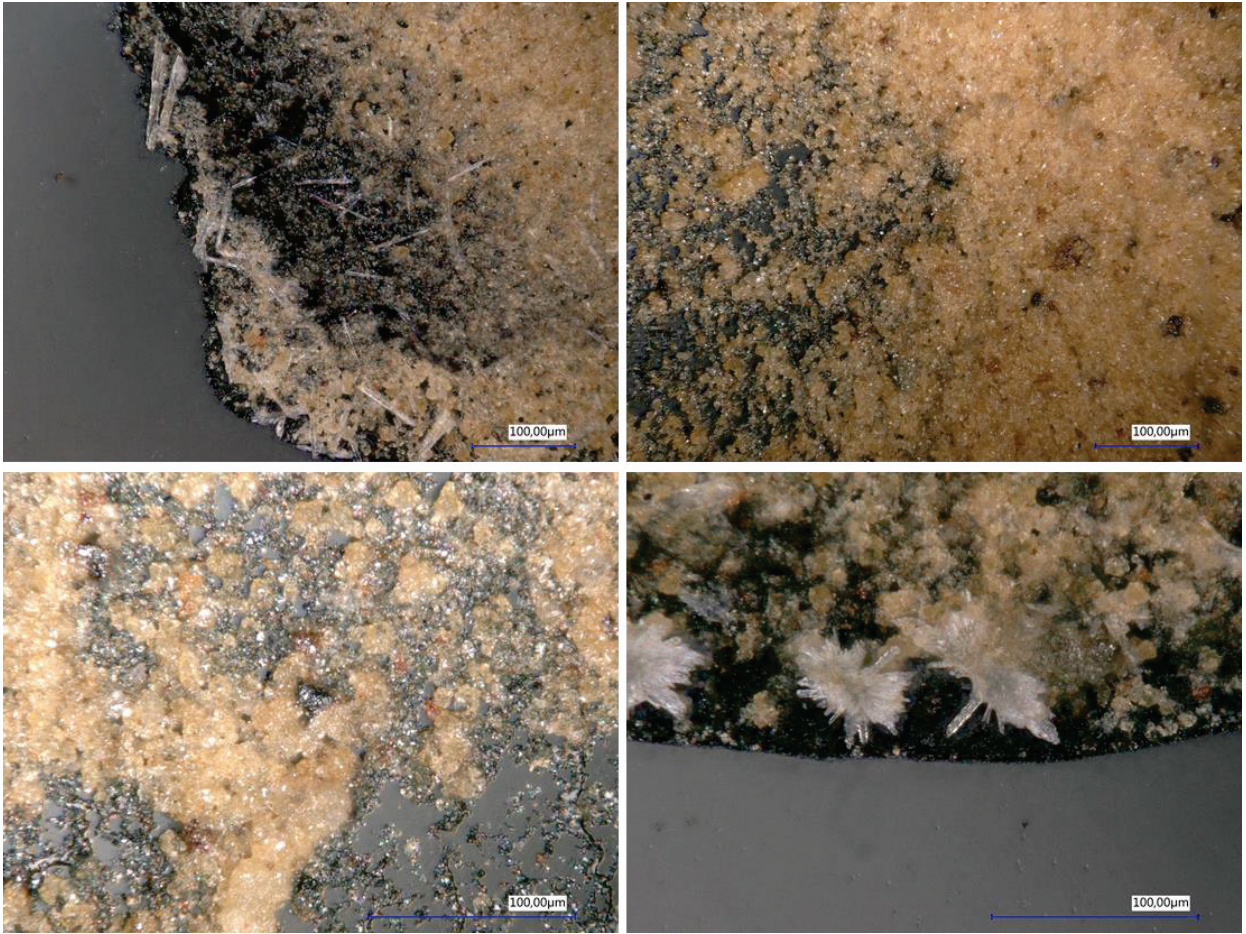
Appendix 1: Jarosite material from zinc production showing euhedral gypsum crystals.	149
Appendix 2: XRF analysis of a jarosite from zinc production (pressed powder pellet). ...	150
Appendix 3: XRF analysis of a jarosite from zinc production (pressed powder pellet). ...	151
Appendix 4: SEM-EDX element mapping of a representative section of jarosite from zinc production.....	152
Appendix 5: SEM-EDX measurements on different fractions from magnetic separation of a jarosite residue from zinc production.....	153
Appendix 6: SEM-EDX measurements of a residue from jarosite from zinc production after leaching in aqua regia for chemical analysis.....	154
Appendix 7: SEM-EDX measurements of a residue from jarosite from zinc production after leaching in aqua regia for chemical analysis (continuation).....	155
Appendix 8: XRD patterns of a jarosite residue and two grain-size fractions of the same material.	156
Appendix 9: RAMAN measurement of a magnetite in a jarosite residue from zinc production.....	156
Appendix 10: RAMAN measurement of a jarosite particle in a jarosite residue from zinc production.....	157
Appendix 11: RAMAN measurement of a sphalerite in a jarosite residue from zinc production.....	157
Appendix 12: Selected SEM-EDX measurements on a polished section of slag produced during pyrometallurgical treatment of jarosite residue from zinc production.	158
Appendix 13: Four XRF measurements (powder discs) of the same jarosite material (Zn production).....	159
Appendix 14: SEM-EDX element measurements of a silver-bearing particle from jarosite residue from zinc production.....	159
Appendix 15: SEM-EDX element measurements of a silver-bearing particle from jarosite residue from zinc production (continuation 1).....	160
Appendix 16: SEM-EDX element measurements of a silver-bearing particle from jarosite residue from zinc production (continuation 2).....	161
Appendix 17: SEM-EDX element measurements of a silver-bearing particle from jarosite residue from zinc production (continuation 3).....	162

Appendix 18: SEM-EDX element measurements of a silver-bearing particle from jarosite residue from zinc production (continuation 4).....	163
Appendix 19: SEM-EDX element measurements of a silver-bearing particle from jarosite residue from zinc production (continuation 5).....	164
Appendix 20: SEM-EDX element measurements of a silver-bearing particle from jarosite residue from zinc production (continuation 6).....	165
Appendix 21: Grain size distribution (sieve analysis) of four jarosite samples from the same material (Zn production).....	165
Appendix 22: Sieve curves referring to Appendix 21.	166
Appendix 23: Settings and throughput of HGMS trials on jarosite from zinc production.	167
Appendix 24: Chemical composition of different fraction from HGMS trials with jarosite from zinc production.....	167
Appendix 25: Calculation of atoms per formula unit based on SEM-EDX and EMP-WDX measurements (jarosite from zinc production).	168
Appendix 26: Calculation of atoms per formula unit based on SEM-EDX and EMP-WDX measurements (jarosite from zinc production , continuation).	169
Appendix 27: STEM image and EDX measurement of a jarosite from zinc production....	170
Appendix 28: STEM image and EDX measurement of a jarosite from zinc production....	170
Appendix 29: SEM-WDX measurements of jarosite material from platinum production.	171
Appendix 30: SEM-WDX measurements of jarosite material from platinum production (continuation).....	172
Appendix 31: Calcination trials with jarosite from zinc production. Upper left: jarosite pellets ready for calcination. Upper right: calcination in the TBRC. Middle: tapping of the calcine. Bottom: calcine.....	173
Appendix 32: Reduction trials with jarosite from zinc production. Upper left: calcine. Upper right and middle left: reduction in the electric furnace. Middle left: tapping. bottom left: slag. bottom right: slag and alloy.	174
Appendix 33: SEM-EDX measurements on calcine and slag from pyrometallurgical trials on jarosite from platinum production.	175
Appendix 34: SEM-EDX measurements on calcine and slag from pyrometallurgical trials on jarosite from platinum production (continuation 1).	176

Appendix 35: SEM-EDX measurements on calcine and slag from pyrometallurgical trials on jarosite from platinum production (continuation 2).	177
Appendix 36: RAMAN measurement of a jarosite particle in a jarosite residue from platinum production.....	178
Appendix 37: RAMAN measurement of a hematite particle in a jarosite residue from platinum production.	178
Appendix 38: SEM-EDX analyses of the calcine of jarosite from platinum production after calcination trial 1.....	179
Appendix 39: SEM-EDX analyses of slag from jarosite from platinum production after reduction trial 1.....	180
Appendix 40: SEM-EDX analyses of the calcine of jarosite from platinum production after calcination trial 2.1.....	181
Appendix 41: SEM-EDX analyses of the calcine of jarosite from platinum production after calcination trial 2.2.....	182
Appendix 42: SEM-EDX analyses of slag from jarosite from platinum production after reduction trial 2.2.....	183
Appendix 43: SEM-EDX analyses of the calcine of jarosite from platinum production after calcination trial 3.1.....	184
Appendix 44: SEM-EDX analyses of slag from jarosite from platinum production after reduction trial 3.1.....	185
Appendix 45: SEM-EDX analyses of the calcine of jarosite from platinum production after calcination trial 3.2.....	186
Appendix 46: SEM-EDX analyses of slag from jarosite from platinum production after reduction trial 3.2.....	187
Appendix 47: Preparation of jarosite from platinum production for pyrometallurgical treatment. Upper left: mixer. Upper right: Jarosite from platinum production mixed with calcium hydroxide. Bottom left: pelletizing disc. Bottom right: pellets ready for calcination.	188
Appendix 48: Calcination trials with jarosite from platinum production. Upper right: charging of the TBRC. Upper right: closed TBRC. Middle left: gas burner. Middle right and bottom left: Tapping of the calcine. Lower right: calcine.....	189

Appendix 49: Reduction trials with jarosite from platinum production. Upper left: Electric furnace prepared for trials. Upper right: sampling during reduction trial. Middle: liquid slag. Bottom: slag and alloy after tapping. 190

18. Appendix



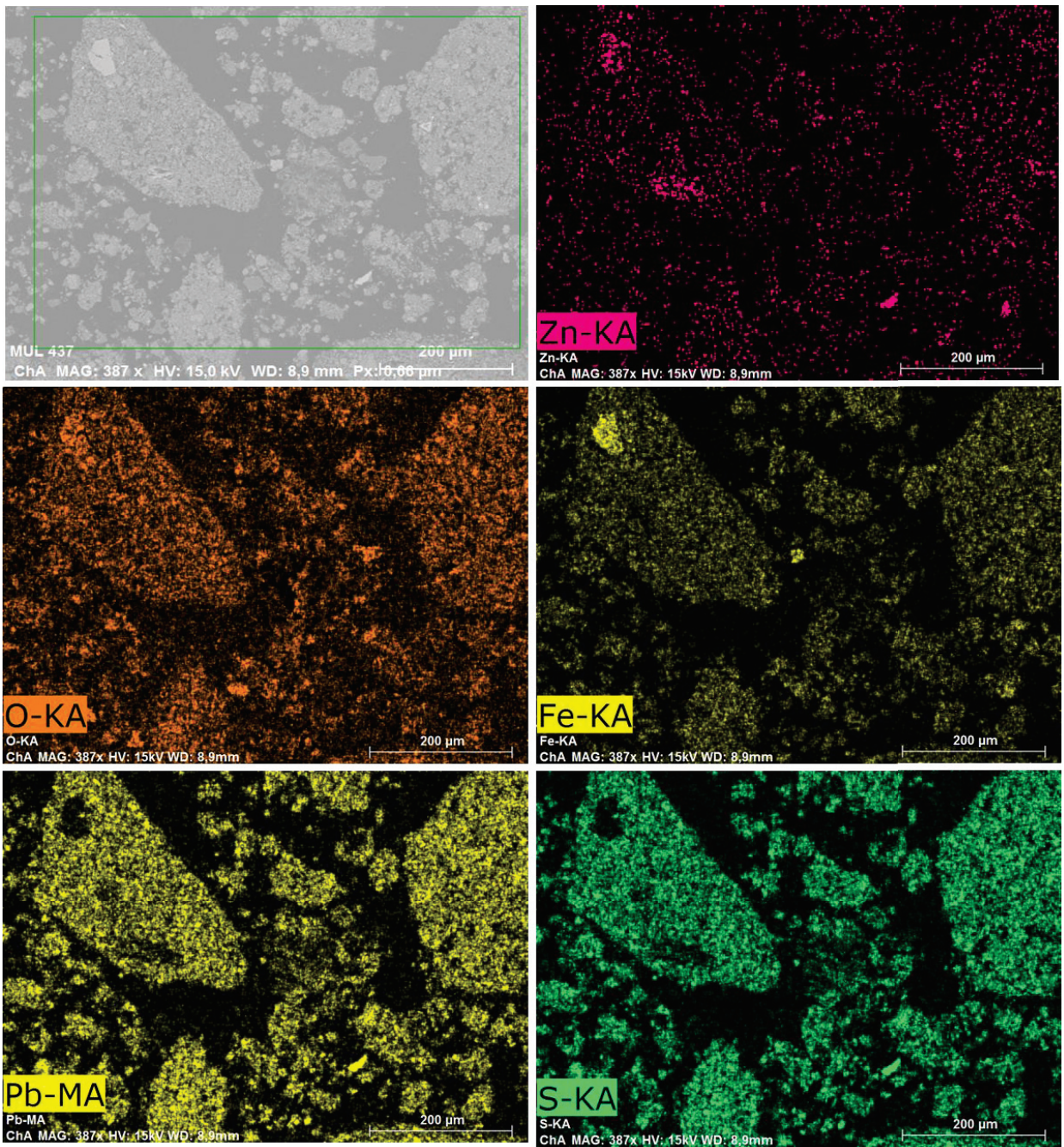
Appendix 1: Jarosite material from zinc production showing euhedral gypsum crystals.

PANalytical		Results quantitative - ProTraceGeo								
Sample name (1-20)		ProTraceG 2078/9081								
Meas. date/time		22.09.2016 13:21		ident	=	2078/9081				
Mod. date/time		22.09.2016 15:07		Method	:	UniQuant				
Version		1		Compound	m/m%	StdErr		El	m/m%	StdErr
Initial	weight	(g)	4.0002	-----	-----	-----		--	-----	-----
Final	weight	(g)	5.0003	Fe2O3	37.93	0.28		Fe	26.53	0.19
Loss On	Ignition	(%)		SO3	26.08	0.26		Sx	10.44	0.10
Sum	of conc.	(%)	67.089	ZnO	5.80	0.12		Zn	4.66	0.10
Result type			Concentration	PbO	5.46	0.02		Pb	5.06	0.02
CaO	Ca	(ppm)	18586	SiO2	5.36	0.07		Si	2.51	0.03
Sc	Sc	(ppm)	11	Na2O	3.16	0.09		Na	2.35	0.07
TiO2	Ti	(ppm)	1334	CaO	1.38	0.06		Ca	0.990	0.042
V	V	(ppm)	41	Al2O3	1.38	0.03		Al	0.731	0.014
Cr	Cr	(ppm)	239	K2O	0.708	0.035		K	0.588	0.029
Mn	Mn	(ppm)	1418	CuO	0.601	0.010		Cu	0.480	0.008
Fe2O3	Fe	(ppm)	508977	BaO	0.569	0.028		Ba	0.510	0.025
Co	Co	(ppm)	11	As2O3	0.387	0.019		As	0.293	0.015
Ni	Ni	(ppm)	13	MgO	0.169	0.008		Mg	0.102	0.005
Cu	Cu	(ppm)	5777	MnO	0.137	0.009		Mn	0.106	0.007
Zn	Zn	(ppm)	65935	CdO	0.0913	0.0046		Cd	0.0799	0.0040
Ga	Ga	(ppm)	315	P2O5	0.0883	0.0044		Px	0.0385	0.0019
Ge	Ge	(ppm)	56	TiO2	0.0788	0.0038		Ti	0.0472	0.0023
As	As	(ppm)	3466	SnO2	0.0658	0.0033		Sn	0.0518	0.0026
Se	Se	(ppm)	36	Sb2O3	0.0572	0.0029		Sb	0.0478	0.0024
Br	Br	(ppm)	33	Sm2O3	0.042	0.013		Sm	0.036	0.011
Rb	Rb	(ppm)	72	Tb4O7	0.034	0.011		Tb	0.0287	0.0096
Sr	Sr	(ppm)	192	Co3O4	0.0301	0.0032		Co	0.0221	0.0023
Y	Y	(ppm)	178	Cl	0.0272	0.0019		Cl	0.0272	0.0019
Zr	Zr	(ppm)	93	Ag2O	0.0222	0.0027		Ag	0.0207	0.0025
Nb	Nb	(ppm)	-8	Cr2O3	0.0208	0.0021		Cr	0.0142	0.0014
Mo	Mo	(ppm)	44	SrO	0.0201	0.0021		Sr	0.0170	0.0018
Ag	Ag	(ppm)	232	In2O3	0.0107	0.0026		In	0.0088	0.0021
Cd	Cd	(ppm)	760	KnownConc=0		REST=0	D/S=	0		
Sb	Sb	(ppm)	469	Sum CONCs	without	normalisation	to	100%	:	89.8
Te	Te	(ppm)	-54	Total %	stripped	Oxygen:	33 938			
I	I	(ppm)	101	Not significant:						
Cs	Cs	(ppm)	137	MoO3	0.0137	0.0050		Mo	0.0091	0.0034
Ba	Ba	(ppm)	6791	Dy2O3	0.0130	0.0087		Dy	0.0113	0.0076
La	La	(ppm)	8	Gd2O3	0.0121	0.0051		Gd	0.0105	0.0045
Ce	Ce	(ppm)	146	Pr6O11	0.0098	0.0083		Pr	0.0081	0.0069
Nd	Nd	(ppm)	5	OsO4	0.009	0.013		Os	0.0069	0.0099
Sm	Sm	(ppm)	-5	Ga2O3	0.0088	0.0031		Ga	0.0065	0.0023
Yb	Yb	(ppm)	21	Re2O7	0.0057	0.0084		Re	0.0044	0.0064
Hf	Hf	(ppm)	-4	Bi2O3	0.0052	0.0046		Bi	0.0047	0.0041
Ta	Ta	(ppm)	103	PtO2	0.0035	0.0060		Pt	0.0030	0.0052
W	W	(ppm)	-114	ZrO2	0.0022	0.0026		Zr	0.0016	0.0019
Hg	Hg	(ppm)	12	La2O3	0.0015	0.0032		La	0.0013	0.0027
Tl	Tl	(ppm)	220	Sc2O3	0.0006	0.0014		Sc	0.00037	0.00089
Pb	Pb	(ppm)	54642	V2O5	0.0004	0.0019		V	0.0002	0.0011
Bi	Bi	(ppm)	143	Yb2O3	0.0004	0.0048		Yb	0.0004	0.0042
Th	Th	(ppm)	-53	CeO2	0.0003	0.0067		Ce	0.0002	0.0054
U	U	(ppm)	-29							

Appendix 2: XRF analysis of a jarosite from zinc production (pressed powder pellet).

PANalytical		Results quantitative - ProTraceGeo								
Sample name (1-20)		ProTraceGe 2078/9080		Sample	ident =	2078/9080				
Meas. date/time		22.09.2016 15:27		Method	:	UniQuant				
Mod. date/time		22.09.2016 17:13								
Version			1	Compound	m/m%	StdErr		El	m/m%	StdErr
Initial weight	(g)		4.0026	-----	-----	-----		--	-----	-----
Final weight	(g)		5.0039	Fe2O3	35.30	0.27		Fe	24.69	0.19
Loss On Ignition	(%)			SO3	29.75	0.27		Sx	11.91	0.11
Sum of conc.	(%)		79.164	PbO	6.87	0.02		Pb	6.38	0.02
Result type			Concentration	ZnO	5.75	0.12		Zn	4.62	0.10
CaO	Ca	(ppm)	76339	CaO	4.90	0.11		Ca	3.51	0.08
Sc	Sc	(ppm)	12	SiO2	4.25	0.06		Si	1.99	0.03
TiO2	Ti	(ppm)	765	As2O3	1.07	0.05		As	0.808	0.039
V	V	(ppm)	41	Na2O	0.973	0.049		Na	0.722	0.036
Cr	Cr	(ppm)	188	Al2O3	0.736	0.016		Al	0.390	0.009
Mn	Mn	(ppm)	2042	BaO	0.480	0.024		Ba	0.430	0.021
Fe2O3	Fe	(ppm)	540789	CuO	0.321	0.005		Cu	0.256	0.004
Co	Co	(ppm)	31	K2O	0.164	0.008		K	0.136	0.007
Ni	Ni	(ppm)	135	MnO	0.162	0.011		Mn	0.126	0.008
Cu	Cu	(ppm)	3106	SrO	0.0939	0.0047		Sr	0.0794	0.0040
Zn	Zn	(ppm)	72391	CdO	0.0876	0.0044		Cd	0.0767	0.0038
Ga	Ga	(ppm)	458	MgO	0.0620	0.0048		Mg	0.0374	0.0029
Ge	Ge	(ppm)	85	P2O5	0.0568	0.0028		Px	0.0248	0.0012
As	As	(ppm)	10414	Sb2O3	0.0515	0.0030		Sb	0.0430	0.0025
Se	Se	(ppm)	126	TiO2	0.0459	0.0022		Ti	0.0275	0.0013
Br	Br	(ppm)	43	Co3O4	0.0372	0.0030		Co	0.0273	0.0022
Rb	Rb	(ppm)	66	Ag2O	0.0257	0.0028		Ag	0.0239	0.0026
Sr	Sr	(ppm)	848	SnO2	0.0255	0.0028		Sn	0.0201	0.0022
Y	Y	(ppm)	226	Bi2O3	0.0239	0.0050		Bi	0.0214	0.0045
Zr	Zr	(ppm)	67	In2O3	0.0209	0.0028		In	0.0173	0.0023
Nb	Nb	(ppm)	-15	Cr2O3	0.0158	0.0022		Cr	0.0108	0.0015
Mo	Mo	(ppm)	45	GeO2	0.0120	0.0026		Ge	0.0083	0.0018
Ag	Ag	(ppm)	267	Ga2O3	0.0102	0.0034		Ga	0.0076	0.0025
Cd	Cd	(ppm)	764	SeO2	0.0102	0.0026		Se	0.0073	0.0018
Sn	Sn	(ppm)	291							
Sb	Sb	(ppm)	510	KnownConc=0	REST=0	D/S=	0			
Te	Te	(ppm)	-8	Sum CONCs without	normalisation to	100% :				91.3
I	I	(ppm)	124	Total % stripped	Oxygen:	34 917				
Cs	Cs	(ppm)	173							
Ba	Ba	(ppm)	5710	Not significant:						
La	La	(ppm)	-8							
Ce	Ce	(ppm)	178	Tb4O7	0.011	0.011		Tb	0.0092	0.0096
Nd	Nd	(ppm)	1	MoO3	0.0052	0.0050		Mo	0.0035	0.0033
Sm	Sm	(ppm)	-20	NiO	0.0031	0.0028		Ni	0.0024	0.0022
Yb	Yb	(ppm)	26	V2O5	0.0021	0.0021		V	0.0012	0.0012
Hf	Hf	(ppm)	-1	RuO4	0.0020	0.0035		Ru	0.0015	0.0026
Ta	Ta	(ppm)	118	Gd2O3	0.0020	0.0057		Gd	0.0017	0.0049
W	W	(ppm)	-115	La2O3	0.0013	0.0034		La	0.0011	0.0029
Hg	Hg	(ppm)	14	Sm2O3	0.001	0.013		Sm	0.001	0.011
Tl	Tl	(ppm)	253	OsO4	0.001	0.015		Os	0.001	0.012
Pb	Pb	(ppm)	74871							
Bi	Bi	(ppm)	405							
Th	Th	(ppm)	-67							
U	U	(ppm)	-43							

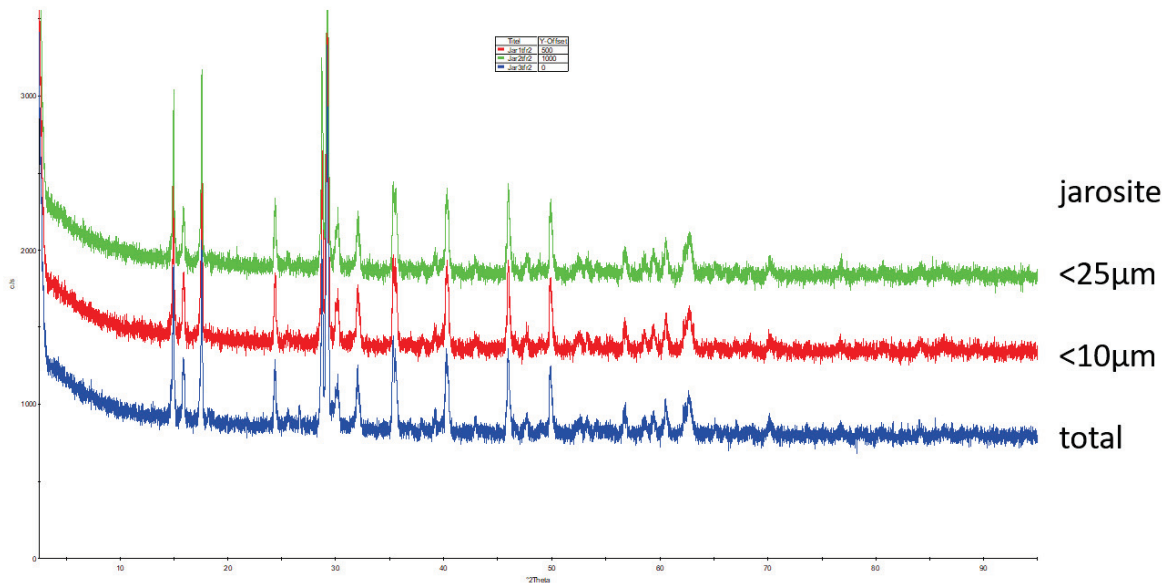
Appendix 3: XRF analysis of a jarosite from zinc production (pressed powder pellet).



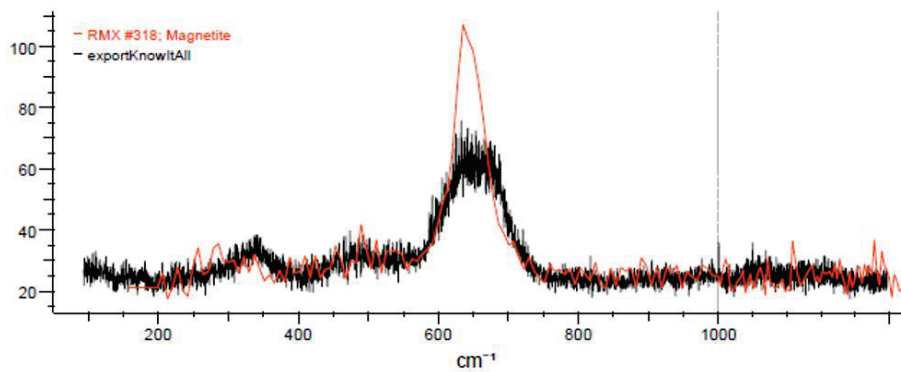
Appendix 4: SEM-EDX element mapping of a representative section of jarosite from zinc production.

Bruker Nano GmbH, Germany																
Quantax																
Quantifizierungs-Ergebnisse																
Massenprozent (%)																
Datum: 19.06.2019																
Spektrum	C	O	Na	Mg	Al	Si	S	K	Ca	Mn	Fe	Cu	Zn	As	Ba	Pb
FV4 konz 1	0	25.86	0.77		0.98	2.43	7.04		3.03		10.38		2.07			5.28
FV6 konz 2	0	29.84	0.95		1.33	3.13	6.16	0.38	2.81	0.48	13.96		3.05	1.20		7.32
FV6 konz 3	0	30.45	0.77		0.69	2.44	6.72	0.49	3.00	0.45	13.07		2.64			8.73
HGMS V4 unmag 4	0	31.16	0.89	0.20	1.40	4.83	5.80	0.49	0.86		13.00	0.74	3.25			10.94
HGMS V4 unmag 5	0	32.97	0.59		1.35	5.79	5.39	0.44	0.90		14.67	0.65	2.92		0.88	10.98
HGMS V4 mag 6	0	25.72	1.22	0.60	1.91	3.92	2.88	0.35		0.80	18.44		4.17			3.85
HGMS V4 mag 7	0	28.49		0.45	1.65	3.68	3.34	0.39	0.30	0.81	17.91	0.50	5.11			6.76
FV6 Berge 8	0	37.40	0.38		0.88	5.69	12.47		14.94		6.42		1.93			4.21
FV6 Berge 9	0	36.65	0.43		0.95	4.65	12.08	0.25	15.21		6.15		1.89			4.16
FV4 Berge 10	0	35.01	0.53		0.83	4.43	11.84	0.34	14.23		7.18		2.20			5.18
FV4 Berge 11	0	34.67	0.53		1.03	4.03	10.60	0.32	11.00	0.37	8.18		2.29			5.97
Mittelwert	0	31.66	0.71	0.42	1.18	4.09	7.67	0.38	6.63	0.58	11.76	0.63	2.87	1.20	0.88	6.67
Sigma:	0	4.05	0.26	0.20	0.38	1.14	3.50	0.08	6.38	0.21	4.41	0.12	1.01	0.00	0.00	2.58
Sigma Mittelwert:	0	1.22	0.08	0.06	0.11	0.34	1.06	0.02	1.92	0.06	1.33	0.04	0.30	0.00	0.00	0.78

Appendix 5: SEM-EDX measurements on different fractions from magnetic separation of a jarosite residue from zinc production.

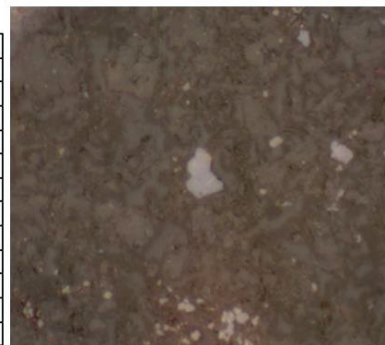


Appendix 8: XRD patterns of a jarosite residue and two grain-size fractions of the same material.

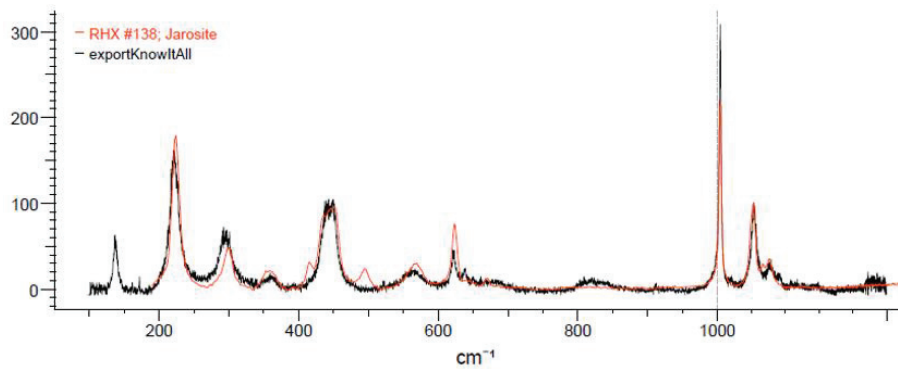


Manuelle Korrekturen: Keine
 Suchbereiche: Voll
 Suchalgorithmus: Korrelation
 Pfad des Suchspektrums: n. zutr.

Name:	Wert
Ergebnis-HQI	90.77
Datenbankkürzung	RMX
Datenbanktitel	Raman - Minerals - HORIBA
Datensatzkennung	318
Name:	Magnetite
Classification	oxide
Comments	O.D.2
Formula	Fe3O4
Instrument Name	HORIBA LabRAM 300 gr/mm
Raman Laser Power	632.8
Source of Spectrum	HORIBA Scientific
Substance Type	spinel



Appendix 9: RAMAN measurement of a magnetite in a jarosite residue from zinc production.

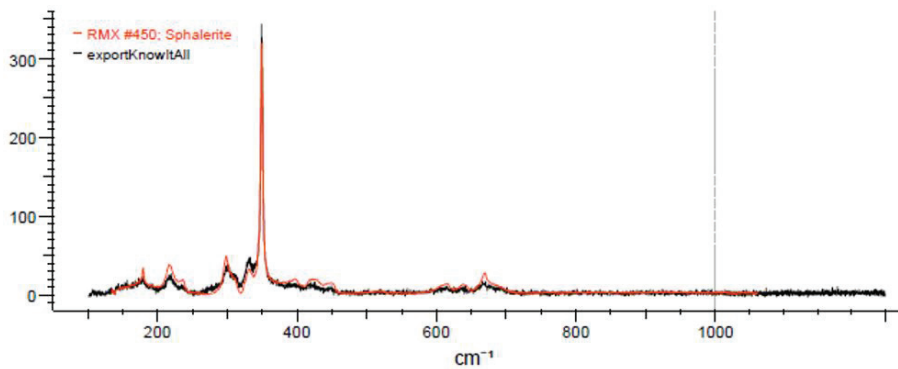


Manuelle Korrekturen: Keine
 Suchbereiche: Voll
 Suchalgorithmus: Korrelation
 Pfad des Suchspektrums: n. zutr.

Name:	Wert
Ergebnis-HQI	92.75
Datenbankabkürzung	RHX
Datenbanktitel	Raman - Forensic - HORIBA
Datensatzkennung	138
Name:	Jarosite
CAS Registry Number	12449-90-0
Classification	mineral
Comments	California, USA
Formula	$\text{KFe}(\text{SO}_4)_2(\text{OH})_6$
Instrument Name	HORIBA
Raman Laser Power	785
Source of Sample	Caltech USA
Source of Spectrum	HORIBA Scientific
Substance Type	sulfate hydroxide



Appendix 10: RAMAN measurement of a jarosite particle in a jarosite residue from zinc production.



Manuelle Korrekturen: Keine
 Suchbereiche: Voll
 Suchalgorithmus: Korrelation
 Pfad des Suchspektrums: n. zutr.

Name:	Wert
Ergebnis-HQI	95.95
Datenbankabkürzung	RMX
Datenbanktitel	Raman - Minerals - HORIBA
Datensatzkennung	450
Name:	Sphalerite
Classification	sulfide
Formula	ZnS
Instrument Name	HORIBA LabRAM
Raman Laser Power	632.8
Source of Spectrum	HORIBA Scientific
Substance Type	Blende



Appendix 11: RAMAN measurement of a sphalerite in a jarosite residue from zinc production.

Bruker Nano GmbH, Germany																		
Quantax																		
Quantifizierungs-Ergebnisse																		
Massenprozent (%)																		
Datum: 03.11.2017																		
Spektrum	C	O	Na	Mg	Al	Si	S	K	Ca	Ti	Cr	Mn	Fe	Cu	Zn	As	Ba	Pb
17-1623 25	0.00	22.38		2.36	9.59	0.35			0.50	0.26	18.29		20.18		7.25			
17-1623 24	0.00	28.31		3.25		12.12			17.61			1.11	27.80		2.43			
17-1623 23	0.00	1.67					10.40						1.16	0.84		4.31		58.44
17-1623 22	0.00						29.44						11.36		39.13			
17-1623 21	0.00	2.82					9.79						0.98	0.92				65.36
17-1623 20	0.00	0.88											0.66	56.48		21.96		
17-1623 19	0.00						0.00											83.21
17-1623 18	0.00	8.75			0.83	0.35	20.19			0.40			25.14		28.08			
17-1623 17	0.00				0.39	1.05	27.73		0.40				15.24		37.11			
17-1623 16	0.00	28.63			1.83	13.04		0.40	0.94			0.92	27.08		3.23			
17-1623 15	0.00	28.81			6.56	14.14	0.62	6.71	6.35				10.66		3.03			2.11
17-1623 14	0.00	24.55			10.20	0.42			0.39	0.77	23.46		20.27		7.37			
17-1623 13	0.00	24.85			8.58				0.35	0.56	25.93		17.64		7.52			
17-1623 12	0.00	9.11			2.44	5.70	18.39	3.10	2.63				17.97		19.82			13.99
17-1623 11	0.00	5.75			1.85	3.84	24.90	1.40	1.46				20.87		30.32			
17-1623 10	0.00	11.14	2.52	0.52	2.79	7.24	17.72	2.22	4.98				26.22	0.77	14.46			
17-1623 8	0.00	22.36		1.77	4.58				0.41	0.45	21.82		13.56	0.48	5.62			33.04
17-1623 7	0.00	24.08	1.08	2.51	7.84	0.32			0.50	0.33	19.87		22.54		7.01			
17-1623 6	0.00	24.59		2.47	8.74				0.27	0.49	25.42		17.08		8.81			
17-1623 5	0.00	3.22			0.59	2.29	24.83	0.74	1.74				15.90		34.03			
17-1623 4	0.00	1.69					11.13						4.40	0.76	1.64	2.96		61.68
17-1623 3	0.00						30.61						32.10		21.62			
17-1623 2	0.00	26.67	1.43	2.26	9.16	1.25		0.57	0.65	0.96	20.20		19.47		8.05			
17-1623 1	0.00	29.55		4.10		12.82			17.38			1.28	25.51		2.76			
Mittelwert	0.00	16.49	1.68	2.37	5.01	5.35	17.37	2.04	4.44	0.53	22.14	1.10	17.12	10.04	14.47	9.74	2.11	52.62
Sigma:	0.00	11.11	0.75	0.89	3.76	5.46	10.32	2.09	6.31	0.23	2.91	0.18	8.96	22.75	12.73	10.60	0.00	24.86
Sigma Mittelw	0.00	2.27	0.15	0.18	0.77	1.12	2.11	0.43	1.29	0.05	0.59	0.04	1.83	4.64	2.60	2.16	0.00	5.07

Appendix 12: Selected SEM-EDX measurements on a polished section of slag produced during pyrometallurgical treatment of jarosite residue from zinc production.

RFA-Eingangsanalysen								
	Probe 1		Probe 2		Probe 4		Probe 5	
Na ₂ O	3.186	%	3.150	%	3.746	%	3.950	%
MgO	0.143	%	0.285	%	0.245	%	0.216	%
Al ₂ O ₃	2.119	%	2.153	%	2.345	%	2.399	%
SiO ₂	6.304	%	6.821	%	7.371	%	7.267	%
P ₂ O ₅	0.115	%	0.128	%	0.120	%	0.119	%
SO ₃	25.79	%	25.975	%	27.643	%	27.906	%
Cl	0.016	%	0.021	%	0.023	%	0.021	%
K ₂ O	0.812	%	0.751	%	0.750	%	0.761	%
CaO	1.006	%	1.190	%	1.307	%	1.313	%
TiO ₂	0.073	%	0.088	%	0.075	%	0.075	%
Cr ₂ O ₃	0.038	%	0.030	%	0.034	%	0.027	%
MnO	0.168	%	0.169	%	0.175	%	0.174	%
Fe ₂ O ₃	45.234	%	44.524	%	42.426	%	42.039	%
NiO	0.014	%	0.013	%	0.011	%	0.014	%
CuO	0.739	%	0.726	%	0.527	%	0.661	%
ZnO	6.042	%	5.884	%	5.741	%	5.513	%
GeO ₂	0.016	%	0.015	%	0.015	%	0.016	%
SrO	0.028	%	0.029	%	0.027	%	0.027	%
MoO ₃	0.013	%	0.011	%	0.008	%	0.009	%
Ag ₂ O	0.037	%	0.035	%	0.033	%	0.031	%
CdO	0.072	%	0.072	%	0.066	%	0.060	%
SbO	0.077	%	0.087	%	0.073	%	0.065	%
BaO	0.671	%	0.677	%	0.631	%	0.668	%
Tl ₂ O ₃	0.025	%	0.022	%	0.020	%	0.023	%
PbO	7.231	%	7.098	%	6.557	%	6.529	%
Bi ₂ O ₃	0.019	%	0.029	%	0.023	%	0.023	%
Rh	0.011	%	0.009	%	0.008	%		%

Appendix 13: Four XRF measurements (powder discs) of the same jarosite material (Zn production).

Spektrum: Nh_Jori_St3_38						
El	OZ	Serie	unn. C [Gew.-%]	norm. C [Gew.-%]	Atom. C [At.-%]	Fehler (1 Sigma) [Gew.-%]
C	6	K-Serie	0,00	0,00	0,00	0,00
O	8	K-Serie	13,52	16,00	46,40	2,04
Na	11	K-Serie	0,80	0,95	1,91	0,09
Mg	12	K-Serie	0,26	0,31	0,58	0,04
Al	13	K-Serie	1,39	1,65	2,83	0,10
Si	14	K-Serie	1,66	1,96	3,24	0,10
S	16	K-Serie	1,07	1,27	1,84	0,07
Cl	17	K-Serie	9,06	10,72	14,03	0,33
Fe	26	K-Serie	0,31	0,37	0,31	0,04
Cu	29	K-Serie	0,39	0,46	0,33	0,05
Ag	47	L-Serie	56,02	66,32	28,52	1,77
Summe:			84,47	100,00	100,00	

Appendix 14: SEM-EDX element measurements of a silver-bearing particle from jarosite residue from zinc production.

Spektrum: Kk_Hy30_ 9						
El OZ	Serie	unn. C [Gew. %]	norm. C [Gew. %]	Atom. C [At. %]	Fehler (1 Sigma) [Gew. %]	
C 6	K-Serie	0,00	0,00	0,00	0,00	
O 8	K-Serie	1,54	2,01	5,77	0,63	
S 16	K-Serie	25,92	33,69	48,28	0,98	
Cu 29	K-Serie	48,06	62,48	45,18	1,45	
Ag 47	L-Serie	1,40	1,82	0,77	0,11	
Summe:		76,92	100,00	100,00		

Spektrum: Kk_Hy30_ 10						
El OZ	Serie	unn. C [Gew. %]	norm. C [Gew. %]	Atom. C [At. %]	Fehler (1 Sigma) [Gew. %]	
C 6	K-Serie	0,00	0,00	0,00	0,00	
O 8	K-Serie	0,65	0,75	5,62	0,41	
S 16	K-Serie	10,07	11,66	43,64	0,41	
Pb 82	L-Serie	75,63	87,59	50,74	2,75	
Summe:		86,35	100,00	100,00		

Spektrum: Kk_Hy30_ 11						
El OZ	Serie	unn. C [Gew. %]	norm. C [Gew. %]	Atom. C [At. %]	Fehler (1 Sigma) [Gew. %]	
C 6	K-Serie	0,00	0,00	0,00	0,00	
O 8	K-Serie	1,95	2,47	7,04	0,73	
S 16	K-Serie	26,72	33,85	48,03	1,01	
Fe 26	K-Serie	0,47	0,59	0,48	0,07	
Cu 29	K-Serie	47,86	60,64	43,42	1,44	
Ag 47	L-Serie	1,93	2,44	1,03	0,13	
Summe:		78,92	100,00	100,00		

Spektrum: Jori_St_ 5						
El OZ	Serie	unn. C [Gew. %]	norm. C [Gew. %]	Atom. C [At. %]	Fehler (1 Sigma) [Gew. %]	
C 6	K-Serie	0,00	0,00	0,00	0,00	
O 8	K-Serie	38,73	50,86	73,00	5,48	
Na 11	K-Serie	2,76	3,62	3,61	0,24	
Al 13	K-Serie	0,88	1,15	0,98	0,09	
Si 14	K-Serie	0,84	1,10	0,90	0,08	
S 16	K-Serie	10,38	13,64	9,77	0,42	
Fe 26	K-Serie	19,16	25,16	10,34	0,61	
Cu 29	K-Serie	0,68	0,90	0,32	0,09	
Zn 30	K-Serie	1,73	2,27	0,80	0,13	
Ag 47	L-Serie	0,99	1,30	0,28	0,09	
Summe:		76,15	100,00	100,00		

Appendix 15: SEM-EDX element measurements of a silver-bearing particle from jarosite residue from zinc production (continuation 1).

Spektrum: Jori_St_ 6						
El OZ	Serie	unn. C [Gew. %]	norm. C [Gew. %]	Atom. C [At. %]	Fehler (1 Sigma) [Gew. %]	
C 6	K-Serie	0,00	0,00	0,00		0,00
O 8	K-Serie	17,95	26,84	47,73		3,42
Na 11	K-Serie	2,21	3,30	4,08		0,21
Al 13	K-Serie	0,49	0,73	0,77		0,07
Si 14	K-Serie	0,73	1,09	1,10		0,08
S 16	K-Serie	24,92	37,27	33,06		0,95
Fe 26	K-Serie	6,26	9,37	4,77		0,29
Zn 30	K-Serie	11,08	16,57	7,21		0,45
Ag 47	L-Serie	3,24	4,84	1,28		0,18
Summe:		66,88	100,00	100,00		

Spektrum: Jori_St_ 7						
El OZ	Serie	unn. C [Gew. %]	norm. C [Gew. %]	Atom. C [At. %]	Fehler (1 Sigma) [Gew. %]	
C 6	K-Serie	0,00	0,00	0,00		0,00
O 8	K-Serie	22,68	25,93	58,44		3,21
Na 11	K-Serie	1,00	1,15	1,80		0,10
Al 13	K-Serie	0,76	0,87	1,16		0,07
Si 14	K-Serie	0,51	0,58	0,75		0,05
S 16	K-Serie	8,77	10,03	11,28		0,35
Cl 17	K-Serie	4,18	4,78	4,86		0,17
Fe 26	K-Serie	3,87	4,42	2,86		0,15
Cu 29	K-Serie	1,81	2,07	1,17		0,10
Zn 30	K-Serie	3,69	4,22	2,33		0,16
Ag 47	L-Serie	40,17	45,94	15,36		1,29
Summe:		87,44	100,00	100,00		

Spektrum: Jori_St_ 8						
El OZ	Serie	unn. C [Gew. %]	norm. C [Gew. %]	Atom. C [At. %]	Fehler (1 Sigma) [Gew. %]	
C 6	K-Serie	0,00	0,00	0,00		0,00
O 8	K-Serie	31,38	33,28	66,73		4,23
Na 11	K-Serie	1,64	1,74	2,42		0,14
Al 13	K-Serie	1,01	1,07	1,27		0,08
Si 14	K-Serie	0,72	0,76	0,87		0,06
S 16	K-Serie	5,59	5,93	5,93		0,23
Cl 17	K-Serie	4,17	4,42	4,00		0,17
Fe 26	K-Serie	6,69	7,10	4,08		0,22
Cu 29	K-Serie	1,39	1,48	0,75		0,09
Zn 30	K-Serie	3,88	4,11	2,02		0,17
Ag 47	L-Serie	37,81	40,10	11,93		1,21
Summe:		94,28	100,00	100,00		

Appendix 16: SEM-EDX element measurements of a silver-bearing particle from jarosite residue from zinc production (continuation 2).

Spektrum: Jori_St_10						
El	OZ	Serie	unn. C [Gew. %]	norm. C [Gew. %]	Atom. C [At. %]	Fehler (1 Sigma) [Gew. %]
C	6	K-Serie	0,00	0,00	0,00	0,00
O	8	K-Serie	15,62	18,11	44,05	2,43
Mg	12	K-Serie	1,03	1,19	1,91	0,10
Al	13	K-Serie	1,83	2,12	3,05	0,13
Si	14	K-Serie	1,52	1,77	2,45	0,10
S	16	K-Serie	13,14	15,23	18,48	0,50
Cl	17	K-Serie	2,38	2,76	3,03	0,12
Mn	25	K-Serie	0,42	0,49	0,35	0,05
Fe	26	K-Serie	1,46	1,70	1,18	0,08
Zn	30	K-Serie	18,66	21,64	12,87	0,57
Ag	47	L-Serie	30,18	34,99	12,62	0,98
Summe:			86,25	100,00	100,00	

Spektrum: Jori_St_11						
El	OZ	Serie	unn. C [Gew. %]	norm. C [Gew. %]	Atom. C [At. %]	Fehler (1 Sigma) [Gew. %]
C	6	K-Serie	0,00	0,00	0,00	0,00
O	8	K-Serie	5,70	7,24	19,03	1,03
Mg	12	K-Serie	0,56	0,71	1,23	0,07
Al	13	K-Serie	0,90	1,14	1,78	0,08
Si	14	K-Serie	0,77	0,97	1,46	0,07
S	16	K-Serie	23,65	30,05	39,42	0,88
Mn	25	K-Serie	0,80	1,02	0,78	0,06
Fe	26	K-Serie	1,20	1,53	1,15	0,07
Zn	30	K-Serie	39,72	50,49	32,47	1,13
Ag	47	L-Serie	5,38	6,84	2,67	0,21
Summe:			78,68	100,00	100,00	

Spektrum: Jori_St_12						
El	OZ	Serie	unn. C [Gew. %]	norm. C [Gew. %]	Atom. C [At. %]	Fehler (1 Sigma) [Gew. %]
C	6	K-Serie	0,00	0,00	0,00	0,00
O	8	K-Serie	26,92	27,84	48,39	3,77
Na	11	K-Serie	3,28	3,39	4,10	0,28
Mg	12	K-Serie	1,50	1,55	1,78	0,14
Al	13	K-Serie	1,71	1,77	1,82	0,13
Si	14	K-Serie	19,75	20,44	20,23	0,89
S	16	K-Serie	11,81	12,22	10,60	0,47
Mn	25	K-Serie	0,46	0,48	0,24	0,05
Fe	26	K-Serie	1,78	1,84	0,92	0,09
Zn	30	K-Serie	23,50	24,31	10,34	0,70
Ag	47	L-Serie	5,96	6,16	1,59	0,24
Summe:			96,67	100,00	100,00	

Appendix 17: SEM-EDX element measurements of a silver-bearing particle from jarosite residue from zinc production (continuation 3).

Spektrum: Jori_St_ 13						
El OZ	Serie	unn. C [Gew.-%]	norm. C [Gew.-%]	Atom. C [At.-%]	Fehler (1 Sigma) [Gew.-%]	
C 6	K-Serie	0,00	0,00	0,00		0,00
O 8	K-Serie	24,55	31,02	51,38		3,53
Na 11	K-Serie	2,95	3,73	4,30		0,25
Mg 12	K-Serie	1,08	1,37	1,49		0,11
Al 13	K-Serie	1,34	1,69	1,66		0,11
Si 14	K-Serie	15,69	19,83	18,71		0,71
S 16	K-Serie	10,46	13,22	10,92		0,42
Mn 25	K-Serie	0,69	0,87	0,42		0,06
Fe 26	K-Serie	6,33	7,99	3,79		0,22
Zn 30	K-Serie	11,63	14,69	5,95		0,38
Ag 47	L-Serie	4,42	5,58	1,37		0,19
Summe:		79,15	100,00	100,00		

Spektrum: Jori_St_ 17						
El OZ	Serie	unn. C [Gew.-%]	norm. C [Gew.-%]	Atom. C [At.-%]	Fehler (1 Sigma) [Gew.-%]	
C 6	K-Serie	0,00	0,00	0,00		0,00
O 8	K-Serie	30,16	37,15	66,00		4,21
Na 11	K-Serie	2,23	2,75	3,40		0,19
Mg 12	K-Serie	1,81	2,24	2,61		0,14
Al 13	K-Serie	1,28	1,57	1,66		0,10
Si 14	K-Serie	0,69	0,85	0,86		0,06
S 16	K-Serie	7,16	8,82	7,82		0,29
Cl 17	K-Serie	3,76	4,63	3,71		0,16
Mn 25	K-Serie	0,44	0,54	0,28		0,05
Fe 26	K-Serie	4,39	5,41	2,75		0,17
Zn 30	K-Serie	6,72	8,27	3,60		0,25
Ag 47	L-Serie	22,55	27,78	7,32		0,74
Summe:		81,18	100,00	100,00		

Spektrum: Jori_St_ 18						
El OZ	Serie	unn. C [Gew.-%]	norm. C [Gew.-%]	Atom. C [At.-%]	Fehler (1 Sigma) [Gew.-%]	
C 6	K-Serie	0,00	0,00	0,00		0,00
O 8	K-Serie	42,71	52,22	72,94		5,36
Na 11	K-Serie	4,10	5,01	4,87		0,31
Mg 12	K-Serie	1,29	1,58	1,45		0,11
Al 13	K-Serie	1,15	1,40	1,16		0,09
Si 14	K-Serie	2,21	2,70	2,15		0,13
S 16	K-Serie	9,89	12,10	8,43		0,39
Fe 26	K-Serie	12,35	15,10	6,04		0,38
Cu 29	K-Serie	0,45	0,55	0,19		0,06
Zn 30	K-Serie	5,03	6,15	2,10		0,20
Ag 47	L-Serie	2,60	3,18	0,66		0,12
Summe:		81,78	100,00	100,00		

Appendix 18: SEM-EDX element measurements of a silver-bearing particle from jarosite residue from zinc production (continuation 4).

Spektrum: Jsit1_Nh_ 1						
El OZ	Serie	unn. C [Gew. %]	norm. C [Gew. %]	Atom. C [At. %]	Fehler (1 Sigma) [Gew. %]	
C 6	K-Serie	0,00	0,00	0,00	0,00	
O 8	K-Serie	1,55	1,77	5,84	0,40	
Al 13	K-Serie	0,07	0,07	0,15	0,03	
S 16	K-Serie	23,13	26,36	43,46	0,86	
Fe 26	K-Serie	3,31	3,78	3,57	0,12	
Cu 29	K-Serie	7,09	8,08	6,73	0,23	
Zn 30	K-Serie	38,56	43,95	35,53	1,04	
Ag 47	L-Serie	2,39	2,72	1,34	0,11	
Pb 82	L-Serie	11,63	13,26	3,38	0,41	
Summe:		87,72	100,00	100,00		

Spektrum: Nh_grob2_ 17						
El OZ	Serie	unn. C [Gew. %]	norm. C [Gew. %]	Atom. C [At. %]	Fehler (1 Sigma) [Gew. %]	
C 6	K-Serie	0,00	0,00	0,00	0,00	
O 8	K-Serie	6,20	6,89	18,55	1,30	
Al 13	K-Serie	1,28	1,42	2,27	0,11	
Si 14	K-Serie	2,53	2,80	4,30	0,16	
S 16	K-Serie	22,60	25,09	33,72	0,85	
Fe 26	K-Serie	1,19	1,33	1,02	0,11	
Cu 29	K-Serie	49,03	54,42	36,91	1,76	
Ag 47	L-Serie	7,26	8,05	3,22	0,30	
Summe:		90,09	100,00	100,00		

Spektrum: Nh_grob2_ 18						
El OZ	Serie	unn. C [Gew. %]	norm. C [Gew. %]	Atom. C [At. %]	Fehler (1 Sigma) [Gew. %]	
C 6	K-Serie	0,00	0,00	0,00	0,00	
O 8	K-Serie	39,51	39,96	58,64	5,80	
Al 13	K-Serie	10,14	10,25	8,92	0,53	
Si 14	K-Serie	28,35	28,67	23,97	1,24	
K 19	K-Serie	10,07	10,18	6,11	0,37	
Cu 29	K-Serie	1,07	1,08	0,40	0,14	
Ag 47	L-Serie	5,93	6,00	1,30	0,26	
Ba 56	L-Serie	3,82	3,87	0,66	0,21	
Summe:		98,87	100,00	100,00		

Appendix 19: SEM-EDX element measurements of a silver-bearing particle from jarosite residue from zinc production (continuation 5).

Spektrum: Nh_grob2_ 19						
El	OZ	Serie	unn. C [Gew.%]	norm. C [Gew.%]	Atom. C [At.%]	Fehler (1 Sigma) [Gew.%]
C	6	K-Serie	0,00	0,00	0,00	0,00
O	8	K-Serie	34,15	36,18	57,66	5,08
Al	13	K-Serie	8,42	8,92	8,42	0,44
Si	14	K-Serie	21,09	22,34	20,28	0,93
S	16	K-Serie	3,72	3,94	3,13	0,18
K	19	K-Serie	7,44	7,89	5,14	0,29
Cu	29	K-Serie	3,62	3,83	1,54	0,26
Ag	47	L-Serie	12,86	13,62	3,22	0,48
Ba	56	L-Serie	3,10	3,29	0,61	0,18
Summe:			94,40	100,00	100,00	

Appendix 20: SEM-EDX element measurements of a silver-bearing particle from jarosite residue from zinc production (continuation 6).

Eingangs-Korngrößenverteilung									
		Probe 1		Probe 2		Probe 4		Probe 5	
200	>200	2.05	g	0.75	g	0.97	g	0.93	g
160	160-200	0.63	g	0.21	g	0.28	g	0.26	g
125	125-160	0.87	g	0.52	g	0.62	g	0.64	g
100	100-125	1.539	g	0.7	g	0.56	g	0.71	g
90	90-100	0.77	g	0.29	g	0.43	g	0.38	g
71	71-90	3.07	g	1.27	g	1.14	g	1.23	g
63	63-71	1.98	g	0.76	g	0.08	g	0.73	g
45	45-63	6.06	g	2.21	g	2.67	g	2.71	g
32	32-45	7.27	g	2.81	g	2.59	g	2.97	g
25	25-32	5.09	g	2.36	g	2.28	g	2.29	g
16	16-25	28.62	g	18.93	g	25.58	g	20.2	g
10	Okt.16	58.63	g	46.81	g	46.85	g	47.92	g
	<10	154.71	g	176.22	g	169.54	g	173.84	g

Appendix 21: Grain size distribution (sieve analysis) of four jarosite samples from the same material (Zn production).

Jarosit HGMS-Versuche		
Versuch 1	Tap 1	Düse: 6 Matrix XM0
mag.	2.52 g	
unmag.	25.76 g	
Versuch 2	Tap 2	Düse: 6 Matrix XM0
mag.	6.34 g	
unmag.	21.74 g	
Versuch 3	Tap 3	Düse: 6 Matrix XM0
mag.	10.38 g	
unmag.	17.32 g	
Versuch 4	Tap 4	Düse: 6 Matrix XM0
mag.	12.72 g	
unmag.	15.04 g	
Versuch 5	Tap 5	Düse: 6 Matrix XM0
mag.	13.64 g	
unmag.	13.92 g	
V1-V5 ferromag: 3.21g		
Versuch 6	Aufgabe 300 g	Düse: 6 Matrix XM0
Tap 1 mag.	12.17 g	
Tap 2 mag.	14.61 g	
Tap 3 mag.	15.2 g	
Tap 4 mag.	14.71 g	
Tap 5 mag.	13.97 g	
Berge	205.94 g	

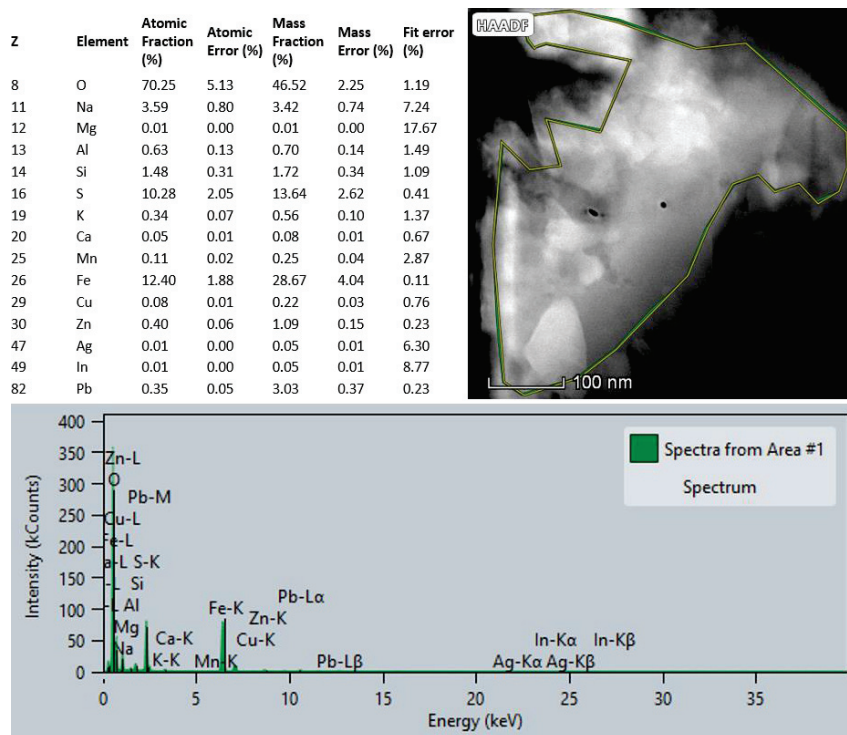
Appendix 23: Settings and throughput of HGMS trials on jarosite from zinc production.

%	Jarosit										V6 Berge		Sample-Mix	
	V1 mag	V1 unmag.	V2 mag.	V2 unmag.	V3 mag.	V3 unmag.	V4 mag.	V4 unmag.	V5 mag.	V5 unmag.	V6 Tap 1	V6 Tap 2		V6 Tap 3
NazO	4.157	3.503	3.905	3.54	3.658	3.698	3.473	3.466	5.037	4.74	4.318	3.656	4.181	4.119
MgO	0.08	0.11	0.152	0.111	0.115	0.145	0.147	0.123	0.392	0.259	0.185	0.091	0.144	0.187
Al ₂ O ₃	2.366	2.063	2.161	1.995	2.055	2.061	1.959	2.04	2.115	2.63	2.636	2.409	2.227	2.381
SiO ₂	7.074	5.971	4.381	6.502	3.562	7.287	3.275	7.258	10.84	7.766	6.037	4.736	3.842	7.102
P ₂ O ₅	0.651	0.615	0.626	0.646	0.61	0.613	0.624	0.653	0.568	0.576	0.608	0.602	0.633	0.603
SO ₃	24.98	24.05	21.34	24.04	21.99	24.09	21.99	23.32	10.84	18.07	22.75	24.02	23.61	25.36
Cl	0.022	0.036	0.043	0.043	0.038	0.038	0.036	0.036	0.018	0.018	0.018	0.031	0.023	0.023
K ₂ O	0.885	0.884	0.788	0.844	0.816	0.855	0.817	0.867	0.39	0.621	0.776	0.824	0.851	0.791
CaO	0.385	0.527	0.323	0.456	0.315	0.5	0.313	0.478	0.386	0.343	0.292	0.298	0.335	0.397
TiO ₂	0.093	0.099	0.099	0.087	0.102	0.087	0.094	0.098	0.093	0.103	0.105	0.1	0.1	0.098
Cr ₂ O ₃	0.04	0.036	0.039	0.039	0.036	0.045	0.039	0.042	0.049	0.038	0.033	0.035	0.04	0.052
MnO	0.111	0.099	0.195	0.102	0.181	0.094	0.177	0.106	0.438	0.302	0.201	0.154	0.139	0.137
Fe ₂ O ₃	45.8	47.86	50.25	47.6	50.77	47.06	61.08	47.61	57.22	48.13	46.85	48.05	49.48	45.34
Co ₃ O ₄					0.012				0.111	0.092	0.088	0.102		0.098
NiO	0.019	0.033	0.02	0.042	0.018	0.012		0.027	0.037	0.019	0.016		0.017	0.014
CuO	0.75	0.824	0.769	0.771	0.847	0.517	0.821	0.516	0.718	0.655	0.494	0.537	0.791	0.704
ZnO	4.561	4.606	7.157	4.548	6.713	4.511	6.951	4.609	14.59	9.313	6.988	5.747	5.464	3.953
SrO	0.027	0.03	0.025	0.03	0.025	0.029	0.026	0.03	0.02	0.026	0.024	0.025	0.028	0.026
Ag ⁺ O	0.038	0.047	0.029	0.049	0.032	0.048	0.034	0.052	0.016	0.025	0.027	0.026	0.037	0.036
Sb ₂ O ₃	0.079	0.081	0.075	0.091	0.069	0.09	0.068	0.1	0.103	0.103	0.085	0.072	0.064	0.075
BaO	0.776	0.803	0.72	0.797	0.746	0.813	0.734	0.871	0.588	0.683	0.771	0.704	0.775	0.696
PbO	7.039	7.606	6.82	7.563	7.111	7.305	7.286	7.599	3.112	5.044	6.197	7.064	7.603	6.596

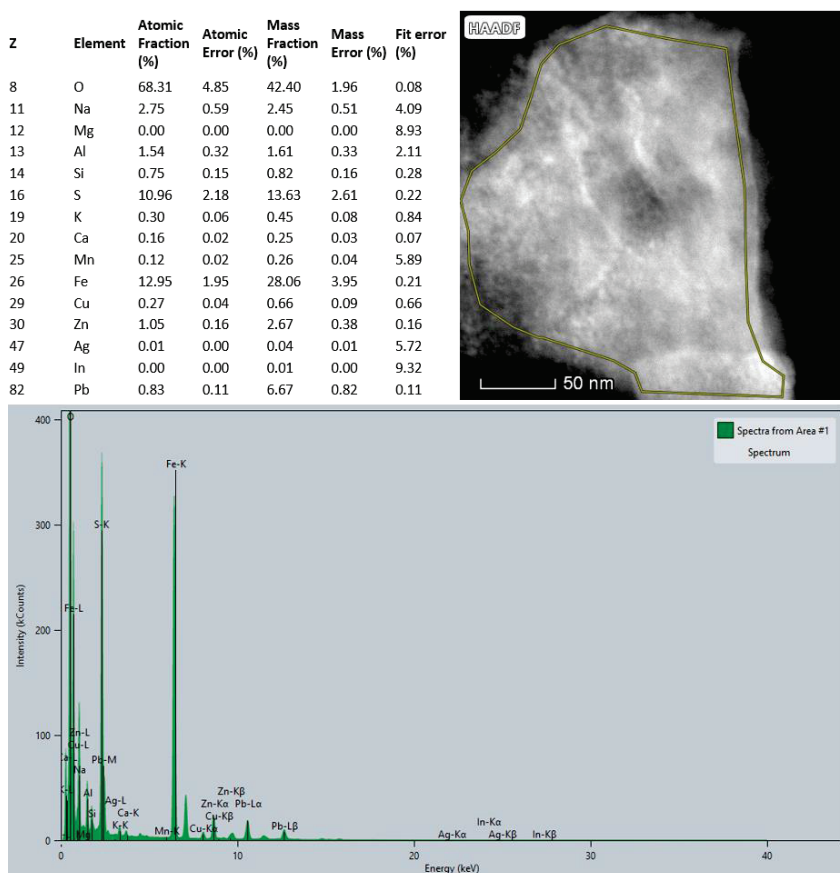
Appendix 24: Chemical composition of different fraction from HGMS trials with jarosite from zinc production.

atoms per formula unit		1.90	2.10	1.89	2.02	2.01	2.10	2.10	2.03	1.97	1.87	2.03	1.91	1.93	1.82	1.83	1.81	1.90	1.83	1.83	1.99	2.07	2.11	2.15	2.01	1.95	2.00	2.06	2.06	2.06
S	apfu	2.21	2.46	2.57	2.82	2.65	2.58	2.56	2.26	2.35	2.28	2.38	2.44	2.37	2.86	2.79	2.39	2.18	2.37	2.30	2.38	2.23	2.57	2.20	2.26	3.00	2.56	2.54		
Fe	apfu	0.55	0.19	0.22	0.16	0.25	0.19	0.21	0.42	0.31	0.31	0.24	0.39	0.32	0.37	0.34	0.19	0.17	0.16	0.20	0.10	0.17	0.00	0.40	0.28	0.00	0.26	0.24		
Zn	apfu	0.40	0.16	0.11	0.11	0.16	0.15	0.20	0.19	0.25	0.37	0.27	0.18	0.29	0.31	0.19	0.22	0.23	0.25	0.25	0.16	0.21	0.11	0.29	0.24	0.00	0.00	0.00		
Al	apfu	0.05	0.06	0.34	0.00	0.00	0.00	0.00	0.33	0.00	0.12	0.00	0.04	0.03	0.00	0.00	0.32	0.32	0.29	0.06	0.03	0.19	0.00	0.13	0.27	0.00	0.00	0.00		
Si	apfu	0.00	0.00	0.00	0.00	0.00	0.00	0.00	0.00	0.17	0.12	0.07	0.16	0.15	0.00	0.00	0.06	0.06	0.04	0.07	0.05	0.07	0.00	0.00	0.00	0.00	0.00	0.00		
Cu	apfu	0.00	0.00	0.00	0.00	0.00	0.00	0.00	0.00	0.00	0.08	0.00	0.00	0.00	0.00	0.00	0.00	0.16	0.05	0.03	0.13	0.00	0.00	0.00	0.00	0.00	0.00	0.00	0.00	
As	apfu	0.00	0.00	0.00	0.00	0.00	0.00	0.00	0.00	0.00	0.05	0.00	0.00	0.00	0.00	0.00	0.00	0.00	0.02	0.02	0.00	0.00	0.00	0.00	0.00	0.00	0.00	0.00	0.00	
Tl	apfu	0.00	0.00	0.00	0.00	0.00	0.00	0.00	0.00	0.00	0.00	0.00	0.00	0.00	0.00	0.00	0.00	0.00	0.00	0.00	0.00	0.00	0.00	0.00	0.00	0.00	0.00	0.00	0.00	
Ba	apfu	0.00	0.00	0.00	0.00	0.00	0.00	0.00	0.00	0.00	0.00	0.00	0.00	0.02	0.00	0.00	0.01	0.01	0.11	0.00	0.00	0.00	0.03	0.02	0.01	0.00	0.00	0.00	0.00	
Mg	apfu	0.00	0.00	0.00	0.00	0.00	0.00	0.00	0.00	0.00	0.00	0.00	0.00	0.00	0.00	0.00	0.04	0.00	0.00	0.00	0.00	0.00	0.00	0.00	0.00	0.00	0.00	0.00	0.00	
Ca	apfu	0.00	0.00	0.00	0.00	0.00	0.00	0.00	0.00	0.00	0.00	0.00	0.00	0.00	0.00	0.00	0.16	0.13	0.04	0.00	0.06	0.00	0.00	0.01	0.00	0.00	0.00	0.00	0.00	
Ag	apfu	0.00	0.00	0.00	0.00	0.00	0.00	0.00	0.00	0.00	0.00	0.00	0.00	0.00	0.00	0.00	0.00	0.00	0.00	0.00	0.00	0.00	0.00	0.00	0.00	0.00	0.00	0.00	0.00	
Na	apfu	0.62	0.81	0.70	0.67	0.86	0.73	1.00	0.62	0.44	0.72	0.82	0.65	0.63	0.00	0.67	0.80	0.80	0.83	1.21	0.99	0.78	0.96	0.41	0.59	1.00	0.81	0.83		
K	apfu	0.05	0.07	0.11	0.09	0.11	0.10	0.12	0.09	0.00	0.07	0.09	0.07	0.08	0.06	0.08	0.09	0.09	0.06	0.07	0.10	0.00	0.06	0.09	0.09	0.00	0.09	0.09	0.09	
Pb	apfu	0.41	0.00	0.00	0.00	0.00	0.00	0.00	0.00	0.48	0.21	0.22	0.43	0.38	0.38	0.31	0.00	0.15	0.18	0.14	0.00	0.00	0.00	0.30	0.23	0.00	0.29	0.33		
Summe	apfu	4.29	3.77	4.05	3.85	4.04	3.75	3.87	3.70	4.10	4.32	4.09	4.36	4.28	3.98	4.38	4.15	4.42	4.35	4.35	4.01	3.72	3.73	3.84	3.98	4.00	4.00	4.02		
Fe pos		3.16	2.82	2.90	3.09	3.07	2.92	2.75	2.66	3.18	3.07	2.96	3.16	3.13	3.54	3.32	2.77	3.07	2.84	2.82	2.76	2.68	2.68	2.90	2.78	3.00	2.82	2.78		
A pos		1.08	0.88	0.81	0.76	0.97	0.83	1.12	0.71	0.92	1.00	1.13	1.15	1.11	0.44	1.07	0.90	1.04	1.18	1.42	1.09	0.84	1.05	0.81	0.92	1.00	1.18	1.24		

Appendix 26: Calculation of atoms per formula unit based on SEM-EDX and EMP-WDX measurements (jarosite from zinc production , continuation).



Appendix 27: STEM image and EDX measurement of a jarosite from zinc production.



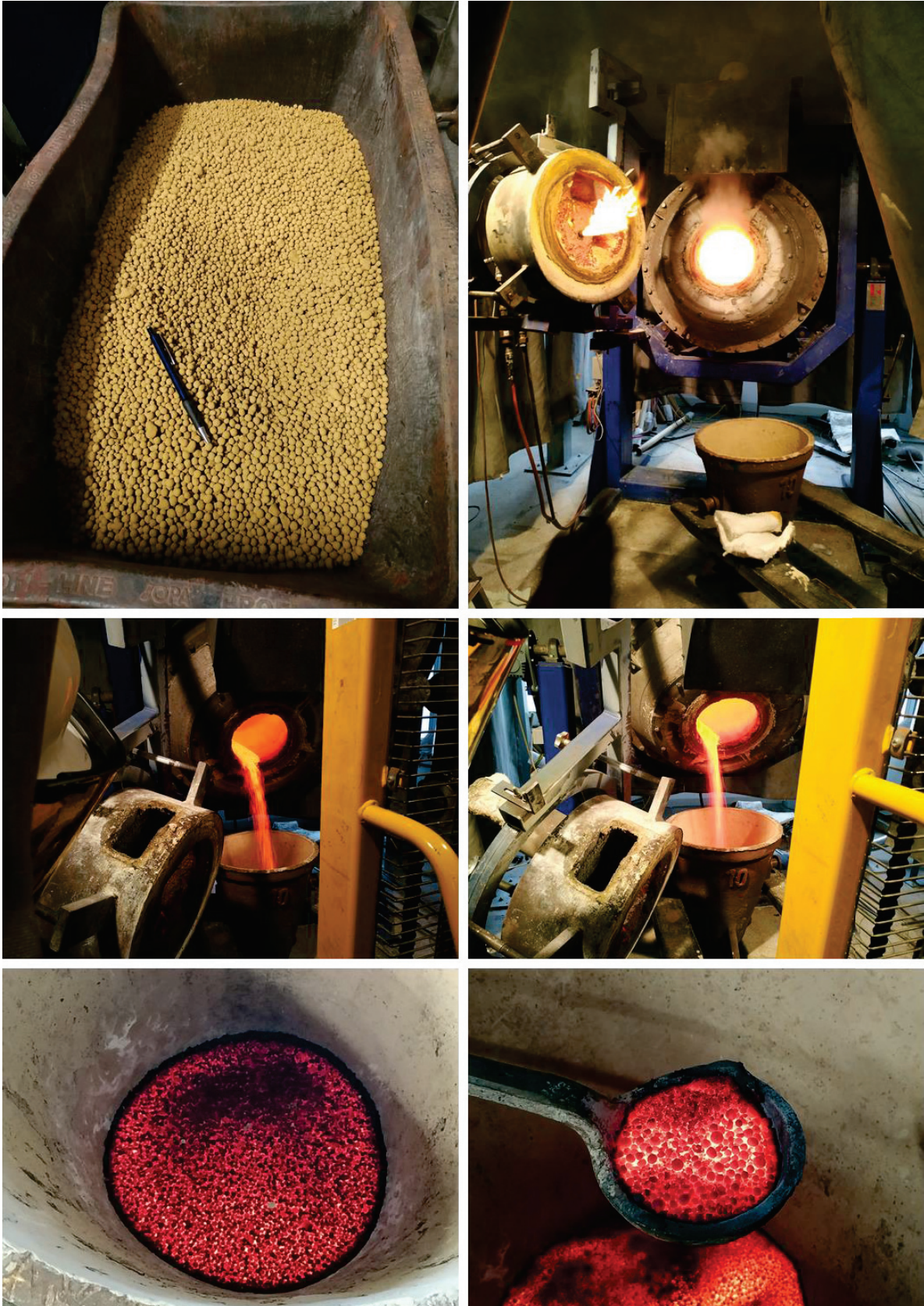
Appendix 28: STEM image and EDX measurement of a jarosite from zinc production.

Bruker Nano GmbH, Germany											
Quantax											
Quantifizierungs-Ergebnisse											
Massenprozent (%)											
Datum: 17.07.2017											
Spektrum	C	O	Na	Al	Si	S	K	Fe	Ni	As	Summe
NiJsit2 1	0.000	35.596		0.394	0.303	8.922		39.628	3.257	0.843	88.944
NiJsit2 2	0.000	31.368			0.493	1.619		55.538	3.661	2.635	95.315
NiJsit2 3	0.000	32.133		0.419	1.176	1.523		54.015	4.020	1.300	94.585
NiJsit2 4	0.000	32.521			0.404	1.546		60.903	3.383	1.801	100.558
NiJsit2 5	0.000	34.357		0.160	0.824	2.179		50.757	3.499	3.319	95.095
NiJsit2 6	0.000	34.376			0.222	7.264		39.113	1.760	1.268	84.003
NiJsit2 7	0.000	35.005			0.352	3.953		49.127	2.933	3.260	94.630
NiJsit2 8	0.000	40.376	0.613	0.385	0.527	9.740		33.966	2.687	0.831	89.126
NiJsit2 9	0.000	29.546			0.702	1.603		53.789	2.613	2.200	90.452
NiJsit2 10	0.000	34.805		0.320	0.720	1.716		54.156	3.628	2.893	98.238
NiJsit2 11	0.000	35.854				12.158		32.305	1.823	0.289	82.429
NiJsit2 12	0.000	36.100			0.362	5.735		44.792	3.393	1.348	91.731
NiJsit2 13	0.000	30.204		0.216	0.562	1.597		58.334	3.800	1.279	95.992
NiJsit2 14	0.000	33.766		0.239	0.981	2.591		51.166	4.464	1.191	94.400
NiJsit2 15	0.000	34.478				8.230		38.139	1.857	0.439	83.143
NiJsit2 16	0.000	29.505		0.396	1.047	2.052		54.635	5.881	0.988	94.504
NiJsit2 17	0.000	30.086			0.775	1.835		53.579	4.547	0.552	91.375
NiJsit2 18	0.000	30.007			0.317	4.454		52.075	2.863	0.641	90.357
NiJsit2 19	0.000	29.903			0.583	1.761		62.338	4.146	1.270	100.002
NiJsit2 20	0.000	25.028			0.687	1.630		62.413	3.943	1.175	94.876
NiJsit2 21	0.000	30.289		0.295	0.400	5.487		42.109	3.397	1.249	83.227
NiJsit2 22	0.000	34.361		0.465	1.012	2.024		55.421	4.024	2.101	99.409
NiJsit2 23	0.000	27.955		0.883	2.706	2.242		42.696	12.154	0.583	89.218
NiJsit2 24	0.000	29.793			1.981	1.354		52.790	5.609	0.502	92.029
NiJsit2 25	0.000	22.186		1.513	3.876	2.658		16.398	20.631	0.103	67.364
NiJsit2 26	0.000	31.356		0.282	0.968	2.807		51.062	6.070	1.861	94.406
NiJsit2 27	0.000	30.467		0.166	0.523	1.680		57.854	3.981	1.505	96.176
NiJsit2 28	0.000	34.235			0.754	1.759		56.235	3.761	1.495	98.239
NiJsit2 29	0.000	30.737			0.831	1.371		53.488	3.718	1.973	92.119
NiJsit2 30	0.000	33.313		0.714	1.023	1.924		56.534	6.853	1.504	101.864
NiJsit2 31	0.000	33.891		0.423	0.798	6.476		44.916	4.526	1.130	92.160
NiJsit2 32	0.000	30.326		0.423	0.815	1.764		54.635	4.489	0.763	93.215
NiJsit2 33	0.000	31.431			0.329	1.749		57.229	3.476	0.988	95.202
NiJsit2 34	0.000	30.215		0.239	0.633	1.943		55.069	4.345	1.388	93.833
NiJsit2 35	0.000	33.358		0.270	0.701	1.680		52.876	4.368	3.123	96.375

Appendix 29: SEM-WDX measurements of jarosite material from platinum production.

NiJsit2 36	0.000	30.949		1.136	1.642	6.219		41.068	6.645	0.811	88.470
NiJsit2 37	0.000	32.525			0.538	1.488		55.247	3.931	1.661	95.391
NiJsit2 38	0.000	33.180		0.233	0.648	1.773		54.202	4.553	1.680	96.270
NiJsit2 39	0.000	31.827			0.470	1.449		60.571	2.989	1.201	98.507
NiJsit2 40	0.000	30.231		0.348	0.615	1.368		54.277	4.208	5.547	96.593
NiJsit2 41	0.000	35.576		0.330	0.931	4.977		44.714	5.461	1.431	93.419
NiJsit2 42	0.000	32.066		0.115	0.492	1.652		58.435	3.601	0.860	97.221
NiJsit2 43	0.000	33.579		1.239	1.607	1.588		59.057	4.461	0.837	102.369
NiJsit2 44	0.000	29.082		5.841	5.989	1.153	1.910	42.963	3.492	0.429	90.859
NiJsit2 45	0.000	30.884		0.255	0.498	1.852		54.519	4.577	1.561	94.146
NiJsit2 46	0.000	30.238		0.140	0.751	1.618		57.234	4.257	0.322	94.560
NiJsit2 47	0.000	27.463			0.786	1.604		62.904	3.846	0.857	97.459
NiJsit2 48	0.000	31.578		0.265	0.673	4.135		54.081	4.901	1.025	96.658
NiJsit2 49	0.000	31.156			0.999	1.892		58.840	5.584	1.132	99.603
NiJsit2 50	0.000	29.610		0.743	2.646	1.369		54.223	5.683	1.372	95.647
NiJsit2 51	0.000	33.701			0.238	5.632		48.286	2.599	1.425	91.881
NiJsit2 52	0.000	33.797				8.161		40.720	2.212	0.871	85.760
NiJsit2 53	0.000	31.282		0.340	0.659	2.839		57.515	3.897	1.451	97.983
NiJsit2 54	0.000	30.262		0.554	0.864	1.743		54.745	5.963	1.159	95.291
NiJsit2 55	0.000	24.519		1.264	1.971	2.434		40.742	12.702	1.482	85.114
NiJsit2 56	0.000	29.162			0.323	1.727		54.237	2.848	2.949	91.246
NiJsit2 57	0.000	30.297		0.232	0.461	10.917		34.092	3.760	0.920	80.679
NiJsit2 58	0.000	32.435			0.390	1.809		60.308	4.180	0.776	99.897
NiJsit2 59	0.000	34.903			0.249	3.727		52.745	2.451	0.883	94.957
NiJsit2 60	0.000	30.606		0.452	1.122	2.167		55.600	5.512	2.016	97.474
NiJsit2 61	0.000	32.351			0.385	1.404		61.477	3.107	1.565	100.289
NiJsit2 62	0.000	21.758		1.950	9.458	1.578	0.866	24.605	13.093		73.308
NiJsit2 63	0.000	33.063			0.591	2.874		48.441	4.116	2.915	92.000
NiJsit2 64	0.000	33.590				8.013		38.270	2.077	1.456	83.406
NiJsit2 65	0.000	30.695		0.388	0.659	1.688		58.996	4.952	0.616	97.994
NiJsit2 66	0.000	31.447			0.285	1.597		59.794	2.556	0.907	96.586
NiJsit2 67	0.000	31.790			1.148	1.759		55.253	5.579	0.519	96.048
NiJsit2 68	0.000	31.684			0.485	2.307		57.585	3.750	0.731	96.542
NiJsit2 69	0.000	32.547		0.886	0.699	7.653		37.986	4.456	1.087	85.314
NiJsit2 70	0.000	31.646		0.138	0.600	1.732		53.823	4.227	1.526	93.692
NiJsit2 71	0.000	26.845		0.659	1.118	2.412		47.673	12.417	1.018	92.143
NiJsit2 72	0.000	30.302			0.460	1.393		59.832	3.236	0.725	95.948
NiJsit2 73	0.000	30.484			0.557	1.499		55.811	3.338	1.439	93.127
Mittelwert	0.000	31.480	0.613	0.643	1.020	3.154	1.388	50.972	4.668	1.374	
Sigma:	0.000	3.003	0.000	0.937	1.353	2.581	0.738	9.176	2.951	0.872	
Sigma Mittelv	0.000	0.352	0.000	0.110	0.158	0.302	0.086	1.074	0.345	0.102	

Appendix 30: SEM-WDX measurements of jarosite material from platinum production (continuation).



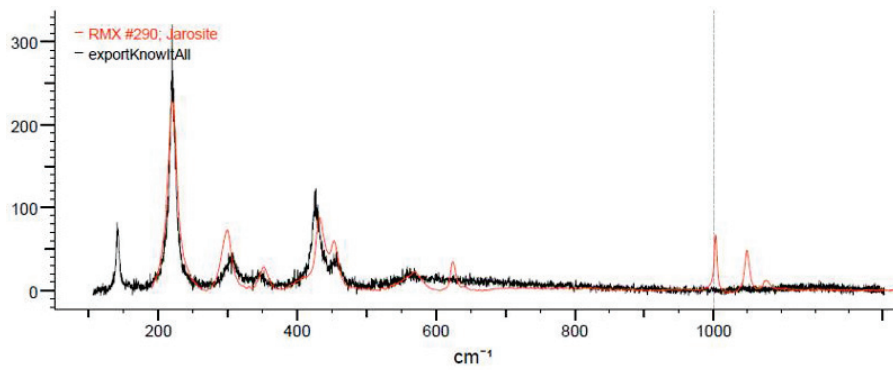
Appendix 31: Calcination trials with jarosite from zinc production. Upper left: jarosite pellets ready for calcination. Upper right: calcination in the TBRC. Middle: tapping of the calcine. Bottom: calcine.



Appendix 32: Reduction trials with jarosite from zinc production. Upper left: calcine. Upper right and middle left: reduction in the electric furnace. Middle left: tapping. bottom left: slag. bottom right: slag and alloy.

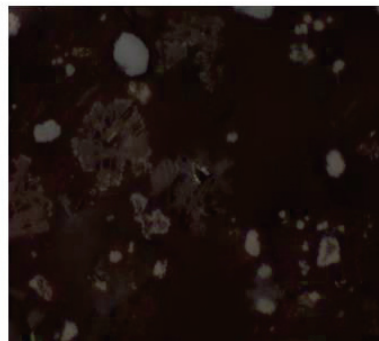
Bruker Nano GmbH, Germany		C	O	F	Na	Mg	Al	Si	P	S	Cl	K	Ca	Ti	Cr	Mn	Fe	Ni	As	Zr	Mo	Ag	Sn	La	Ce	Nd	Pb
Quantax		0.00	1.02			1.08				24.61			0.86				1.68	70.75									
Quantifizierungs-Ergebnisse		0.00				1.41							0.88				7.40	90.32									
Norm. Massenprozent (%)		28.63				20.62	1.16						0.38			2.27	30.17	16.78									
Datum:		0.00															91.92	8.08									
22.01.2019		0.00															92.18	7.82									
Spektrum		30.99				1.22	1.42	3.46					61.71				1.20										
RV 3.1 slag 7		39.61				4.94	5.90	16.27				1.29	27.85			1.44	2.69										
RV 3.1 slag 6		23.96						0.28		0.95			6.22				66.15		2.45								
RV 3.1 slag 5		23.09					0.20			0.43			3.23				71.82		1.23								
RV 3.1 slag 4		25.88								1.96			18.31				34.24		9.68								
RV 3.1 slag 3		41.64				6.74	6.35	16.52		1.29			0.51	26.41		0.53											
RV 3.1 slag 2		40.90				5.71	6.35	15.99		0.96			0.50	28.69		0.52											
RV 3.1 slag 1		41.53	1.35			1.41	1.01	4.06		16.03			6.96				5.54										
V 1.1 roasted 16		42.18				0.76	2.70	2.13	4.72	14.41			0.14	14.24		1.61	20.48										
V 1.1 roasted 15		42.81				9.08	6.82	17.66		1.19			0.48	21.96		0.88	13.15										
V 1.1 roasted 14		41.17				0.44	5.69	6.23	16.46	0.97			28.43														
V 1 slag 7		41.93				6.65	6.69	17.06		1.01			26.65														
V 1 slag 6		40.33				0.74	6.44	6.24	16.25			0.26	28.36				0.39	0.98									
V 1 slag 5		37.98				3.73	10.69	11.03				1.10	12.38	4.33		3.22	15.53										
V 1 slag 4		0.00								32.02							32.89	35.09									
V 1 slag 3		0.00																									
V 1 slag 2		0.00																									
V 1 slag 1		0.00																									
RV 3.2 slag 11		0.00																									
RV 3.2 slag 10		0.00																									
RV 3.2 slag 9		0.00																									
RV 3.2 slag 8		0.00																									
RV 3.2 slag 7		0.00																									
RV 3.2 slag 6		0.00	4.32				1.20	1.84		30.25			2.70			1.83	57.87										
RV 3.2 slag 5		0.00	4.35				1.30	1.66		26.50			0.84	1.46		2.10	58.05										
RV 3.2 slag 4		37.26				1.81	10.50	11.41				3.30	12.87	3.53		4.01	15.32										

Appendix 33: SEM-EDX measurements on calcine and slag from pyrometallurgical trials on jarosite from platinum production.

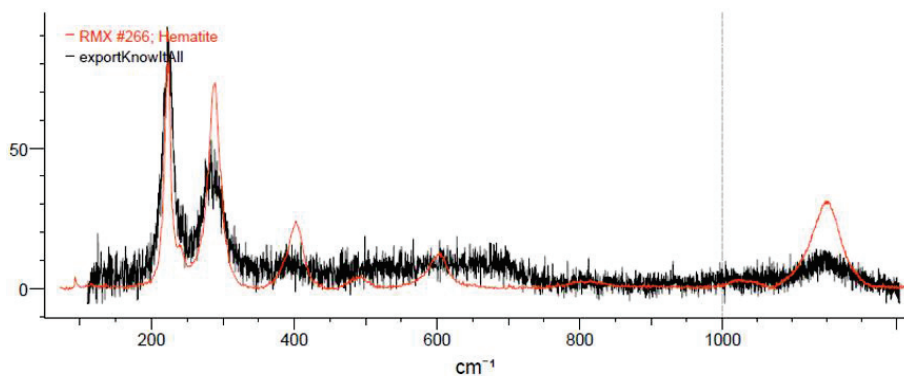


Manuelle Korrekturen: Keine
 Suchbereiche: Voll
 Suchalgorithmus: Korrelation
 Pfad des Suchspektrums: n. zutr.

Name:	Wert
Ergebnis-HQI	82.98
Datenbankkürzung	RMX
Datenbanktitel	Raman - Minerals - HORIBA
Datensatzkennung	290
Name:	Jarosite
Classification	sulfate; hydroxide
Comments	Barium Queen Mine, Barstow, California, USA; con.H
Formula	$KFe_3(SO_4)_2(OH)_6$
Instrument Name	HORIBA
Raman Laser Power	785
Source of Sample	Caltech
Source of Spectrum	HORIBA Scientific

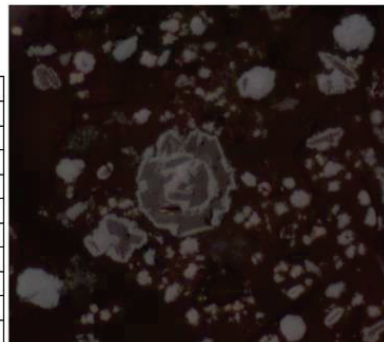


Appendix 36: RAMAN measurement of a jarosite particle in a jarosite residue from platinum production.



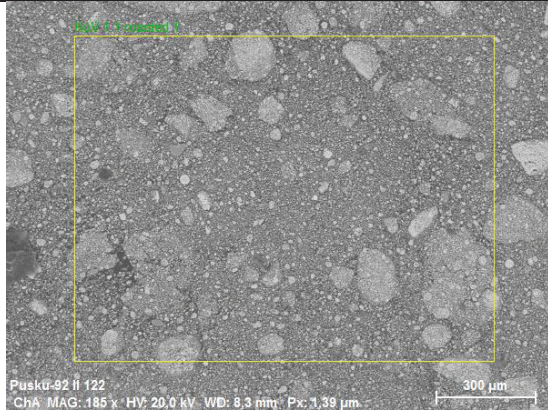
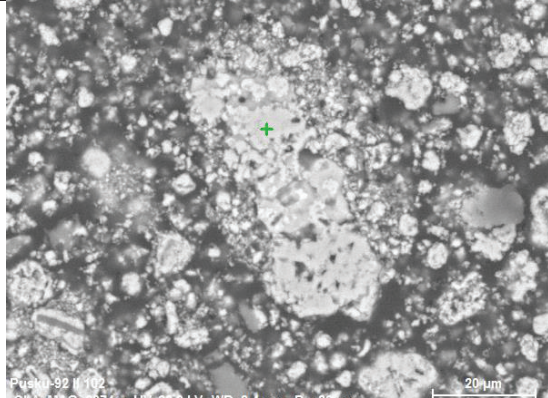
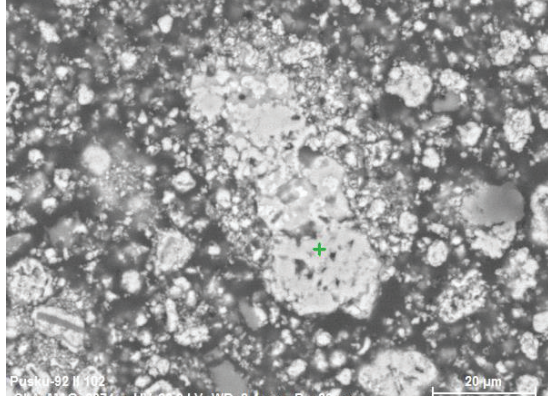
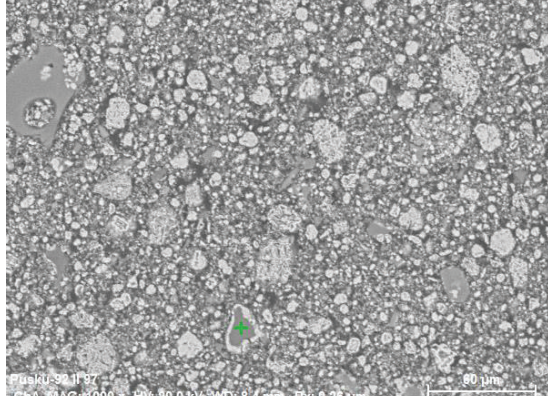
Manuelle Korrekturen: Basislinie
 Suchbereiche: Voll
 Suchalgorithmus: Korrelation
 Pfad des Suchspektrums: n. zutr.

Name:	Wert
Ergebnis-HQI	67.90
Datenbankkürzung	RMX
Datenbanktitel	Raman - Minerals - HORIBA
Datensatzkennung	266
Name:	Hematite
Classification	oxide
Formula	$\alpha\text{-Fe}_2\text{O}_3$
Instrument Name	HORIBA LabRAM
Raman Laser Power	632.8
Source of Spectrum	HORIBA Scientific



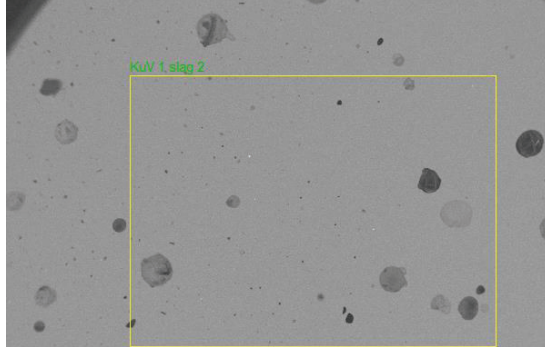
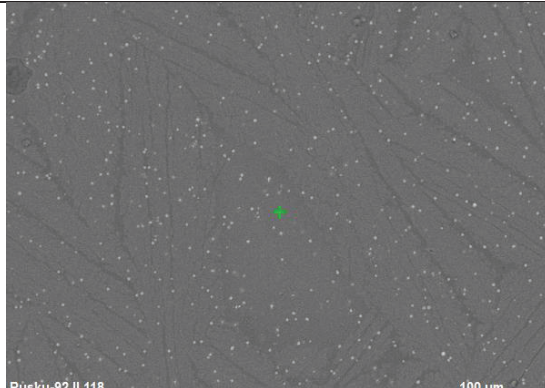
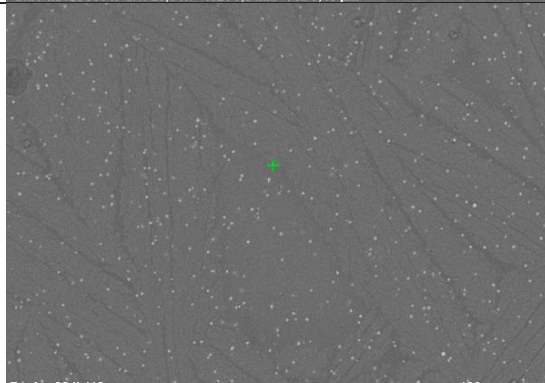
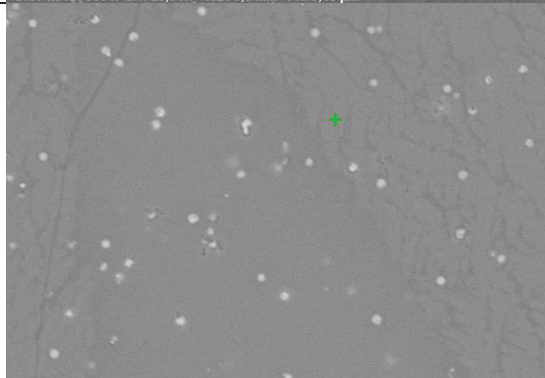
Appendix 37: RAMAN measurement of a hematite particle in a jarosite residue from platinum production.

1st trial calcine

	<table border="1"> <thead> <tr> <th></th> <th>wt.%</th> </tr> </thead> <tbody> <tr> <td>O</td> <td>27.85</td> </tr> <tr> <td>Al</td> <td>1.41</td> </tr> <tr> <td>Si</td> <td>3.13</td> </tr> <tr> <td>S</td> <td>2.80</td> </tr> <tr> <td>Ca</td> <td>2.91</td> </tr> <tr> <td>Fe</td> <td>54.73</td> </tr> <tr> <td>Ni</td> <td>7.13</td> </tr> </tbody> </table>		wt.%	O	27.85	Al	1.41	Si	3.13	S	2.80	Ca	2.91	Fe	54.73	Ni	7.13
	wt.%																
O	27.85																
Al	1.41																
Si	3.13																
S	2.80																
Ca	2.91																
Fe	54.73																
Ni	7.13																
	<table border="1"> <thead> <tr> <th></th> <th>wt.%</th> </tr> </thead> <tbody> <tr> <td>O</td> <td>22.31</td> </tr> <tr> <td>Al</td> <td>0.45</td> </tr> <tr> <td>Ca</td> <td>0.66</td> </tr> <tr> <td>Fe</td> <td>55.66</td> </tr> <tr> <td>Ni</td> <td>20.91</td> </tr> </tbody> </table>		wt.%	O	22.31	Al	0.45	Ca	0.66	Fe	55.66	Ni	20.91				
	wt.%																
O	22.31																
Al	0.45																
Ca	0.66																
Fe	55.66																
Ni	20.91																
	<table border="1"> <thead> <tr> <th></th> <th>wt.%</th> </tr> </thead> <tbody> <tr> <td>O</td> <td>22.46</td> </tr> <tr> <td>Al</td> <td>0.41</td> </tr> <tr> <td>Fe</td> <td>77.13</td> </tr> </tbody> </table>		wt.%	O	22.46	Al	0.41	Fe	77.13								
	wt.%																
O	22.46																
Al	0.41																
Fe	77.13																
	<table border="1"> <thead> <tr> <th></th> <th>wt.%</th> </tr> </thead> <tbody> <tr> <td>O</td> <td>46.01</td> </tr> <tr> <td>Na</td> <td>3.12</td> </tr> <tr> <td>Al</td> <td>10.56</td> </tr> <tr> <td>Si</td> <td>29.09</td> </tr> <tr> <td>K</td> <td>10.15</td> </tr> <tr> <td></td> <td></td> </tr> <tr> <td>Fe</td> <td>1.07</td> </tr> </tbody> </table>		wt.%	O	46.01	Na	3.12	Al	10.56	Si	29.09	K	10.15			Fe	1.07
	wt.%																
O	46.01																
Na	3.12																
Al	10.56																
Si	29.09																
K	10.15																
Fe	1.07																

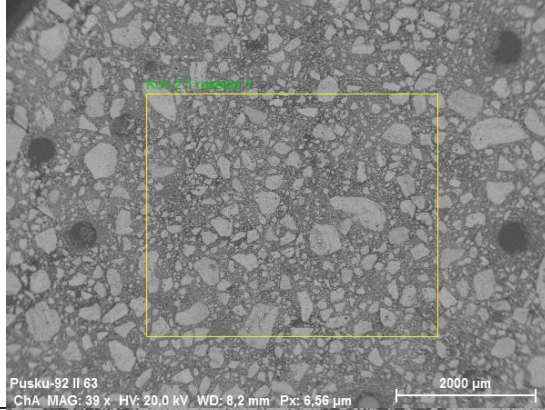
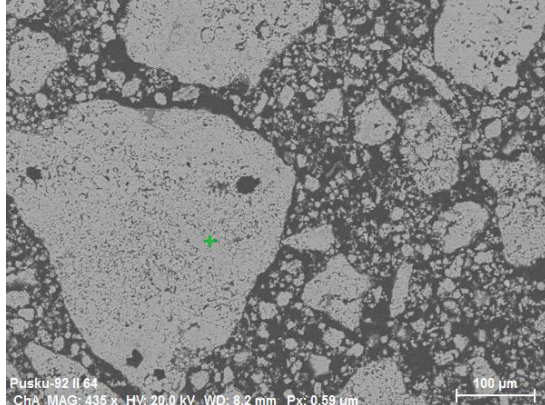
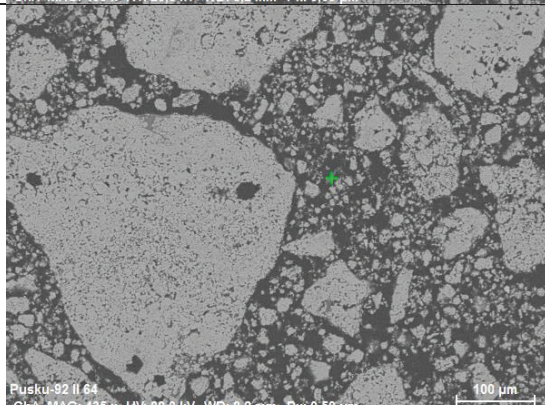
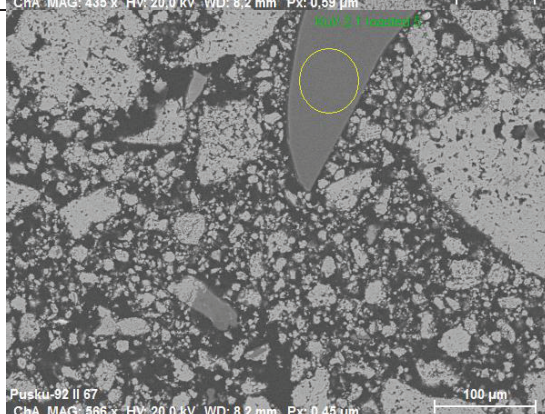
Appendix 38: SEM-EDX analyses of the calcine of jarosite from platinum production after calcination trial 1.

1st trial, slag

 <p>Pusk-92 II 121 ChA MAG: 37 x HV: 20,0 kV WD: 8,9 mm Px: 6,91 µm</p> <p>2000 µm</p>	<table border="1"> <thead> <tr> <th></th> <th>wt.%</th> </tr> </thead> <tbody> <tr> <td>O</td> <td>41.27</td> </tr> <tr> <td>Na</td> <td>0.41</td> </tr> <tr> <td>Mg</td> <td>6.18</td> </tr> <tr> <td>Al</td> <td>6.40</td> </tr> <tr> <td>Si</td> <td>15.07</td> </tr> <tr> <td>S</td> <td>1.99</td> </tr> <tr> <td>K</td> <td>0.61</td> </tr> <tr> <td>Ca</td> <td>27.05</td> </tr> <tr> <td>Mn</td> <td>1.03</td> </tr> </tbody> </table>		wt.%	O	41.27	Na	0.41	Mg	6.18	Al	6.40	Si	15.07	S	1.99	K	0.61	Ca	27.05	Mn	1.03
	wt.%																				
O	41.27																				
Na	0.41																				
Mg	6.18																				
Al	6.40																				
Si	15.07																				
S	1.99																				
K	0.61																				
Ca	27.05																				
Mn	1.03																				
 <p>Pusk-92 II 118 ChA MAG: 600 x HV: 20,0 kV WD: 9,0 mm Px: 0,43 µm</p> <p>100 µm</p>	<table border="1"> <thead> <tr> <th></th> <th>wt.%</th> </tr> </thead> <tbody> <tr> <td>O</td> <td>41.93</td> </tr> <tr> <td>Mg</td> <td>6.65</td> </tr> <tr> <td>Al</td> <td>6,69</td> </tr> <tr> <td>Si</td> <td>17.06</td> </tr> <tr> <td>S</td> <td>1.01</td> </tr> <tr> <td>Ca</td> <td>26.65</td> </tr> </tbody> </table>		wt.%	O	41.93	Mg	6.65	Al	6,69	Si	17.06	S	1.01	Ca	26.65						
	wt.%																				
O	41.93																				
Mg	6.65																				
Al	6,69																				
Si	17.06																				
S	1.01																				
Ca	26.65																				
 <p>Pusk-92 II 118 ChA MAG: 600 x HV: 20,0 kV WD: 9,0 mm Px: 0,43 µm</p> <p>100 µm</p>	<table border="1"> <thead> <tr> <th></th> <th>wt.%</th> </tr> </thead> <tbody> <tr> <td>O</td> <td>42.81</td> </tr> <tr> <td>Mg</td> <td>9.08</td> </tr> <tr> <td>Al</td> <td>6.82</td> </tr> <tr> <td>Si</td> <td>17.66</td> </tr> <tr> <td>S</td> <td>1.19</td> </tr> <tr> <td>K</td> <td>0.48</td> </tr> <tr> <td>Ca</td> <td>21.96</td> </tr> </tbody> </table>		wt.%	O	42.81	Mg	9.08	Al	6.82	Si	17.66	S	1.19	K	0.48	Ca	21.96				
	wt.%																				
O	42.81																				
Mg	9.08																				
Al	6.82																				
Si	17.66																				
S	1.19																				
K	0.48																				
Ca	21.96																				
 <p>Pusk-92 II 119 ChA MAG: 1896 x HV: 20,0 kV WD: 8,9 mm Px: 0,13 µm</p> <p>30 µm</p>	<table border="1"> <thead> <tr> <th></th> <th>wt.%</th> </tr> </thead> <tbody> <tr> <td>O</td> <td>40.90</td> </tr> <tr> <td>Na</td> <td>0.38</td> </tr> <tr> <td>Mg</td> <td>5.71</td> </tr> <tr> <td>Al</td> <td>6.35</td> </tr> <tr> <td>Si</td> <td>15.99</td> </tr> <tr> <td>S</td> <td>0.96</td> </tr> <tr> <td>K</td> <td>0.50</td> </tr> <tr> <td>Ca</td> <td>28.69</td> </tr> <tr> <td>Mn</td> <td>0.52</td> </tr> </tbody> </table>		wt.%	O	40.90	Na	0.38	Mg	5.71	Al	6.35	Si	15.99	S	0.96	K	0.50	Ca	28.69	Mn	0.52
	wt.%																				
O	40.90																				
Na	0.38																				
Mg	5.71																				
Al	6.35																				
Si	15.99																				
S	0.96																				
K	0.50																				
Ca	28.69																				
Mn	0.52																				

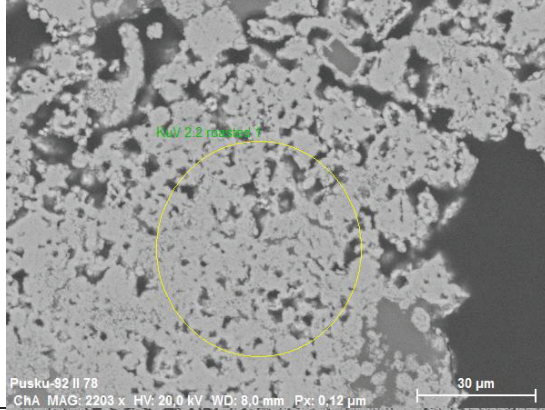
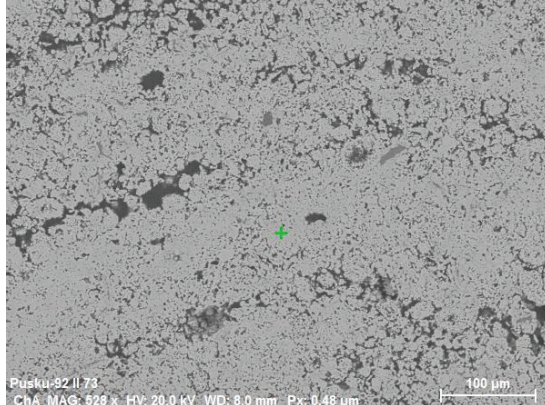
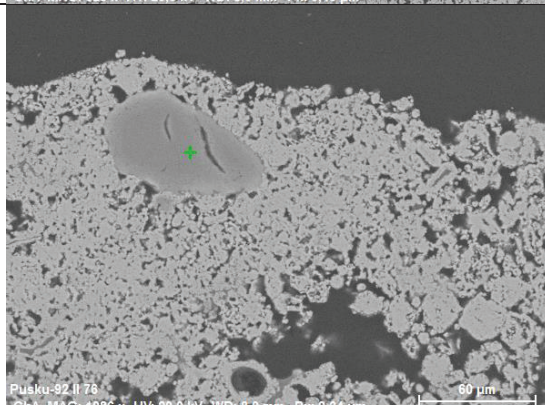
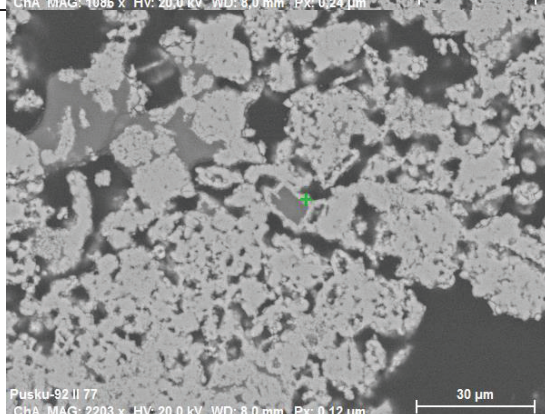
Appendix 39: SEM-EDX analyses of slag from jarosite from platinum production after reduction trial 1.

Trial 2.1, calcine

	<table border="1"> <thead> <tr> <th></th> <th>wt.%</th> </tr> </thead> <tbody> <tr> <td>O</td> <td>23.08</td> </tr> <tr> <td>Si</td> <td>1.24</td> </tr> <tr> <td>Fe</td> <td>74.84</td> </tr> <tr> <td>Ni</td> <td>0.84</td> </tr> </tbody> </table>		wt.%	O	23.08	Si	1.24	Fe	74.84	Ni	0.84		
	wt.%												
O	23.08												
Si	1.24												
Fe	74.84												
Ni	0.84												
	<table border="1"> <thead> <tr> <th></th> <th>wt.%</th> </tr> </thead> <tbody> <tr> <td>O</td> <td>24.40</td> </tr> <tr> <td>Al</td> <td>0.72</td> </tr> <tr> <td>Si</td> <td>2.73</td> </tr> <tr> <td>Fe</td> <td>70.70</td> </tr> <tr> <td>Ni</td> <td>1.44</td> </tr> </tbody> </table>		wt.%	O	24.40	Al	0.72	Si	2.73	Fe	70.70	Ni	1.44
	wt.%												
O	24.40												
Al	0.72												
Si	2.73												
Fe	70.70												
Ni	1.44												
	<table border="1"> <thead> <tr> <th></th> <th>wt.%</th> </tr> </thead> <tbody> <tr> <td>O</td> <td>48.55</td> </tr> <tr> <td>Al</td> <td>2.32</td> </tr> <tr> <td>Si</td> <td>37.99</td> </tr> <tr> <td>Fe</td> <td>11.14</td> </tr> </tbody> </table>		wt.%	O	48.55	Al	2.32	Si	37.99	Fe	11.14		
	wt.%												
O	48.55												
Al	2.32												
Si	37.99												
Fe	11.14												
	<table border="1"> <thead> <tr> <th></th> <th>wt.%</th> </tr> </thead> <tbody> <tr> <td>O</td> <td>49.96</td> </tr> <tr> <td>Al</td> <td>25.41</td> </tr> <tr> <td>Si</td> <td>23.81</td> </tr> <tr> <td>Fe</td> <td>0.82</td> </tr> </tbody> </table>		wt.%	O	49.96	Al	25.41	Si	23.81	Fe	0.82		
	wt.%												
O	49.96												
Al	25.41												
Si	23.81												
Fe	0.82												


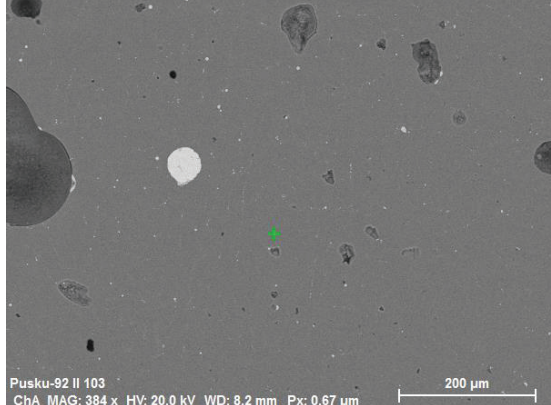
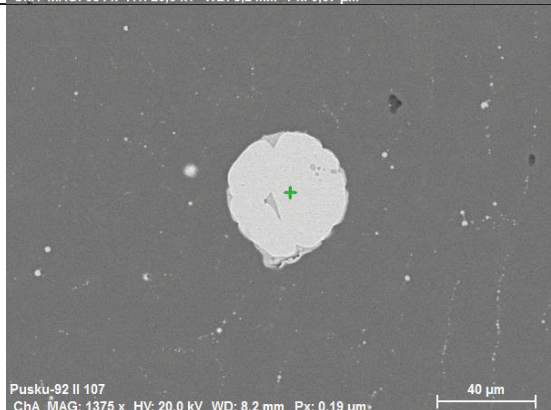
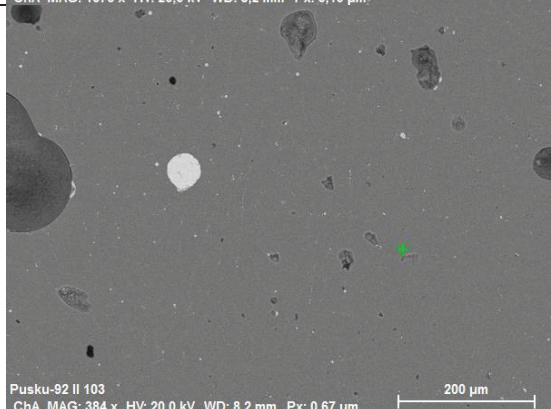
Appendix 40: SEM-EDX analyses of the calcine of jarosite from platinum production after calcination trial 2.1.

Trial 2.2, calcine

 <p>Puskku-92 II 78 CHA MAG: 2203 x HV: 20.0 kV WD: 8.0 mm Px: 0.12 µm</p>	<table border="1"> <thead> <tr> <th></th> <th>wt.%</th> </tr> </thead> <tbody> <tr> <td>O</td> <td>23.71</td> </tr> <tr> <td>Al</td> <td>0.74</td> </tr> <tr> <td>Si</td> <td>1.71</td> </tr> <tr> <td>Fe</td> <td>69.69</td> </tr> <tr> <td>Ni</td> <td>4.14</td> </tr> </tbody> </table>		wt.%	O	23.71	Al	0.74	Si	1.71	Fe	69.69	Ni	4.14		
	wt.%														
O	23.71														
Al	0.74														
Si	1.71														
Fe	69.69														
Ni	4.14														
 <p>Puskku-92 II 73 CHA MAG: 528 x HV: 20.0 kV WD: 8.0 mm Px: 0.48 µm</p>	<table border="1"> <thead> <tr> <th></th> <th>wt.%</th> </tr> </thead> <tbody> <tr> <td>O</td> <td>22.99</td> </tr> <tr> <td>Si</td> <td>1.14</td> </tr> <tr> <td>Fe</td> <td>72.48</td> </tr> <tr> <td>Ni</td> <td>3.40</td> </tr> </tbody> </table>		wt.%	O	22.99	Si	1.14	Fe	72.48	Ni	3.40				
	wt.%														
O	22.99														
Si	1.14														
Fe	72.48														
Ni	3.40														
 <p>Puskku-92 II 76 CHA MAG: 1086 x HV: 20.0 kV WD: 8.0 mm Px: 0.24 µm</p>	<table border="1"> <thead> <tr> <th></th> <th>wt.%</th> </tr> </thead> <tbody> <tr> <td>O</td> <td>37.10</td> </tr> <tr> <td>F</td> <td>1.55</td> </tr> <tr> <td>P</td> <td>14.78</td> </tr> <tr> <td>Cl</td> <td>1.15</td> </tr> <tr> <td>Ca</td> <td>44.39</td> </tr> <tr> <td>Fe</td> <td>1.03</td> </tr> </tbody> </table>		wt.%	O	37.10	F	1.55	P	14.78	Cl	1.15	Ca	44.39	Fe	1.03
	wt.%														
O	37.10														
F	1.55														
P	14.78														
Cl	1.15														
Ca	44.39														
Fe	1.03														
 <p>Puskku-92 II 77 CHA MAG: 2203 x HV: 20.0 kV WD: 8.0 mm Px: 0.12 µm</p>	<table border="1"> <thead> <tr> <th></th> <th>wt.%</th> </tr> </thead> <tbody> <tr> <td>O</td> <td>24.72</td> </tr> <tr> <td>Al</td> <td>0.74</td> </tr> <tr> <td>Si</td> <td>3.36</td> </tr> <tr> <td>Fe</td> <td>59.51</td> </tr> <tr> <td>Ni</td> <td>11.67</td> </tr> </tbody> </table>		wt.%	O	24.72	Al	0.74	Si	3.36	Fe	59.51	Ni	11.67		
	wt.%														
O	24.72														
Al	0.74														
Si	3.36														
Fe	59.51														
Ni	11.67														

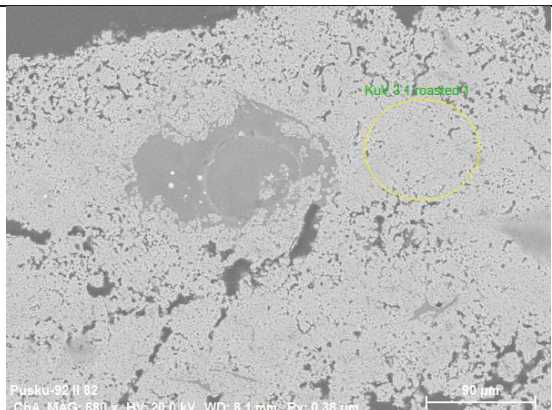
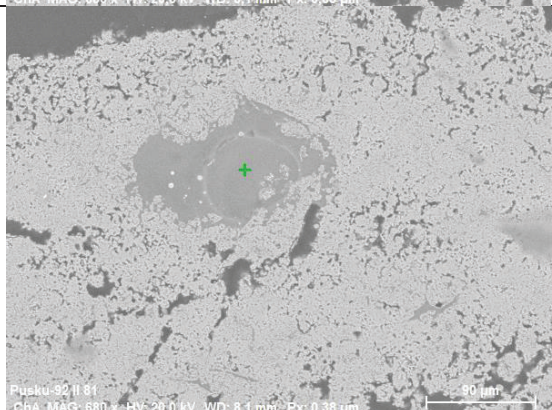
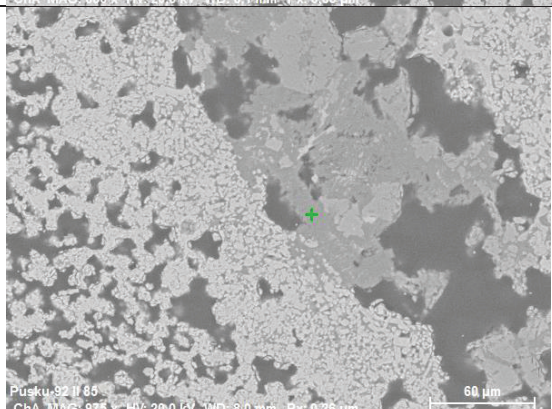
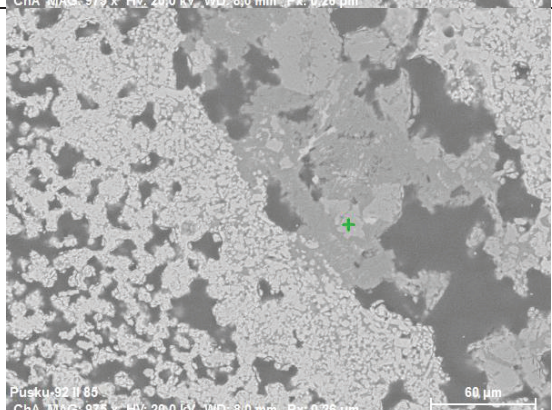
Appendix 41: SEM-EDX analyses of the calcine of jarosite from platinum production after calcination trial 2.2.

Trial 2.2, slag

	<table border="1"> <thead> <tr> <th></th> <th>wt.%</th> </tr> </thead> <tbody> <tr> <td>O</td> <td>40.43</td> </tr> <tr> <td>Mg</td> <td>6.22</td> </tr> <tr> <td>Al</td> <td>7.65</td> </tr> <tr> <td>Si</td> <td>15.84</td> </tr> <tr> <td>Ca</td> <td>25.90</td> </tr> <tr> <td>Mn</td> <td>1.07</td> </tr> <tr> <td>Fe</td> <td>2.89</td> </tr> </tbody> </table>		wt.%	O	40.43	Mg	6.22	Al	7.65	Si	15.84	Ca	25.90	Mn	1.07	Fe	2.89
	wt.%																
O	40.43																
Mg	6.22																
Al	7.65																
Si	15.84																
Ca	25.90																
Mn	1.07																
Fe	2.89																
	<table border="1"> <thead> <tr> <th></th> <th>wt.%</th> </tr> </thead> <tbody> <tr> <td>O</td> <td>39.69</td> </tr> <tr> <td>Mg</td> <td>4.73</td> </tr> <tr> <td>Al</td> <td>6.11</td> </tr> <tr> <td>Si</td> <td>15.51</td> </tr> <tr> <td>Ca</td> <td>33.22</td> </tr> <tr> <td>Fe</td> <td>0.73</td> </tr> </tbody> </table>		wt.%	O	39.69	Mg	4.73	Al	6.11	Si	15.51	Ca	33.22	Fe	0.73		
	wt.%																
O	39.69																
Mg	4.73																
Al	6.11																
Si	15.51																
Ca	33.22																
Fe	0.73																
	<table border="1"> <thead> <tr> <th></th> <th>wt.%</th> </tr> </thead> <tbody> <tr> <td>Fe</td> <td>100</td> </tr> </tbody> </table>		wt.%	Fe	100												
	wt.%																
Fe	100																
	<table border="1"> <thead> <tr> <th></th> <th>wt.%</th> </tr> </thead> <tbody> <tr> <td>O</td> <td>41.00</td> </tr> <tr> <td>Mg</td> <td>4.90</td> </tr> <tr> <td>Al</td> <td>7.33</td> </tr> <tr> <td>Si</td> <td>17.09</td> </tr> <tr> <td>Ca</td> <td>29.06</td> </tr> <tr> <td>Fe</td> <td>0.62</td> </tr> </tbody> </table>		wt.%	O	41.00	Mg	4.90	Al	7.33	Si	17.09	Ca	29.06	Fe	0.62		
	wt.%																
O	41.00																
Mg	4.90																
Al	7.33																
Si	17.09																
Ca	29.06																
Fe	0.62																

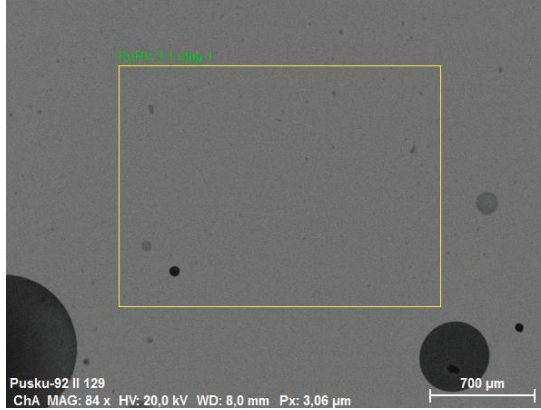
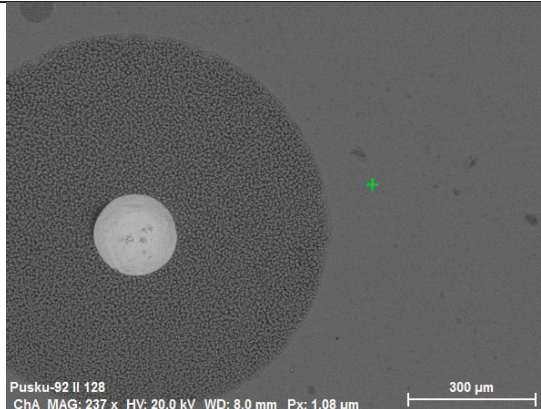
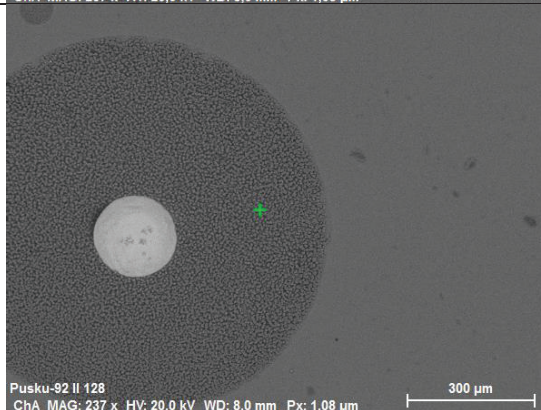
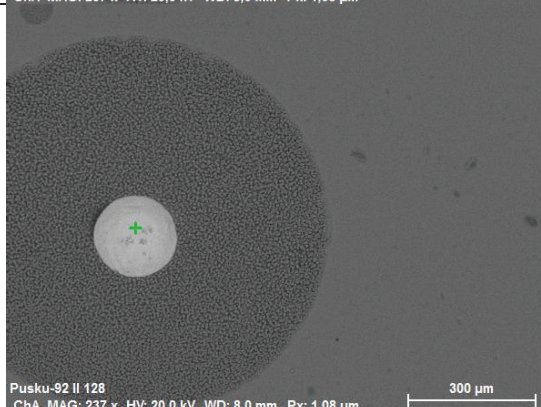
Appendix 42: SEM-EDX analyses of slag from jarosite from platinum production after reduction trial 2.2.

Trial 3.1, calcine

 <p>Pusku-92 II 82 CHA MAG: 680 X HV: 20.0 kV WD: 8.1 mm Px: 0.38 µm</p>	<table border="1"> <thead> <tr> <th></th> <th>wt.%</th> </tr> </thead> <tbody> <tr> <td>O</td> <td>25.03</td> </tr> <tr> <td>Al</td> <td>0.67</td> </tr> <tr> <td>Si</td> <td>2.27</td> </tr> <tr> <td>Fe</td> <td>68.22</td> </tr> <tr> <td>Ni</td> <td>4.81</td> </tr> </tbody> </table>		wt.%	O	25.03	Al	0.67	Si	2.27	Fe	68.22	Ni	4.81				
	wt.%																
O	25.03																
Al	0.67																
Si	2.27																
Fe	68.22																
Ni	4.81																
 <p>Pusku-92 II 81 CHA MAG: 680 X HV: 20.0 kV WD: 8.1 mm Px: 0.38 µm</p>	<table border="1"> <thead> <tr> <th></th> <th>wt.%</th> </tr> </thead> <tbody> <tr> <td>O</td> <td>46.76</td> </tr> <tr> <td>Na</td> <td>1.77</td> </tr> <tr> <td>Al</td> <td>6.05</td> </tr> <tr> <td>Si</td> <td>33.68</td> </tr> <tr> <td>K</td> <td>5.18</td> </tr> <tr> <td>Fe</td> <td>3.96</td> </tr> <tr> <td>Pb</td> <td>2.60</td> </tr> </tbody> </table>		wt.%	O	46.76	Na	1.77	Al	6.05	Si	33.68	K	5.18	Fe	3.96	Pb	2.60
	wt.%																
O	46.76																
Na	1.77																
Al	6.05																
Si	33.68																
K	5.18																
Fe	3.96																
Pb	2.60																
 <p>Pusku-92 II 85 CHA MAG: 975 X HV: 20.0 kV WD: 8.0 mm Px: 0.26 µm</p>	<table border="1"> <thead> <tr> <th></th> <th>wt.%</th> </tr> </thead> <tbody> <tr> <td>O</td> <td>44.82</td> </tr> <tr> <td>Na</td> <td>1.49</td> </tr> <tr> <td>Mg</td> <td>0.76</td> </tr> <tr> <td>Al</td> <td>19.63</td> </tr> <tr> <td>Si</td> <td>17.92</td> </tr> <tr> <td>Ca</td> <td>13.41</td> </tr> <tr> <td>Fe</td> <td>1.97</td> </tr> </tbody> </table>		wt.%	O	44.82	Na	1.49	Mg	0.76	Al	19.63	Si	17.92	Ca	13.41	Fe	1.97
	wt.%																
O	44.82																
Na	1.49																
Mg	0.76																
Al	19.63																
Si	17.92																
Ca	13.41																
Fe	1.97																
 <p>Pusku-92 II 85 CHA MAG: 975 X HV: 20.0 kV WD: 8.0 mm Px: 0.26 µm</p>	<table border="1"> <thead> <tr> <th></th> <th>wt.%</th> </tr> </thead> <tbody> <tr> <td>O</td> <td>34.47</td> </tr> <tr> <td>Mg</td> <td>9.07</td> </tr> <tr> <td>Al</td> <td>20.25</td> </tr> <tr> <td>Cr</td> <td>1.09</td> </tr> <tr> <td>Fe</td> <td>28.97</td> </tr> <tr> <td>Ni</td> <td>6.15</td> </tr> </tbody> </table>		wt.%	O	34.47	Mg	9.07	Al	20.25	Cr	1.09	Fe	28.97	Ni	6.15		
	wt.%																
O	34.47																
Mg	9.07																
Al	20.25																
Cr	1.09																
Fe	28.97																
Ni	6.15																

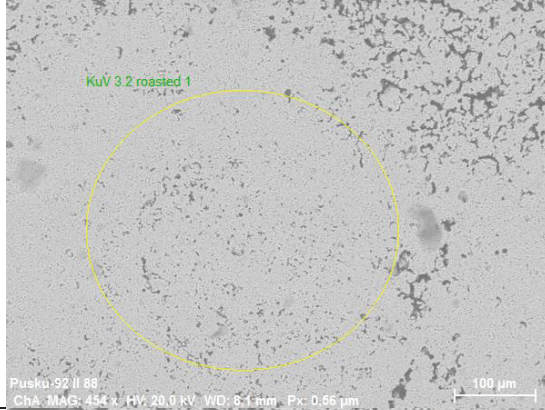
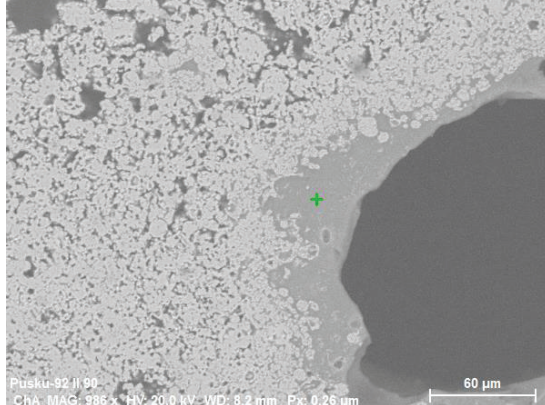
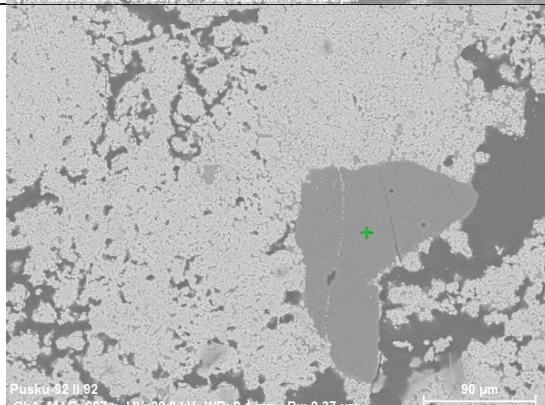
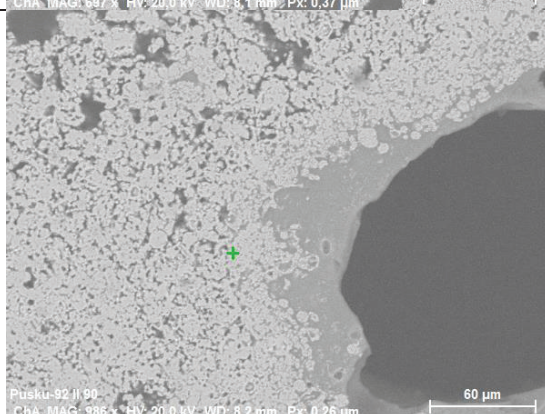
Appendix 43: SEM-EDX analyses of the calcine of jarosite from platinum production after calcination trial 3.1.

Trial 3.1, slag

	<table border="1"> <thead> <tr> <th></th> <th>wt.%</th> </tr> </thead> <tbody> <tr> <td>O</td> <td>40.04</td> </tr> <tr> <td>Na</td> <td>0.42</td> </tr> <tr> <td>Mg</td> <td>6.83</td> </tr> <tr> <td>Al</td> <td>6.86</td> </tr> <tr> <td>Si</td> <td>15.67</td> </tr> <tr> <td>K</td> <td>1.06</td> </tr> <tr> <td>Ca</td> <td>25.56</td> </tr> <tr> <td>Mn</td> <td>1.11</td> </tr> <tr> <td>Fe</td> <td>2.44</td> </tr> </tbody> </table>		wt.%	O	40.04	Na	0.42	Mg	6.83	Al	6.86	Si	15.67	K	1.06	Ca	25.56	Mn	1.11	Fe	2.44
	wt.%																				
O	40.04																				
Na	0.42																				
Mg	6.83																				
Al	6.86																				
Si	15.67																				
K	1.06																				
Ca	25.56																				
Mn	1.11																				
Fe	2.44																				
	<table border="1"> <thead> <tr> <th></th> <th>wt.%</th> </tr> </thead> <tbody> <tr> <td>O</td> <td>39.61</td> </tr> <tr> <td>Mg</td> <td>4.94</td> </tr> <tr> <td>Al</td> <td>5.90</td> </tr> <tr> <td>Si</td> <td>16.27</td> </tr> <tr> <td>K</td> <td>1.29</td> </tr> <tr> <td>Ca</td> <td>27.85</td> </tr> <tr> <td>Mn</td> <td>1.44</td> </tr> <tr> <td>Fe</td> <td>2.69</td> </tr> </tbody> </table>		wt.%	O	39.61	Mg	4.94	Al	5.90	Si	16.27	K	1.29	Ca	27.85	Mn	1.44	Fe	2.69		
	wt.%																				
O	39.61																				
Mg	4.94																				
Al	5.90																				
Si	16.27																				
K	1.29																				
Ca	27.85																				
Mn	1.44																				
Fe	2.69																				
	<table border="1"> <thead> <tr> <th></th> <th>wt.%</th> </tr> </thead> <tbody> <tr> <td>O</td> <td>30.99</td> </tr> <tr> <td>Mg</td> <td>1.22</td> </tr> <tr> <td>Al</td> <td>1.42</td> </tr> <tr> <td>Si</td> <td>3.46</td> </tr> <tr> <td>Ca</td> <td>61.71</td> </tr> <tr> <td>Fe</td> <td>1.20</td> </tr> </tbody> </table>		wt.%	O	30.99	Mg	1.22	Al	1.42	Si	3.46	Ca	61.71	Fe	1.20						
	wt.%																				
O	30.99																				
Mg	1.22																				
Al	1.42																				
Si	3.46																				
Ca	61.71																				
Fe	1.20																				
	<table border="1"> <thead> <tr> <th></th> <th>wt.%</th> </tr> </thead> <tbody> <tr> <td>Fe</td> <td>92.18</td> </tr> <tr> <td>Ni</td> <td>7.82</td> </tr> </tbody> </table>		wt.%	Fe	92.18	Ni	7.82														
	wt.%																				
Fe	92.18																				
Ni	7.82																				

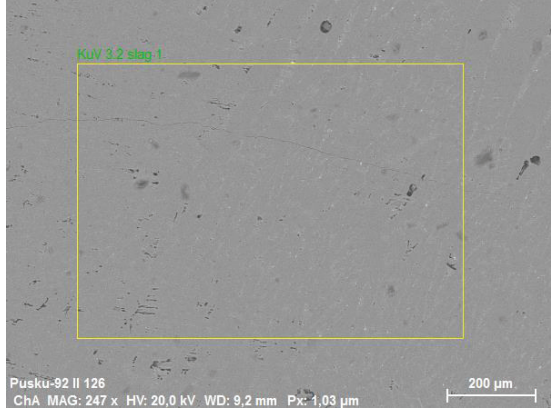
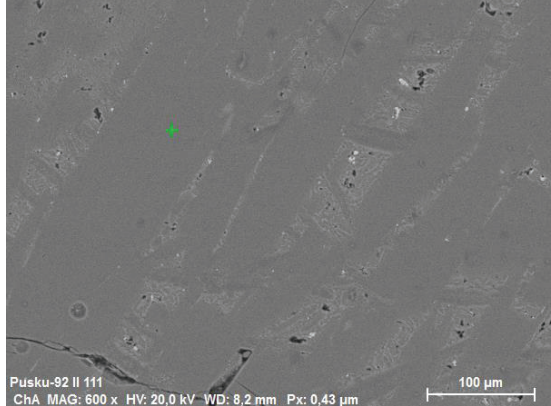


Appendix 44: SEM-EDX analyses of slag from jarosite from platinum production after reduction trial 3.1.

Trial 3.2, calcine

	<table border="1"> <thead> <tr> <th></th> <th>wt.%</th> </tr> </thead> <tbody> <tr> <td>O</td> <td>23.12</td> </tr> <tr> <td>Si</td> <td>1.34</td> </tr> <tr> <td>Fe</td> <td>71.69</td> </tr> <tr> <td>Ni</td> <td>3.85</td> </tr> </tbody> </table>		wt.%	O	23.12	Si	1.34	Fe	71.69	Ni	3.85								
	wt.%																		
O	23.12																		
Si	1.34																		
Fe	71.69																		
Ni	3.85																		
	<table border="1"> <thead> <tr> <th></th> <th>wt.%</th> </tr> </thead> <tbody> <tr> <td>O</td> <td>45.46</td> </tr> <tr> <td>Na</td> <td>3.39</td> </tr> <tr> <td>Mg</td> <td>0.70</td> </tr> <tr> <td>Al</td> <td>8.40</td> </tr> <tr> <td>Si</td> <td>29.80</td> </tr> <tr> <td>K</td> <td>4.34</td> </tr> <tr> <td>Fe</td> <td>4.26</td> </tr> <tr> <td>Pb</td> <td>3.65</td> </tr> </tbody> </table>		wt.%	O	45.46	Na	3.39	Mg	0.70	Al	8.40	Si	29.80	K	4.34	Fe	4.26	Pb	3.65
	wt.%																		
O	45.46																		
Na	3.39																		
Mg	0.70																		
Al	8.40																		
Si	29.80																		
K	4.34																		
Fe	4.26																		
Pb	3.65																		
	<table border="1"> <thead> <tr> <th></th> <th>wt.%</th> </tr> </thead> <tbody> <tr> <td>O</td> <td>52.93</td> </tr> <tr> <td>Si</td> <td>46.25</td> </tr> <tr> <td>Fe</td> <td>0.82</td> </tr> </tbody> </table>		wt.%	O	52.93	Si	46.25	Fe	0.82										
	wt.%																		
O	52.93																		
Si	46.25																		
Fe	0.82																		
	<table border="1"> <thead> <tr> <th></th> <th>wt.%</th> </tr> </thead> <tbody> <tr> <td>O</td> <td>23.04</td> </tr> <tr> <td>Al</td> <td>0.60</td> </tr> <tr> <td>Si</td> <td>0.74</td> </tr> <tr> <td>Fe</td> <td>75.62</td> </tr> </tbody> </table>		wt.%	O	23.04	Al	0.60	Si	0.74	Fe	75.62								
	wt.%																		
O	23.04																		
Al	0.60																		
Si	0.74																		
Fe	75.62																		

Appendix 45: SEM-EDX analyses of the calcine of jarosite from platinum production after calcination trial 3.2.

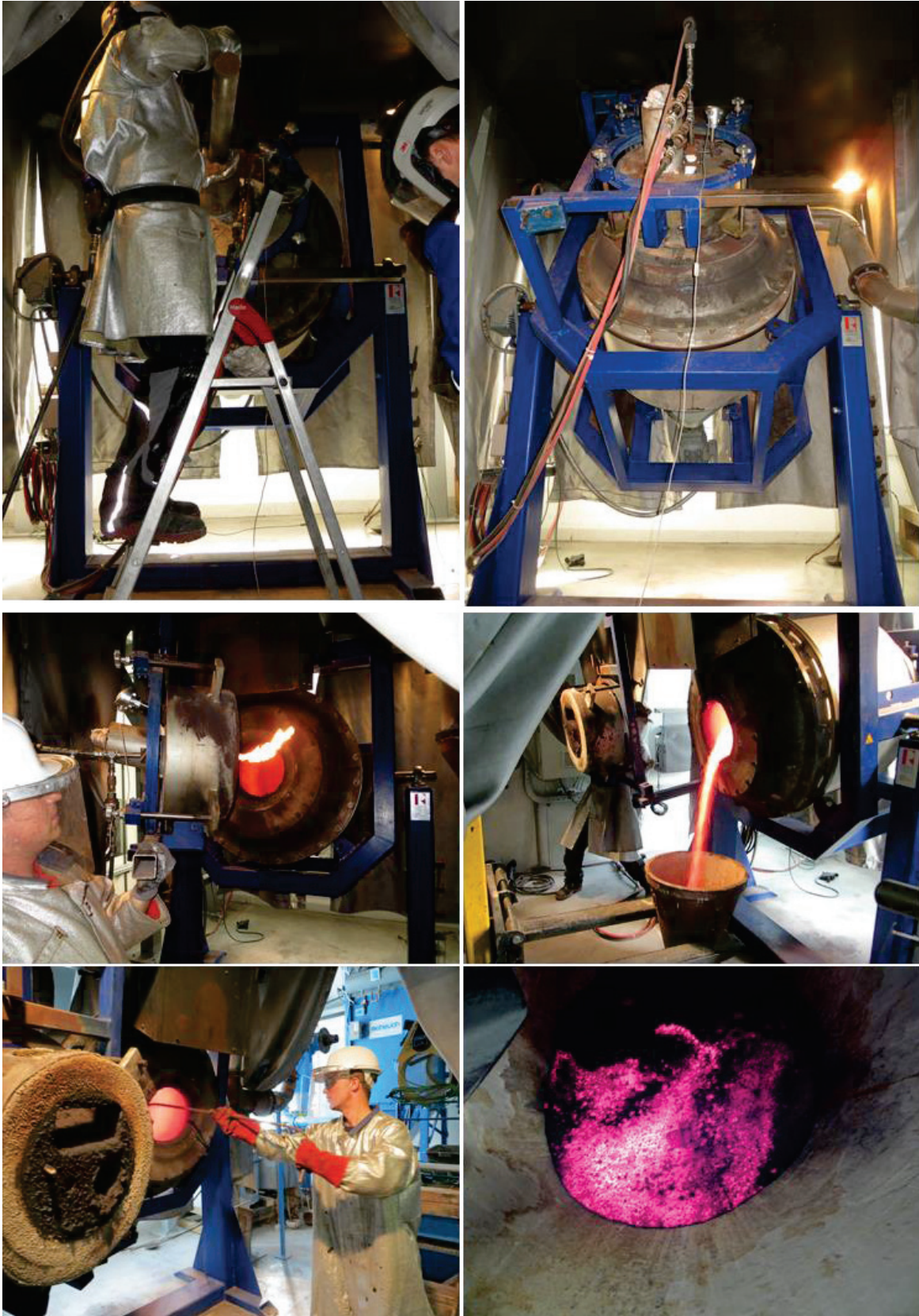
Trial 3.2, slag

	<table border="1"> <thead> <tr> <th></th> <th>wt.%</th> </tr> </thead> <tbody> <tr><td>O</td><td>39.42</td></tr> <tr><td>Na</td><td>0.28</td></tr> <tr><td>Mg</td><td>5.98</td></tr> <tr><td>Al</td><td>6.19</td></tr> <tr><td>Si</td><td>15.57</td></tr> <tr><td>K</td><td>1.04</td></tr> <tr><td>Ca</td><td>24.42</td></tr> <tr><td>Ti</td><td>0.36</td></tr> <tr><td>Mn</td><td>1.50</td></tr> <tr><td>Fe</td><td>5.24</td></tr> </tbody> </table>		wt.%	O	39.42	Na	0.28	Mg	5.98	Al	6.19	Si	15.57	K	1.04	Ca	24.42	Ti	0.36	Mn	1.50	Fe	5.24
	wt.%																						
O	39.42																						
Na	0.28																						
Mg	5.98																						
Al	6.19																						
Si	15.57																						
K	1.04																						
Ca	24.42																						
Ti	0.36																						
Mn	1.50																						
Fe	5.24																						
	<table border="1"> <thead> <tr> <th></th> <th>wt.%</th> </tr> </thead> <tbody> <tr><td>O</td><td>40.07</td></tr> <tr><td>Na</td><td>0.66</td></tr> <tr><td>Mg</td><td>5.93</td></tr> <tr><td>Al</td><td>6.41</td></tr> <tr><td>Si</td><td>15.80</td></tr> <tr><td>K</td><td>0.43</td></tr> <tr><td>Ca</td><td>29.66</td></tr> <tr><td>Fe</td><td>1.04</td></tr> </tbody> </table>		wt.%	O	40.07	Na	0.66	Mg	5.93	Al	6.41	Si	15.80	K	0.43	Ca	29.66	Fe	1.04				
	wt.%																						
O	40.07																						
Na	0.66																						
Mg	5.93																						
Al	6.41																						
Si	15.80																						
K	0.43																						
Ca	29.66																						
Fe	1.04																						
	<table border="1"> <thead> <tr> <th></th> <th>wt.%</th> </tr> </thead> <tbody> <tr><td>O</td><td>37.26</td></tr> <tr><td>Mg</td><td>1.81</td></tr> <tr><td>Al</td><td>10.50</td></tr> <tr><td>Si</td><td>11.41</td></tr> <tr><td>K</td><td>3.30</td></tr> <tr><td>Ca</td><td>12.87</td></tr> <tr><td>Ti</td><td>3.53</td></tr> <tr><td>Mn</td><td>4.01</td></tr> <tr><td>Fe</td><td>15.32</td></tr> </tbody> </table>		wt.%	O	37.26	Mg	1.81	Al	10.50	Si	11.41	K	3.30	Ca	12.87	Ti	3.53	Mn	4.01	Fe	15.32		
	wt.%																						
O	37.26																						
Mg	1.81																						
Al	10.50																						
Si	11.41																						
K	3.30																						
Ca	12.87																						
Ti	3.53																						
Mn	4.01																						
Fe	15.32																						
	<table border="1"> <thead> <tr> <th></th> <th>wt.%</th> </tr> </thead> <tbody> <tr><td>O</td><td>4.32</td></tr> <tr><td>Al</td><td>1.20</td></tr> <tr><td>Si</td><td>1.84</td></tr> <tr><td>s</td><td>30.25</td></tr> <tr><td>Ca</td><td>2.70</td></tr> <tr><td>Mn</td><td>1.83</td></tr> <tr><td>Fe</td><td>57.87</td></tr> </tbody> </table>		wt.%	O	4.32	Al	1.20	Si	1.84	s	30.25	Ca	2.70	Mn	1.83	Fe	57.87						
	wt.%																						
O	4.32																						
Al	1.20																						
Si	1.84																						
s	30.25																						
Ca	2.70																						
Mn	1.83																						
Fe	57.87																						

Appendix 46: SEM-EDX analyses of slag from jarosite from platinum production after reduction trial 3.2.



Appendix 47: Preparation of jarosite from platinum production for pyrometallurgical treatment. Upper left: mixer. Upper right: Jarosite from platinum production mixed with calcium hydroxide. Bottom left: pelletizing disc. Bottom right: pellets ready for calcination.



Appendix 48: Calcination trials with jarosite from platinum production. Upper right: charging of the TBRC. Upper right: closed TBRC. Middle left: gas burner. Middle right and bottom left: Tapping of the calcine. Lower right: calcine.



Appendix 49: Reduction trials with jarosite from platinum production. Upper left: Electric furnace prepared for trials. Upper right: sampling during reduction trial. Middle: liquid slag. Bottom: slag and alloy after tapping.